5.0 LICENSING DOCUMENTS

This section contains documents generated as a result of U.S. Nuclear Regulatory Commission (NRC) review of previous versions of this topical report. Sections 5.1 and 5.2 contain responses to rounds one and two questions, respectively, for revision 1 of this report. These documents were previously issued in the approved proprietary and non-proprietary versions as appendices H and I. Section 5.3 contains the Safety Evaluation Report (SER) issued for revision 1.

Section 5.4 and 5.5 contain responses to NRC questions on revisions 2 and 3, respectively, of this report. Section 5.6 contain supplemental information to revisions 2 and 3. Section 5.7 contains the SER issued for revisions 2 and 3. Section 5.8 contains responses to NRC questions on revision 4. Section 5.9 contains the SER issued for revision 4. Finally, Section 5.10 contains the pages removed or replaced from revision 3 to create revision 4 and Section 5.11 contains pages that were replaced due to SER direction and typographical errors.

This page intentionally left blank.

5.1 Responses to Round 1 Request for Additional Information

This section contains round one questions transmitted to B&W by M.W. Hodges of the NRC in his letter of March 31, 1988, and responses transmitted by B&W to the NRC in letters dated August 15, 1988, November 23, 1988, and December 23, 1988.

1. Question: The RELAP5/MOD2 - B&W code manual (BAW-10164P) was reviewed and compared to the RELAP5/MOD2 code manual (NUREG/CR-4312, EGG-2396). Some discrepancies between the two manuals were noted in the equations shown below. Clarify why the equations are different and verify that the equations in the RELAP5/MOD2 - B&W manual reflect the actual coding in the program.

   a. Eq. 2.2.1-27 in RELAP5/MOD2 B&W versus Eq. 528 in RELAP5/MOD2.

   b. Eq. 2.2.1-33 in RELAP5/MOD2 B&W versus Eq. 534 in RELAP5/MOD2.

   c. Eq. 2.2.1-34 in RELAP5/MOD2 B&W versus Eq. 535 in RELAP5/MOD2.

   d. Eq. 2.2.1-37 in RELAP5/MOD2 B&W versus Eq. 538 in RELAP5/MOD2.

   e. Eq. 2.2.2-13 in RELAP5/MOD2 B&W versus h_{mic} on pg. 107 in RELAP5/MOD2.

   f. Eq. 2.2.2-38 in RELAP5/MOD2 B&W versus A_{wf} on pg. 111 in RELAP5/MOD2.

   g. Eq. 2.2.2-58 in RELAP5/MOD2 B&W versus the condensation model given on pg. 116 in RELAP5/MOD2.

   h. Eq. 2.3.2-2 in RELAP5/MOD2 B&W versus Eq. 575 in RELAP5/MOD2.

   i. Eq. 2.3.2-3 in RELAP5/MOD2 B&W versus Eq. 576 in RELAP5/MOD2.

j. Eq. 2.3.2-5 in RELAP5/MOD2 B&W versus Eq. 577 in RELAP5/MOD2.

k. Eq. 2.3.2-10 in RELAP5/MOD2 B&W versus Eq. 592 in RELAP5/MOD2.

l. Eq. 2.3.2-11 in RELAP5/MOD2 B&W versus Eq. 593 in RELAP5/MOD2.

m. Eq. 2.1.3-24 in RELAP5/MOD2 B&W versus Eq. 181 in RELAP5/MOD2.

n. Eq. 2.1.3-53 in RELAP5/MOD2 B&W versus Eq. 210 in RELAP5/MOD2.

o. Eq. 2.1.3-97 in RELAP5/MOD2 B&W versus Eq. 253 in RELAP5/MOD2.

p. Eq. 2.1.3-102 in RELAP5/MOD2 B&W versus Eq. 258 in RELAP5/MOD2.

q. Eq. 2.3.1-8 in RELAP5/MOD2 B&W versus Eq. 659 in RELAP5/MOD2.

Response: The following text responds by parts:

a. The term d_m in the difference approximation for the m^{th} interior mesh point for the one dimensional heat conduction solution in BAW-10164P is defined correctly by Equation 2.2.1-27. The RELAP5/MOD2 coding (subroutine HT1TDP) agrees with Equation 2.2.1-27. Equation 528 of NUREG/CR-4312 and EGG-2396 contains two typographical errors.

In Equation 2.2.1-24 of BAW-10164 and Equation 525 of NUREG/CR-4312 and EGG-2396 K^n_{lm} should be k^n_{lm}.

In Equation 2.2.1-26 of BAW-10164 and Equation 527 of NUREG/CR-4312 and EGG-2396 K_{rm}^{n} should be k_{rm}^{n}.

There should be a minus "-" sign on the right hand side of Equation 2.2.1-32 of BAW-10164 and Equation 533 of NUREG/CR-4312 and EGG-2396.

Changes to BAW-10164 will be prepared and released in the first revision to the document.

b. The term d_1 in the left boundary condition for the conduction solution (Equation 2.2.1-30) in BAW-10164 is defined correctly by Equation 2.2.1-33. The RELAP5/MOD2 coding (subroutine HT1TDP) agrees with Equation 2.2.1-33. Equation 534 of NUREG/CR-4312 and EGG-2396 contains two typographical errors.

c. There are several typographical errors in both Equation 535 of NUREG/CR-4312 and EGG-2396 and Equation 2.2.1-34 of BAW-10164. Equation 2.2.1-34 should read as follows:

$\sigma c_1^n T_2^n$ should be $-\sigma c_1^n T_2^n$,

$$- \frac{k_{r1} \, \delta_1^b \, c_1 \Delta t}{B_1^n} \text{ should be } - \frac{k_{r1} \, \delta_1^b \, C_1^n \Delta t}{B_1^n}, \text{ and}$$

$Q_{rl} \, \delta_{rl}$ in the last term should be $Q_{r1} \, \delta_{r1}^v$.

The equation is coded correctly in RELAP5/MOD2.

Changes to BAW-10164 will be prepared and released in the first revision to the document.

d. Equation 2.2.1-37 of BAW-10164 is correct and the coding of RELAP5/MOD2 agrees with the equation. There are two typographical errors in NUREG/CR-4312 and EGG-2396 Equation 538.

In the first line of text after Equation 2.2.1-38

$C_m^n = A_m^n \, T_m^n - D_m^n$ should be replaced by $C_M^n = A_M^n \, T_M^n - D_M^n$

A similar typographical error exists on page 245 of NUREG/CR-4312 and EGG-2396.

e. Equation 2.2.2-13 of BAW-10164 is incorrect. It should read:

$$h_{mic} = 0.00122 \left\{ \frac{K_f^{0.79} \, C_{pf}^{0.45} \, \rho_f^{0.49}}{\sigma^{0.5} \, \mu_f^{0.29} \, h_{fg}^{0.24} \, \rho_g^{0.24}} \right\} \Delta T_{sat}^{0.24} \, \Delta P^{0.75} S$$

The Equation on page 107 of NUREG/CR-4312 and EGG-2396 is correct. The coding of RELAP5/MOD2 is correct and agrees with the above equation.

Changes to BAW-10164 will be prepared and released in the first revision to the document.

f. The F_L factor given by Equation 2.2.2-38 of BAW-10164 is the fraction of wall surface area wetted and equivalent to A_{Wf}/A_W on page 111 of the RELAP5/MOD2 manual. Equation 2.2.2-38 is correct whereas the form of the correlation on page 111 of NUREG/CR-4312 and EGG-2396 is incorrect. The coding for RELAP5/MOD2 agrees with the equation in BAW-10164. Note should be taken of the difference in units for these correlations in the two reports. SI units are used for Equation 2.2.2-38 in BAW-10164 while British units are used on page 111 of NUREG/CR-4312 and EGG-2396.

g. The volumetric vapor generation rate, Γ_w, for condensation is given correctly by Equation 2.2.2-58 of BAW-10164. The coding for RELAP5/MOD2 agrees with this equation. The equation on page 116 of NUREG/CR-4312 and EGG-2396 misrepresents Γ_w for condensation.

h. The core heat transfer models, Section 2.3.2 and 2.3.3 of BAW-10164, are essentially new models which were added to RELAP5/MOD2-B&W to enhance the reactor core simulation. The original RELAP5/MOD2 heat transfer model has been maintained in RELAP5/MOD2-B&W and is referred to as the System Heat Transfer Model. The System Heat Transfer Model is applied to the reactor coolant system exterior to the reactor core and to the secondary side. While maintaining the basic heat structure form of RELAP5/MOD2, the Core Heat Transfer Model contains new heat transfer coefficients, a pin model with a different gap conductance approach, a pin rupture model, and a metal-water reaction model. There is unlikely to be good correspondence between BAW-10164 and NUREG/CR-4312 and EGG-2396 within the features of the core heat transfer and fuel pin packages.

Equation 2.3.2-2 is part of the new fuel pin model for the core. It is printed correctly and the coding in RELAP5/MOD2-B&W agrees with the equation.

Note: The formulation of Equation 2.3.2-2 is identical to the formulation used in FRAP-T6-B&W, BAW-10165, Equations 2.1.3-1 and 2.1.3-2.

i. Equation 2.3.2-3 is incorrect. It should be:

$$r_n = \left(\frac{2n - 1}{N} \right) r_g .$$

There is no intended correspondence to Equation 576 of NUREG/CR-4312 and EGG-2396. Equation 2.3.2-3 is a simplified form of the FRAP-T6-B&W, BAW-10165, formulation of Equation 2.1.3-3 with r_o' always taken as the average hot fuel to cladding gap width.

Changes to BAW-10164 will be prepared and released in the first revision to the document.

j. Equation 2.3.2-5 is stated correctly for the new core heat transfer and fuel pin models. Equation 577 of NUREG/CR-4312 and EGG-2396 is incorrect.

k. Equation 2.3.2-10 of BAW-10164 contains a typographical error. It should read:

$$K_{gas} = \sum_{i=1}^{N_g} K_i X_i \Bigg/ \left[X_i + \sum_{j=1}^{N_g} \phi_{ij} X_j \right] ,$$

The coding of RELAP5/MOD2 is correct and agrees with the above equation.

Changes to BAW-10164 will be prepared and released in the first revision to the document.

l. Equation 2.3.2-11 of BAW-10164 and Equation 593 of NUREG/CR-4312 and EGG-2396 are equivalent but in different forms.

m. Equation 2.1.3-24 in BAW-10164 correctly defines the critical Weber Number. The coding of RELAP5/MOD2 corresponds to Equation 2.1.3-24. Equation 181 of

NUREG/CR-4312 and EGG-2396 contains a typographical error.

n. Equation 2.1.3-53 correctly defines the relationship between the Lockhart - Martinelli parameter "x" and the ratio of the phasic pressure drops. There is a typographical error in equation 210 of NUREG/CR-4312 and EGG-2396.

Equation 2.1.3-53 enters into the coding through Equation 2.1.3-77 whose exponents are specified by the definition of the "x" term. Equations 2.1.3-53 and 2.1.3-77 are consistent as given in BAW-10164 and the coding of RELAP5/MOD2 is properly represented by Equation 2.1.3-77.

Equation 2.1.3-71 contains a typographical error. The second term of the quadratic C_x should be C x.

Changes to BAW-10164 will be prepared and released in the first revision to the document.

o. The definition of the friction factor, $\lambda_{L,T}$, for the transition regime between laminar and turbulent flow is calculated correctly by Equation 2.1.3-97 in BAW-10164. Equation 253 of NUREG/CR-4312 and EGG-2396 contains typographical errors.

Equation 2.1.3-97 enters into the coding as part of the derivation for Equation 2.1.3-107 which corresponds to RELAP5/MOD2 as programed. Equation 2.1.3-107 can not be derived from Equation 253 of NUREG/CR-4312 and EGG-2396.

Equations 2.1.3-98 of BAW-10164 and Equation 254 of NUREG/CR-4312 and EGG-2396 are both incorrect and should read as follows:

$$0 \leq 5.285 \left[1.189 - \left(\frac{4000}{R} \right)^{0.25} \right] \leq 1.0$$

The coding of RELAP5/MOD2 is correct and agrees with the above equation.

$L(2-R^*)$ in Equation 2.1.3-107 of BAW-10164 and in Equation 263 of NUREG/CR-4312 and EGG-2396 should be replaced by $L\ [\ 5.285\ (\ 1.189 - R^*\ )\ ]$.

The coding of RELAP5/MOD2 is correct and agrees with the above.

Changes to BAW-10164 will be prepared and released in the first revision to the document.

p. The critical Reynold's number is properly given by Equation 2.1.3-102 BAW-10164 and the coding of RELAP5/MOD2 corresponds to Equation 2.1.3-102. Equation 258 of NUREG/CR-4312 and EGG-2396 contains typographical errors.

q. Equation 2.3.1-8 of BAW-10164 contains a typographical error. It should read:

$$P_{\alpha j}(t) = \lambda_{\alpha j} \quad \gamma_{\alpha j} \quad = a_{\alpha j} \exp(-\lambda_{\alpha j} t).$$

The coding of RELAP5/MOD2 is correct and agrees with the above equation.

Changes to BAW-10164 will be prepared and released in the first revision to the document.

2. Question: Verify the correctness or typographic error for each of the following items.

a. Verify that Eq. 2.2.2-25 is shown correctly. Define delta-T_{NVG}. Also, should T_f be T_W?

b. Are R_2 and R_3 defined correctly on pg. 2.2-30?

c. Page 2.2-30 refers to Eq. 2.2.2-34/35. Should this page actually refer to Eq. 2.2.2-40/41.

d. On page 2.1-46 reference is made to Eq. 2.1.3-1. Should reference be to Eq. 2.1.3-2?

Response: The following text responds by parts:

a. Equation 2.2.2-25 and the use of T_f are correct in BAW-10164. The term ΔT_{NVG} is defined as:

$$\Delta T_{NVG} = T_{sat} - T_{fNVG} ,$$

where

T_{fNVG} = the liquid temperature above which net vapor generation can occur.

This modeling agrees with RELAP5/MOD2 coding.

b. Equation 2.2.2-45 and its subcomponents, namely R_1, R_2, and R_3, are correct in BAW-10164. Typographical errors exist in NUREG/CR-4312 and EGG-2396 on pages 126 and 127 for these terms. Reference can be made to K. H. Sun, J. M. Gonzales, and C. L. Tien, "Calculation of Combined Radiation and Convection Heat Transfer in Rod Bundles under Emergency Cooling Conditions," Journal o Heat Transfer, Transactions of ASME, 98, 1976 page 414.

c. The references in the last paragraph on page 2.2-30 to Equations 2.2.2-34 and 2.2.2-35 are in error; reference should be made to Equations 2.2.2-40 and 2.2.2-41 respectively.

Changes to BAW-10164 will be prepared and released in the first revision to the document.

d. The reference in the middle paragraph on page 2.1-46 to Equation 2.1.3-1 is not correct; reference should be made to Equation 2.1.3-2.

Changes to BAW-10164 will be prepared and released in the first revision to the document.

3. Question: Eq. 2.2.2-51 is a Nusselt condensation correlation. Describe where and how this correlation is used in the code.

Response: In the RELAP5/MOD2 and RELAP5/MOD2-B&W computer codes, a form of the Nusselt laminar film condensation correlation is used that differs from the form given by Equation 2.2.2-51 of BAW-10164 (and also on page 114 of NUREG/CR-4312). The correlation as used in these codes depends on the orientation of the condensing surface as described below.

a. Horizontal Surface (inclination angle of the volume to the horizontal is zero)

For condensation on a horizontal surface, laminar film condensation in a horizontal tube with stratified flow is assumed, and a modified form of the Nusselt equation (page 341 of Reference 44 in BAW-10164), given by

$$h_{nlf} = 0.296 \left[\frac{\rho_f (\rho_f - \rho_g)\ g\ h_{fg}\ k_f^3}{D_e \mu_f\ (T_{sat} - T_w)} \right]^{0.25},$$

is used.

b. Vertical Surface

For condensation on a vertical surface, the Nusselt laminar film condensation correlation (Reference 44 in BAW-10164), given by

$$h_{nlf} = 0.943 \left[\frac{\rho_f (\rho_f - \rho_g)\ g\ \sin\theta\ h_{fg} k_f^3}{\mu_f\ L_v\ (T_{sat} - T_w)} \right]^{0.25},$$

where

θ = angle of inclination to the horizontal

and

L_V = volume length,

is used.

When the volume average liquid velocity is less than or equal to 0.001 m/s, only laminar film condensation is used. These changes will be incorporated into the next revision to BAW-10164.

4. Question: Clarify why Eq. 2.2.2-54 is multiplied by the min(1.0, 10*VOIDG).

Response: Equation 2.2.2-54 would be more clearly written as,

$$h_{Wg} = h_{con} \cdot (\alpha_g \, MIN(1.0, 10 \, \alpha_g)).$$

The weighting of h_{con} by void fraction is to restrict the surface area available for condensation. At high void fraction straight α_g weighting is adequate; however, at very low void fraction α_g weighting may under predict the rate of condensation. The term $MIN(1.0, 10 \, \alpha_g)$ is applied to adjust the weighting at low void fractions.

This weighting of h_{con} exists in the RELAP5/MOD2 coding.

5. Question: Clarify why the coefficient in the Rohsenow-Choi correlation is 4.36 in the system model (Eq. 2.2.2-7) but 4.0 in the core model (Eq. 2.3.3-15).

Response: The coefficient in the Rohsenow-Choi correlation, as originally given (W. M. Rohsenow and H. Y. Choi; Heat, Mass, and Momentum Transfer; Prentice-Hall, Inc.; 1961;page 166), depends on the wall conditions:

Wall Condition	Coefficient
Uniform T_W	3.66
Uniform heat flux	4.36

Y. Y. Hsu recommends a value of 4.0 for this coefficient for blowdown heat transfer. This is a compromise between the laminar forced convection condition of uniform heat flux and the uniform temperature condition. Refer to Thermohydraulics of Two-Phase Systems for Industrial Design and Nuclear Engineering; Edited by J. M. Delhaye, M. Giot, and M. L. Reithmuller, Hemisphere Publishing Corporation, 1981, pages 261 and 262. B&W feels that the compromise coefficient is more appropriate for the conditions in the core than the uniform heat flux value.

On page 2.3-71 of BAW-10164 an incorrect reference was given for the Rohsenow-Choi correlation. The correct reference is given above.

Changes to BAW-10164 will be prepared and released in the first revision to the document.

6. Question: All of the heat transfer coefficients are coded with a user input multiplier. Clarify whether a multiplier other than 1.0 will ever be used in a licensing calculation, and provide justifications or bases for those multipliers with values other than 1.0.

Response: The incorporation of multipliers on the heat transfer was to provide some degree of user flexibility for general code use and to allow for sensitivity studies which may form part of a plant licensing basis. The multipliers to be used in evaluations are documented in the applicable evaluation model report (BAW-10168 for applications to Westinghouse designed NSSS).

Note: As of 7/8/88 it is B&W's intention to use a multiplier of 1.0 on all RELAP5/MOD2-B&W heat transfer coefficients for application on Westinghouse designed NSSS with the exception of certain sensitivity studies.

7. Question: Eq. 2.3.3-59 sets the film boiling heat transfer coefficient to the maximum of the CSO film boiling correlation and the Rohsenow-Choi correlation. Clarify the applicability of the Rohsenow-Choi correlation to film boiling heat transfer and why the film boiling heat transfer coefficient is calculated in this manner.

Response: The lower bound of single phase wall to vapor convective heat transfer is given by the Rohsenow-Choi correlation (Equation 2.3.3-66 of BAW-10164). The lower bound for flow film boiling is convective heat transfer to vapor. Therefore it is reasonable to use the lower bound convective heat transfer correlation as the lower bound for the flow film boiling regime. The CSO correlation is, in fact, the product of a convective to vapor heat transfer term (Equation 2.3.3-60 of BAW-10164) and liquid content based enhancement term, $(1 + \dot{F}_S)$.

Recent modifications to RELAP5/MOD2-B&W, FRAP-T6-B&W, and the B&W Evaluation Model for Westinghouse-designed NSSS's have replaced the CSO flow film boiling correlation with the Condie-Bengston IV correlation (K. G. Condie, S. J. Bengston and S. L. Richlin; Post-CHF Heat Transfer Data Analysis, Comparison and Correlation; EG&G unpublished report). The same reasoning applies to the lower bound of the flow film boiling heat transfer regime and the use of Rohsenow-Choi is maintained.

A telephone conversation has been conducted with the NRC informing them of the change. A letter formally advising of this modification to the RELAP5/MOD2-B&W and FRAP-T6-B&W is being prepared for submittal in the near future.

Appropriate changes to BAW-10164, RELAP5/MOD2-B&W, and BAW-10165, FRAP-T6-B&W, will be prepared and released in the first revision to those documents. The B&W evaluation model report for Westinghouse-designed NSSS, BAW-10168, as submitted on July 25, 1988, uses and properly reflects the use of the Condie-Bengston correlation.

8. Question: Provide an assessment of the CSO film boiling heat transfer correlation and the McEligot single-phase steam correlation to verify the correlations' accuracy for calculating film boiling and single-phase steam heat transfer.

Response: In the RELAP5/MOD2-B&W EM heat transfer package, the film boiling heat transfer coefficient is calculated using either the CSO or the Condie-Bengston IV correlation. For EM applications, B&W will use the Condie-Bengston IV correlation to calculate film boiling heat transfer. Therefore, an assessment of the Condie-Bengston correlation instead of the CSO correlation will be made in response to this question. The applicability of Condie-Bengston IV and McEligot correlations for LBLOCA applications is demonstrated by the simulation of the Semiscale MOD1 test S-04-6, which is discussed in detail as a response to question 12. Additional assessments of these correlations are discussed below.

Assessment of the Condie-Bengston IV Correlation

Yoder[8.1] evaluated the Condie-Bengston IV correlation using the available rod bundle film boiling data base. Figure 4.3 of Reference 8.1 shows the comparison between the correlation predicted heat flux and the film boiling data. From this figure, the correlation can be characterized as producing reasonable to conservative predictions. Yoder, in fact, concluded that "the Condie-Bengston IV correlation does a reasonable job in predicting film boiling heat fluxes." Therefore, B&W concludes that the Condie-Bengston IV correlation is appropriate for the prediction of film boiling heat transfer in the B&W RSG LOCA Evaluation Model.

McEligot Single-Phase Steam Correlation

The McEligot convective steam cooling correlation has been used in other approved computer code for EM applications. It is also the approved correlation used by the Japanese Nuclear Safety Commission to calculate convective heat transfer to steam in their evaluation model. Experimental studies of convective steam cooling heat transfer in single tubes and rod bundles support the use of the McEligot correlation to calculate convective heat transfer to steam.

Larsen and Lord[8.4] studied convection and radiation heat transfer to superheated steam in heated tubes. Their results (Figure 12 in Reference 8.4) show that the correlation properly predicts convective heat transfer to steam for bulk Reynolds numbers, Re_b, (calculated based on the bulk steam temperature) above 5000, but overpredicts the heat transfer for Reynolds numbers below 5000. However, in rod bundles, such as in a nuclear core, the convective heat transfer at low Re_b would be higher than in a single tube due to the mixed convection in rod bundles.

Wong and Hochreiter[8.5] studied low Reynolds number forced convection steam cooling using the 161-rod FLECHT-SEASET bundle. The inlet Reynolds number was varied from 2500 to 17,000. Their results show that the Dittus-Boelter correlation underpredicts the heat transfer over this range of Reynolds numbers and that the degree of underprediction increases with decreasing Reynolds number. For a given set of conditions, the Dittus-Boelter correlation predicts larger heat transfer coefficients than does the McEligot correlation. Therefore, from the Wong and Hochreiter study it can be concluded that the McEligot correlation will in general underpredict the heat transfer for Reynolds numbers below 17,000.

Yoder[8.1] also evaluated the rod bundle steam cooling data base. The results (Figure 4.9 of Reference 8.1) show that the Dittus-Boelter correlation is appropriate for use in calculating convective heat transfer to steam for Re_b less than 20,000. This is consistent with the study by Wong and Hochreiter. Thus, from Yoder's work, it can also be concluded that the McEligot correlation is valid for use at low Reynolds numbers. Sozer, Anklam and Dodds also reached this same conclusion.

Recently, Kumamaru, et al[8.7] evaluated various convective steam cooling correlations using the uncovered bundle heat transfer test data under high pressure boil-off conditions in the Two-Phase Flow Test Facility (TPTF). These tests covered a pressure range from 3 to 12 MPa and vapor Reynolds numbers from 10,000 to 62,000. The results of the evaluation (Figure 13 in Reference 8.7) showed that the McEligot correlation reasonably predicts convective heat transfer to steam.

From the evaluation of the available literature on convective heat transfer to steam, it is concluded that the McEligot correlation is reasonable and appropriate for use in calculating convective heat transfer to steam in both the transition (low Reynolds number) and the turbulent (high Reynolds number) flow regimes.

References

8.1 G. L. Yoder, Rod Bundle Film Boiling and Steam Cooling Data Base and Correlation Evaluation, NUREG/CR-4394, ORNL-TM-9628, August 1986.

8.2 F. M. Bordelon, et al, LOCTA-IV Program: Loss of Coolant Transient Analysis, WCAP-8305, June 1974.

8.3 Guideline for the Evaluation of ECCS of Light Water Reactor, Nuclear Safety Commission of Japan, July 20, 1981.

8.4 P. S. Larsen and H. A. Lord, Convective and Radiative Heat Transfer to Superheated Steam in Uniformly and Non-Uniformly Heated Tubes, ORA Project 08742, Dept. of Mech. Eng., University of Michigan, February 1969.

8.5 S. Wong and L. E. Hochreiter, "Low Reynolds Number Forced Convective Steam Cooling Heat Transfer in Rod Bundles," Paper presented at ASME Winter Annual Meeting, November 16-21, 1980, Chicago, Illinois.

8.6 A. Sozer, T. M. Anklam and H. L. Dodds, "Convection-Radiation Heat Transfer to Steam in Rod Bundle Geometry," Nuc. Technology 67, pp. 452-462, December 1984.

8.7 H. Kumamaru, et al, "Investigation of Uncovered Bundle Heat Transfer Under High Pressure Boil-Off Conditions," Nuc. Eng. and Design, 96, pp. 81-94, 1986.

9. Question: The Schrock and Grossman correlation is applied at pressures greater than 1000 psia. However, based on the information in the THETA1-B code manual, the data base for the correlation only goes to 505 psia. Clarify the accuracy and applicability of this correlation for pressures greater than 1000 psia.

Response: The data base for the Schrock and Grossman correlation is limited to below 505 psia. However, the correlation has been used in NRC-approved codes for licensing applications and in audit calculation codes (for example WREM, FRAPT-6, and TOODEE2). Extension of the correlation for use at high pressures is supported by its sound theoretical development which accounts for pressure effects.

The heat-momentum analogy is used in the development of the Schrock and Grossman correlation. Analogies between heat, mass and momentum transfer have been successfully used by the thermal hydraulic research community to transfer information between these parameters. Schrock and Grossman assumed that the ratio between the two-phase and the single-phase liquid heat transfer coefficients, h_{TP}/h_{ℓ}, was a function of the Lockhart-Martinelli parameter, X_{tt}, given by Equation 2.3.3-23 in the RELAP5/MOD2-B&W topical report (BAW-10164).

$$h_{TP} / h_{\ell} = f(X_{tt}) \quad ,$$

where the single-phase liquid heat transfer coefficient is given by the Dittus-Boelter correlation. It should also be noted that the Lockhart-Martinelli parameter is the squareroot of the ratio between the single-phase liquid pressure drop and the single-phase vapor pressure drop (Equation 2.1.3-53 in BAW-10164). The two-phase pressure drop is calculated using the assumption that the pressure ratio between the two-phase and the single-phase is a function of X_{tt}. This approach has been successfully applied in calculating two-phase pressure drops over the range from atmospheric pressure to the critical pressure. Based on this result, it is concluded that the Schrock and Grossman correlation is applicable at pressures above 1000 psia.

10. Question: Provide an assessment of the fuel behavior models (gap conductance, clad deformation, and metal-water reaction) added to RELAP5/MOD2-B&W.

Response: The fuel behavior models incorporated into RELAP5/MOD2-B&W by B&W were obtained from current technology computer codes, such as FRAPT-6, RELAP5/MOD2 and MATPRO-Version 11, and implemented according to the requirements of 10CFR50.46 Appendix K. An assessment of each of these models is presented below.

Gap Conductance

The RELAP5/MOD2-B&W gap conductance model was developed based on the models in FRAPT-6 and RELAP5/MOD2. Recently, EG&G[10.2] evaluated the RELAP5/MOD2 dynamic gap conductance model using the Power Burst Facility (PBF) test LOC-11C. Figure 9-10, in Reference 10.2, shows the variation of fuel centerline temperature with local fuel rod power; the calculated results using FRAPT-6 are also shown. From the results shown in this figure, it can be concluded that the gap conductance models in both RELAP5/MOD2 and FRAPT-6 realistically predict fuel temperatures. The FRAPT-6 code has been widely used in calculating cladding and fuel thermal and mechanical responses during transients. In addition, RELAP5/MOD2-B&W gap conductance at steady-state is adjusted, using the gap multiplier M_g (discussed below), to match the NRC-approved fuel pin code results. Based on this assessment, it can be concluded that RELAP5/MOD2-B&W would calculate realistic fuel rod temperatures. The sources of each of the terms in the gap conductance model are given below.

The correlation for the gap conductance in RELAP5/MOD2-B&W (Equation 2.3.2-2 in BAW-10164) is the same as that used in FRAP-T6-B&W (BAW-10165 Equation 2.1.3-2). It is to be noted that the constant 3.6 in Equation 2.3.2-2 is the same as that used in FRAP-T6 code, even though the FRAP-T6 manual (NUREG/CR-2148, Equation 2) states 3.2.

The correlation for the temperature jump distance term, (g_1 + g_2), in RELAP5/MOD2-B&W (Equation 2.3.2-5 in BAW-10164) is the same as that in FRAPT-6 (Equation 4 in NUREG/CR-2148). RELAP5/MOD2-B&W uses a value of 0.74 for the constant term in the equation for the accommodation coefficient of Xenon, while FRAPT-6 uses a value of 0.749, which is consistent with the value reported by Lanning and Hann.[10.1] It is concluded that the value used in RELAP5/MOD2-B&W should be updated to 0.749. This was accomplished in Revision 2 to BAW-10164. The gap radiation heat transfer in RELAP5/MOD2-B&W (Equation 2.3.2-4 in BAW-10164) is calculated in the same way as in FRAPT-6 (Equation 7 in NUREG/CR-2148).

RELAP5/MOD2-B&W (Equations 2.3.2-10 and 2.3.2-11 in BAW-10164) and FRAPT-6 (based on the coding) use the same correlation to calculate the thermal conductivity of the gas mixture, K_{gas}. The individual gas thermal conductivities, k_i, in RELAP5/MOD2-B&W are calculated using the correlations given in MATPRO Version 11 (Revision 2). These same correlations are also used in RELAP5/MOD2.

The gap width at the mid-point of the n-th azimuthal segment, r_n, is calculated using a simplified form of the equation given in FRAPT-6. This would have a minimal impact on the results because of the use of the gap multiplier, M_g, as explained below.

During the steady-state initialization of RELAP5/MOD2-B&W, h_{gap} is adjusted using the multiplier, M_g, such that the gap stored energy calculated by RELAP5/MOD2-B&W is greater than or equal to the value calculated using the NRC-approved fuel pin code, TACO2 (or TACO3 upon NRC approval). The multiplier calculated during steady-state remains constant throughout the transient. A similar method has been used by B&W in the NRC-approved topical report BAW-10104-A.

The transient internal pin pressure, P_g, is calculated using the methodology in the NRC-approved CRAFT2 computer code (BAW-10092-A).

Fuel Rod Swelling, Clad Deformation, and Rupture

The hot fuel-cladding gap distance, r_g, is calculated using Equation 2.3.2-12 in BAW-10164. The fuel thermal expansion, u_{TF} (Equation 2.3.2-14 in BAW-10164), is calculated in the same manner as in RELAP5/MOD2 (NUREG/CR-4312, Equation 583). The fuel radial thermal strain function, ϵ_{TF} (Equation 2.3.2-15 in BAW-10164), the cladding strain function, ϵ_{TC} (Equation 2.3.2-21 in BAW-10164), and Young's modulus of elasticity, E (Equation 2.3.2-28 in BAW-10164), are calculated using the correlations given in MATPRO Version 11 (Revision 2). RELAP5/MOD2 also uses these same correlations in calculating the fuel-cladding gap.

The cladding thermal expansion, u_{TC} (Equation 2.3.2-20 in BAW-10164), required updating in RELAP5/MOD2-B&W. u_{TC} should be calculated based on the cladding thickness rather than the cladding radius as was done in RELAP5/MOD2 (NUREG/CR-4312, Equation 585). This update has been recorded in Revision 2 of BAW-10164.

The steady-state fuel and cladding radii calculated by RELAP5/MOD2-B&W and the corresponding values calculated using the NRC-approved fuel pin code (TACO2 at present or TACO3 after its approval) are made equal by using the over-specification factors, u_{FC} (Equation 2.3.2-13 in BAW-10164) and u_{CC} (Equation 2.3.2-19 in BAW-10164). The values of u_{FC} and u_{CC} remain constant during the transient. In RELAP5/MOD2, similar adjustment parameters can be input to the code. In CRAFT2 and THETA1-B, the cold unstressed dimensions are calculated from the hot stressed dimension code inputs (as determined by the steady-state fuel pin code). These values are used as the basis for calculating the fuel and cladding geometry changes during a transient. Thus, using adjustments in thermal-hydraulic codes to match calculated fuel and cladding radii with values calculated from a steady-state fuel pin computer program is a standard procedure.

The clad swelling and rupture models used in RELAP5/MOD2-B&W are from NUREG-0630. The NUREG-0630 models were developed as licensing standards for LOCA analysis using the data base generated from an extensive research program sponsored by the NRC. During plastic deformation, the normalized ramp rate, H, is calculated using a plastic weighted time average equation (Equation 2.3.2-36 in BAW-10164). Its basis is an NRC letter from G. N. Lauben to L. E. Phillips[10.3] regarding TOODEE2 models for swelling and rupture. It is concluded that RELAP5/MOD2-B&W properly calculates clad swelling and rupture as per NRC requirements.

Metal Water Reaction

The metal-water reaction rate in RELAP5/MOD2-B&W is calculated using the parametric relationship derived by Baker and Just (Reference 120 in BAW-10164) as required by Appendix K.

10.1 D. D. Lanning and C. R. Hann, Review of Methods Applicable to the Calculation of Gap Conductance in Zircaloy-Clad UO_2 Fuel Rods, BNWL-1894.

10.2 R. A. Dimenna, et al, RELAP5/MOD2 Models and Correlations, NUREG/CR-5194, August 1988.

10.3 Letter from Richard P. Denise (Acting Assistant Director for Reactor Safety, Division of Systems Safety), NRC to J. H. Taylor, B&W, January 31, 1980 (Transmitting letter from G. N. Lauben, NRC to L. E. Phillips, NRC, Subject: TOODEE2 Models for Swelling and Rupture, January 15, 1980).

11. Question: Does the fine node option discussed on page 2.3-57 of the RELAP5/MOD2-B&W manual allow for the metal-water reaction to occur no less than 1.5 inches axially from the ruptured point as required by Appendix K?

Response: The fine node option described on page 2.3-57 of BAW-10164 has no restriction on the node size. However, in a system code like RELAP5/MOD2-B&W, it is unlikely to use a node size smaller than 3 inches due to execution time. Furthermore, fuel rod thermal behavior is calculated using FRAP-T6-B&W (BAW-10165), not RELAP5/MOD2-B&W. As such, compliance with Appendix K restrictions on the amount of local and whole core metal-water reaction is demonstrated via FRAP-T6-B&W calculations. Hence, RELAP5/MOD2-B&W metal-water calculations are not significant to the overall result. Core node size used in the RELAP5/MOD2-B&W (and FRAP-T6-B&W) LOCA EM is defined in BAW-10168.

12. Question: In the large break loss-of-coolant (LBLOCA) assessment using data from Semiscale MOD-1 Test S-04-6, the depressurization calculated with the RELAP5/MOD2, cycle 36.04 code was faster than in the experiment (Figures G.1-3 to G.1-9).

a. Clarify why the faster depressurization was calculated even though the break flow in this calculation compared reasonably well to the data.

b. Clarify why the densities upstream of the vessel side break calculated in the two RELAP5/MOD2 calculations were lower than the measured data (Figure G.1-21).

c. Clarify why the mass flow in the intact loop hot leg was underpredicted for the first 10s in both calculations (Figure G.1-14).

d. In Figures G.1-30 and G.1-31, the RELAP5/MOD2-B&W evaluation model (EM) calculation showed slightly better cooling than the RELAP5/MOD2, cycle 36.04 calculation in the period after approximately 12 or 13 s. Clarify what caused this difference between the two calculations.

Response:

The Semiscale MOD1 test S-04-6 was reanalyzed using RELAP5/MOD2-B&W due to the following changes in the B&W evaluation model (BAW-10168):

1. The CSO film boiling correlation was replaced by the Condie-Bengston IV correlation.

2. The B&W-2 CHF correlation was replaced by the BWCMV correlation for the high flow, high pressure flow condition.

3. Moody slip was assumed at the break junction.

4. The ECCS bypass flow modeling was updated (see Section 4.3.4.2 of the LOCA EM topical report, BAW-10168 Volume I).

The test data and BE prediction reported in Section G.1 of BAW-10168 Volume I still remain valid and are reproduced herein for completeness of the comparison with the new EM benchmark. The responses to questions 12 and 13 are incorporated into the following discussion.

Test S-04-6 was one of the 200 percent offset shear double-ended cold leg break tests conducted in the Semiscale MOD1 test facility. RELAP5/MOD2-B&W was used to predict the test, first using the INEL Cycle 36.04 options (base case) and second using the B&W installed evaluation model (EM) options. Both cases predicted higher break mass flow rates than shown by the data, and, as a result, the predicted depressurization rates were higher than the data. The predicted cladding temperature at the peak power location of the high powered rod using the EM option was higher than the Cycle 36.04 prediction. Both cases predicted higher cladding temperatures than the measured data. From this study, it is concluded that the EM option would properly predict the system behavior during the blowdown phase of a PWR large break loss of coolant accident (LBLOCA).

Description of Experiment

An isometric view of the Semiscale MOD1 test facility used for the cold leg break tests is shown in Figure 12.1. It is a small scale model of a typical four-loop recirculating steam generator PWR. It consists of the following major PWR components: a pressure vessel with the core simulator, lower and upper plenums, and downcomer; an intact loop with a steam generator, a pump and a pressurizer; a broken loop with a simulated steam generator and a simulated pump; emergency coolant systems (ECC) in both loops that include an accumulator, and high and low pressure injection pumps; and a pressure suppression system with a suppression tank. The configuration of the electrically-heated 40-rod bundle, shown in Figure 12.2, is typical of a 15 by 15 fuel assembly (0.422 inch rod outside diameter and 0.563 inch pitch) except that the heated length of the test rods is 5.5 feet compared with 12 feet for commercial rods. The bundle has an inlet peaked axial power profile (peak at 26 inches from the bottom of the heated section). Three of the four center rods have a peak power density of 12 kw/ft and the fourth rod is unpowered. Of the remaining 36 rods, 33 rods have a peak power density of 11.46 kw/ft and three rods are unpowered.

The transient was initiated after the system reached steady-state by breaking two rupture assemblies that allowed the flow of the primary fluid into the suppression tank through two blowdown nozzles, each having a break area of 0.00262 ft^2. The suppression system was maintained at a constant pressure of 34.8 psia. At blowdown initiation, the power to the primary coolant pump was reduced and the pump was allowed to coast down to a speed of 1500 rpm, which was then maintained for the duration of the test. During the transient, the power to the core was automatically controlled to simulate the thermal response of nuclear rods. The measurements made during the transient included pressure, flow, density, and fluid temperatures at different locations in the primary and secondary systems, and surface temperatures at different elevations of the selected heated rods. The sequence of events relative to the transient initiation is given in Table 12.1.

RELAP5 Input Model

The nodalization of the RELAP5 input model for the Semiscale MOD1 test facility is shown in Figure 12.3. The nodalization of the primary system is very similar to the RELAP4 model given in Reference 12.3. The geometry and other needed input information for the primary system was obtained from this RELAP4 model.[12.3] The geometry and other input information for the secondary side of the steam generator were obtained from the RELAP5/MOD0 input model given in Reference 12.4. The input information obtained from the RELAP4 and the RELAP5/MOD0 input models were verified using the geometry values given in Reference 12.2.

The RELAP5 base input model consisted of 89 volumes, 98 junctions, and 50 heat structures. Some of the important features of the model are given below.

1. The core was modeled with two channels to account for the radially peaked power profile. The fluid volumes associated with the three high powered rods were modeled as a hot channel. The remaining core fluid volumes were modeled as an average channel. Each channel was axially divided into six volumes in order to make the model consistent with the EM plant model.

The axial division coincided with selected axial steps in the power shape curve. Crossflow junctions were used to connect the hot and average channel volumes.

2. The active heater rods in each channel were modeled using ten heat slabs, that is, one heat slab per power step.

3. The pressurizer was modeled using an eight-equal-volume pipe component.

4. The accumulator was modeled using the accumulator component.

5. The high and low pressure pumps were simulated using time- dependent volumes and junctions.

6. The suppression system was modeled as a time-dependent volume.

7. Break nozzles were modeled as trip valves.

8. The homologous curves for the intact loop pump were obtained from the RELAP4 input model.[12.3] The measured pump speed versus time data were input to simulate the pump coastdown during the transient.

9. The measured power versus time data were input to simulate the electrical power supplied to the heater rods during the transient.

10. The moisture separator on the secondary side of the steam generator was simulated using the separator component.

11. Nonequilibrium and nonhomogeneous options were selected for each volume and junction.

12. The break junctions and the pressurizer surge line junction were treated as choked flow junctions using a discharge coefficient of one.

EM Input Options

The following modifications to the base model were made to select the EM options. These options are the same as those used in the EM plant model reported in BAW-10168 Volume I.

1. The equilibrium option was selected for the core inlet, outlet, and core volumes.

2. The homogeneous option was selected for the core inlet, outlet, and the normal (vertical) core junctions.

3. The EM heat transfer option with the B&W high pressure CHF correlation with mixing vanes (BWCMV) was selected for all the core heat slabs. The post-CHF lock-in option, that would force temporary film boiling if CHF is exceeded and conditions would permit a return to nucleate boiling, was used.

4. The 90/10 weighting factor was used in the underrelaxation of the interphase heat transfer.

5. Break junctions used the EM choked flow correlations, Extended Henry-Fauske in the subcooled regime, Moody for the saturated fluid, and Murdock-Bauman for superheated steam, with static properties. A discharge coefficient of one was used for subcooled flow and 0.6

for saturated and superheated flow conditions. These coefficients were chosen to reasonably approximate the leak flow boundary conditions from the test.

6. The break junctions in the base model were selected as EM choked flow junctions. An additional junction and a time- dependent volume were added at each break plane. These junctions were used to switch the flow from choked flow to a flow calculated by the RELAP5 momentum equations when the system pressure was close to the suppression tank pressure and choked flow was no longer appropriate. The non-choking option was selected for these junctions. When the velocity calculated using the orifice equation is less than the choked junction velocity, the choked junction is closed and the second junction is opened, and will remain open during the remainder of the transient.

7. EM ECC bypass flow modeling was used.

8. The EM heat transfer package, including the Condie-Bengston IV film boiling correlation, was used.

Transient Simulation

The base case and the EM case were run with constant boundary conditions to obtain steady-state test conditions. The steam generator secondary side pressure was adjusted to obtain the desired primary system conditions. The measured and the predicted steady-state conditions are given in Table 12.2. Trips were used to initiate the sequence of events, given in Table 12.1, during the transient.

Results and Discussion

The measured and predicted pressure variations near the vessel side break are shown in Figure 12.4. Both Cycle 36.04 and the EM predicted lower pressures than the data during the entire transient. The EM calculated a relatively faster depressurization rate than Cycle 36.04 after about 10 seconds from the transient initiation. As a result, the pressure near the break location reached the suppression tank pressure at about 21.1 seconds in the EM case, and at 25.7 seconds in the base case as compared to 37 seconds in the test.

The pressure response near the pump side break is shown in Figure 12.5. The predicted pressure response near this break location, using the EM option, was similar to the prediction near the vessel side break. Between 1.0 and 8.0 seconds, the base case predicted a higher pressure than the data. The difference between the measured and the input values of the HPI flow rates near this break location is the cause of this difference. The break plane pressure reached the suppression tank pressure at 19.3 seconds in the EM test case, and 25.6 seconds in the base case as compared to 27.0 seconds in the test.

The pressure responses at other locations in the primary system are shown in Figures 12.6 through 12.10. From these figures it can be concluded that the pressure response in the primary system is similar to the pressure response near the vessel side break shown in Figure 12.4. The Cycle 36.04 pressure response near the broken loop simulated pump suction side, as shown in Figure 12.7, supports the conclusion made from Figure 12.5 that the HPI flow rate difference is the cause for the prediction of higher pressure than the data in the 1.0 to 8.0 second time period.

The pressure responses in the intact and the broken loop accumulators, shown in Figures 12.11 and 12.12 respectively, are consistent with the primary system pressure response. The sudden drop in measured pressure in the broken loop accumulator at about 2.5 seconds was caused by the opening of a valve in the surge line before the onset of injection.[12.3] In the present model, the initial pressure in this accumulator was set to 520 psia as was done in the RELAP4 model given in Reference 12.3.

The differential pressure across the pressurizer, which reflects the pressurizer liquid level, is shown in Figure 12.13. Both the EM and Cycle 36.04 predicted a faster decrease in liquid level than the data. Again this is consistent with the system pressure response.

The mass flow rates at different locations in the primary system are shown in Figures 12.14 through 12.20. In the test, the mass flow rate was estimated from the measured density and the volume flow rate. The mass flow rates given in the data report[12.1] were digitized to generate the comparison plots. During the digitalization the oscillations in the original data plots were smoothed out. The vessel side break flow rate for the EM option, shown in Figure 12.14, includes the break junction flow rate and the ECC liquid bypassed.

Figure 12.14 shows that, near the vessel side break, both Cycle 36.04 and the EM predicted higher flow rates than the data during the early part of the transient. Cycle 36.04 correctly predicted the transition from single-phase to two-phase conditions which occurred at about 2.8 seconds, while the EM predicted an earlier transition than the data. The prediction also showed oscillatory flow behavior between two and four seconds from the initiation of the transient. These oscillations are caused by the critical flow transition switching logic from Extended Henry-Fauske to Moody and the non-equilibrium nature of the flow near the break location at this time. In the EM model, the transition from the Extended Henry-Fauske to Moody occurs when the upstream node equilibrium enthalpy is close to the saturation enthalpy. Until this condition is reached only liquid is allowed to flow through the break. Since the non-equilibrium option is selected, vapor can exist in this volume, even though the equilibrium enthalpy is lower than the saturation enthalpy. As a result, the void fraction increases until the condition to switch to Moody is reached. As the choked flow correlation is switched to Moody, the break node void fraction decreases due to the high slip between the phases as calculated by the Moody slip correlation. This reduction in void fraction causes the equilibrium enthalpy to decrease below saturation which in turn causes a switch in the critical flow correlation. The switching between the two choked flow correlations continues until the liquid reaches saturation. When the system pressure was close to the suppression tank pressure, large spikes were observed in the data as well as in the prediction. These spikes were caused by the movement of liquid slugs from the accumulator injection location to the break.

The system depressurization rate depends on the mass and energy crossing the boundaries of the system. In the EM case, the use of the Moody discharge correlation causes the system to loose more energy than mass. This is due to the high slip ratio between the phases at the break location as compared to the RELAP5 Cycle 36.04 choked flow model. Thus, a lower C_D value needs to be used with the Moody correlation to approximate the depressurization rate predicted by Cycle 36.04.

The upper plenum to hot leg flow rates were biased more towards the broken loop than the intact loop for about ten seconds as shown in Figures 12.16 and 12.17. The large flow reversal in the broken loop hot leg, observed in the test at about one second after transient initiation, was not predicted by the code. This flow bias is due to the relative differences between the depressurization rates of the two hot legs.

The data as well as the prediction show that the core inlet flow remains negative during the entire blowdown period as shown in Figure 12.20. For the first second after the initiation of the transient, both cases predicted higher values than the measured negative flow rate. From 7 to 12 seconds, the EM predicted less of a negative flow rate than the data and the Cycle 36.04 prediction.

The flow rates from the intact and the broken loop accumulators are shown in Figures 12.21 and 12.22, respectively. The starting points for the accumulator injection as well as the flow rates are consistent with the pressure response near the injection location. The spike in the broken loop accumulator flow data was caused by the opening of a valve[12.3] and therefore the actual flow did not start until about 3 seconds after transient initiation. The oscillations in the Cycle 36.04 prediction of this accumulator flow were due to the time steps taken by the code. The time steps were larger than those allowed by the Courant limit. Similar oscillations were observed in an EM case when the code used the same time step as in the Cycle 36.04 case. The EM case discussed here was run using time steps which were smaller than that allowed by the Courant limit and it calculated a smooth flow rate as shown in Figure 12.22.

The density variations near the vessel side and the pump side breaks and near the core inlet are shown in Figures 12.23, 12.24, and 12.25, respectively. The spikes in the data as well as in the predictions, during the later part of the transient, were caused by movement of liquid slugs from the ECC injection location to the break. Near the vessel side break the EM calculated density decreased rapidly at about 1.5 seconds after transient initiation. From 1.5 seconds to 5 seconds, oscillation were observed in this density calculation which coincided with the break flow oscillations shown in Figure 12.14. The early decrease in density and its oscillatory behavior are attributable to the switching in the choked flow models as described earlier. After about 5 seconds, the EM calculated density agreed reasonably well with the data until the end of blowdown. Cycle 36.04 underpredicted the density from about 3 to 11 seconds into the transient even though the code predicted the break flow reasonably well (Figure 12.14). Relatively lower slip between the phases, calculated by the Cycle 36.04 choked flow model, caused more than the required amount of liquid to be discharged from the break volume; thus, resulting in a lower volume average density prediction.

Near the pump side break, both the EM and Cycle 36.04 overpredicted the density from 1.5 to 6.0 seconds and underpredicted it during the remainder of the transient which is consistent with the pressure prediction shown in Figure 12.5. Both Cycle 36.04 and the EM overpredicted the density near the core inlet as shown in Figure 12.25. A lower core heat transfer prediction, which is discussed later in this Section, is the major cause of the high density fluid near the core inlet.

Fluid temperature variations at different locations in the primary system are shown in Figures 12.26 through 12.31. The calculated liquid and vapor temperatures are shown in these figures. The figures show that, once the system fluid condition has switched from a subcooled liquid to a two-phase mixture, the liquid and vapor temperatures generally remain near saturation during the major portion of the blowdown period. During the accumulator injection period, the data as well as the prediction show subcooled liquid and saturated steam at the injection location (Figure 12.29). As the liquid slugs move toward the break, the fluid conditions along the path change from a saturation condition to saturated steam and subcooled liquid (Figures 12.27 and 12.28). The effect of lower core heat transfer during the later part of the transient can be observed in the fluid conditions near the core inlet (Figure 12.30) and exit (Figure 12.31).

The cladding temperature variations at the peak power location in the average and the high powered rods are shown in Figures 12.32 and 12.33, respectively. From an examination of the data given in Reference 12.1, it was observed that the cladding temperatures of the rods near the vessel wall were much higher than those of other rods (data D8-27 in Figure 12.32). The unpowered rods in the bundle could reduce the temperatures of the nearby heated rods. However, test S-04-5, which is the counterpart of test S-04-6 (with all rods powered) showed a similar trend in its results. For most of the inner rods, both tests gave about the same temperatures at the peak power locations. Therefore, only the cladding temperatures for the inner rods should be used for comparing the data with predictions.

The predicted cladding surface temperatures are shown in Figures 12.32 and 12.33. In the test, the thermocouples were located in the creases of the inner sheath. In the model, the cladding was modeled using two radial nodes. Therefore, the inner node temperature would and should be closer to the data. However, in RELAP5 only surface temperatures are stored in the plot file. At steady-state, the calculated temperature of the inner node, in both cases, was found to be close to the data. During the transient, the difference between the surface temperature and the inner node temperature was about 10 F. Hence, the surface temperature is sufficient for comparison purposes.

The EM CHF correlations were found to be conservative in predicting DNB. Cycle 36.04 predicted DNB early by about 1 second for the average powered rods and correctly predicted DNB for the high powered rods. The EM predicted DNB within 0.5 seconds for the average powered rods and within 0.1 seconds for the high powered rods after the initiation of the transient. The DNB in the test occurred at about 3 seconds after the initiation of the transient.

Cycle 36.04 and the EM both predicted higher cladding temperatures than the data during the entire transient period with the EM being even higher than Cycle 36.04. The EM calculated cooling of the high and average powered rods, after reaching the peak cladding temperatures, agreed well with the cooling rate for rod D8-27. Both the test and the EM prediction show a slow cooling of the core after 10 seconds from the initiation of the transient while Cycle 36.04 shows a slow heatup during the same period. From Figure 12.20, it can be concluded that the magnitude of the core flow during this period is slightly higher in the test than it is in either predictions. In the test, this higher core flow promotes added core cooling. In the EM calculation, even though the core flow is lower, the very high cladding temperatures before 10 seconds causes a slow cooling of the core during the later part of the transient. In the Cycle 30.04 calculation, the lower core flow calculation in the later part of the blowdown and the approximately correct cladding temperature prediction at 10 seconds cause the cladding temperature to increase slowly during the later part of the transient.

Summary and Conclusion

Semiscale MOD1 large break LOCA test S-04-6 was simulated using RELAP5/MOD2-B&W with one case using the Cycle 36.04 options and the other using the B&W EM options. The EM options selected in this study are the same as those selected for actual plant modeling (BAW-10168). As expected, both cases predicted higher break flow rates, faster system depressurization rates, and higher cladding temperatures than the data; the EM generally predicted higher values for these parameters than Cycle 36.04.

The consistency between the transient behavior predicted by the RELAP5/MOD2-B&W evaluation model version and the test data, given allowances for the effects of the EM discharge and core heat transfer models, supports application of B&W's EM version for conservative calculations of blowdown during large LOCA transients. When applied according to Appendix K requirements, using a spectrum of effective break area-discharge coefficient combinations, RELAP5/MOD2-B&W should prove effective in defining limiting end-of-blowdown conditions.

12.1 H. S. Crapo, et al, Experiment Data Report for Semiscale MOD-1 Test S-04-5 and S-04-6 (Baseline ECC Tests), TREE-NUREG-1045, January 1977.

12.2 L. J. Ball et al, Semiscale Program Description, TREE-NUREG-1210, May 1978.

12.3 M. S. Sahota, Comparisons of RELAP4/MOD2 With Semiscale Blowdown Data, CVAP-TR-78-023, July 1978.

12.4 V. H. Ransom, et al, RELAP5/MOD0 Code Description Volume 2 - RELAP5 Code Development Update and Sample Problems, CDAP-TR-057 (Volume 2), July 1978.

Table 12.1. Sequence of Events During Test S-04-6 .

Event	Time (sec)
Blowdown Initiated	0.0
ECC Accumulators Initiated	0.0
HPI Pumps Started	0.0
Steam Generator Feedwater and Discharge Valves Closed	1.0
LPI Started	30.0

Table 12.2. Conditions at Blowdown Initiation .

Parameter	Data	Cycle 36.04	EM
Core Power, kW	1.44	1.44	1.44
Cold Leg Fluid Temperature, F	543.0	543.5	543.0
Hot Leg Fluid Temperature, F	610.0	610.3	609.5
Pressurizer Pressure, psia	2252.0	2253.3	2252.6
Pump Speed, RPM	2400.0	2400.0	2400.0
ICL Flow Rate, lbm/s	15.5	15.4	15.4
Steam Generator Pressure, psia	850.0	809.5	803.5
Pressure Suppression Tank Pressure, psia	34.8	34.8	34.8

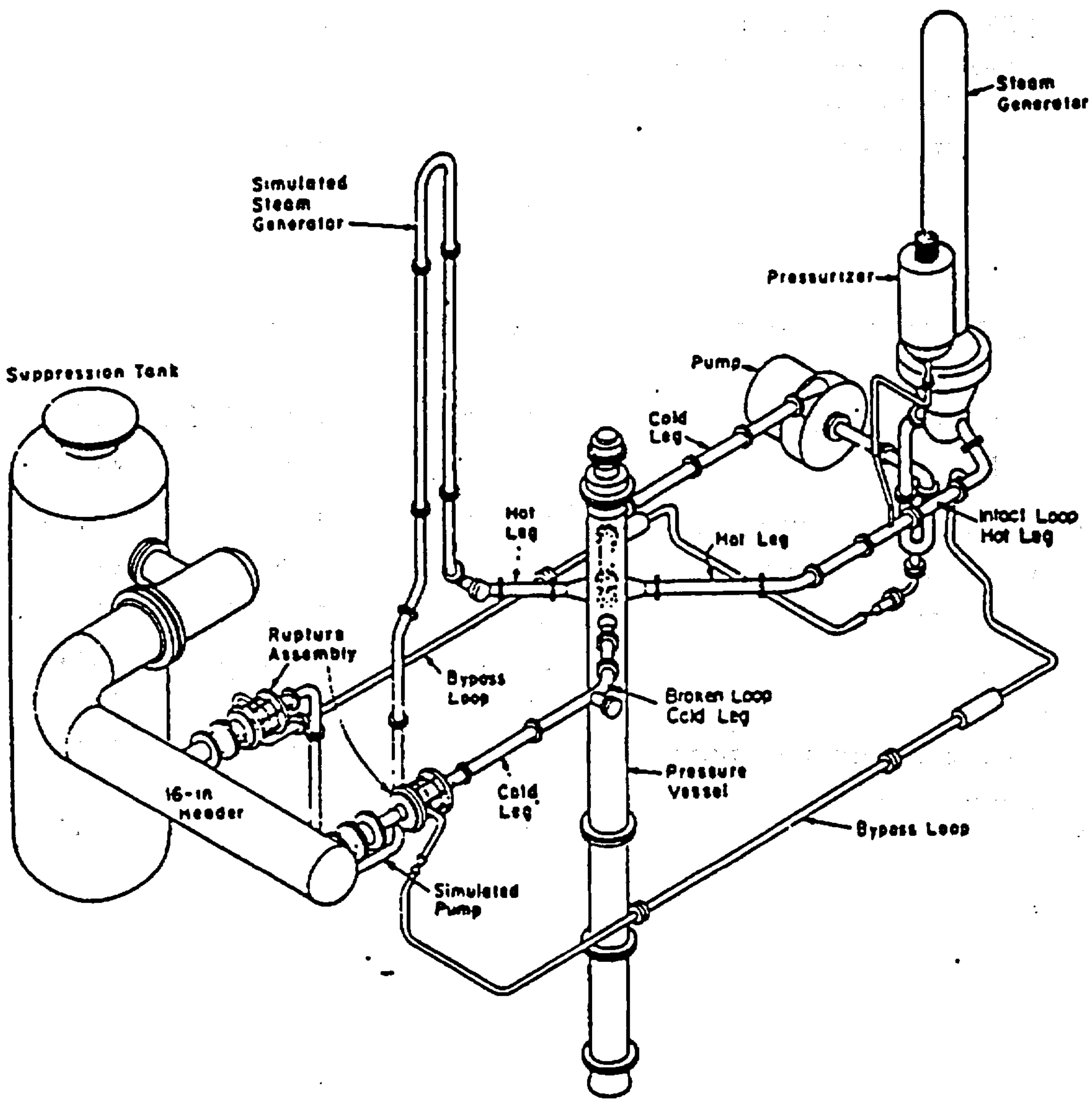

Figure 12.1. Semiscale MOD1 Test Facility - Cold Leg Break Configuration.

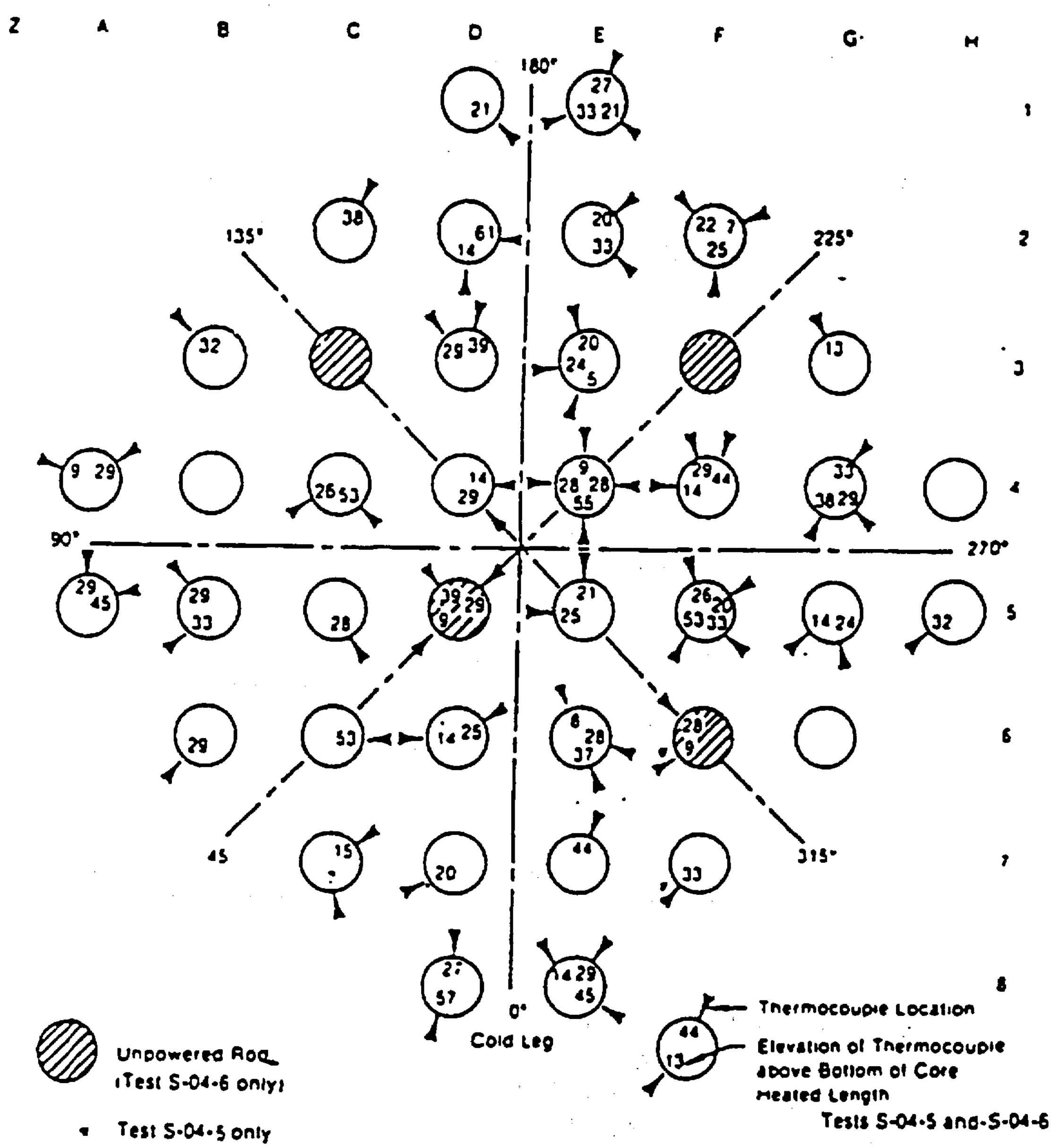

Figure 12.2. Semiscale MOD1 Rod Locations for Test S-04-6.

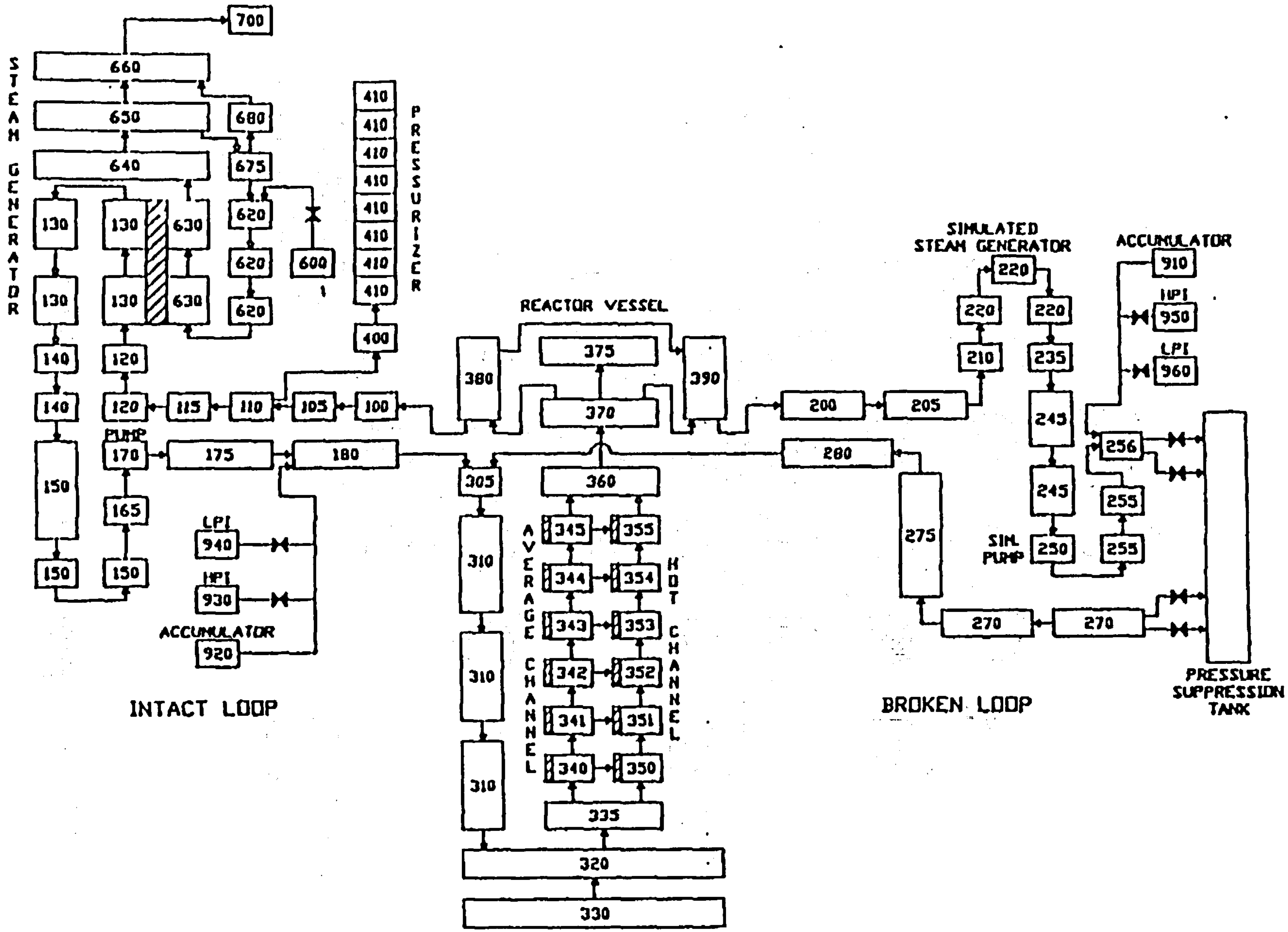

Figure 12.3. RELAP5 Node and Junction Diagram.

FIGURE 12.4. SEMISCALE MOD1 TEST S-04-6; PRESSURE NEAR THE VESSEL SIDE BREAK.

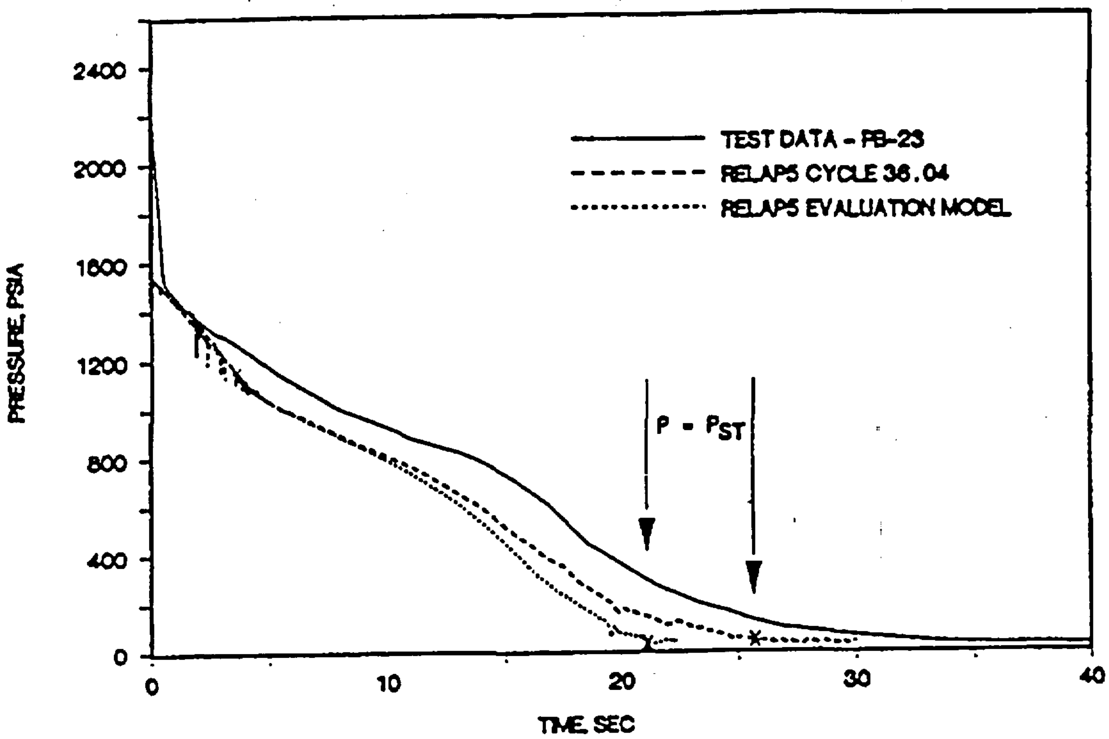

FIGURE 12.5. SEMISCALE MOD1 TEST S-04-6; PRESSURE NEAR THE PUMP SIDE BREAK.

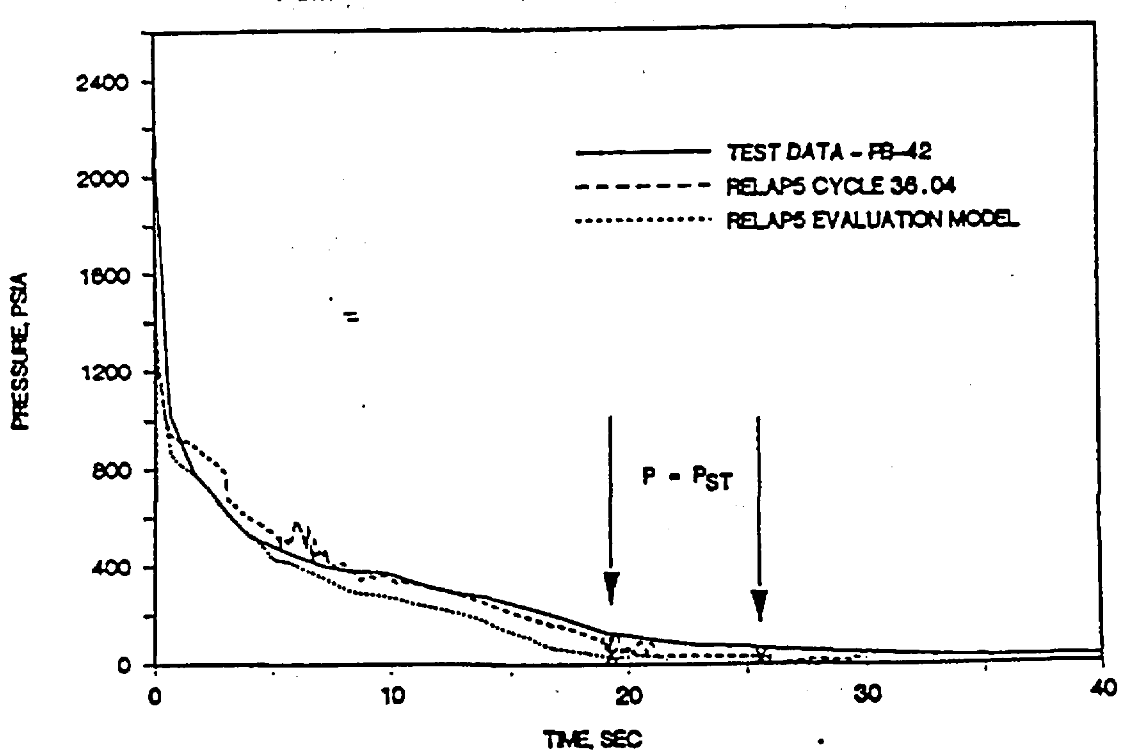

FIGURE 12.6. SEMISCALE MOD1 TEST S-04-6; PRESSURE NEAR THE INTACT LOOP PUMP EXIT.

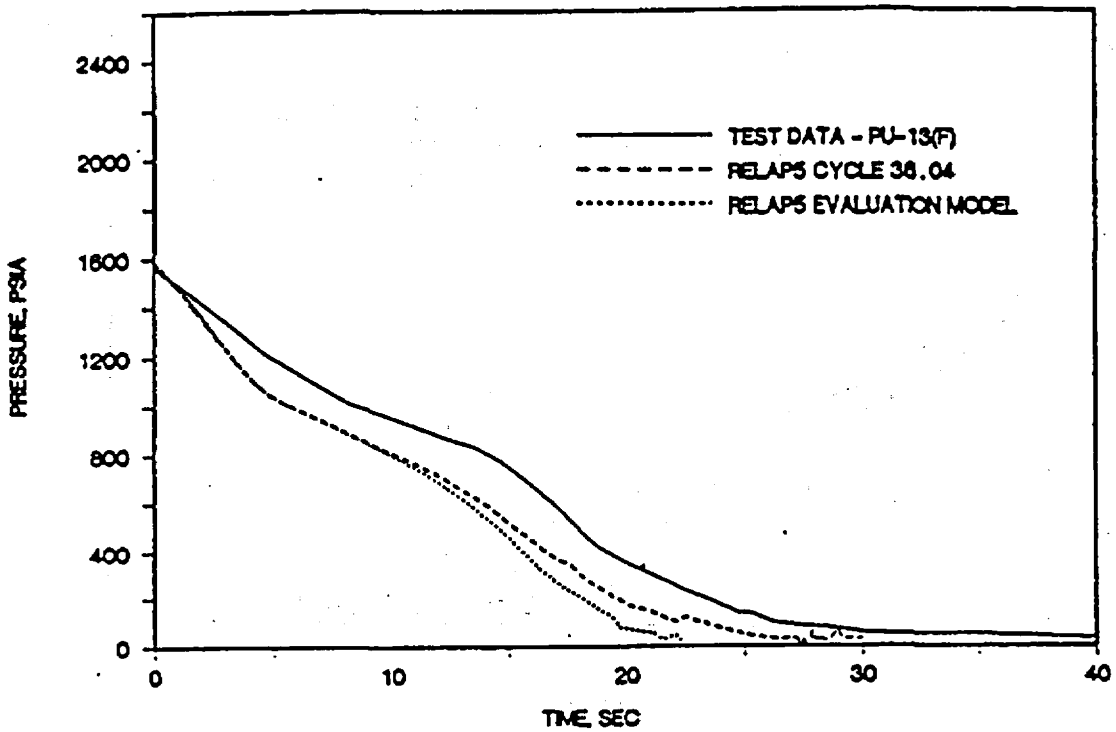

FIGURE 12.7. SEMISCALE MOD1 TEST S-04-6; PRESSURE IN THE BROKEN LOOP NEAR THE PUMP SIMULATOR INLET.

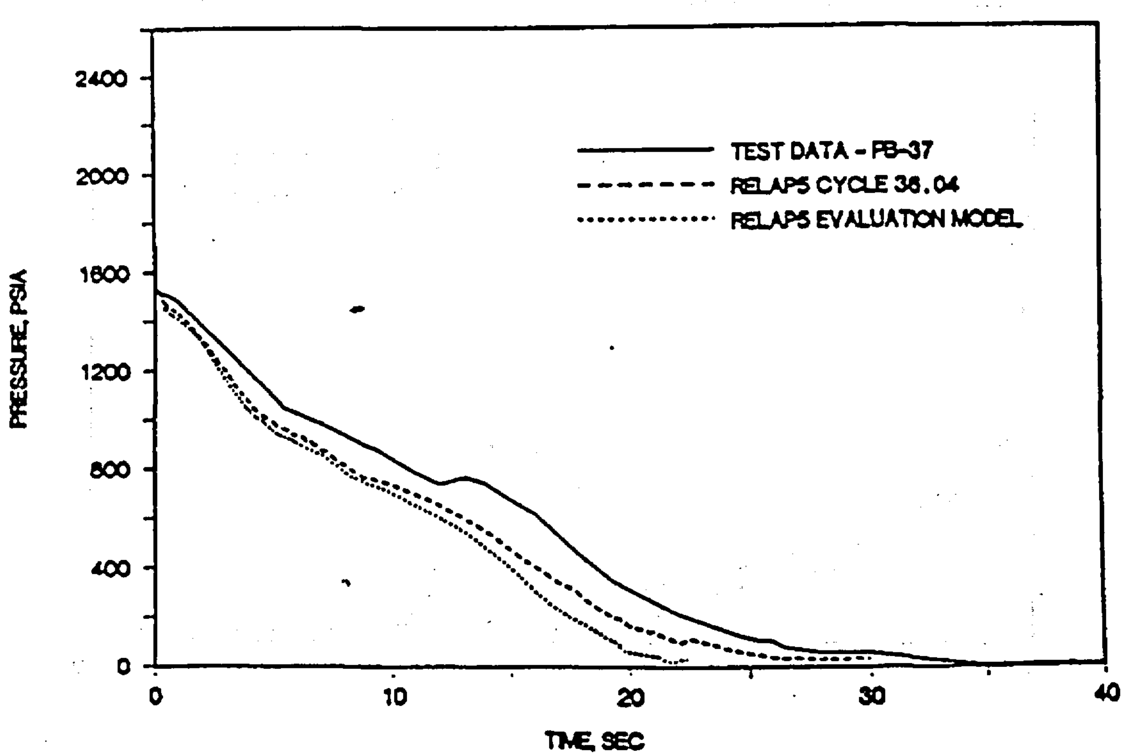

FIGURE 12.8. SEMISCALE MOD1 TEST S-04-6; PRESSURE IN THE LOWER PLENUM.

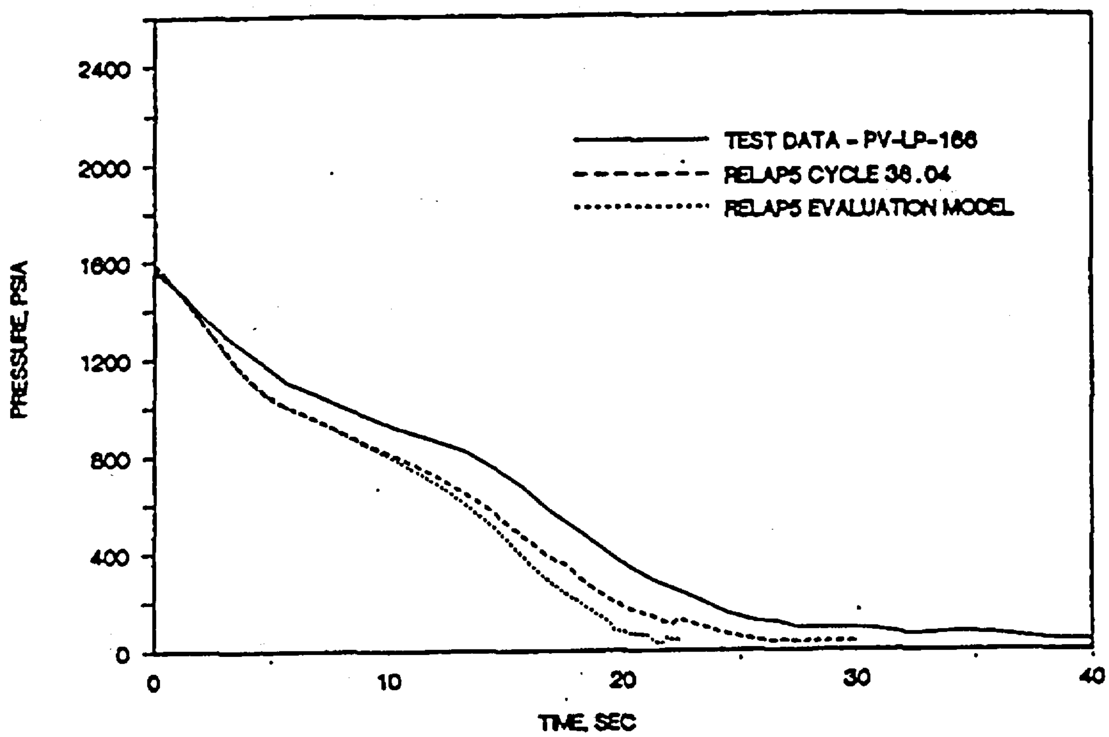

FIGURE 12.9. SEMISCALE MOD1 TEST S-04-6; PRESSURE IN THE UPPER PLENUM.

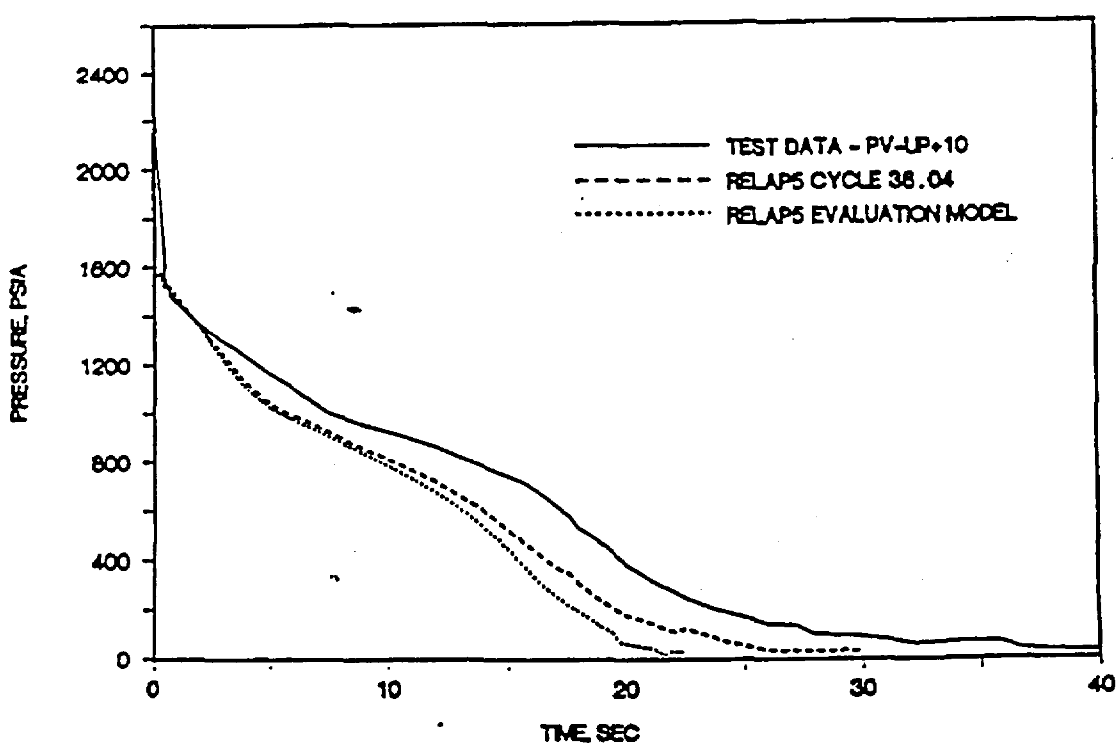

FIGURE 12.10. SEMISCALE MOD1 TEST S-04-6; PRESSURE NEAR THE TOP OF THE PRESSURIZER.

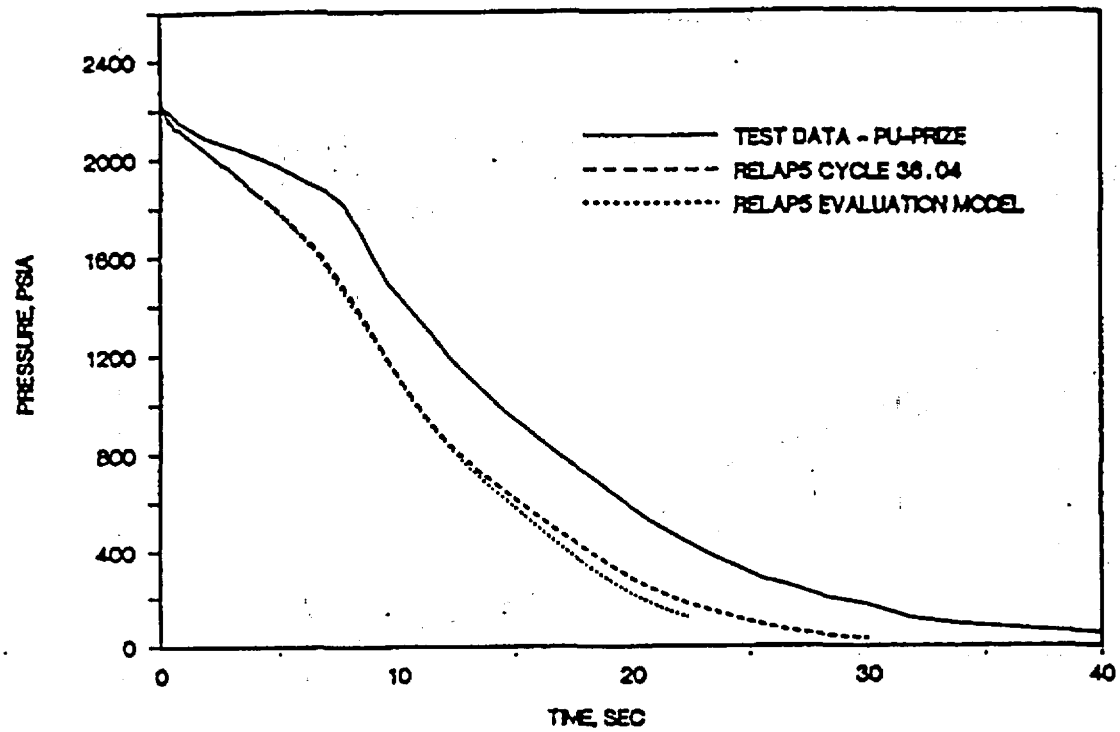

FIGURE 12.11. SEMISCALE MOD1 TEST S-04-6; PRESSURE IN THE INTACT LOOP ACCUMULATOR.

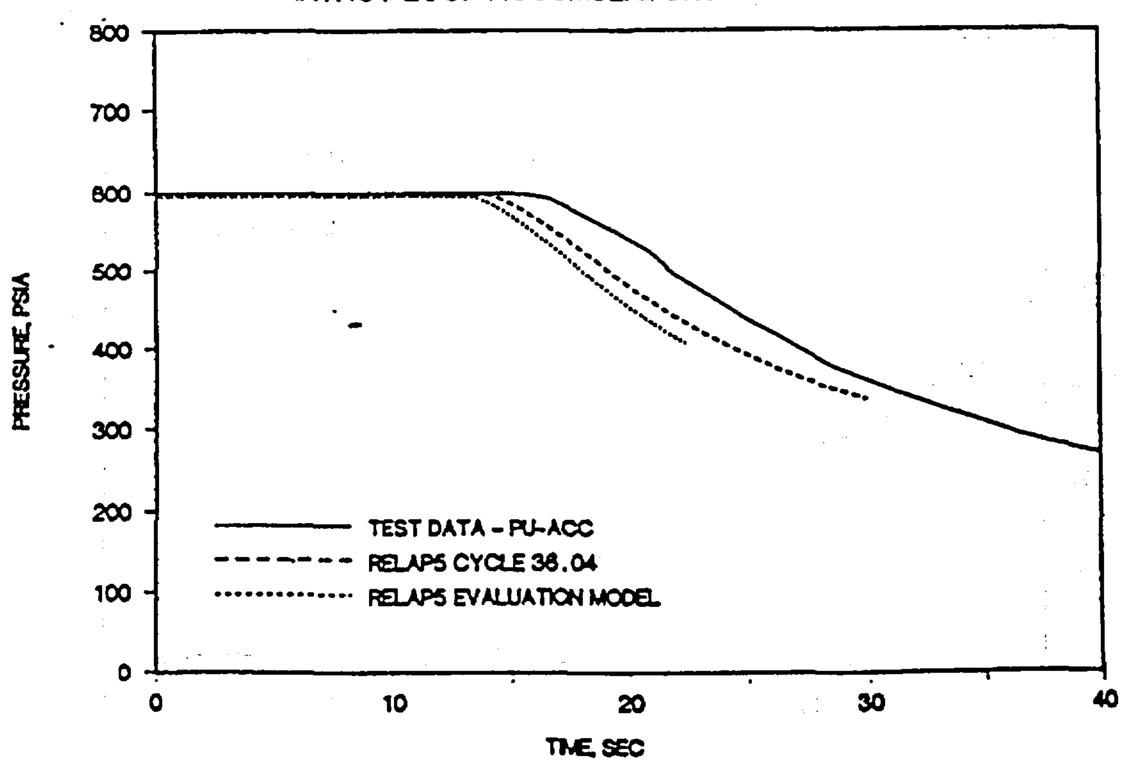

FIGURE 12.12. SEMISCALE MOD1 TEST S-04-6; PRESSURE IN THE BROKEN LOOP ACCUMULATOR.

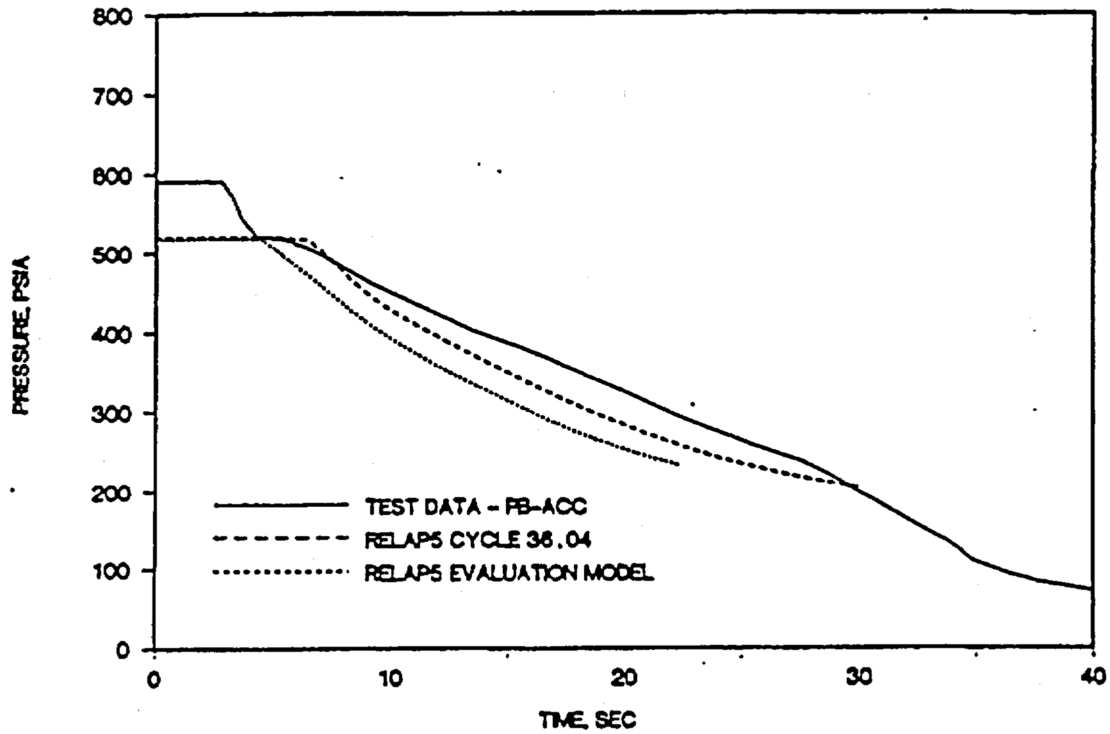

FIGURE 12.13. SEMISCALE MOD1 TEST S-04-6; DIFFERENTIAL PRESSURE IN THE PRESSURIZER.

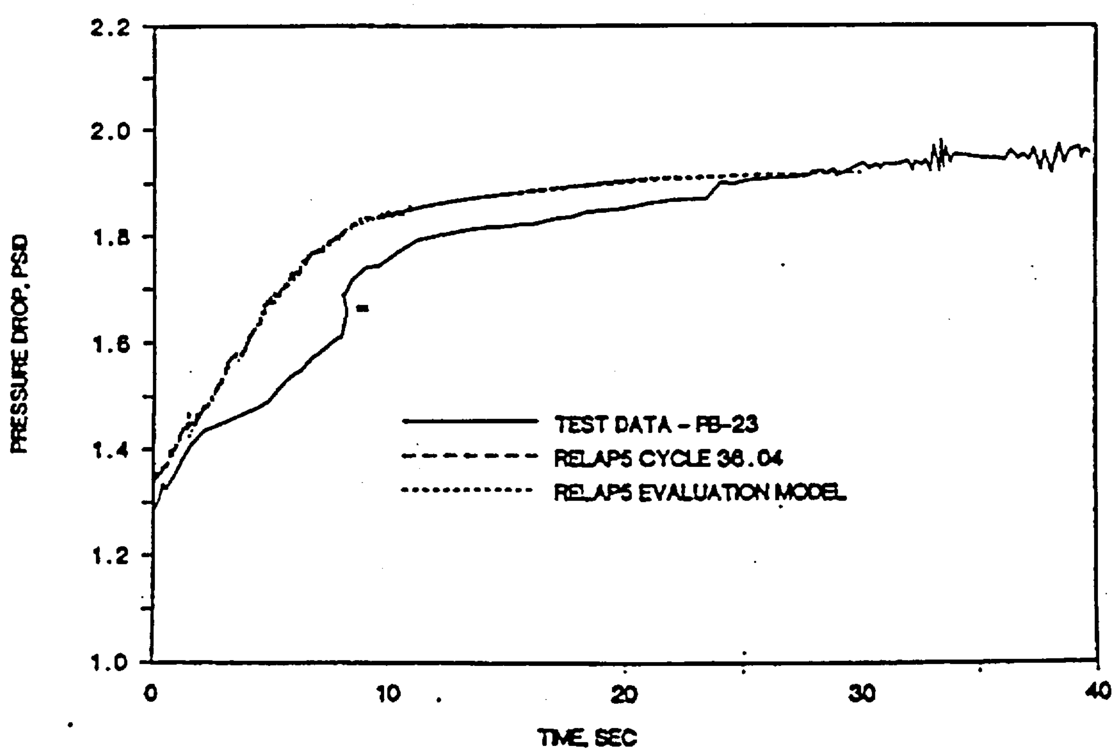

FIGURE 12.14. SEMISCALE MOD1 TEST S-04-6; MASS FLOW RATE NEAR THE VESSEL SIDE BREAK.

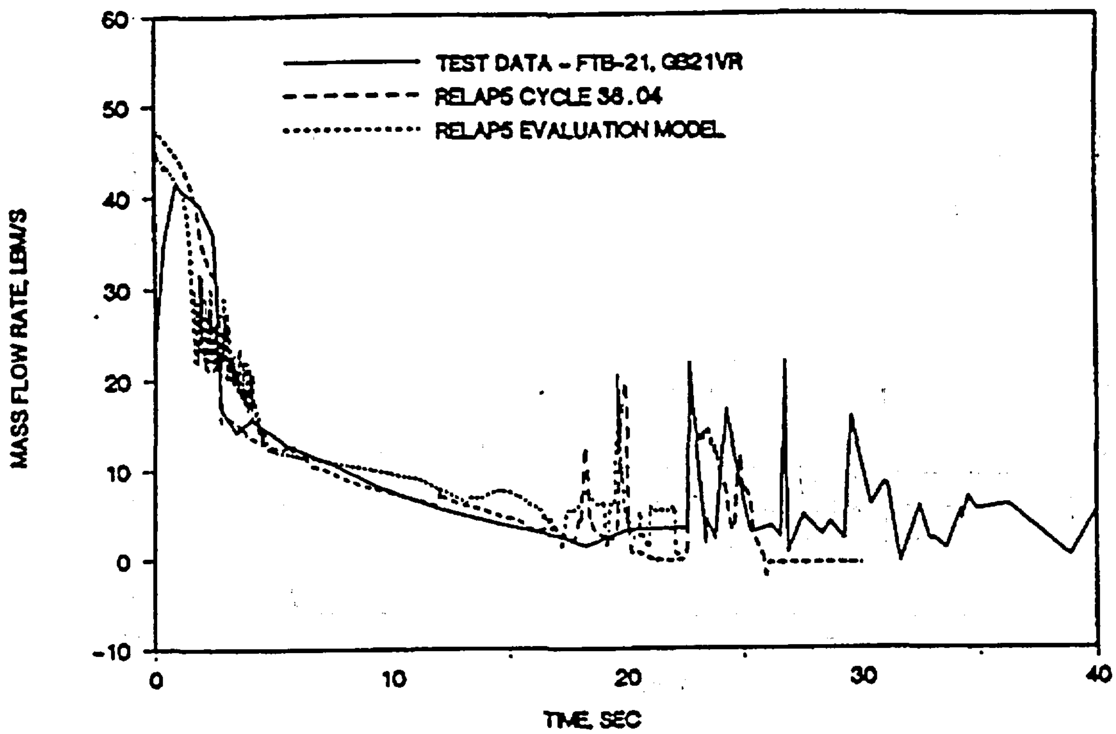

FIGURE 12.15. SEMISCALE MOD1 TEST S-04-6; MASS FLOW RATE NEAR PUMP SIDE BREAK (BEFORE ECC INJECTION POINT).

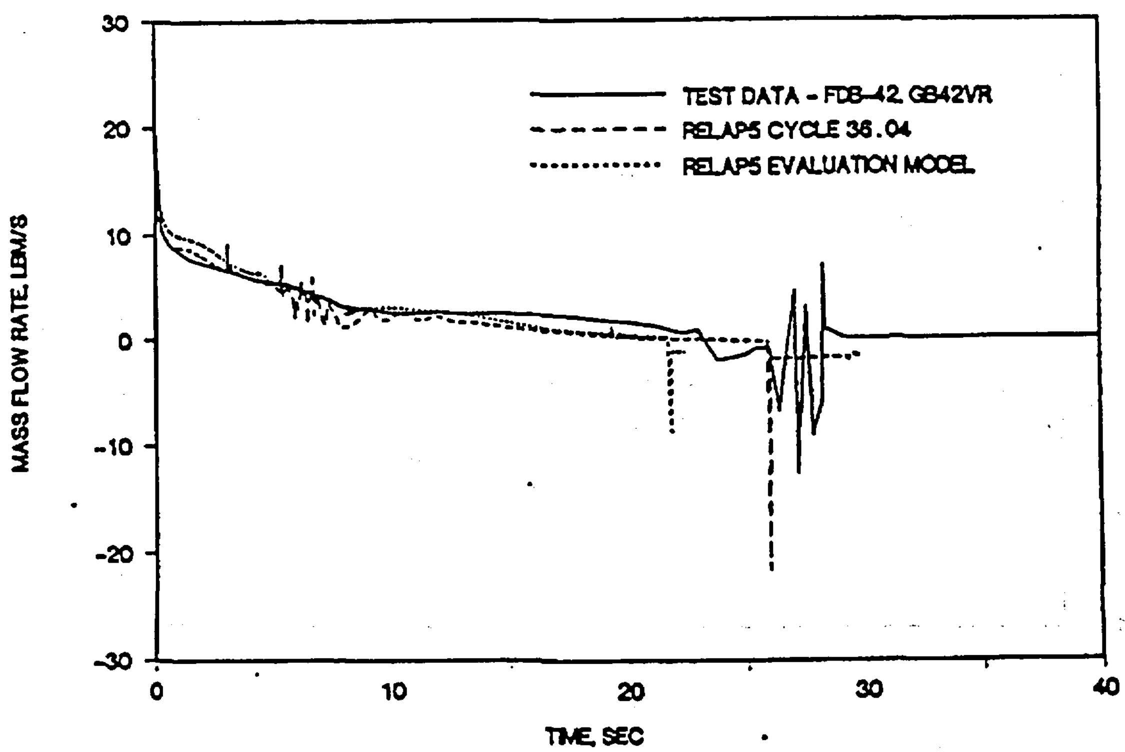

FIGURE 12.16. SEMISCALE MOD1 TEST S-04-6; MASS FLOW RATE IN THE INTACT LOOP HOT LEG.

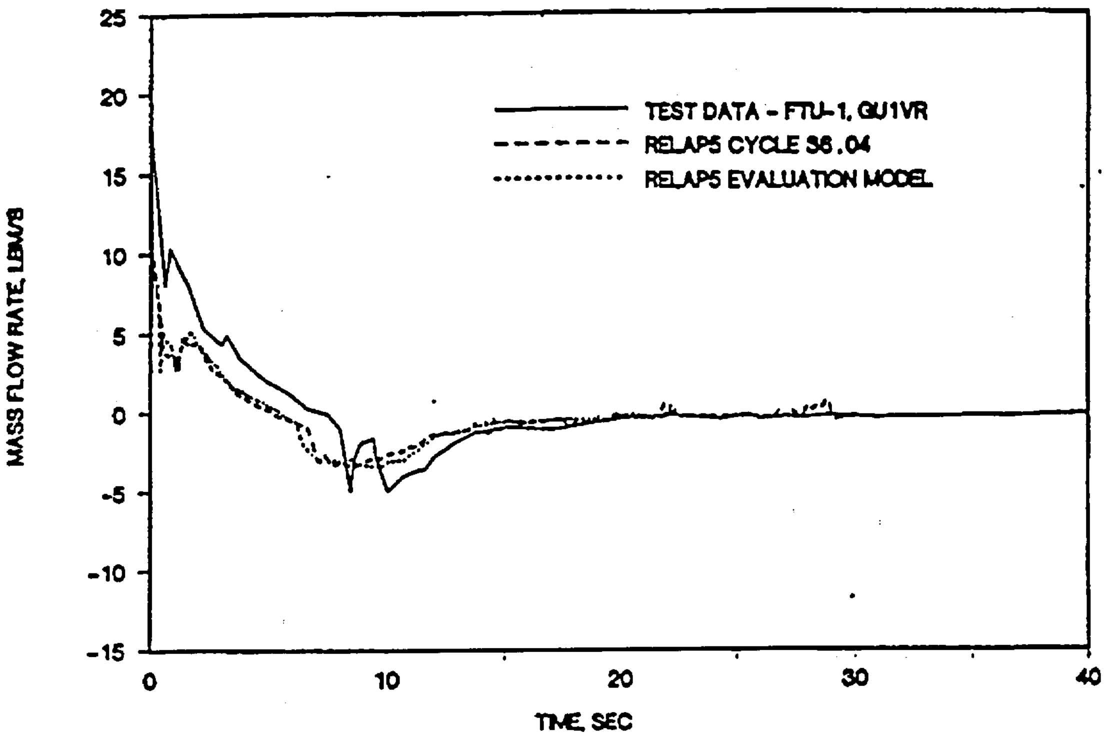

FIGURE 12.17. SEMISCALE MOD1 TEST S-04-6; MASS FLOW RATE NEAR THE PUMP SIMULATOR INLET.

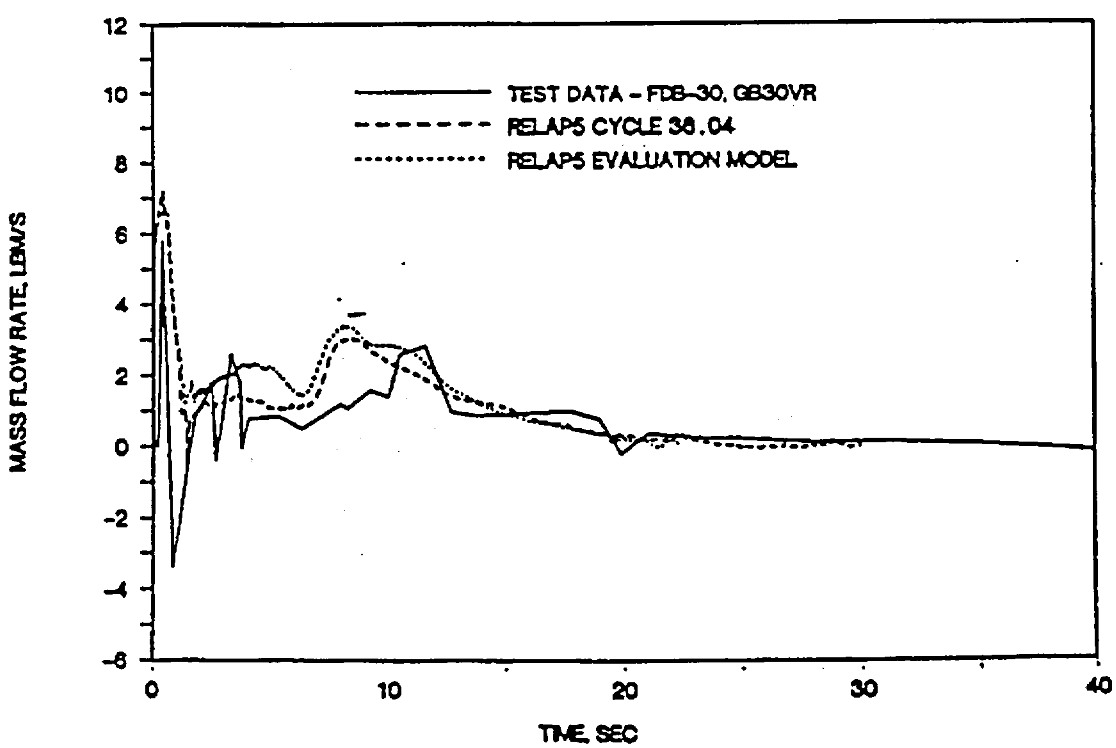

FIGURE 12.18. SEMISCALE MOD1 TEST S-04-6; MASS FLOW RATE IN INTACT LOOP COLD LEG (BEFORE ACCUMULATOR INJECTION POINT).

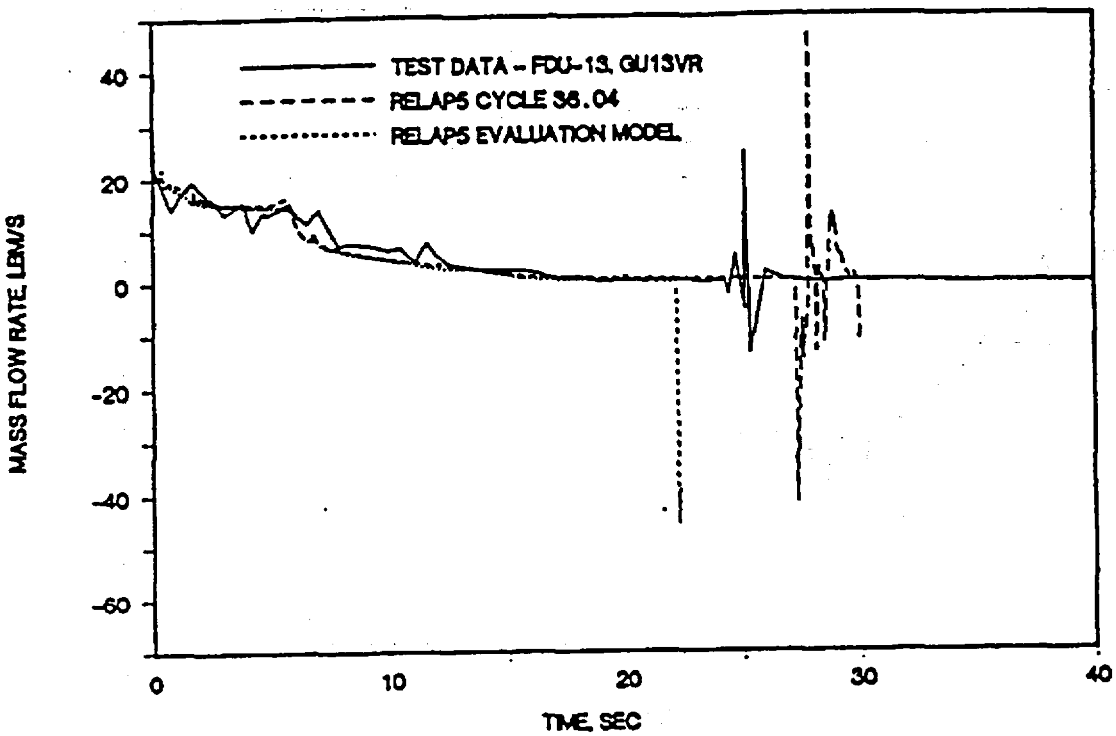

FIGURE 12.19. SEMISCALE MOD1 TEST S-04-6; DOWNCOMER INLET FLOW RATE FROM THE INTACT LOOP.

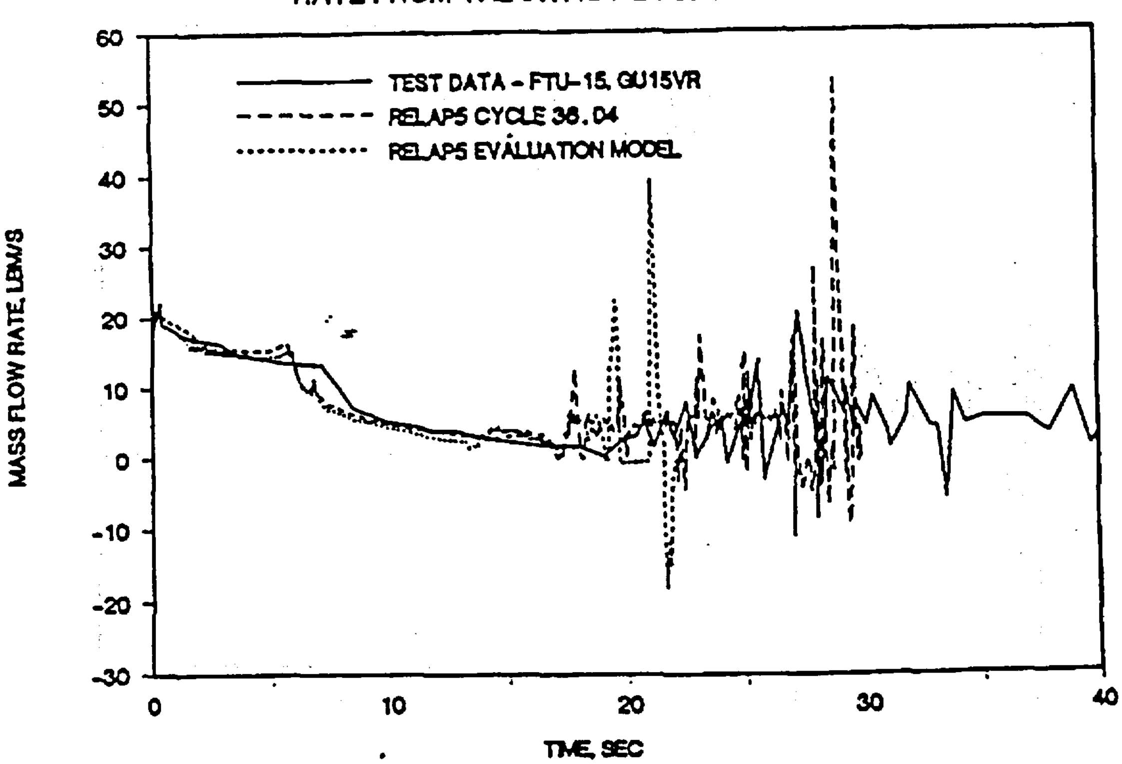

FIGURE 12.20. SEMISCALE MOD1 TEST S-04-6; MASS FLOW RATE AT THE CORE INLET.

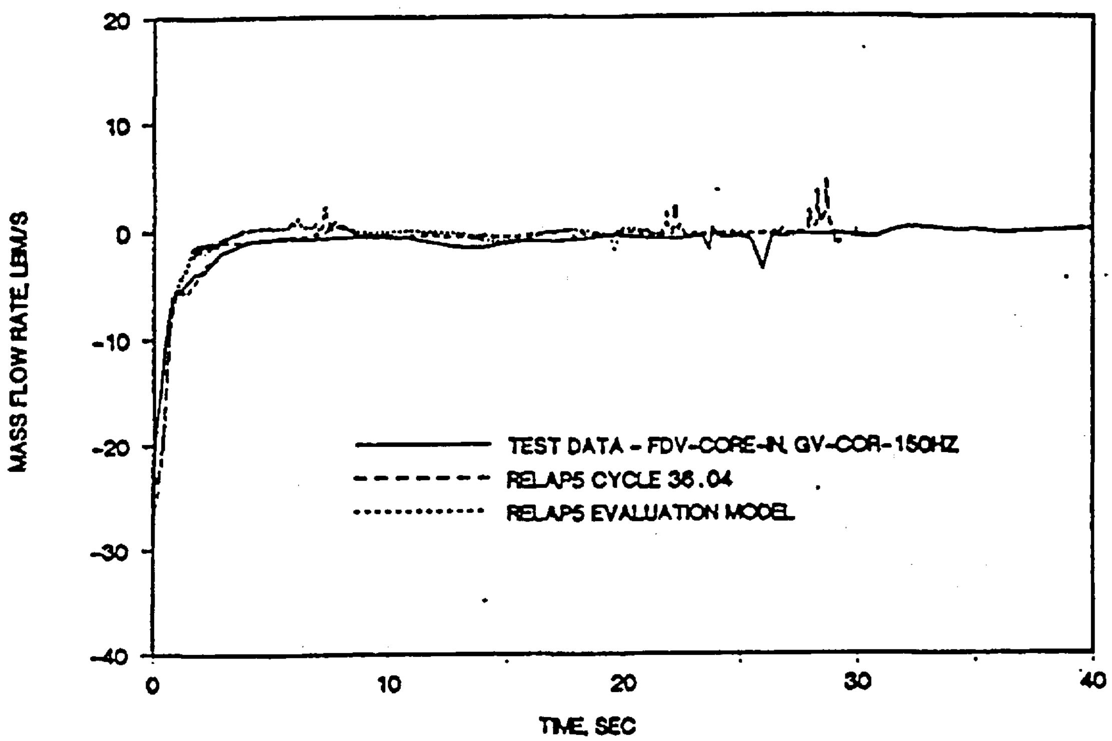

FIGURE 12.21. SEMISCALE MOD1 TEST S-04-6; MASS FLOW RATE FROM THE INTACT LOOP ACCUMULATOR.

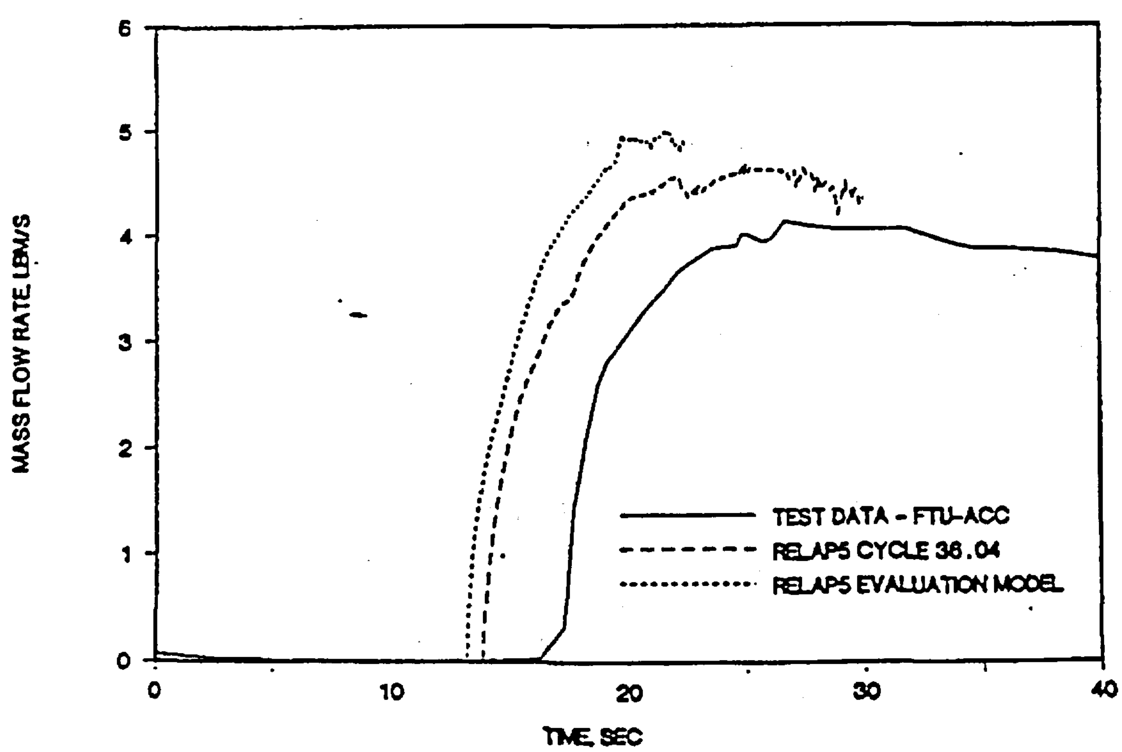

FIGURE 12.22. SEMISCALE MOD1 TEST S-04-6; MASS FLOW RATE FROM THE BROKEN LOOP ACCUMULATOR.

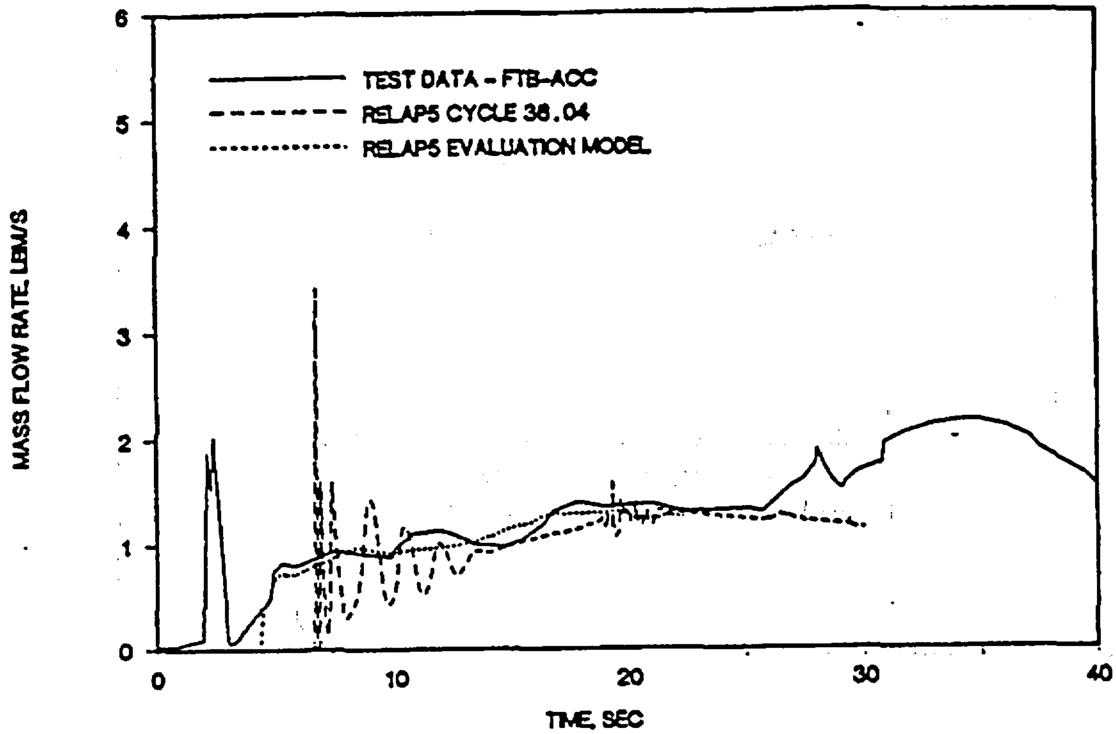

FIGURE 12.23. SEMISCALE MOD1 TEST S-04-6; DENSITY NEAR THE VESSEL SIDE BREAK.

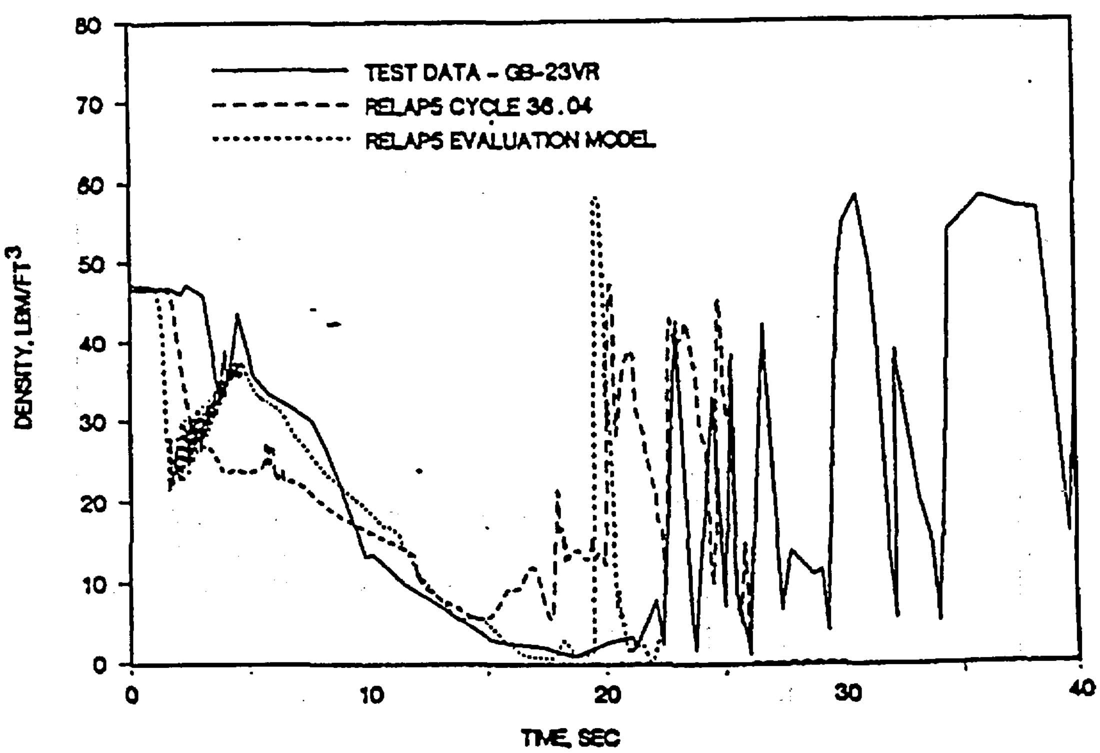

FIGURE 12.24. SEMISCALE MOD1 TEST S-04-6; DENSITY NEAR THE PUMP SIDE BREAK (BEFORE THE ECC INJECTION LOCATION).

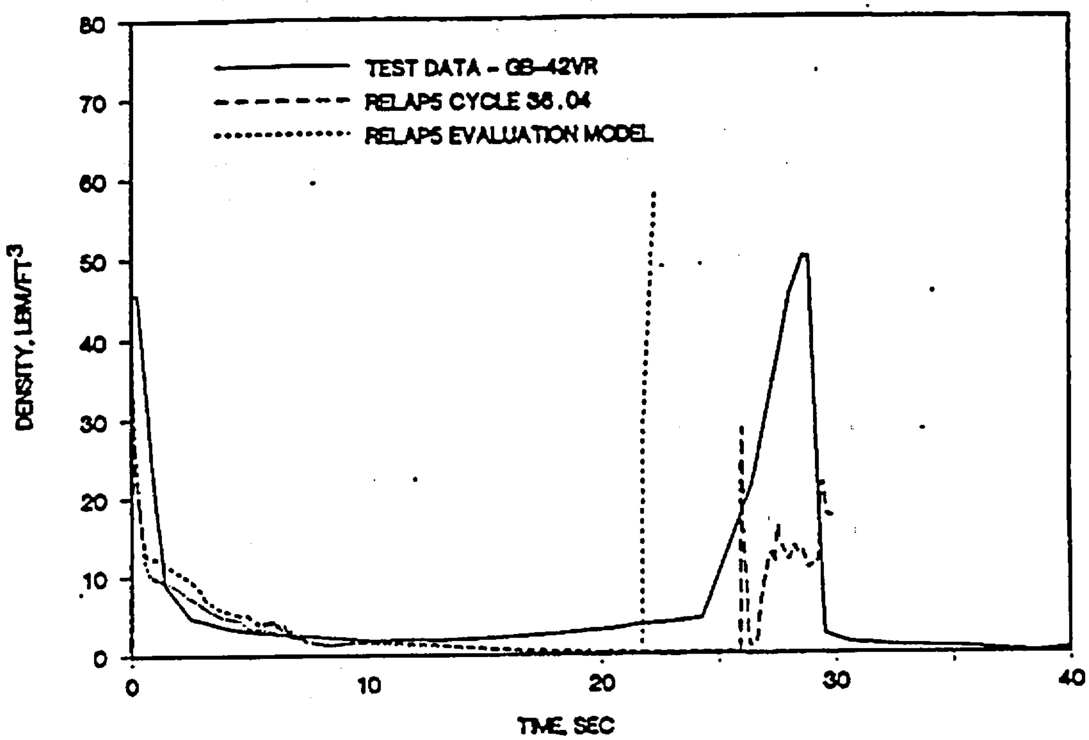

FIGURE 12.25. SEMISCALE MOD1 TEST S-04-6; DENSITY NEAR THE CORE INLET.

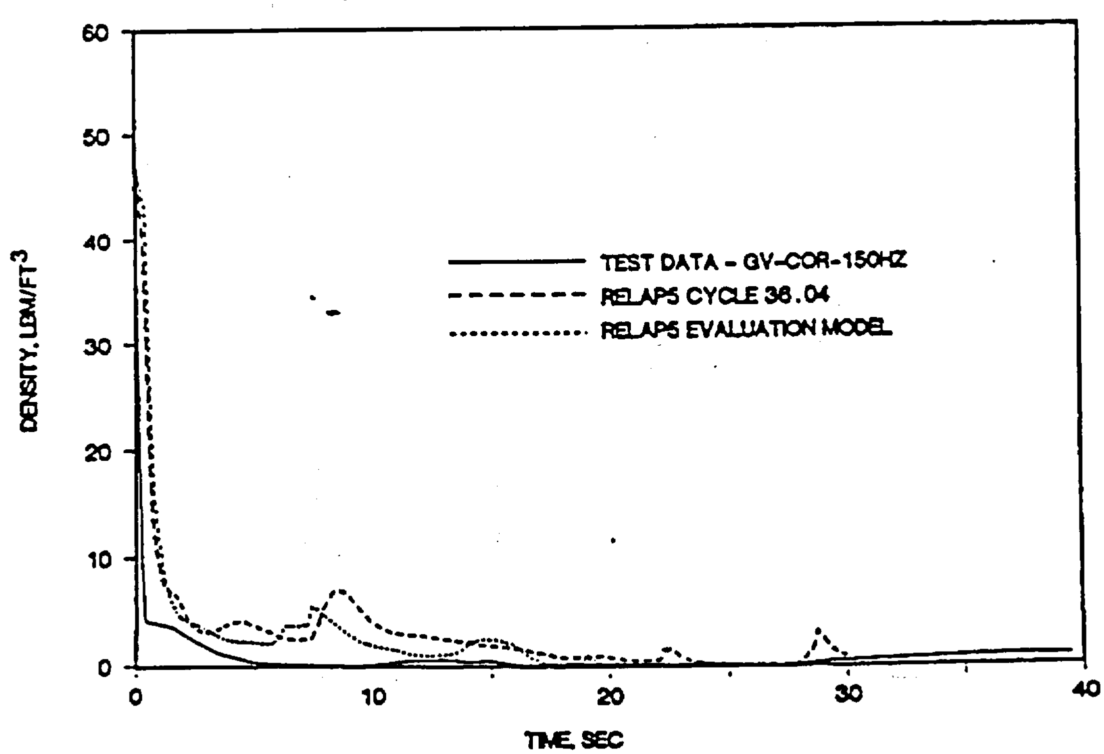

FIGURE 12.26. SEMISCALE MOD1 TEST S-04-6; FLUID TEMPERATURE NEAR THE VESSEL SIDE BREAK.

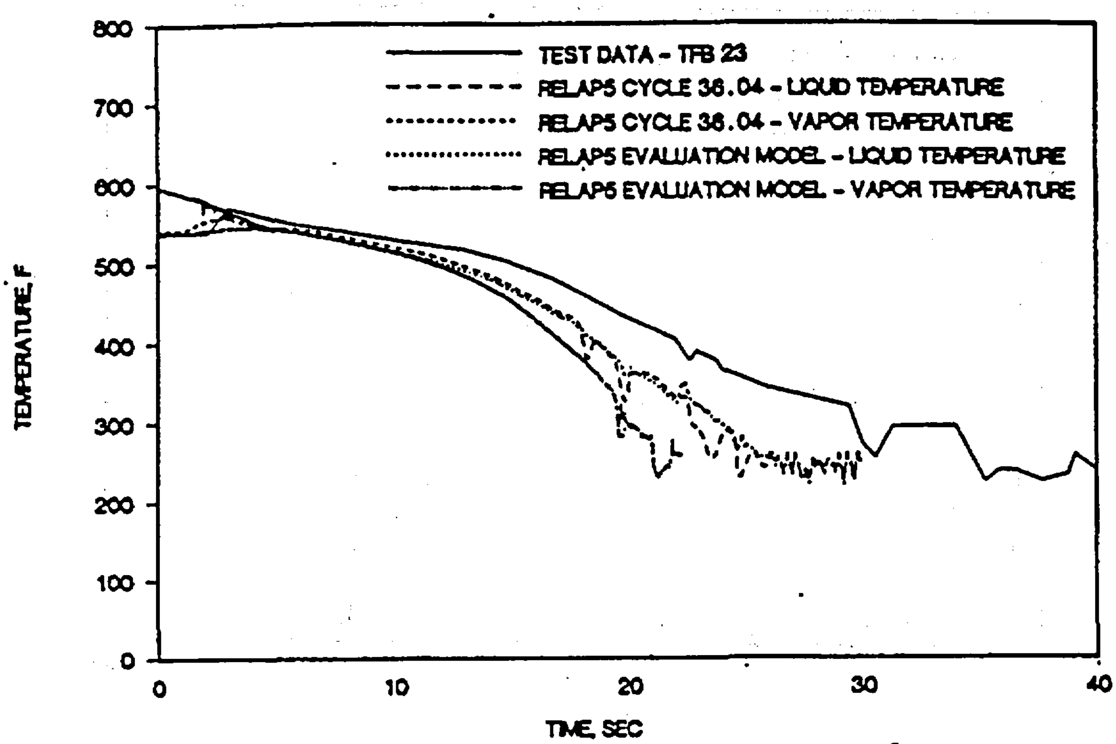

FIGURE 12.27. SEMISCALE MOD1 TEST S-04-6; FLUID TEMPERATURE NEAR PUMP SIDE BREAK (BEFORE ECC INJECTION LOCATION).

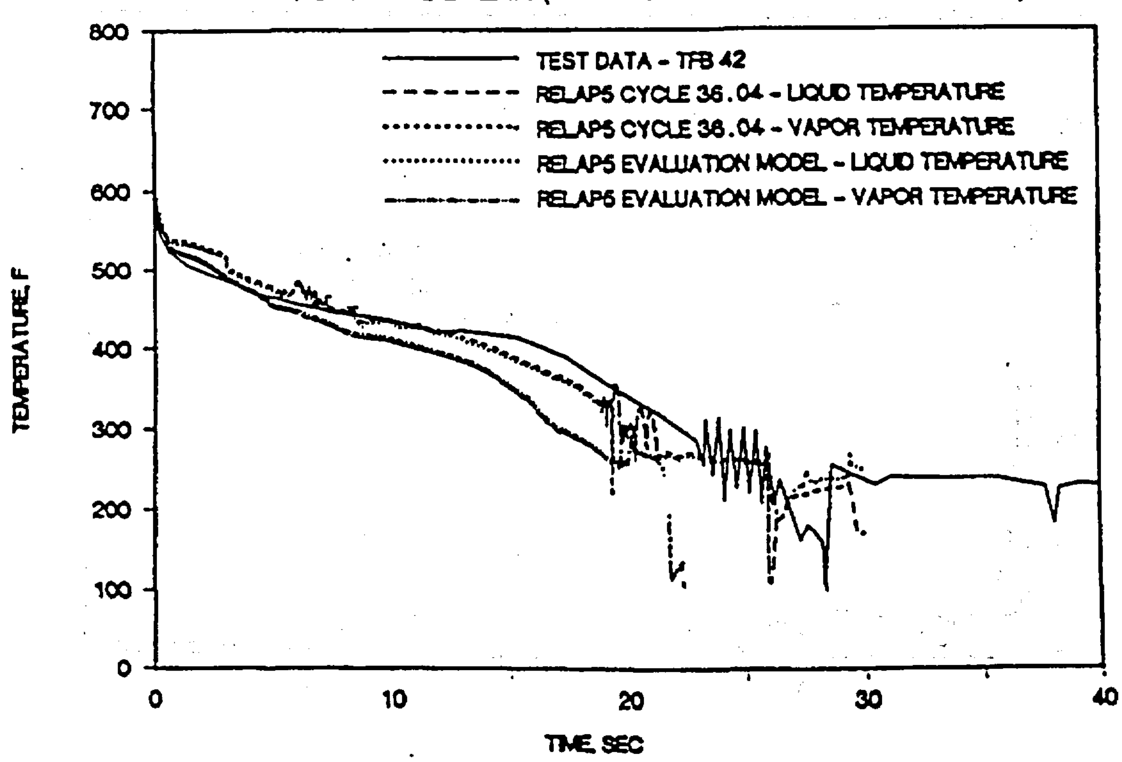

FIGURE 12.28. SEMISCALE MOD1 TEST S-04-6; FLUID TEMPERATURE IN THE INTACT LOOP HOT LEG.

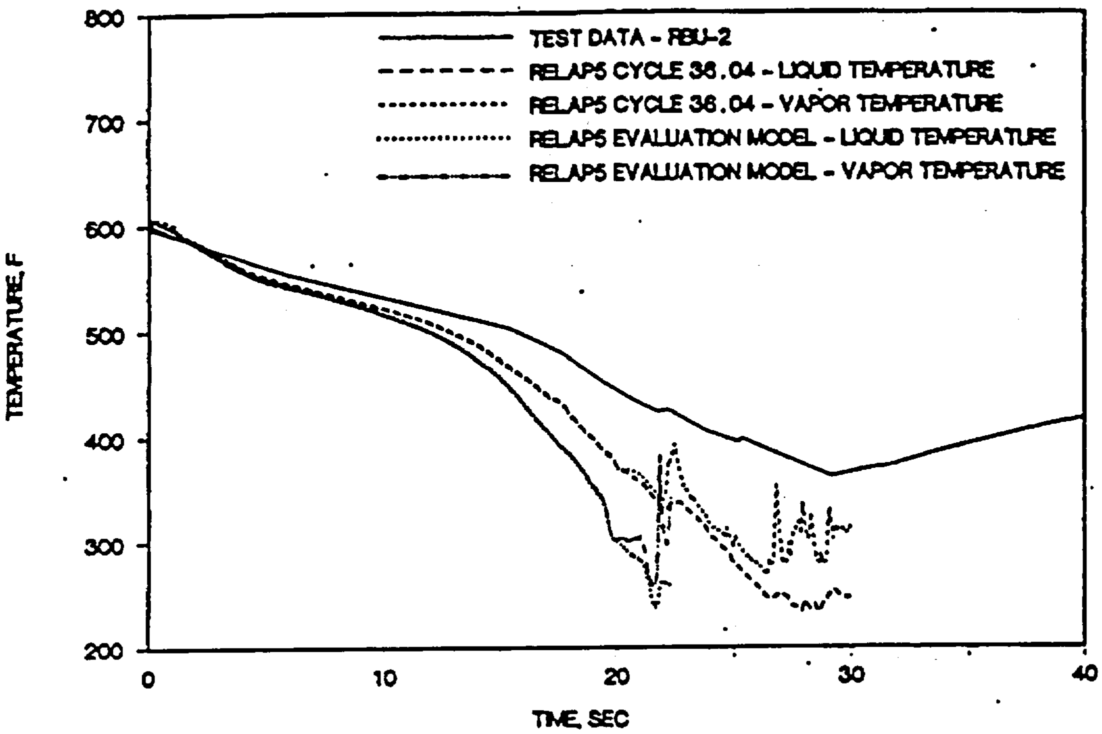

FIGURE 12.29. SEMISCALE MOD1 TEST S-04-6; FLUID TEMPERATURE IN INTACT LOOP COLD LEG (NEAR ECC INJECTION POINT).

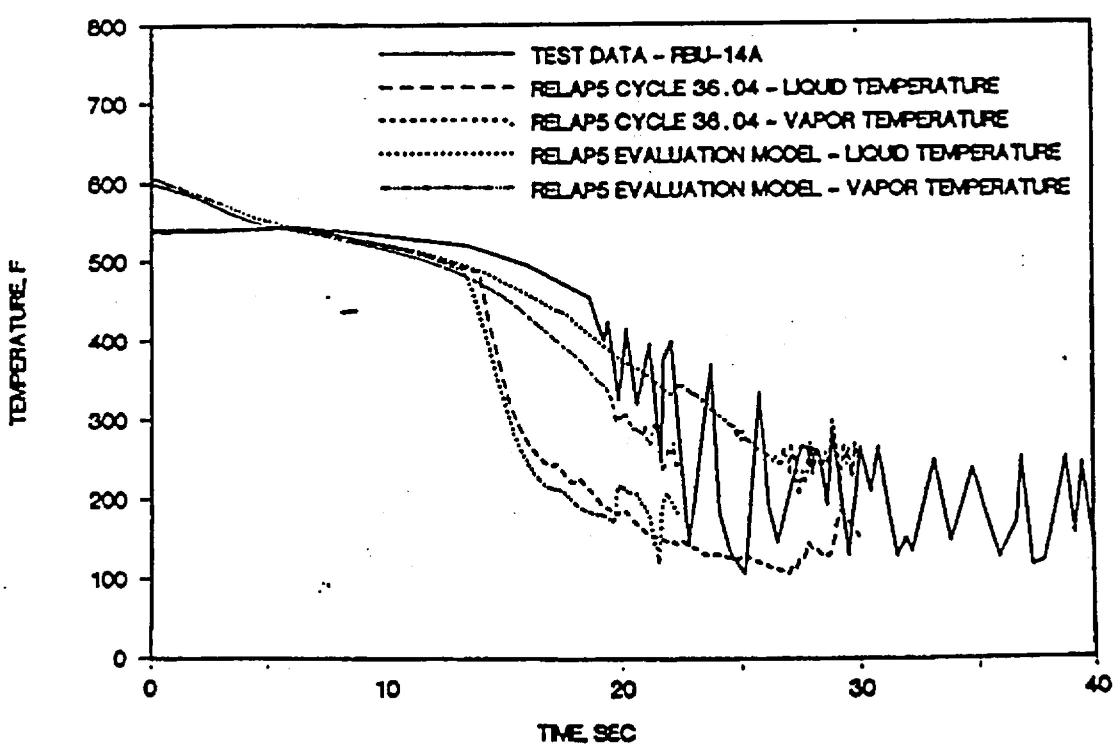

FIGURE 12.30. SEMISCALE MOD1 TEST S-04-6; FLUID TEMPERATURE NEAR THE CORE INLET.

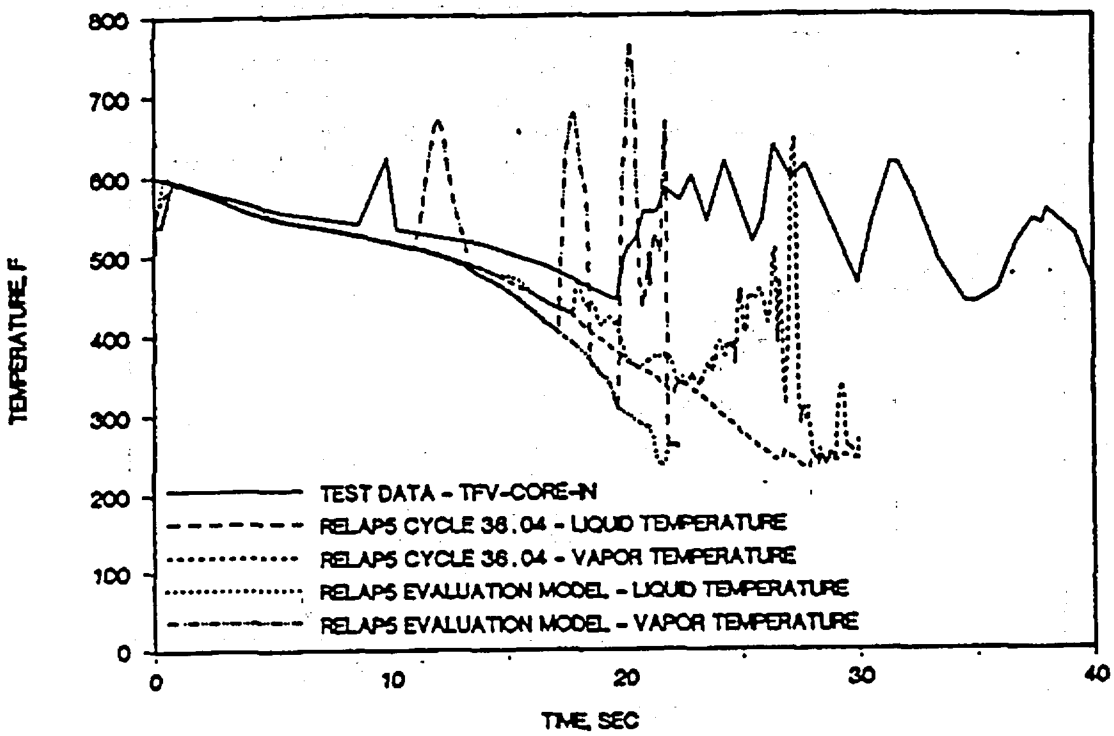

FIGURE 12.31. SEMISCALE MOD1 TEST S-04-6; FLUID TEMPERATURE IN UPPER PLENUM.

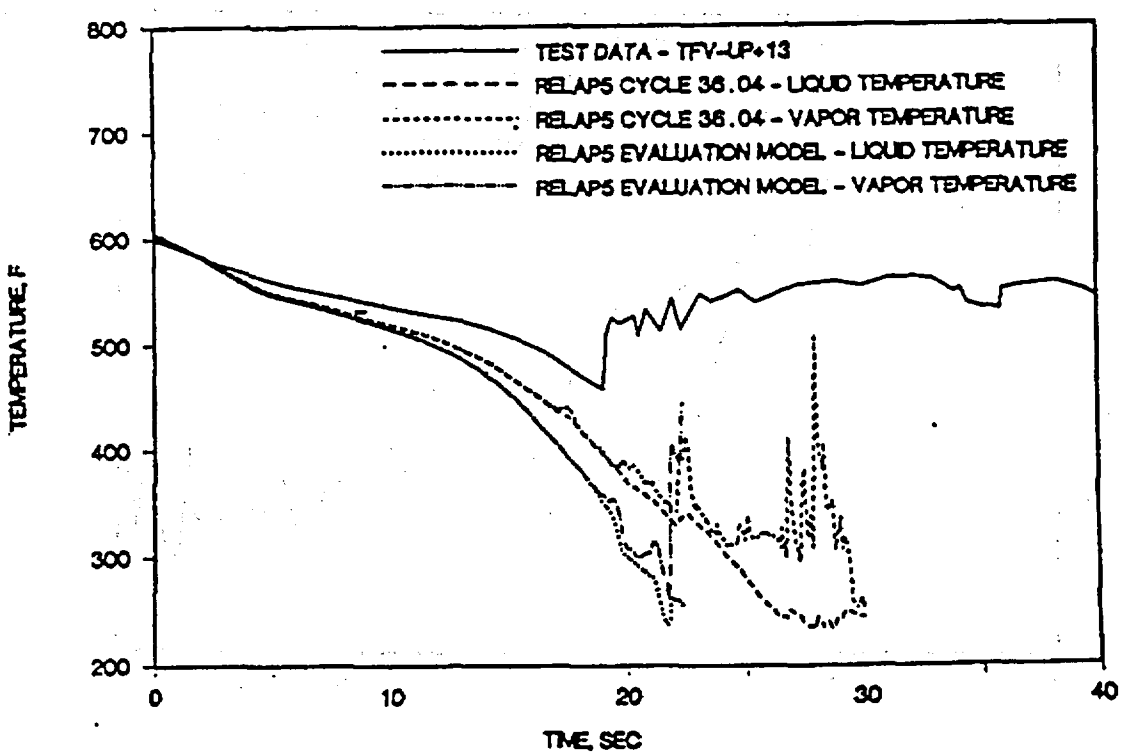

FIGURE 12.32. SEMISCALE MOD1 TEST S-04-6; AVERAGE POWER ROD CLADDING TEMPERATURE AT PEAK POWER LOCATION.

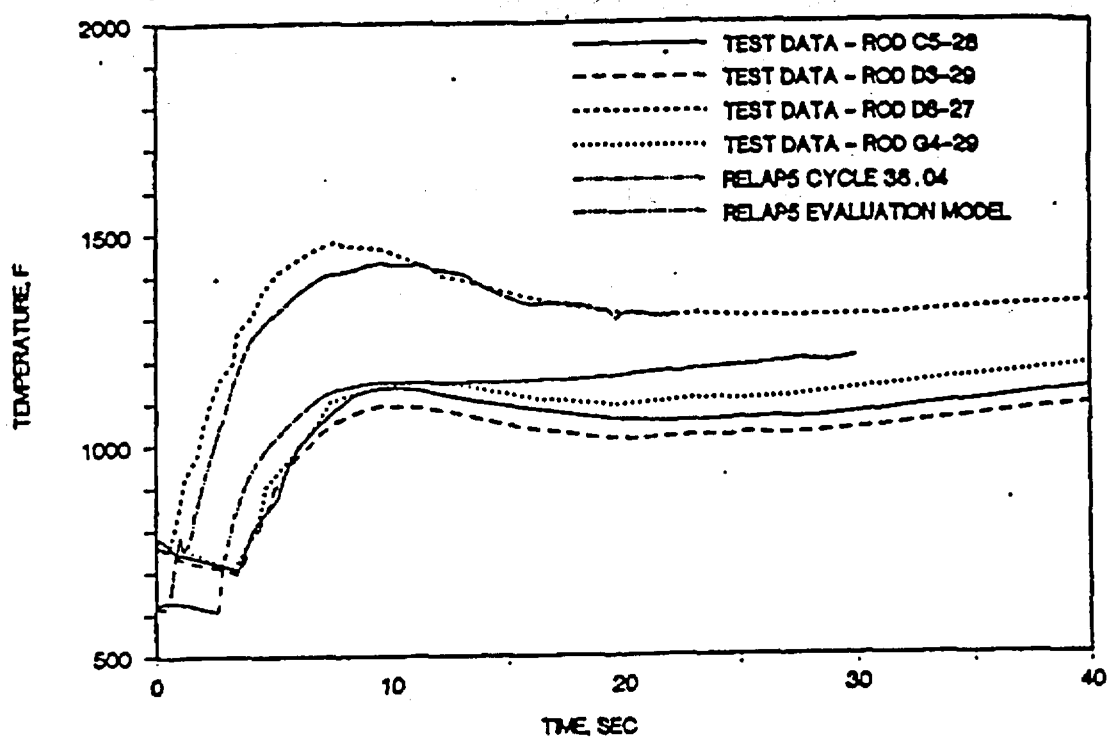

FIGURE 12.33. SEMISCALE MOD1 TEST S-04-6; HIGH POWER ROD CLADDING TEMPERATURE NEAR PEAK POWER LOCATION.

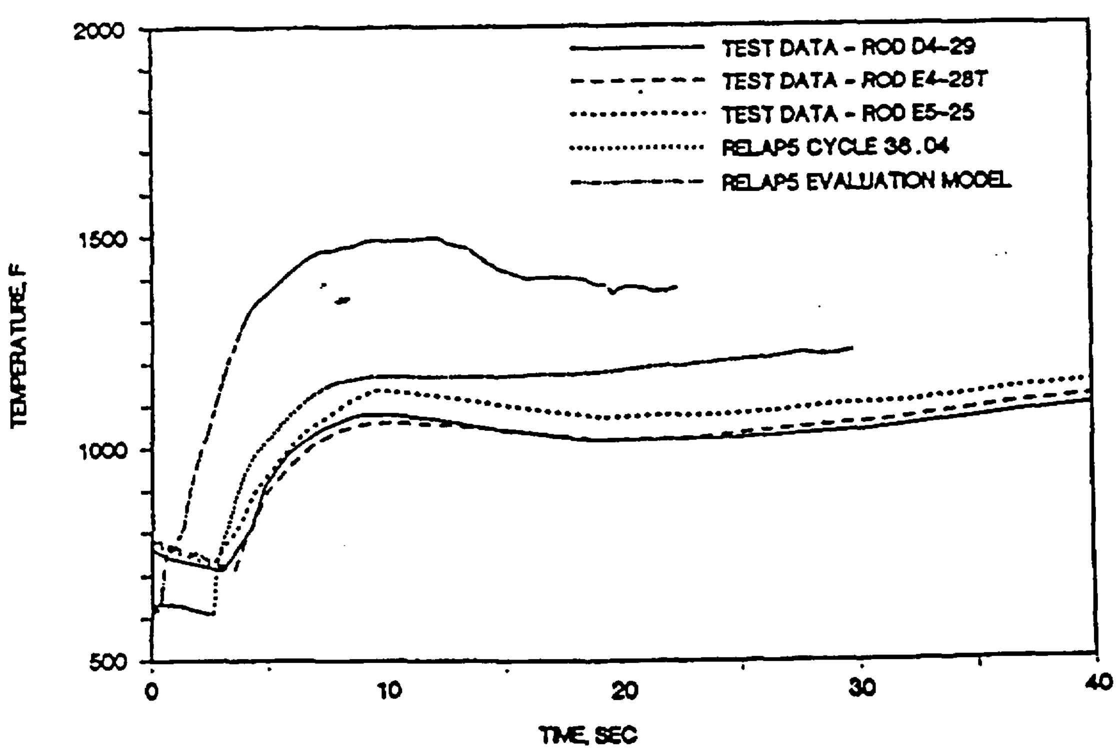

13. Question: The S-04-6 results presented by B&W did not compare the calculated and measured pressurizer level response. Provide this comparison to verify the code and system models B&W intends to use in plant calculations adequately calculate this phenomenon.

Response: See the response to question 12:

14. Question: In small break LOCAs (SBLOCAs), accurately calculating the mass distribution in the primary system is important to predicting the overall system response. The code/data comparisons provided by B&W for the LOFT L3-5 assessment calculation did not include any comparisons that would indicate how well RELAP5/MOD2-B&W calculated the mass distribution.

a. Provide plots comparing calculated and measured densities around the primary system to verify the mass distribution was accurately calculated by the code.

b. Compare the calculated and measured times of loop seal clearing and provide a comparison of the calculated and measured primary system mass inventories.

c. Provide a comparison of the calculated and measured break flows for LOFT L3-5.

d. Clarify why the pump coasted down more rapidly in the calculation for LOFT3-5 than in the experiment (Figure G.2-7).

Response:

As indicated in Section G.2 of BAW-10164, RELAP5/MOD2-B&W predicted the overall system response, including primary and secondary system pressure, pump coastdown, natural circulation and long-term cooling, reasonably well. Despite the underprediction of the BE discharge model, which in large measure reflects the need to use a discharge coefficient greater than one, such uncertainties are generally accounted for in EM applications through a spectrum study. This is equivalent to varying the discharge coefficient in search of the bounding or most severe (highest peak clad temperature) SBLOCA.

a&b. The calculated and measured values for the intact loop hot leg density, cold leg density, loop seal and primary system mass inventory are presented in Figures 14.1, 14.2, 14.3, and 14.4, respectively. The loop seal plot (Figure 14.3) indicates that the loop seal blow-out phenomenon was not observed because core bypass and reflood assisted bypass were utilized in the test. The discrepancy in the loop seal height is due to a difference between the ΔP tap location and the level calculation by RELAP5 control variable that consists of the vertical section of the pump suction piping including the pump volume. Although the upper elevation of the ΔP tap was not available, the main point of this plot is to demonstrate that both the prediction and the test data showed that the loop seal was not cleared due to a core bypass designed to prevent core uncovery. Test measurements during the pump coastdown (0 - 30s in Figure 14.3) do not accurately reflect the actual loop seal liquid level. The calculated hot and cold leg densities and mass inventory are consistently higher than the test data as a result of an underprediction of the BE discharge model.

c. The calculated and measured leak flowrates are presented in Figure 14.5. In general, the RELAP5 BE discharge model underpredicts the discharge flowrate. This is reflected in the primary system pressure shown in Figure G.2-10 (BAW-10164) and the mass inventory plot in Figure 14.4.

d. The pump coastdown is affected by the leak flowrate, which is substantially higher than the measured data during the coastdown period as shown in Figure 14.5. As a result, the reverse flow fluid torque exerted upon the pump reduces its speed more rapidly. This phenomenon is also observed in the benchmark calculation with RELAP4/MOD6. The RELAP4 model was obtained from EGG-LOFT-5089, Best Estimate Prediction for LOFT Nuclear Experiment L3-2, which has the same homologous pump data.

FIGURE 14.1. LOFT TEST L-3-5; HOT LEG DENSITY.

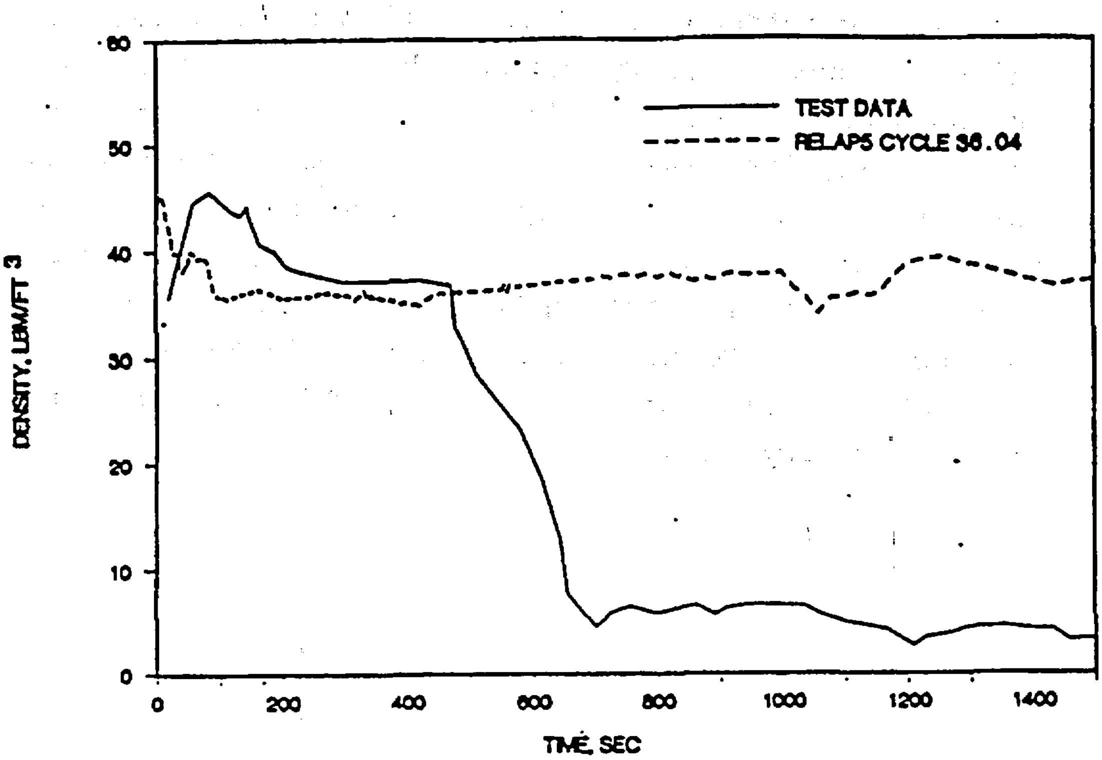

FIGURE 14.2. LOFT TEST L-3-5; COLD LEG DENSITY (PUMP DISCHARGE).

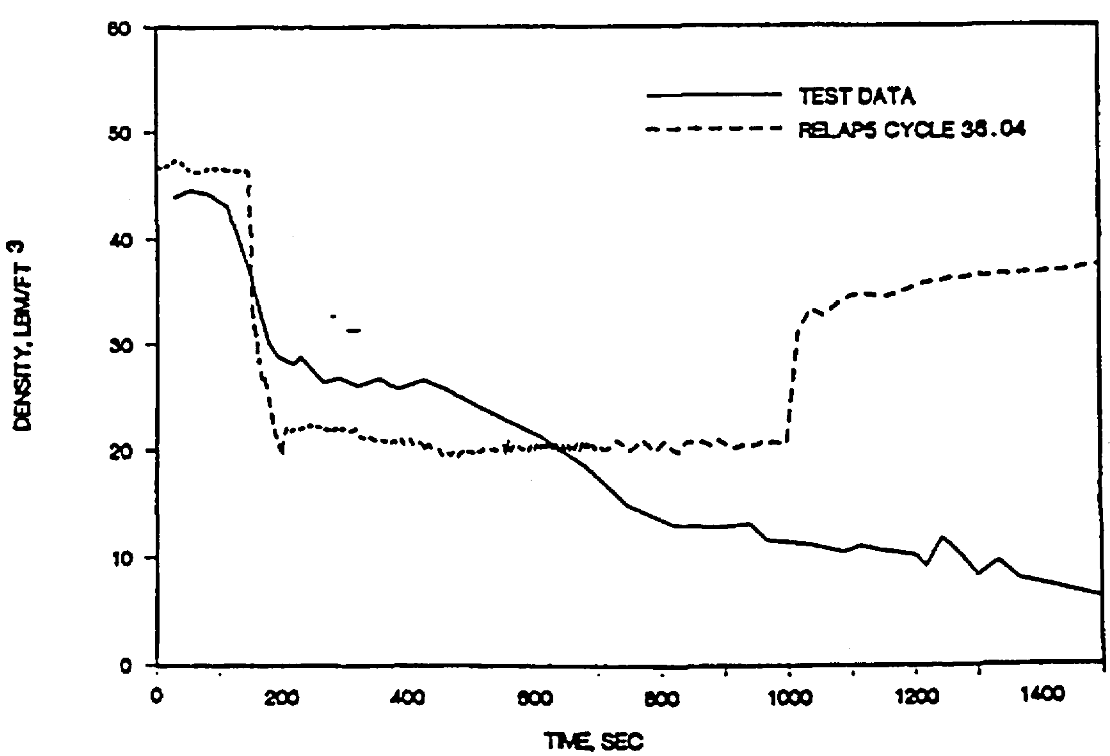

FIGURE 14.3. LOFT TEST L-3-5; LOOP SEAL HEIGHT (PUMP SUCTION PIPE).

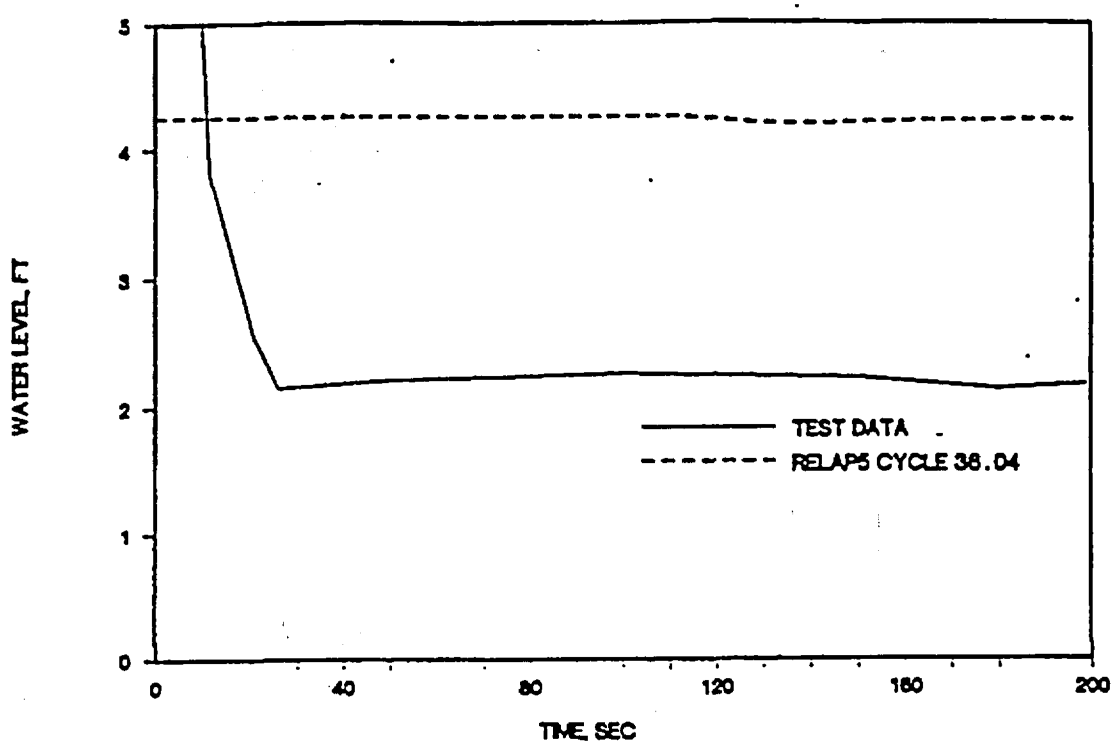

FIGURE 14.4. LOFT TEST L-3-5; NORMALIZED RCS INVENTORY.

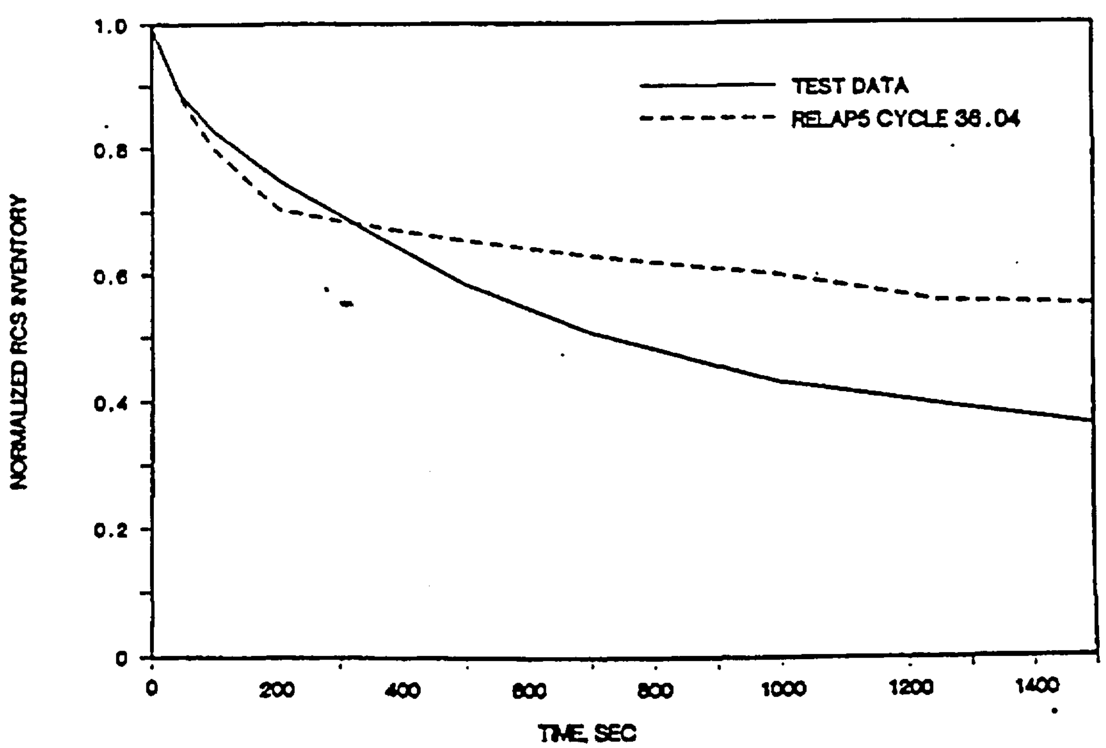

FIGURE 14.5. LOFT TEST L-3-5; LEAK FLOWRATE.

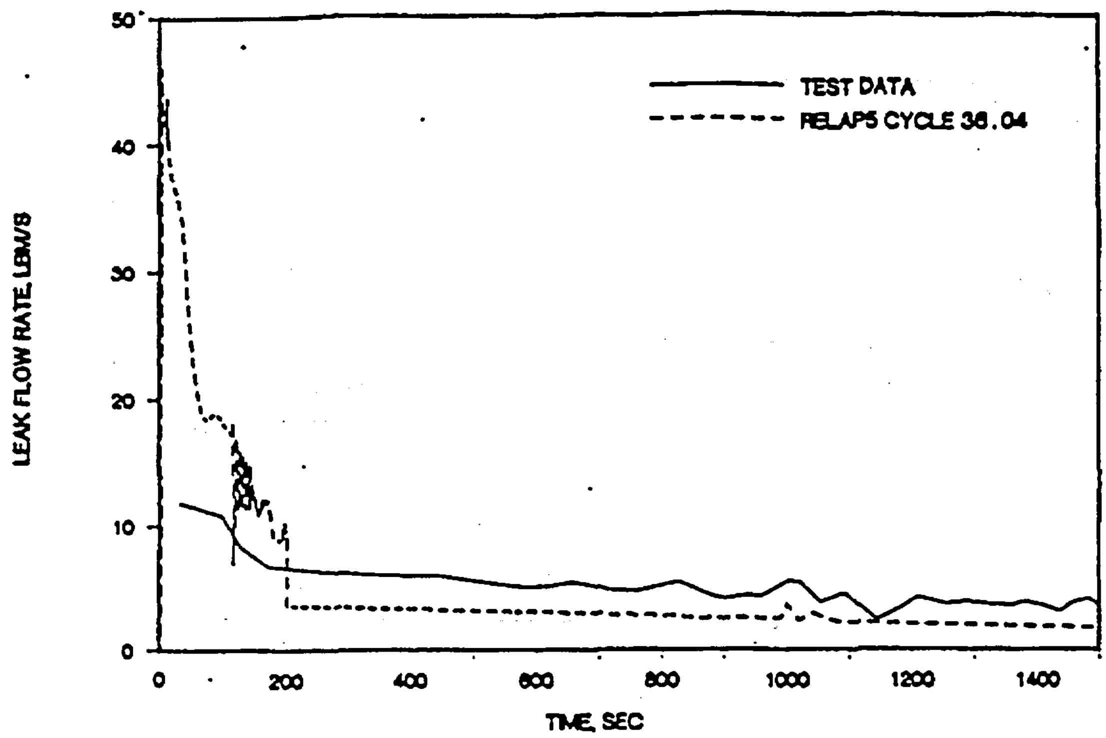

15. Question: In the B&W SBLOCA methodology, RELAP5/MOD2-B&W is used to calculate the system response including partial or total core uncovery. Because LOFT L3-5 did not include core uncovery, the code's ability to calculate the core inventory during core uncovery in a SBLOCA was not demonstrated. To demonstrate this capability of RELAP5/MOD2-B&W, provide the result of SBLOCA assessment calculation involving core uncovery.

Response: To verify RELAP5/MOD2-B&W capability to calculate core uncovery/recovery and loop seal clearing, a benchmark analysis was performed on Semiscale Test S-LH-1. The results of the benchmark are presented in the response to question 17.

16. Question: NUREG-0737, Item II.K3.30, required that codes to be used to perform SBLOCA licensing calculations be verified with respect to their ability to calculate phenomena associated with noncondensibles in the primary system; the single-phase, two-phase, and reflux modes of natural circulation; and condensation heat transfer. The information provided thus far by B&W has not addressed these items. In addition, integral assessment against data for LOFT Test L3-1 and Semiscale Test S-07-10 was requested in NUREG-0737, Item II.K.3.30. The staff agrees that assessment of RELAP5/MOD2-B&W against these specific tests is not required because the SBLOCA data base is considerably larger than when NUREG-0737 was written. However, the tests used to assess the code should cover the range of phenomena typical of small break LOCAs (natural circulation, core uncovery/recovery, loop seal clearing phenomena, pumps on/off, etc.). Provide the assessment calculations needed to verify that RELAP5/MOD2-B&W is capable for accurately calculating all the phenomena expected to occur in SBLOCAs.

Response: The primary system response to SBLOCA is mainly controlled by break size and decay heat removal via the steam generator. The MIST and OTIS benchmark results provided in Chapter 10 of the MIST final report and the RELAP5/MOD2 benchmark of the OTIS Feed and Bleed Test, respectively demonstrate that RELAP5 is capable of properly predicting SBLOCA phenomena. The benchmarks show that the primary system pressure response and primary system mass inventory were well predicted. Further discussion of SBLOCA phenomena, such as liquid entrainment, core uncovery/recovery, loop seal clearing, and pump trip and coastdown, is presented in the response to question 17. The reflux and natural circulation modes of core cooling, and the effect of noncondensible gas on condensation heat transfer are addressed herein.

Noncondensible Gas

A mechanistic model to calculate surface condensation in the presence of noncondensible gas was developed, based on the stagnant film model of Colburn and Hongen, and was incorporated in RELAP5/MOD2-B&W. This model was benchmarked against single tube separate effects tests performed at the B&W Alliance Research Center and at MIT. The results of the benchmark calculation are published in the "Proceedings of the Eighth International Heat Transfer Conference," San Francisco, 1986, pages 1627-1634. The results show that the prediction of RELAP5 is in good agreement with the test data.

Reflux and Natural Circulation

The results of the Westinghouse small break spectrum analysis presented in WCAP-10081A show that the most limiting case is generally predicted for break areas equivalent to between 2 and 6 inches in diameter. The break sizes in this range do not depend heavily on the steam generator to remove decay heat because the primary system pressure rapidly falls below the secondary side pressure. On the other hand, the natural circulation and reflux modes of core cooling become important for smaller breaks (less than 2 inches in diameter - 0.5% break) because the primary system pressure remains above the secondary side pressure for an extended period of time. Thus, for licensing applications, to determine the most limiting break in the SBLOCA category, the ability of RELAP5 to accurately calculate steam generator heat removal will not significantly impact overall results. Furthermore, RELAP5/MOD1 benchmark results of the Semiscale MOD-2A natural circulation tests shown in EGG-SEMI-6315 and NUREG/CR-3690 have demonstrated that the code can qualitatively predict all modes of natural circulation including reflux cooling. The hydrodynamic model improvements made to RELAP5/MOD2 further enhance its accuracy in predicting natural circulation phenomena.

Additional benchmarks on natural circulation and reflux cooling using RELAP5/MOD2 (Cycle 36) were performed separately by S. Guntay of Switzerland, and by K. H. Ardron and P. C. Hall of the United Kingdom. The results of the post-test calculations of OECD-LOFT Experiment LP-SB-03 (0.4% cold leg break) demonstrate that RELAP5/MOD2 generally performed well, predicting all the key events in the correct sequence and with reasonable accuracy in timing. Except for the leak discharge and core heat transfer models, B&W's SBLOCA EM utilizes the BE options in RELAP5/MOD2 for hydrodynamic models, nonhomogeneous frictional flow and nonequilibrium models that were used in the above mentioned analyses. Thus, the B&W version of RELAP5/MOD2-B&W will perform as well as RELAP5/MOD2 Cycle 36.

17. Question: The experience with advanced thermal-hydraulic computer programs has shown an important sensitivity to modeling of the steam generators when analyzing SBLOCAs. Specifically, the modeling of liquid entrainment, condensation, and hydraulic resistance (i.e., flow regime maps) could significantly depress the mixture level in the core. This phenomenon was observed in Semiscale Test S-UT-8 and later studied in Semiscale Tests S-LH-1 and S-LH-2. Recognizing Semiscale's atypicality, the staff nevertheless believes this phenomenon to be real and, therefore, possible in a full scale reactor. It is for this reason that we request validation of your computer program to predict this phenomenon, should it occur in a full scale reactor. Validation with Semiscale Tests S-LH-1 and S-LH-2 or demonstrating that the phenomenon observed in the Semiscale experiments is calculated to occur in a plant calculation would be acceptable. Use of other integral experiments for validation requires that these experiments simulate the hydraulic behavior observed in the Semiscale tests.

Response: In response to the above request, RELAP5/MOD2-B&W was benchmarked against Semiscale test S-LH-1. S-LH-1 is a 5% break at the pump discharge pipe with a 0.9% core bypass flow from the downcomer to the upper head. The simulation of S-LH-1, using RELAP5/MOD2-B&W, demonstrates the capability of the code to predict SBLOCA phenomena, such as core uncovery/recovery, natural circulation including reflux boiling, loop seal clearing, and ECCS performance. The results of the Westinghouse break spectrum analysis in WCAP-10081A show that the peak clad temperature (PCT) is generally predicted for break sizes greater than two inches in diameter (0.5% cross-sectional area of the cold leg pipe). For breaks above this size, the primary system depressurizes rapidly and falls below the secondary side pressure. Thus, decay heat removal via the steam generator is provided only briefly during the early phase of such transients, and the steam generators do not play a significant role in mitigating these accidents. For smaller breaks, that depend mainly on the steam generator for core cooling, numerous benchmarks of Semiscale test series S-NC, that demonstrate the adequacy of RELAP5/MOD2 to predict long-term core cooling by reflux boiling and natural circulation, have been performed.[17-1,17-2] S-LH-1 addresses important SBLOCA phenomena, such as loop seal clearing and core uncovery/recovery, that are observed in larger break size SBLOCAs.

Test Facility

The S-LH-1 test was conducted using the Semiscale MOD-2C facility shown in Figure 17-1. It consisted of a pressure vessel with simulated reactor internals and an external downcomer. The intact loop simulated three unaffected loops of a typical Westinghouse 4-loop PWR, while the broken loop simulated an affected loop in which the break is assumed to occur. The intact loop steam generator contained six inverted U-tubes, and the broken loop steam generator contained two inverted U-tubes. The reactor core simulator was a 5 x 5 bundle with electrically heated rods (23 rods were powered during the test). The upper head region contained a simulated control rod guide tube and two simulated support columns. The bypass line that extended from the external downcomer to the upperhead was used to simulate the core bypass flow. A pressurizer was connected by a surgeline to the intact loop hot leg. Both loops had primary coolant circulation pumps. Emergency core coolant from an accumulator and pumped injection system (LPI and HPI) were routed to the loop cold legs. An open loop secondary coolant system was used to control the secondary side pressure with feedwater and steam control valves.

Model Description

The Semiscale MOD-2C RELAP5 model was originally developed by EG&G for the post-test analysis of experiments S-LH-1 and S-LH-2 (NUREG/CR-4438). The nodalization diagram is shown in Figure 17-2. The model consists of 181 hydrodynamic volumes, 172 junctions, and 256 heat structures. All volume and junction parameters are calculated with nonequilibrium and nonhomogeneous models. Steam generator secondaries, ECC injection, system environmental heat losses, and both vessel and piping external heaters are modelled in detail. The core axial power profile is modelled with twelve stacked heat structures over six two-foot long axial fluid volumes. The upper head region is nodalized to allow for junctions to be connected at the elevations of the top of the control rod guide tube, core bypass line and support columns, and at the elevation of the holes in the guide tube below the upper core support plate.

Several changes were made to the original EG&G model to properly account for and distribute unrecoverable losses due to pipe bends, orifices at the pump discharge pipes, area changes at the steam generator inlet and outlet plenums, and flowmeters in the hot and cold leg pipes. A steady-state calculation was made with these changes to obtain the initial conditions presented in Table 17-1. The calculated initial conditions compared well with the test conditions except for the secondary side masses and pressures. These were adjusted to achieve the desired primary cold leg temperatures. The calculated pump speeds are slightly higher than the test measurements (8% and 3% for the intact and broken loops, respectively) as a result of higher pump discharge orifice resistances calculated by RELAP5.

Prior to transient analysis, additional changes, that do not affect the steady-state initial conditions, were made to incorporate B&W's SBLOCA EM options into the model; they are: the core surface heat transfer model, the leak discharge model (BAW-10164P), and thermal equilibrium in the core region. A leak discharge coefficient of one was applied to both the subcooled and saturated choke flow models. The external heaters were modelled mechanistically in RELAP5, and the measured power to the heaters as a function of time was input as a boundary condition. The core decay power and pump coastdown speeds as a function of time were also input to the model. There was limited secondary side steam valve model information available from this experiment. Since the secondary system responses have an impact on the natural circulation and reflux boiling phases of the transient, the secondary side pressure responses from the experiment were used as boundary conditions in the calculation (see Table 17-2).

Results of Analysis

The sequence of major events is presented in Table 17-2. The transient was initiated at zero seconds by opening the leak, and thereby causing a flow of subcooled primary fluid out the break, resulting in a rapid system depressurization. Figure 17-3 shows good agreement in the leak flowrate between the RELAP5 calculation and the experimental data. The primary system pressure response is controlled by the leak flow, and Figure 17-4 shows that the calculated pressure is in good agreement with the experimental pressure up to 200 seconds. The calculated time to reach the safety injection system (SIS) setpoint of 1827.5 psia (pressurizer) is approximately 3 seconds later than the experiment, primarily due to a slower draining in the pressurizer. This is believed to be caused by a higher overall intact loop resistance observed in the initialization analysis. The calculated steady-state pump speed in the intact loop is approximately 8% higher than that of the experiment.

The draining of the steam generator tubes occurred after the pump speed coasted down to zero at 100 seconds. At this point, the primary system entered a reflux condensation cooling mode. Figures 17-5 through 17-8 show U-tube liquid levels in both the intact and broken loops. It should be noted that the measured liquid levels using differential pressure cells can lead to considerable error during the pump coastdown period (0 - 100 sec).[17-3] Both the prediction and the experimental data show that the upflow side of the U-tube consistently drained later than the downflow side due to de-entrainment and reflux condensation on the tube surface. Following draining of the steam generator U-tubes, a liquid seal was formed in the pump suction of both loops. The seals caused a blockage of steam flow to the break. As a result, the primary system entered a period of manometric level depression in both the downflow side of the pump suction seals and in the core liquid level. To clear the pump suction loop seals, the liquid head imbalance between the downcomer and the core must accrue to the total of the loop seal level plus the liquid holdup, due to reflux condensation, in the upflow side of the U-tubes. As shown in Figures 17-5 and 17-7, the liquid level in the upflow side of the steam generator U-tubes is a significant contributor to the total ΔP, that opposes loop seal clearing. The loop seals cleared at 175 seconds and 214 seconds for the intact loop and the broken loop, respectively.

Figures 17-9 through 17-12 show the liquid level in the pump suction pipes. The intact loop seal cleared first, followed by the broken loop, because the primary-to-secondary heat transfer was terminated earlier in the intact loop than in the broken loop. Clearing of the loop seals produces a continuous path to the break for steam generated in the core. The steam conditions at the leak result in lower leak mass flows, but higher volumetric flows. As a result, the primary system began a rapid depressurization.

Following loop seal clearing, the RELAP5 depressurization rate was faster than was observed in the experiment, in spite of good agreement in discharge mass flowrate between the calculation and the experiment. The energy discharge rate and heat loss to the ambient surroundings of the test, were not available to confirm the reasonable hypothesis that steam venting is the primary cause of the larger depressurization rate in the RELAP5 prediction.

One of the important parameters used as an indicator for SBLOCA mitigation is core collapsed liquid level. This is shown in Figure 17-13. As a result of correctly predicting primary system mass inventory and reflux heat transfer, the agreement in the first core level depression between the calculation and the experiment is excellent. After clearing the loop seals, core decay heat continues to boil-off fluid in the core region and, since the HPIS flow alone is not sufficient to makeup for fluid lost out the break, the core liquid level continues to decrease until accumulator actuation is achieved.

Accumulator injection occurred much earlier in the calculation than in the experiment due to the faster depressurization rate. However, the shortened core boil-off period was compensated for by increased flashing. Thus, the second core level depression was calculated to be nearly the same as the measurement except for its timing. The experiment shows that a more significant and uniform core heat-up occurred during the second core level depression. The ability of RELAP5 to correctly predict the two distinct core liquid level depressions demonstrates that the code can accurately calculate important thermal-hydraulic system parameters, that are used to determine the most limiting SBLOCA. Figure 17-14 shows the normalized primary system mass inventory. It confirms the adequacy of the EM discharge model. The mass inventory increased following accumulator injection. The HPIS injection flow rates for both the intact and broken loops are presented in Figure 17-15 and 17-16, respectively. The calculated flow rates are higher than those of the experiment due to the faster depressurization rate predicted by RELAP5.

<u>Conclusions</u>

In conclusion, the benchmark results show that the calculated overall system responses are in a good agreement with the experimental data. RELAP5/MOD2-B&W calculated the major events of the transient, namely two-phase natural circulation, reflux and liquid holdup, pump suction loop seal clearing, core liquid level depression, ECCS injection and core recovery, in the proper sequence. The benchmark demonstrates that RELAP5/MOD2-B&W can adequately predict the system thermal-hydraulic responses during a SBLOCA.

References

17-1. K. P. Ardron and P. C. Hall, "UK Experience with RELAP5/MOD2," Central Electricity Generating Board, Generation Development and Construction Division, Barnwood, Gloucester, UK (Private Communication).

17-2. P. Ting, R. Hanson, and R. Jenks, International Code Assessment and Applications Program, NUREG-1270, Vol. 1, March 1987.

17-3. G. G. Loomis and J. E. Streit, Results of Semiscale MOD-2C Small-Break (5%) Loss-of Coolant Accident Experiments S-LH-1 and S-LH-2, NUREG/CR-4438, November 1985.

Table 17-1. Comparison of Calculated and Measured Initial Conditions for Semiscale Test S-LH-1.

Parameter	RELAP5	Measured
Pressurizer Pressure, psia	2243.7	2243.8
Core Power, Kw	2014.75	2014.75
Pressurizer Liquid Level, inches	155.5	155.6
Cold Leg Fluid Temperature, F		
Intact Loop	552.1	552.2
Broken Loop	555.6	556.7
Primary System Flowrate, lbm/s		
Intact Loop	15.7	15.6
Broken Loop	5.2	5.2
Core Bypass Flow (% of total core flow)	0.9	1.0
SG Secondary Pressure, psia		
Intact Loop	829.6	859.7
Broken Loop	881.8	857.2
Core ΔT, F	67.8	67.4
SG Secondary Side Mass, lbm		
Intact Loop	421.0	374.8
Broken Loop	94.8	78.0

Table 17-2. Comparison of Calculated and Measured Sequence of Events for Semiscale Test S-LH-1.

Event	Measured (Time, seconds)	RELAP5 (Time, seconds)
Break Opened	0.5	0.0
Pressurizer at 1827.5 psia (SIS)	14.67	17.65
Reactor Scram	19.57	22.60
Pump Coastdown Initiated		
Intact Loop	21.35	24.35
Broken Loop	20.76	23.75
Feedwater Off		
Intact Loop	19.67	22.70
Broken Loop	19.00	22.00
MSIV Closure		
Intact Loop	22.0	25.00
Broken Loop	22.0	25.00
HPIS Initiated		
Intact Loop	41.60	44.60
Broken Loop	40.98	44.60
Pressurizer Emptied	33.90	44.00
Intact Loop Seal Cleared	171.4	175.0
Broken Loop Seal Cleared	262.3	214.0

Table 17-2. Comparison of Calculated and Measured Sequence of Events for Semiscale Test S-LH-1 (continued).

Event	Time, seconds Measured	RELAP5
Accumulator Injection		
Intact Loop	503.8	324.0
Broken Loop	501.4	324.0

SG Secondary Side Pressure Used in the RELAP5 Prediction

Time, seconds	Pressure, PSIA Intact Loop	Broken Loop
0	860	858
20	860	888
40	1016	1021
60	1000	1010
100	995	995
200	989	974
300	958	926
1000	863	700

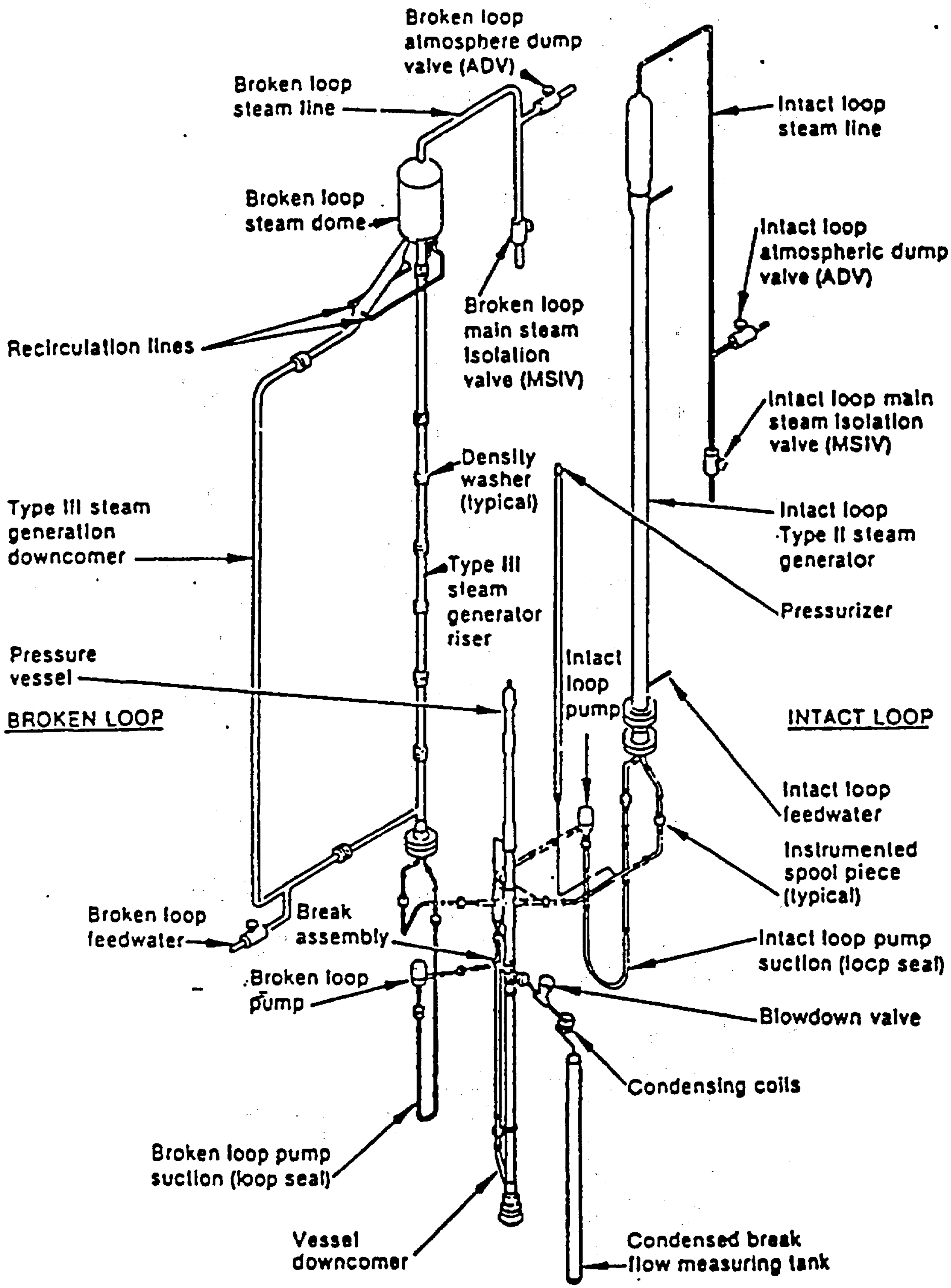

Figure 17-1. Semiscale MOD-2C System Configuration.

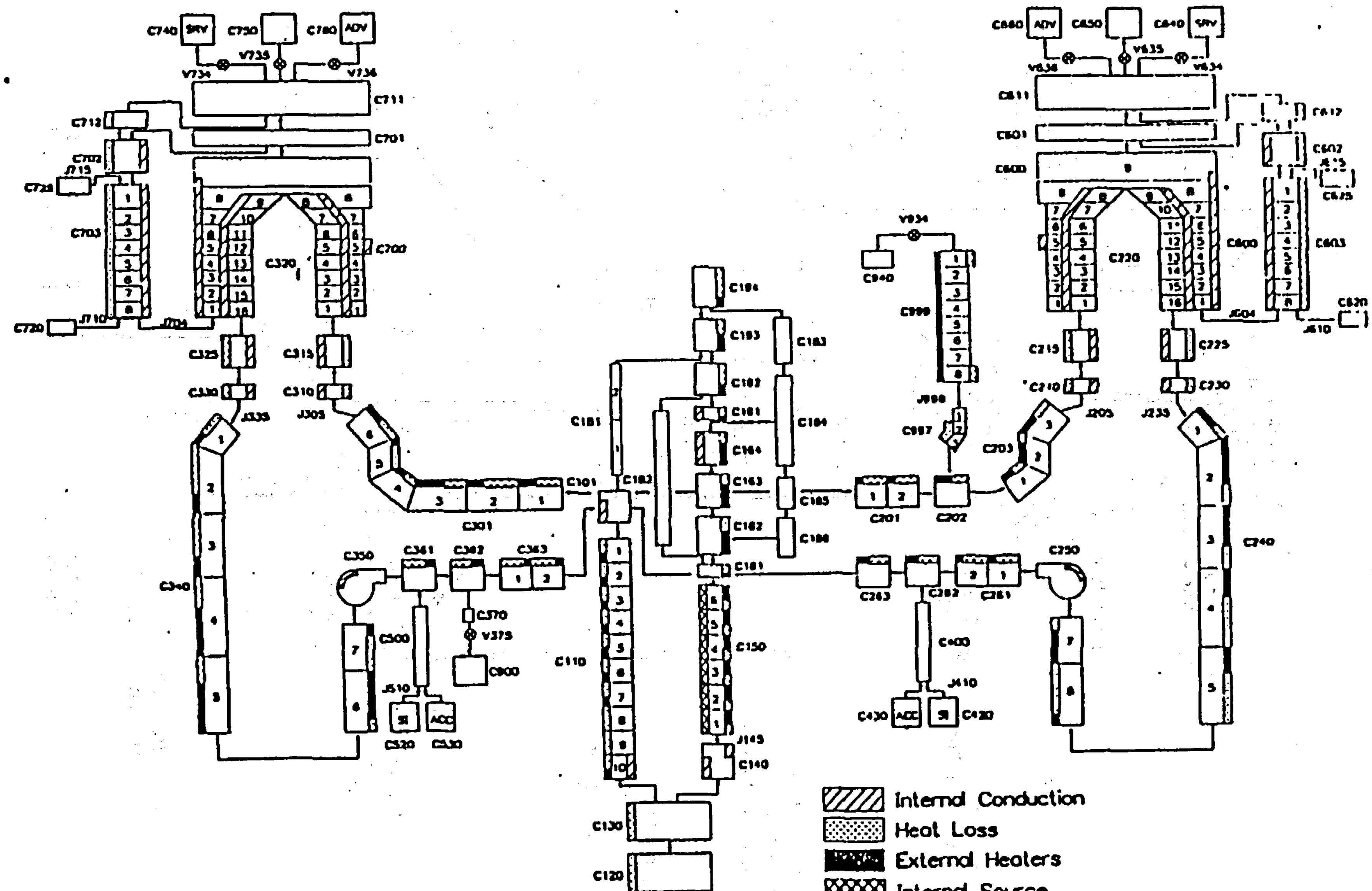

Figure 17-2. Semiscale Test S-LII-1 Noding Diagram.

FIGURE 17-3. SEMISCALE TEST S-LH-1; LEAK FLOW RATE.

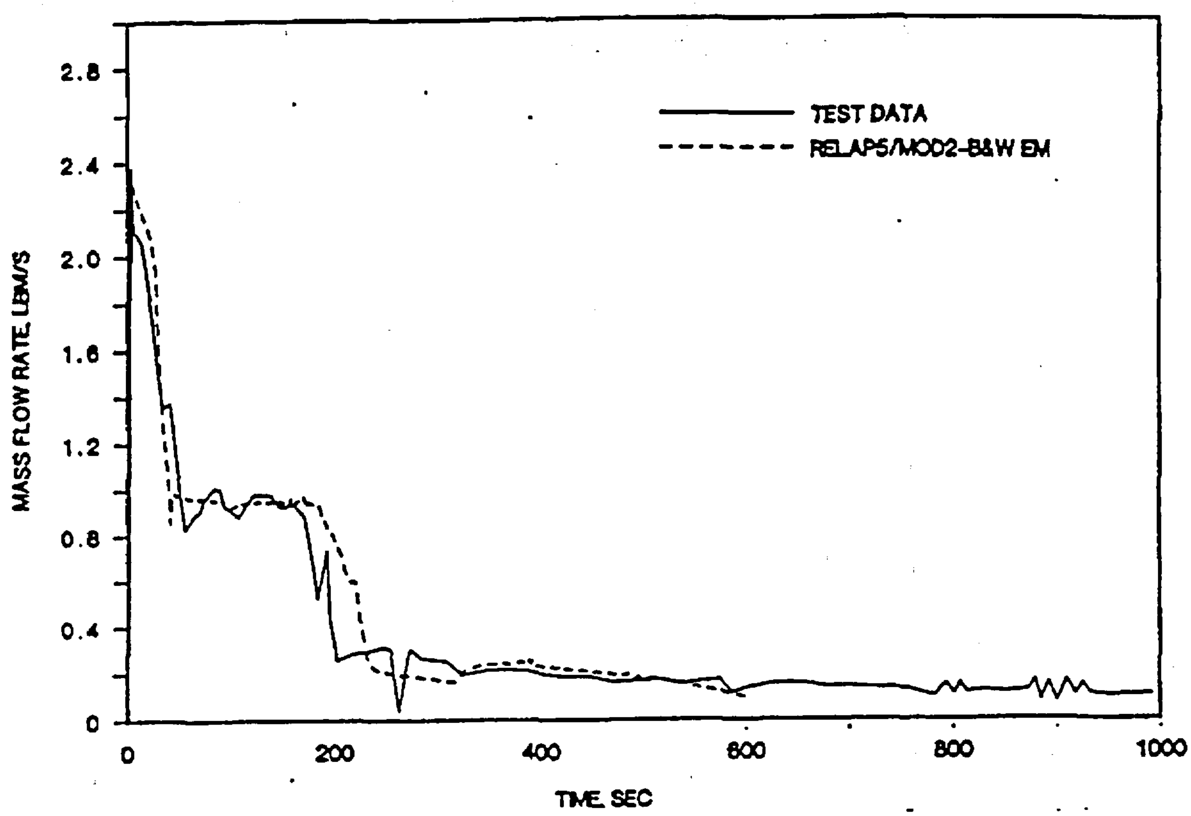

FIGURE 17-4. SEMISCALE TEST S-LH-1; PRIMARY SYSTEM PRESSURE.

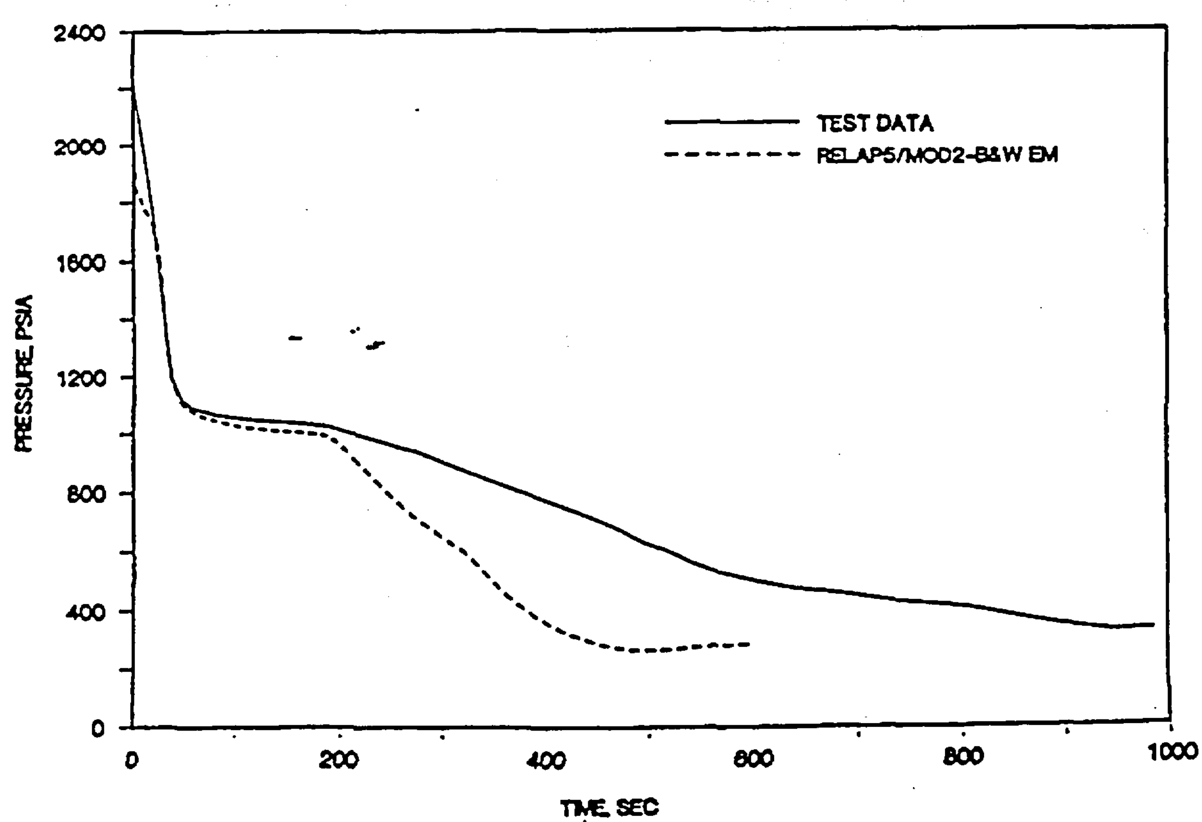

FIGURE 17-5. SEMISCALE TEST S-LH-1; INTACT LOOP STEAM GENERATOR TUBE LEVEL - UP SIDE.

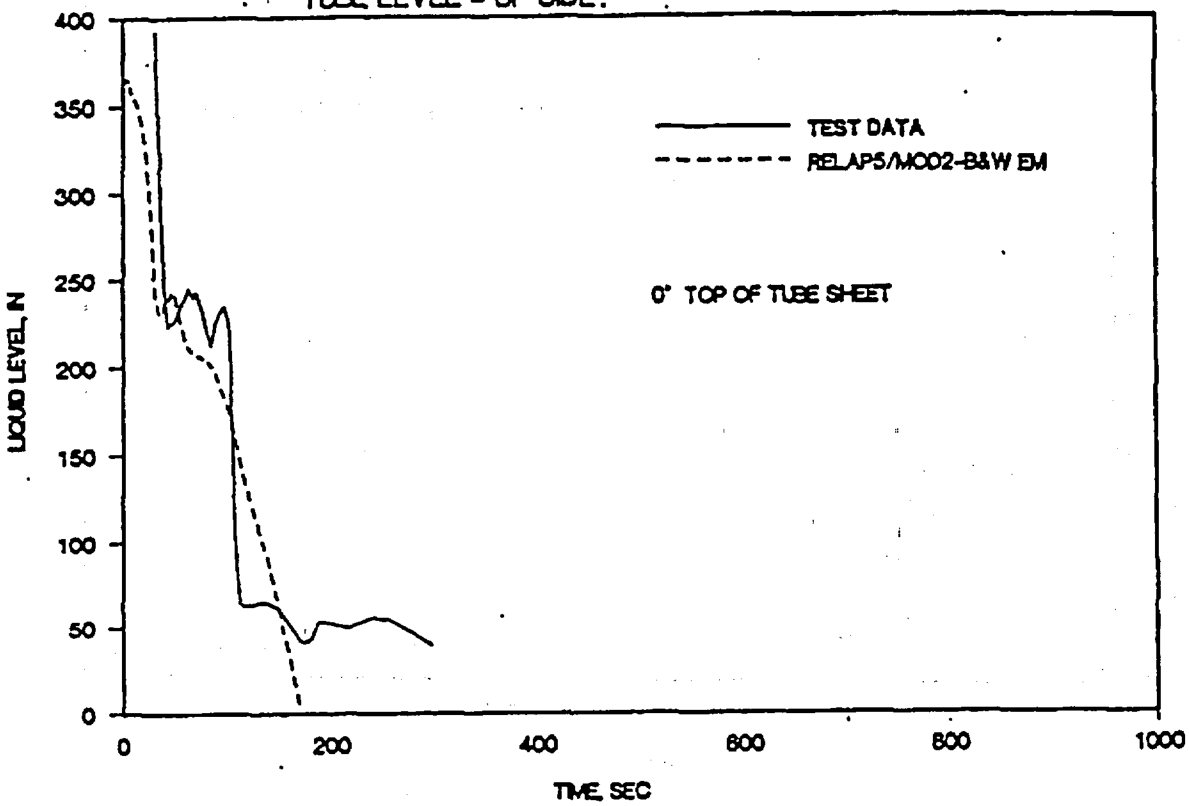

FIGURE 17-6. SEMISCALE TEST S-LH-1; INTACT LOOP STEAM GENERATOR TUBE LEVEL - DOWN SIDE.

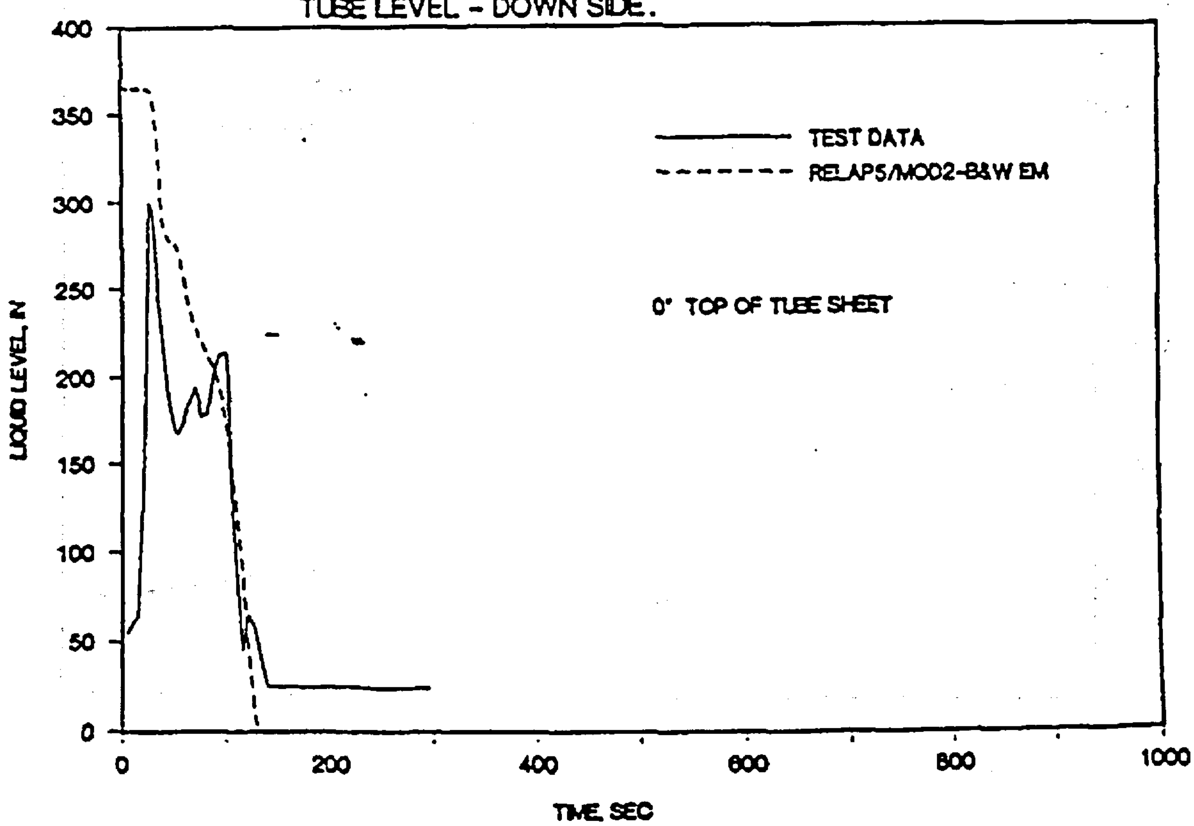

FIGURE 17-7. SEMISCALE TEST S-LH-1; BROKEN LOOP STEAM GENERATOR TUBE LEVEL - UP SIDE.

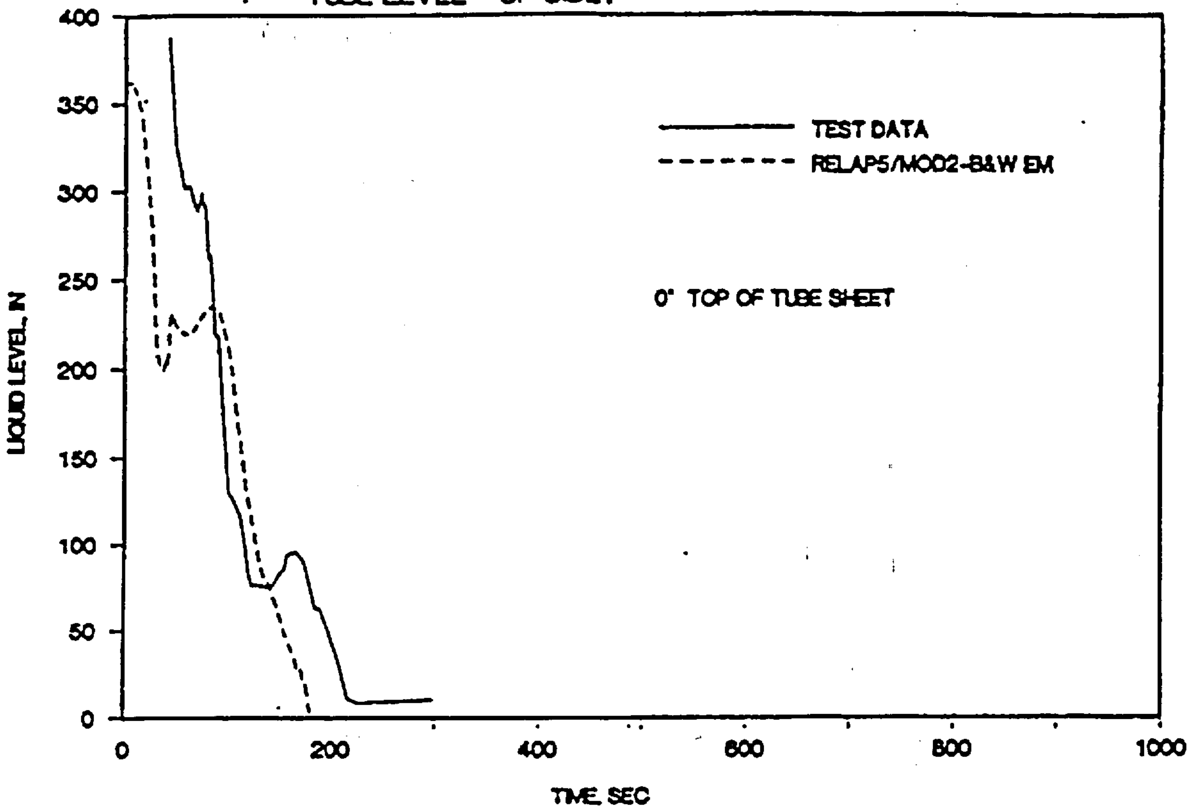

FIGURE 17-8. SEMISCALE TEST S-LH-1; BROKEN LOOP STEAM GENERATOR TUBE LEVEL - DOWN SIDE.

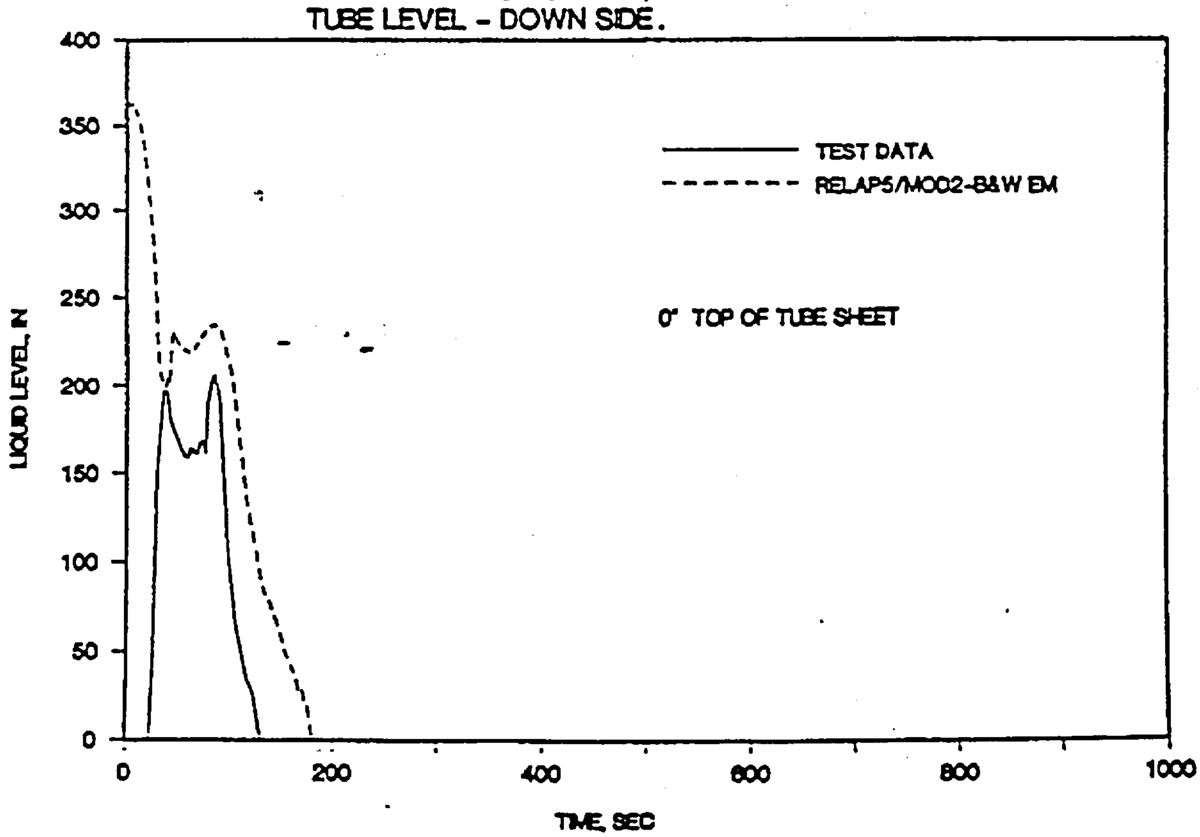

FIGURE 17-9. SEMISCALE TEST S-LH-1; INTACT LOOP PUMP SUCTION LEVEL - DOWN SIDE.

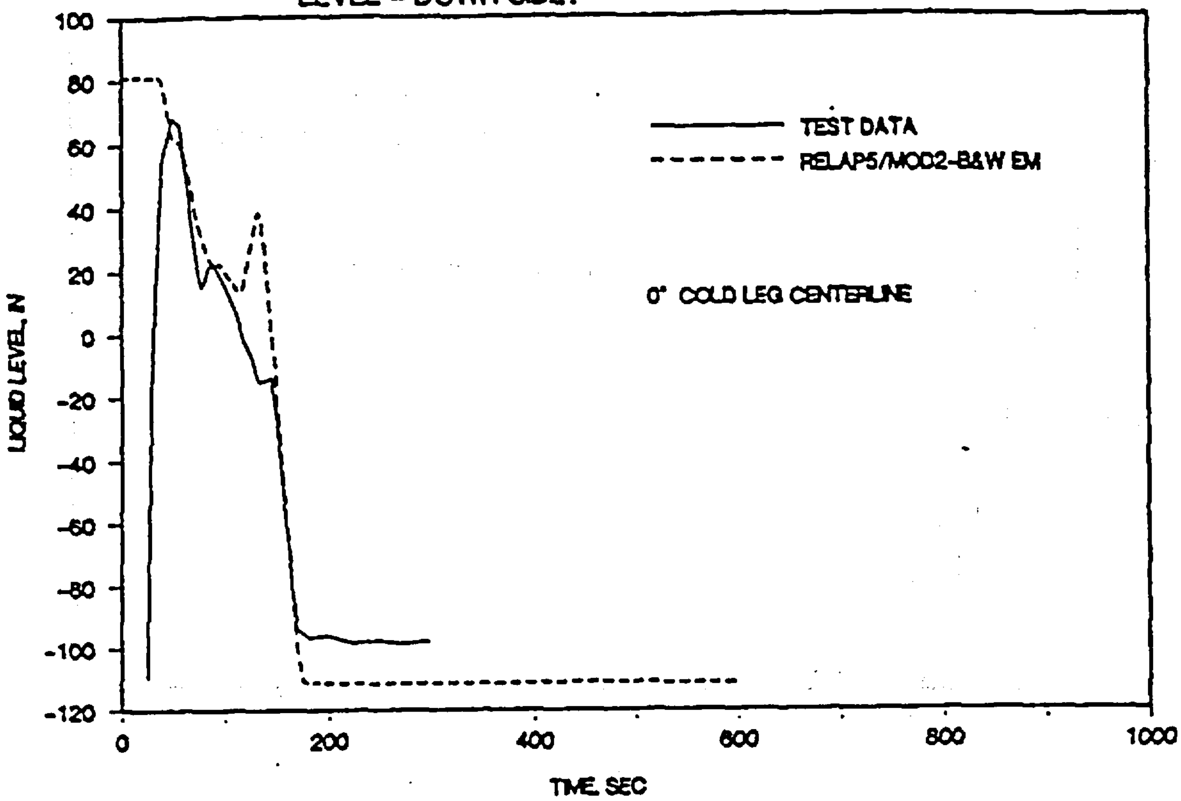

FIGURE 17-10. SEMISCALE TEST S-LH-1; INTACT LOOP PUMP SUCTION LEVEL - UP SIDE.

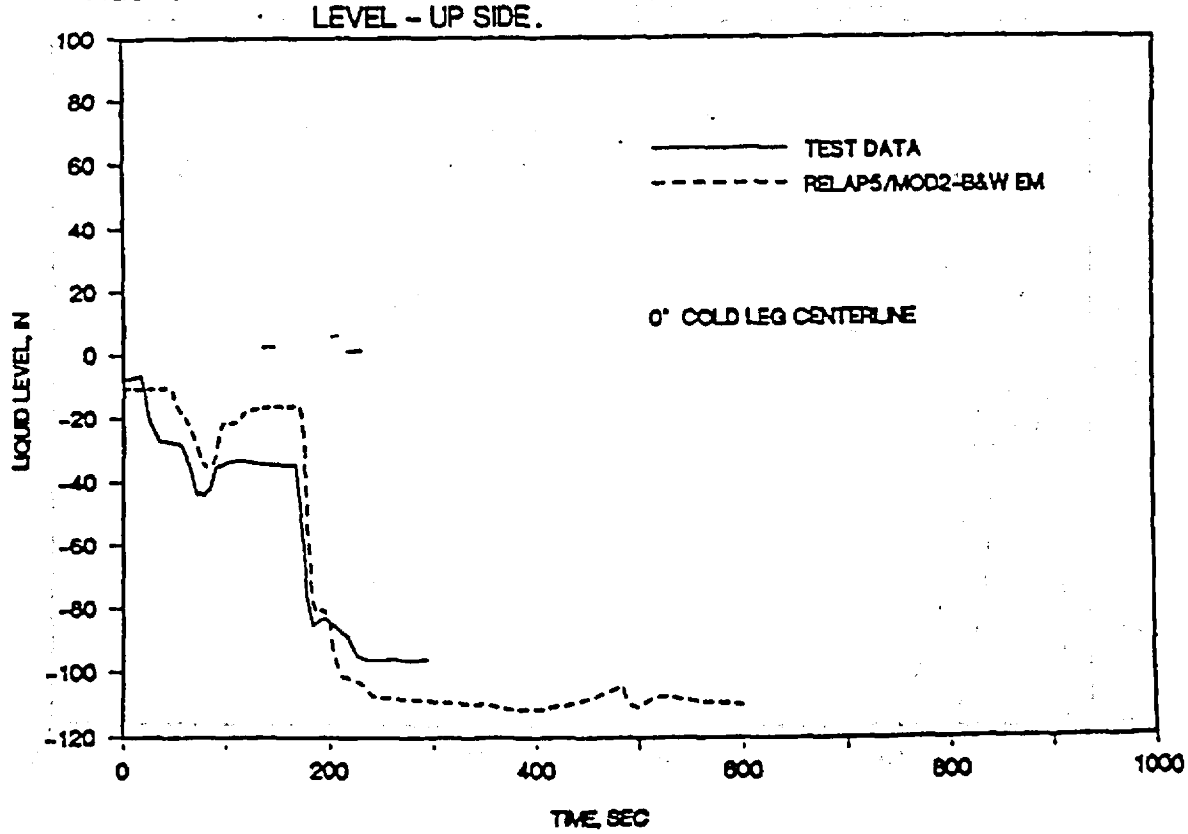

FIGURE 17-11. SEMISCALE TEST S-LH-1; BROKEN LOOP PUMP SUCTION LEVEL - DOWN SIDE.

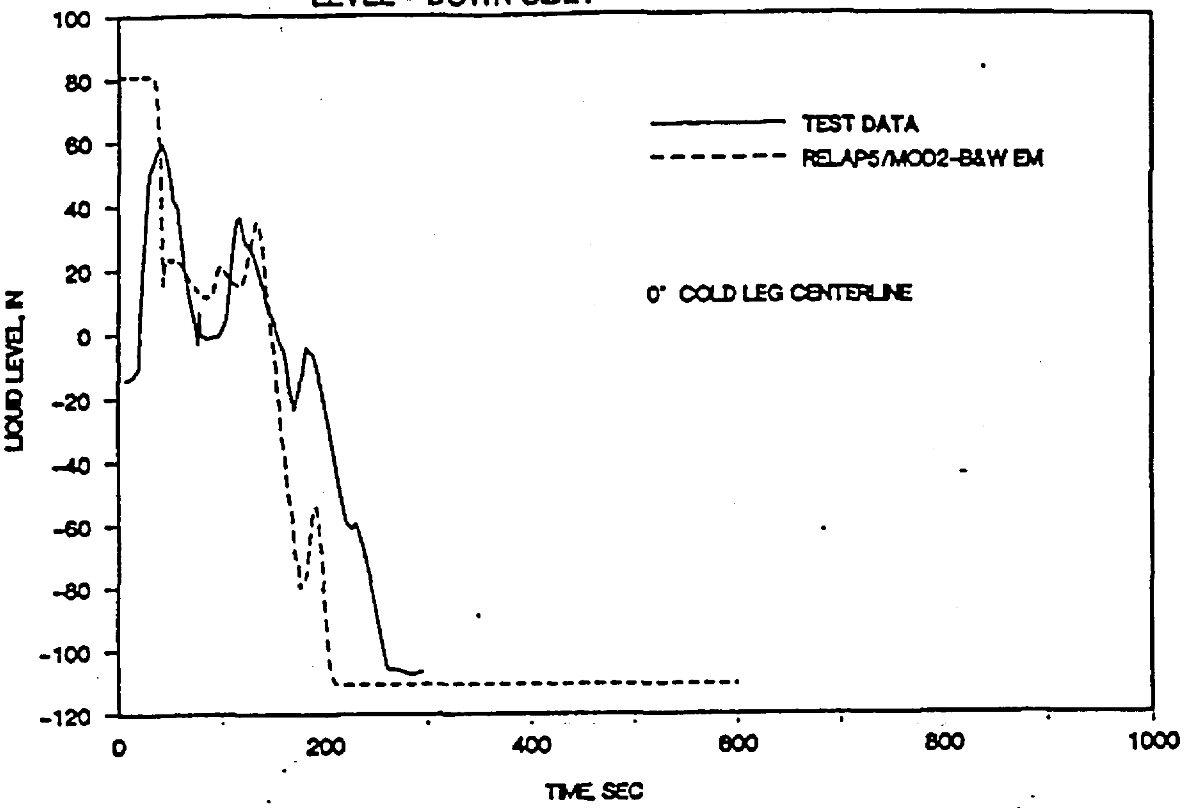

FIGURE 17-12. SEMISCALE TEST S-LH-1; BROKEN LOOP PUMP SUCTION LEVEL - UP SIDE.

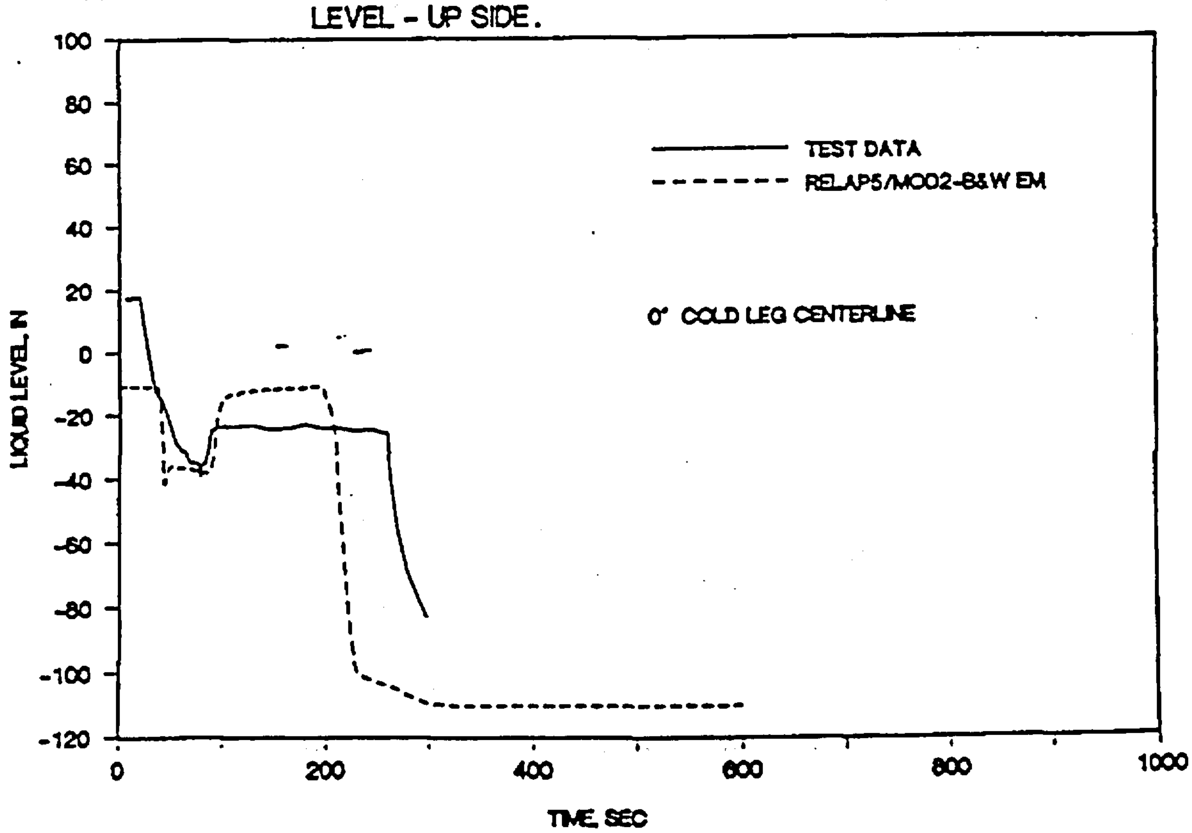

FIGURE 17-13. SEMISCALE TEST S-LH-1; VESSEL LIQUID LEVEL.

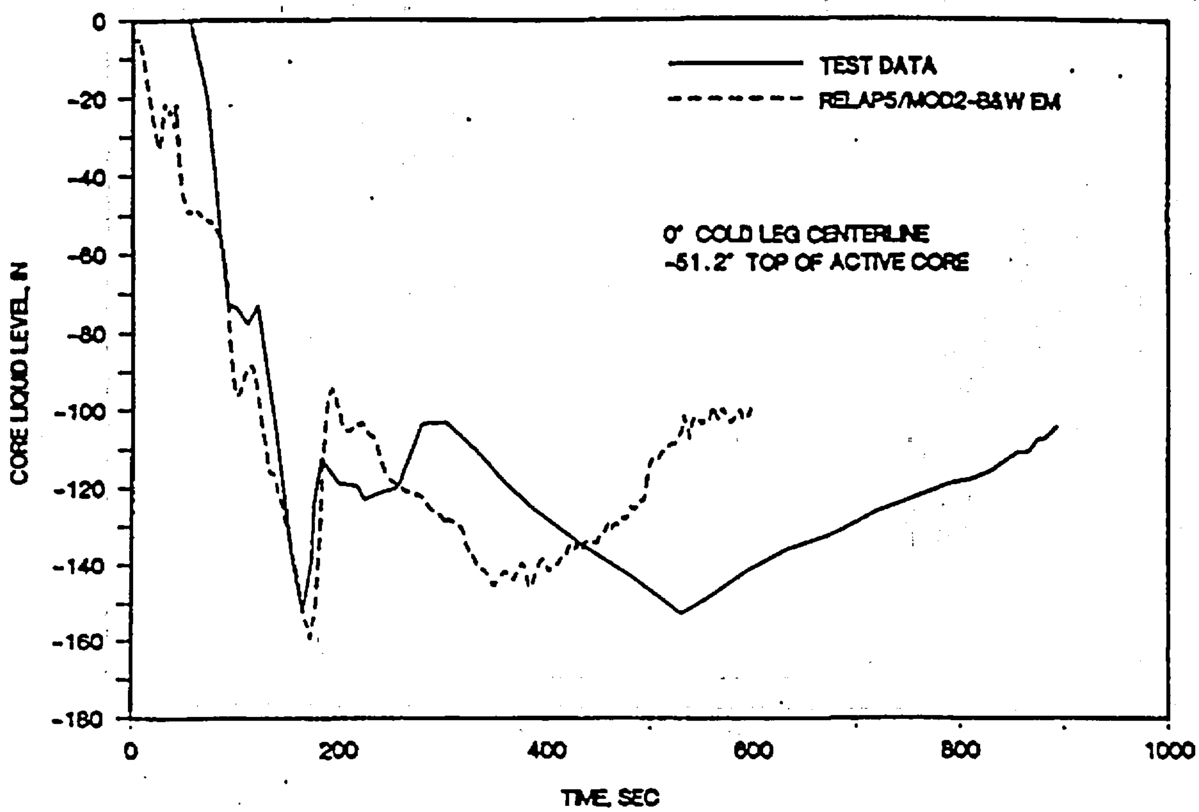

FIGURE 17-14. SEMISCALE TEST S-LH-1; PRIMARY SYSTEM NORMALIZED MASS.

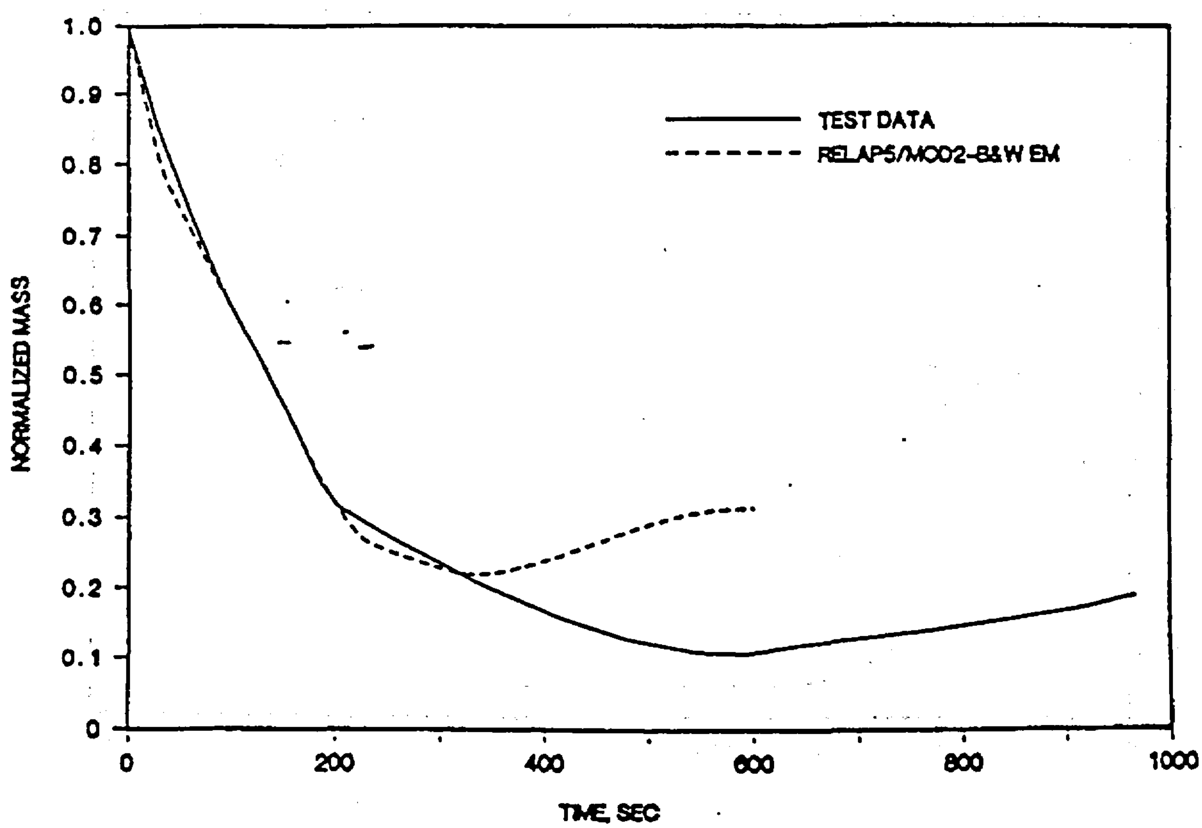

FIGURE 17-15. SEMISCALE TEST S-LH-1; INTACT LOOP ECC FLOW RATE.

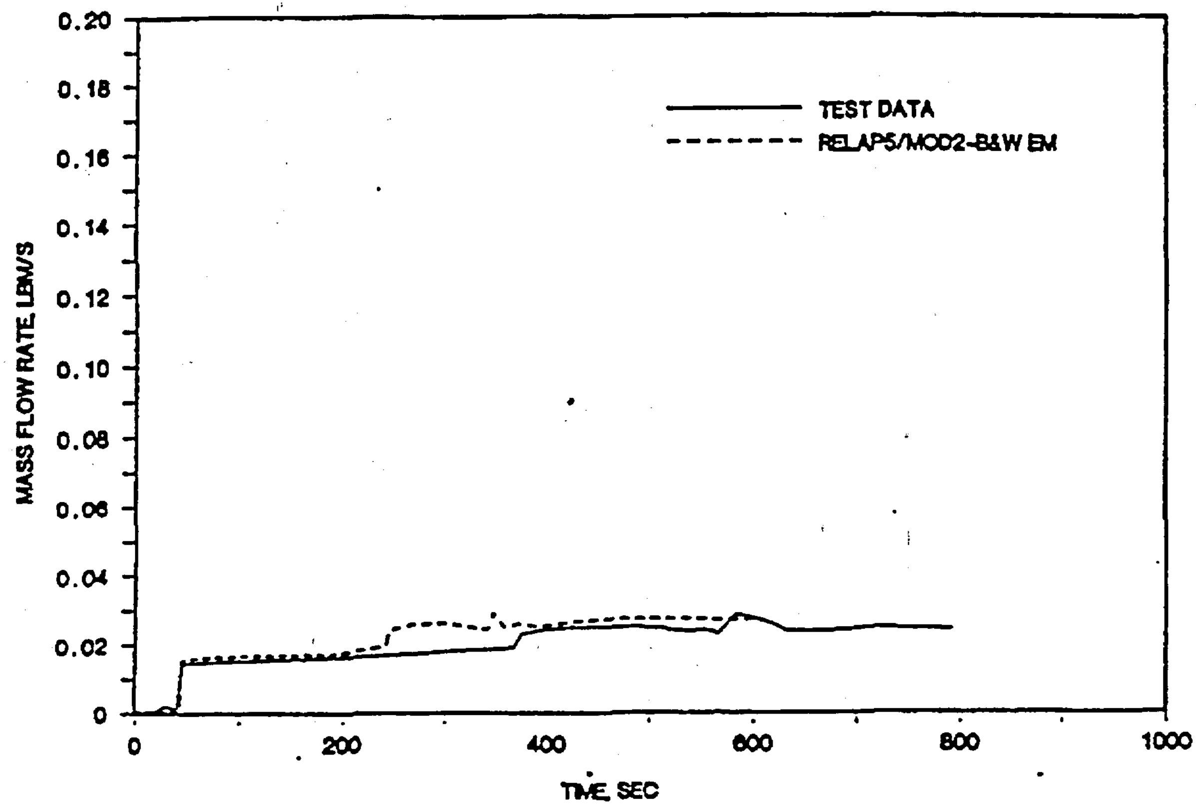

FIGURE 17-16. SEMISCALE TEST S-LH-1; BROKEN LOOP ECC FLOW RATE.

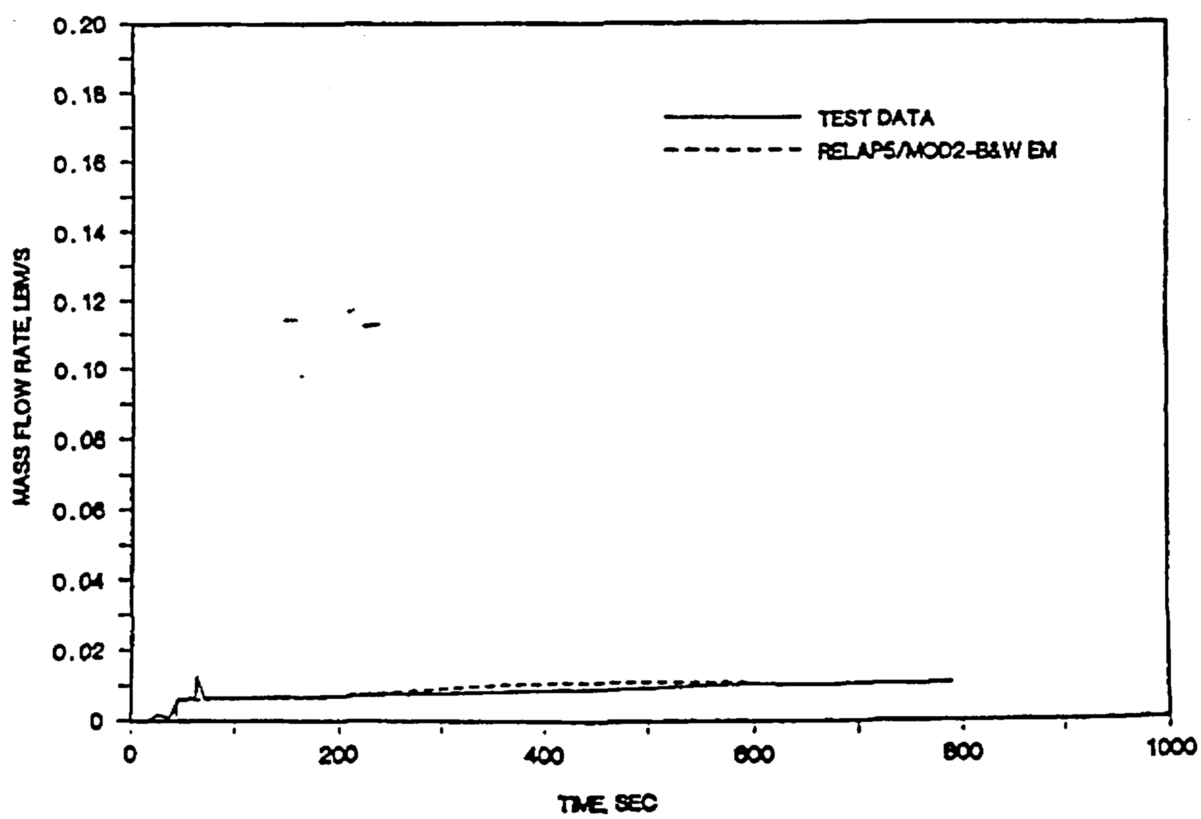

18. Question: In BAW-10168P, B&W Loss-of-Coolant Accident Evaluation Model for Recirculating Steam Generator Plants, B&W stated that the SBLOCA methodology would be applied to breaks up to approximately 1 ft^2. The one SBLOCA assessment provided for review by B&W was LOFT Test L3-5. The break in LOFT Test L3-5 was equivalent to a break size of approximately 0.1 ft^2 in a PWR. Because of the factor of ten difference between the break size analyzed and the largest break size to be analyzed, provide a RELAP5/MOD2-B&W assessment calculation where the break size analyzed is approximately 1 ft^2.

Response: For small breaks, the reactor vessel does not empty, and the LBLOCA phenomena such as ECC bypass, reactor refill (adiabatic heatup period), and reflooding do not occur. Based on experience, B&W selected the 1.0 ft^2 break as a transition point in switching EM methodology. This is consistent with the criterion employed by Westinghouse. Furthermore, over a sustained period of time, Westinghouse has shown that this break size is not the limiting case in either the large or small break LOCA category. As such, B&W believes it is not necessary to perform a demonstration analysis of a 1 ft^2 SBLOCA case.

5.2 Responses to Round 2 Request for Additional Information

This section contains round two questions transmitted to B&W by M.W. Hodges of the NRC in his letter of March 23, 1989 and responses transmitted to the NRC in letters from J. H. Taylor of B&W dated May 11, 1989 and July 20, 1989.

1. Question: The following questions are related to the response to Question 10 in the discussion of the sources of the fuel behavior models added to RELAP5/MOD2-B&W.

   a. The response provided the sources of the gap conductance, clad deformation and metal-water reaction models, but did not provide calculations to verify proper implementation of the models in the code. Provide the results of calculations that demonstrate these models are properly implemented.

   Response: Demonstration of proper implementation of computer models is available in the code predictions and benchmarks that have been supplied within the evaluation model topical reports and in the code certification documentation maintained at B&W. The topical studies provide overall validation of the code and any changes made to it including model interactions. These are already available for review in the topicals. The code certification process provides detailed validation of model implementation on a model by model basis. All models that B&W incorporates into its computer codes are implemented in accordance with B&W procedures for computer code development and certification. The B&W procedure for certification requires that a change be: 1) described in a change specification document. 2) be verified by independent calculations of the coded results (usually manual calculations performed on a time step per time step basis). 3) have the verification calculations independently reviewed and approved for accuracy, comprehensiveness, and conclusions. 4) have all steps documented in files stored permanently at B&W. The process and the files are subject to audit by the B&W quality assurance organization and NRC audit teams. Because of the detail involved in the files, it is not considered practical to publish the results; however, the files are readily available and open for audit at the B&W offices at any time. B&W believes that the procedure and filing of detailed results is sufficient to assure that the code models, as described in the topical reports, are properly implemented.

The following is additional information regarding the implementation of the Baker-Just correlation in RELA5/MOD2-B&W.

Equation 2.3.2-58 in RELAP5/MOD2-B&W is derived based on the Equations 10, B5a and B5b in Reference 120 of BAW-10164. To obtain Equation 2.3.2-58, the plane geometry assumption in Equation 10 is replaced by the cylindrical geometry assumption using Equations B5a and B5b. Equation 2.3.2-58 is reduced to the equation for a plane geometry as given by the Equation 2.2.2-60 which is essentially the same as the Equation 10 in the Reference 120. Equation 10 is also the starting point for the metal water reaction Equation 2.2.2-1 in FRAP-T6-B&W.

The method used in RELAP5/MOD2-B&W to solve the differential equation (Equation 10) is slightly different from the one used in FRAP-T6-B&W. In RELAP5/MOD2-B&W it is assumed that

$$-dx/dt = \psi(t) \;/\; (x_o - x)_{old} ,$$

where $\psi(t)$ represents the remaining terms in Equation 10.

On the other hand, FRAPT6-B&W assumes that

$$dx^2/dt \quad = \psi(t).$$

It is to be noted that the method used in RELAP5/MOD2-B&W is consistent with that used in CRAFT2 and the method used in FRAPT6-B&W is consistent with that used in THETA1B.

b. On comparison of the equations in RELAP5/MOD2-B&W to the source codes, a possible units problem was noted in Section 2.3. On page 2.3-35, the cladding hoop stress is defined in units of kpsi. However, the units for Eqn. 2.3.2-18 would give the hoop stress in units of Pa. Clarify this discrepancy.

Response: As stated in the question, there is an inconsistency in the unit for the hoop stress σ_h in Equations 2.3.2-17 and 2.3.2-18. The inconsistency is in the topical report not in the code. In the code, the hoop stress calculated using Equation 2.3.2-18 is divided by $6.894757*10^6$ (to convert Pa to kpsi) before it is used in Equation 2.3.2-17. In order to make the unit for σ_h consistent in these two equations, Equation 2.3.2-18 should be written as

$$\sigma_h = C_p \left(P_g \, r_{ic_{cold}} - P_f \, r_{oc_{cold}}\right) / \left(r_{oc_{cold}} - r_{ic_{cold}}\right)$$

where

$$C_p \quad = 1/6.894757*10^6,$$

and the other variables are defined in the topical report.

This modification to Equation 2.3.2-18 will be made in the next revision to the topical report.

2. Question: The following questions are regarding the new assessment calculation for Semiscale Mod-1 Test S-04-6 provided in response to Question 12.

a. The EM and BE calculations over-predicted the system depressurization rate and the peak cladding temperature. Clarify if the PCT would still be over predicted if the calculated pressures matched the measured pressure.

Response: From Figures 12.32 and 12.33 in Round-1 question 12, it can be seen that the main reason for the EM calculation of higher cladding temperature is the prediction of the early CHF. In the EM calculation the CHF occurred within 0.2 seconds whereas in the test CHF occurred at about 3 seconds after the initiation of the transient. From Figures 12.8 and 12.9 it can be seen that during the first 3 seconds of the transient the code predicted the core pressure response reasonably well. Therefore the over-prediction of the cladding temperature in the EM calculation will not change even if the calculated pressure matched the data during the later part of the transient.

In an attempt to match the calculated pressure response with the data, the EM case was rerun using CD = 0.4 during the two phase and steam blowdown period. It is to be noted that CD = 0.6 was used in the EM calculations given in the response to question 12. From Figure 2.1 it can be seen that the code calculated pressure response agreed reasonably well with the data. The calculated cladding temperature is lower than the CD = 0.6 case during the later part of the transient, as shown in Figure 2.2. However, it is still much higher than the data. All other parameters, except the density near the core inlet, Figure 2.3, showed similar behavior as in the CD = 0.6 case. From about 7.5 seconds to 14 seconds the CD = 0.4 case calculated density was higher than the data. During this period the intact loop cold leg (ICL) flow rate was higher than the broken loop cold leg (BCL) flow rate. The excess flow from the ICL flowed down to lower plenum through the downcomer. As a result of the flow reversal in the downcomer, high density fluid from the lower plenum entered the core inlet volume (volume 335). It is to be noted that the code calculated density is a volume average density in the lower plenum (volume 235 in Figure 12.3) where as the measurement is at a local point.

From this study it can be concluded that the EM would calculate higher cladding temperatures than the data even if the correct depressurization rate is calculated. A similar trend is expected in the BE calculation even though the difference between the calculated and the measured cladding temperature would be much smaller.

b. The response noted the EM and BE RELAP5/MOD2-B&W calculations predicted a faster decrease in the pressurizer liquid level (Figure 12.13) than the data and stated this was consistent with the system pressure response. The response, however, does not explain why the level decreases were different. Clarify why the calculated and measured levels were different.

Response: The faster decrease in the calculated pressurizer level shown in Figure 12.13 was primarily caused by the pump side break flow rate shown in Figure 12.15. From Figure 12.15 and 12.17 it can be seen that during the early part of the transient the flow in the broken loop hot leg is higher than the data. As a result, the intact loop hot leg flow rate is lower than the data as shown in Figure 12.16. From Figure 12.19 it can be seen that the intact loop cold leg flow rate is in reasonable agrement with the data. This flow is mainly controlled by the pump. The lower intact loop hot leg flow rate caused the pump to pull additional flow from the pressurizer.

c. The response stated the calculated upper plenum to hot leg flows (Figures 12.16 and 12.17) were biased towards the broken loop over the intact loop due to relative differences in the depressurization rates between the two hot legs. B&W also noted that a flow reversal in the broken loop hot leg at 1 s observed in the test was not calculated in either analysis. Clarify the reasons for the differences between the measured data and the calculated results.

Response: The difference between the calculated flow rates and data in the intact and the broken loop hot legs is mainly due to the over-prediction of the pump side break flow as discussed with the response to question 2b.

d. The oscillations in the calculated EM break flow after 2 s (FiguPe 12.14) were attributed to the critical flow switching logic between the Extended Henry-Fauske and Moody models. Was the same switching logic used in the original Test S-04-6 calculation? If so, why were the oscillation only seen in the new S-04-6 calculation? Also Section 4.3.4.1 of BAW-10168P discussed an EM method of smoothing the transition from the Extended Henry-Fauske model to the Moody model using a linear weighting technique over the very low quality range. Clarify if this technique was used and, if so, clarify why it was not effective in providing a smooth transition between the critical flow models.

Response: The main cause for the oscillations in the EM calculated vessel flow rate, shown in Figure 12.14, from 2 to 4 seconds after the initiation of the transient was due to the use of CD = 1.0 for subcooled and CD = 0.6 for the saturated and two phase break flow conditions. Even though the extended Henry-Fauske and the Moody correlation flow rates are made continuous at the transition boundary, the use of a smaller CD value for the Moody calculated flow rate causes the flow discontinuity at the transition point. The discontinuity in the CD along with the criteria used to switch between the two correlations, as explained in question 12, caused the flow to oscillate for about 2 seconds. After about 4 seconds the flow remained two-phase and the calculated flow rate was smooth.

In the EM applications the same CD value is used with the extended Henry-Fauske and the Moody break flow correlations. Therefore, these flow oscillations will not be present in the EM calculations.

It is to be noted that the method used to smooth the flow rate at the transition point is different from that given in Section 4.3.4.1 of the EM topical report BAW-10168. Instead of linear weighting, an under relaxation of velocity as described by the equation 2.1.4-47 of RELAP5/MOD2-B&W topical report BAW 10164 is used. This is further discussed in response to question 12 of the first set of questions on the EM topical report BAW-10168.

e. An early decrease and subsequent oscillations in the density near the vessel side break in the EM calculation from 1.5 to 5 s were attributed to the switching in the choked flow model (See Figure 12.23). During the oscillatory period from 1.5 to 5 s, the EM calculated density showed an increasing trend that contributed to the good agreement between the EM calculation and the test data after 5 s. Was this increasing trend also caused by the switching in the choked flow model? If so, was the good agreement after 5 s fortuitous because the switching in the choked flow model is an unphysical condition? If not, clarify why the density increased in the EM calculation. Because the early density decrease was also calculated in the old EM analysis (and the BE calculation), clarify further how the early decrease was caused by the switching logic.

Response: The causes for the vessel side break flow oscillations during the 1.5 to 3.5 seconds transient period(Figure 12.14) are the discontinuities in the break flow at the subcooled to saturated transition boundary as discussed with the response to question 2d. As a result of these discontinuities, the density near the vessel side break shows similar oscillations during this period (Figure 12.23). Once the break flow condition stabilizes and becomes completely two phase (after about 5 seconds) the break flow and the density near the break show smooth behavior. The good agreement between the density calculation and the data after 5 seconds is not fortuitous, but caused by accurate code predictions after the calculated flow regime passes the transition zone and becomes two phase. This result shows that for the test S-04-6 two different CD values have to be used with the EM break flow model, in order to calculate the correct system behavior. The flow behavior in the transition zone could be made smoother if the CD in the transition zone is made continuous. It is to be noted that the two CD values in this test simulation are used to match the break flow boundary condition with the data. In the EM applications, the same CD value is used during subcooled, two phase and single phase vapor flow conditions. Therefore, the discontinuities in the break flow and the density near the break will not exist in the EM calculations.

f. Better cooling of the cladding after 12 s in the EM calculation as compared to the BE calculation was related to differences in core flow and the higher cladding temperatures in the EM calculation. Provide additional information on calculated heat transfer coefficients, heat fluxes, etc., to support the discussion in the response.

Response: In the EM calculation of Semiscale test S-04-6, the better cooling of the cladding after 12 seconds (Figures 12.32 and 12.33 of Round-1 question 12 related to RELAP5/MOD2-B&W topical report 10164) as compared to the Cycle 36.04 calculation was related to differences in core flow and higher cladding temperatures in the EM calculations.

From Figures 12.32 and 12.33 it can be observed that the EM calculated cladding temperatures are higher than the Cycle 36.04 calculation. Figure 2.4 shows the calculated core flow rates near the peak power location in the hot channel. It can be seen that after about 12 seconds the EM flow rate is generally larger than that of Cycle 36.04. As a result, the EM calculated a higher heat transfer coefficient than the Cycle 36.04 prediction as shown in Figure 2.5. The higher wall temperature and higher heat transfer coefficient prediction in the EM calculation results in a higher heat flux prediction than Cycle 36.04 as shown in Figure 2.6. The prediction of higher heat flux after 12 seconds in the EM calculation caused better cooling of the cladding as shown in Figures 12.32 and 12.33.

FIGURE 2.1. SEMISCALE MOD1 TEST S-04-6; PRESSURE IN THE LOWER PLENUM.

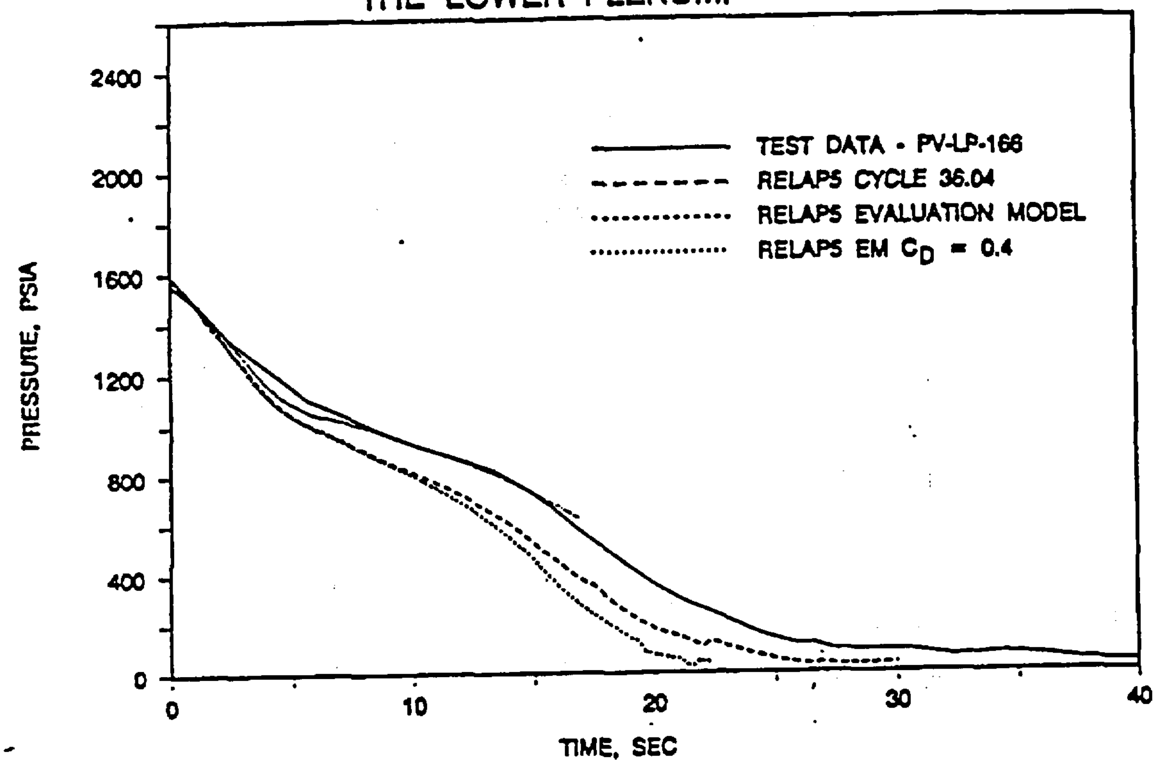

FIGURE 2.2. SEMISCALE MOD1 TEST S-04-6; HIGH POWER ROD CLAD TEMPERATURE NEAR THE PEAK POWER LOCATION.

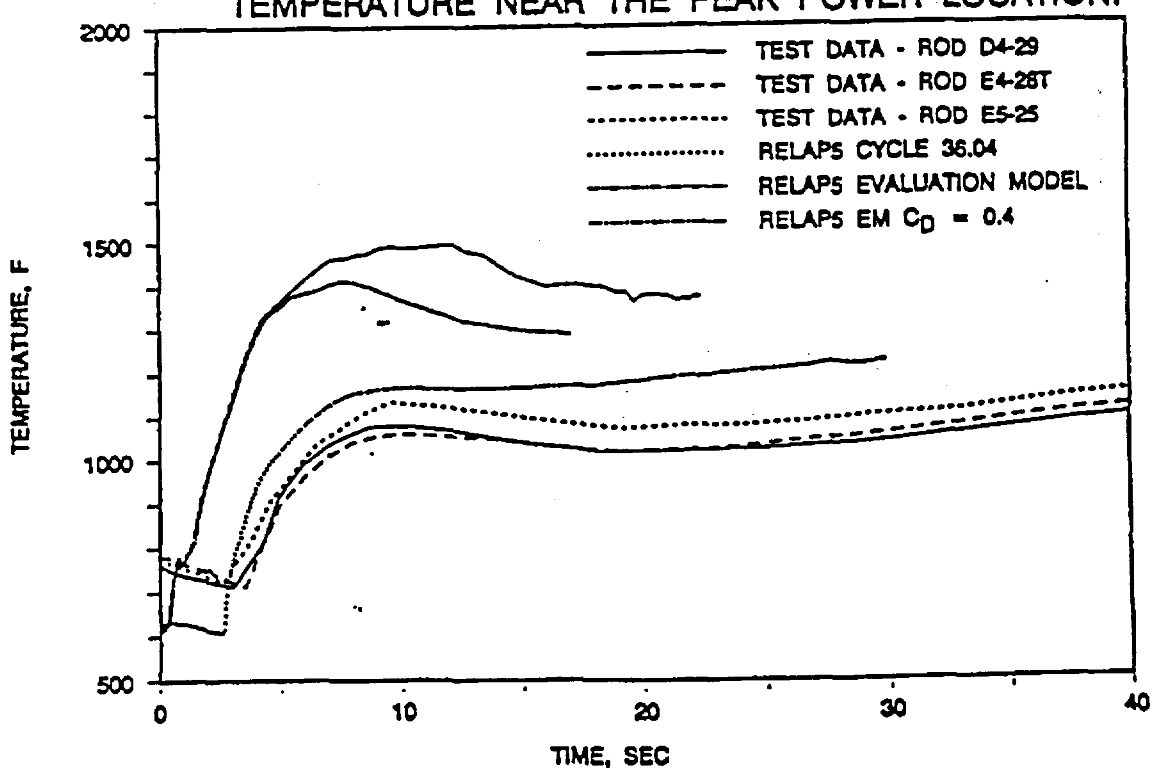

FIGURE 2.3. SEMISCALE MOD1 TEST S-04-6; DENSITY NEAR THE CORE INLET.

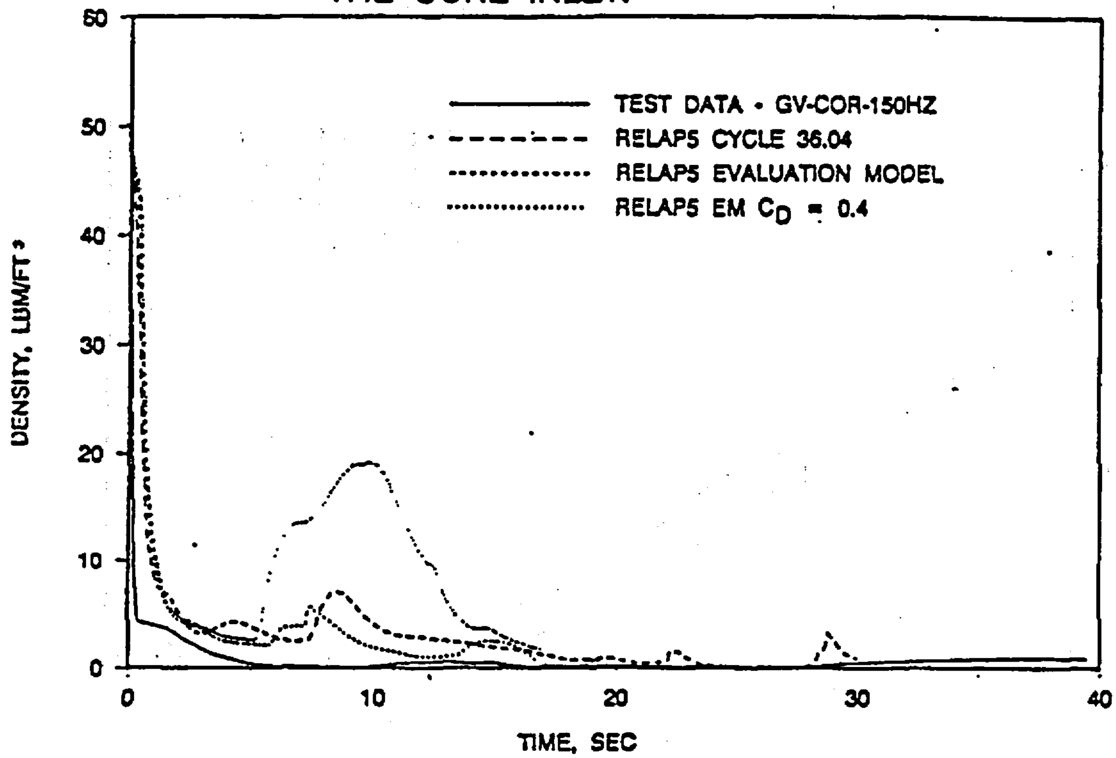

FIGURE 2.4. SEMISCALE MOD1 TEST S-04-6; MASS FLOW RATE IN THE HOT CHANNEL AT THE HIGH POWER LOCATION.

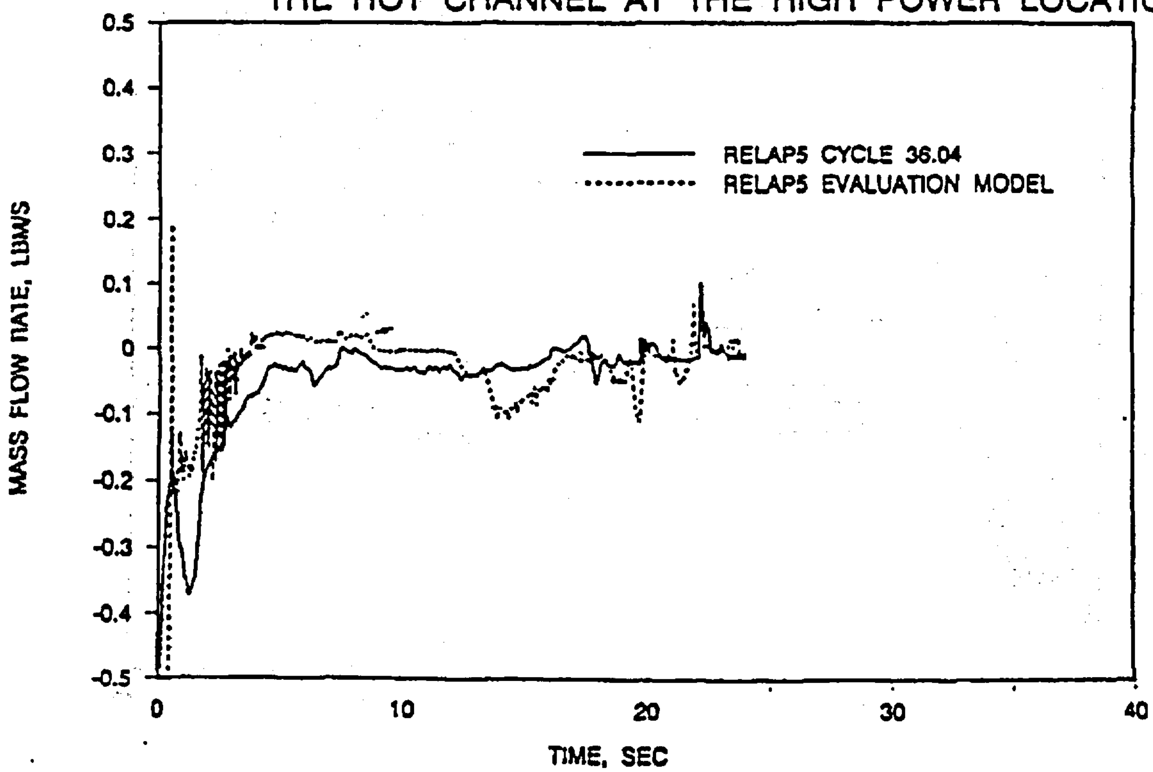

FIGURE 2.5. SEMISCALE MOD1 TEST S-04-6; HEAT TRANSFER COEFFICIENT IN THE HOT CHANNEL AT THE HIGH POWER LOCATION.

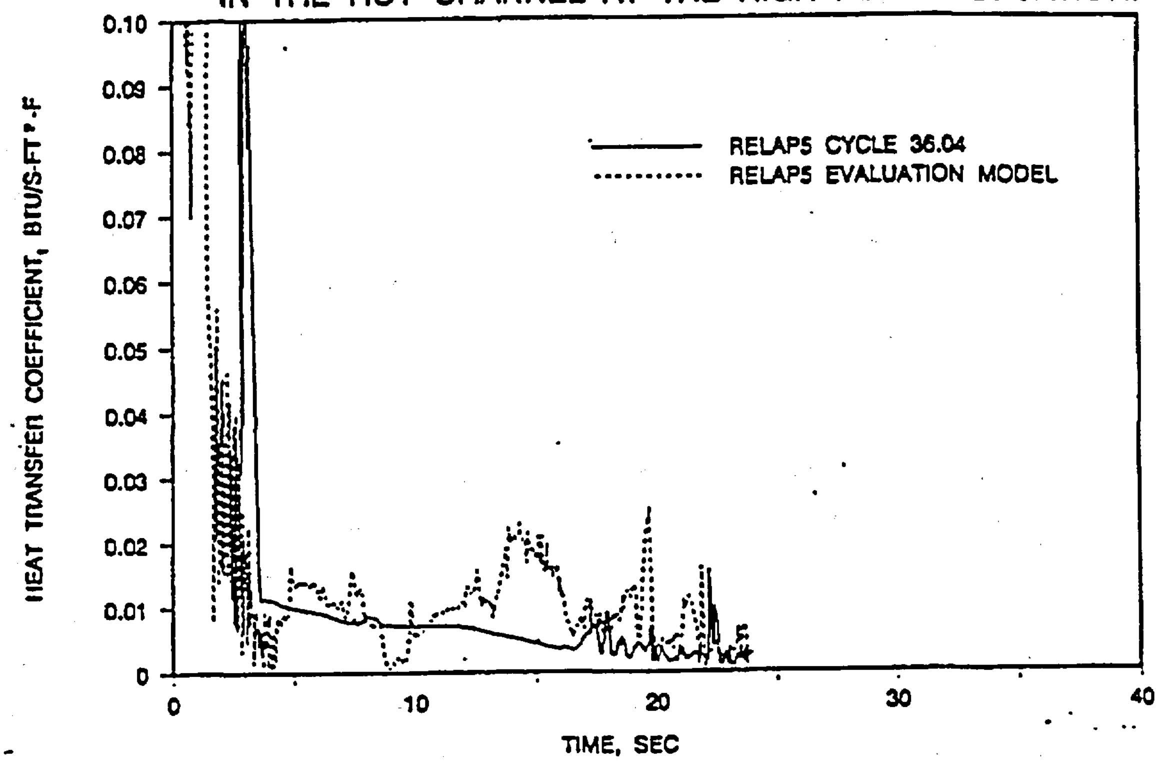

FIGURE 2.6. SEMISCALE MOD1 TEST S-04-6; HEAT FLUX IN THE HOT CHANNEL AT THE HIGH POWER LOCATION.

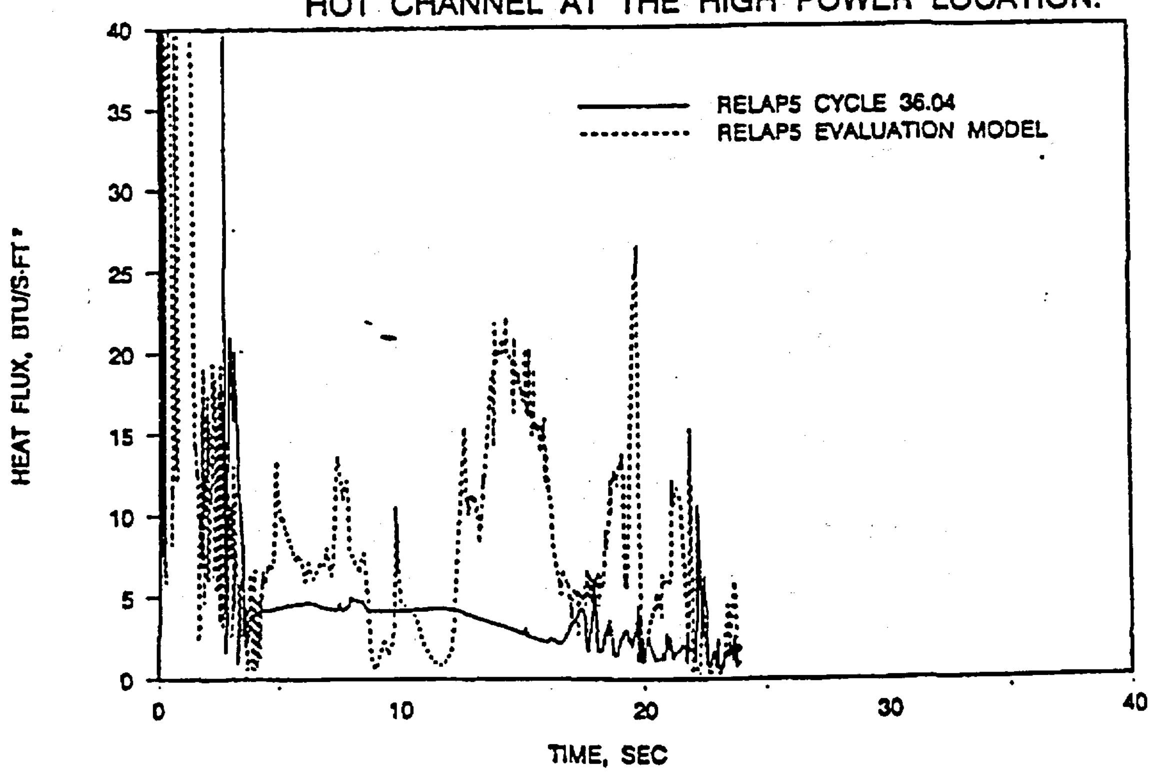

3. The following questions are related to the information provided in the response to Question 14 on LOFT L3-5 benchmark calculation.

a. For several of the parameters presented, the differences between the calculated and measured results were related to the underprediction of the break flow in the RELAP5/MOD2-B&W calculation (see Figure 14.5). Clarify why the break flow was under-predicted.

Response: The purpose of the LOFT L-3-5 benchmark analysis presented in Appendix G Section 2 of BAW 10164P is to demonstrate that the B&W version of RELAP5/MOD2-36.04 can adequately predict the small break phenomena observed in the L-3-5 experiment. Although this version is not used for the licensing application, it is important to establish a baseline for the development of the SBLOCA EM. As discussed in Appendix G Section 2, the Ransom-Trapp discharge model in RELAP5/MOD2-36.04 under-predicted the two-phase discharge flow rate. As a result, the calculated primary system inventory is higher than the experiment, and the primary system depressurization is slower for the RELAP5 calculation than for the experiment.

B&W has reanalyzed the L-3-5 experiment with the EM discharge models using discharge coefficients of 1.0 and 0.6 respectively for subcooled and saturated blowdown. In addition, the core bypass resistance from the inlet annulus to the upper plenum region is reduced to achieve approximately 6.1% bypass flow (estimated bypass flow rate is 6.6% per EGG-LOFT5480). The original analysis has approximately 4.4% bypass flow. The results of this reanalysis form the basis for the response to this question.

The blowdown was initiated 4.8 seconds after the reactor scram as shown in Table 3.1. The RC pump trip, main feedwater isolation, and auxiliary feedwater initiation are identical to the original analysis presented in Table G.2-2. A comparison of the timing of events during the early phase of the blowdown between the two cases shows good agreement. This confirms the consistent subcooled leak flow calculations between the B&W EM and Ranson-Trapp discharge models. As the primary system enters the saturated discharge phase, the discharge rate between the two models vary substantially. The EM discharge model calculates a higher leak flow rate then the measurements as shown in Figure 3-1. The effects of a higher leak flow rate are reflected in the primary system depressurization rate and normalized mass inventory presented in Figures 3-2 and 3-3 respectively. Although the experimental data for the leak flow during the early phase of the blowdown are not available, Figure 3-3 seems to indicate that the calculated subcooled leak flow is higher than the test data.

A comparison of the calculated hot leg and cold leg densities with those of the experiment shows that RELAP5 can correctly calculate the primary system mass distribution. Water in the hot leg drained at approximately 600 seconds as shown in Figure 3-4. As a result of the higher leak flow calculated by the EM discharge model, water in the cold leg pipe drained earlier than the experiment as shown in Figure 3-5. This causes a sudden reduction in the leak flow rate at 670 seconds as the fluid density changes drastically following the draining.

The secondary side pressure exceeds the primary side pressure at 707 seconds, approximately 43 seconds earlier than the experiment due to the higher depressurization rate calculated by the EM discharge model. This leads to a loss of natural circulation and is conservative for the SBLOCA analysis.

The results of the analysis demonstrate that RELAP5-MOD2-B&W can adequately predict the important phenomena observed in the L-3-5 experiment such as pressurizer draining, pump coastdown, natural circulation, ECC injection, loss of natural circulation, hot let draining, and long-term cooling. Furthermore, the comparison plots confirm that B&W's SBLOCA evaluation model is conservative in predicting the overall system thermal hydraulic responses to a small break LOCA.

b. The response also stated that the pump in the RELAP5/MOD2-B&W calculation had a faster coastdown than the pump in the test because of greater reverse flow fluid torque acting on the pump in the calculation during the coastdown period, and that the faster reverse flow torque was due to the larger break flow calculated. The connection between the reverse flow fluid torque acting on the pump and the break flow rate is not clear. Clarify how the break flow affected the pump performance. Also, in Figure 14.5, the measured break flow during the pump coastdown period (approximately the first 30 s) is not shown. How was the conclusion reached that the calculated break flow was larger than the measured break flow during this period?

Response: The response to question 14-3 with regard to the pump coastdown was inaccurate. The break flow has only a slight effect on the RC pump coast down. The difference in pump coast down appears to be due to the pump descriptive data used in the analysis. The initial several seconds of coast down are governed by the moment of inertia and the frictional torques of the pump and motor. Fluid interactions with the pump during small breaks do not contribute significantly. In order to predict the coast down observed in the test, the reported moment of inertia must be increased by a factor of 4 to 5 or the frictional torques reduced by the same factor. A comparison of the moment of inertia reported for the LOFT facility to a typical RC pump value shows that the moment of inertia of the LOFT pump is 0.0001 that of a full sized pump. This small a value is surprising in light of the scaling of the LOFT facility. At present B&W can only speculate along the line described to explain the pump behavior in the L-3-5 test prediction.

As discussed in the response to part a of this question, the lack of experimental data in the first 30 seconds of the transient and the uncertainty associated with the measurements available, make it difficult to confirm that the calculated leak flow is higher than the experiment. However, the comparison of the primary systems mass inventory logically leads to that conclusion.

Table 3.1. Sequence of Events for LOFT L-3-5 with EM Discharge Models

Events	Time (sec) Experiment	RELAP5/MOD2 with EM Discharges
Reactor scrammed	0.0	0.0
LOCA Initiated	4.8	4.8
RC Pump Tripped	5.6	5.6
HPIS Initiated	8.8	9.3
Pressurizer Emptied	27.0	39.0
RC Pump Coastdown	35.0	20.0
SG Auxiliary Feedwater Initiated	67.8	67.8
Secondary side Pressure Exceeded Primary Side	749.8	706.6
SG Auxiliary Feedwater Terminated	1804.8	----
Leak Isolation	2313.9	----

FIGURE 3-1. LOFT TEST L-3-5, LEAK FLOW RATE.

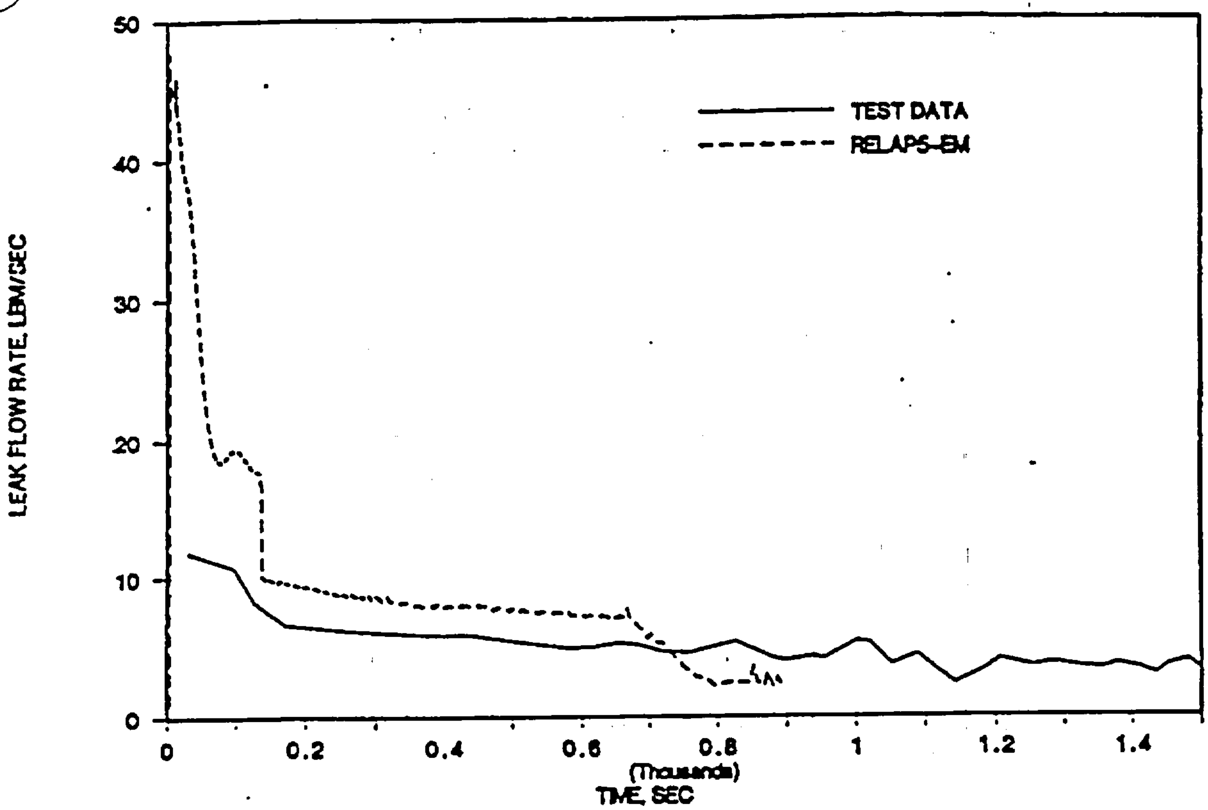

FIGURE 3-2. LOFT TEST L-3-5, LEAK NODE PRESSURE.

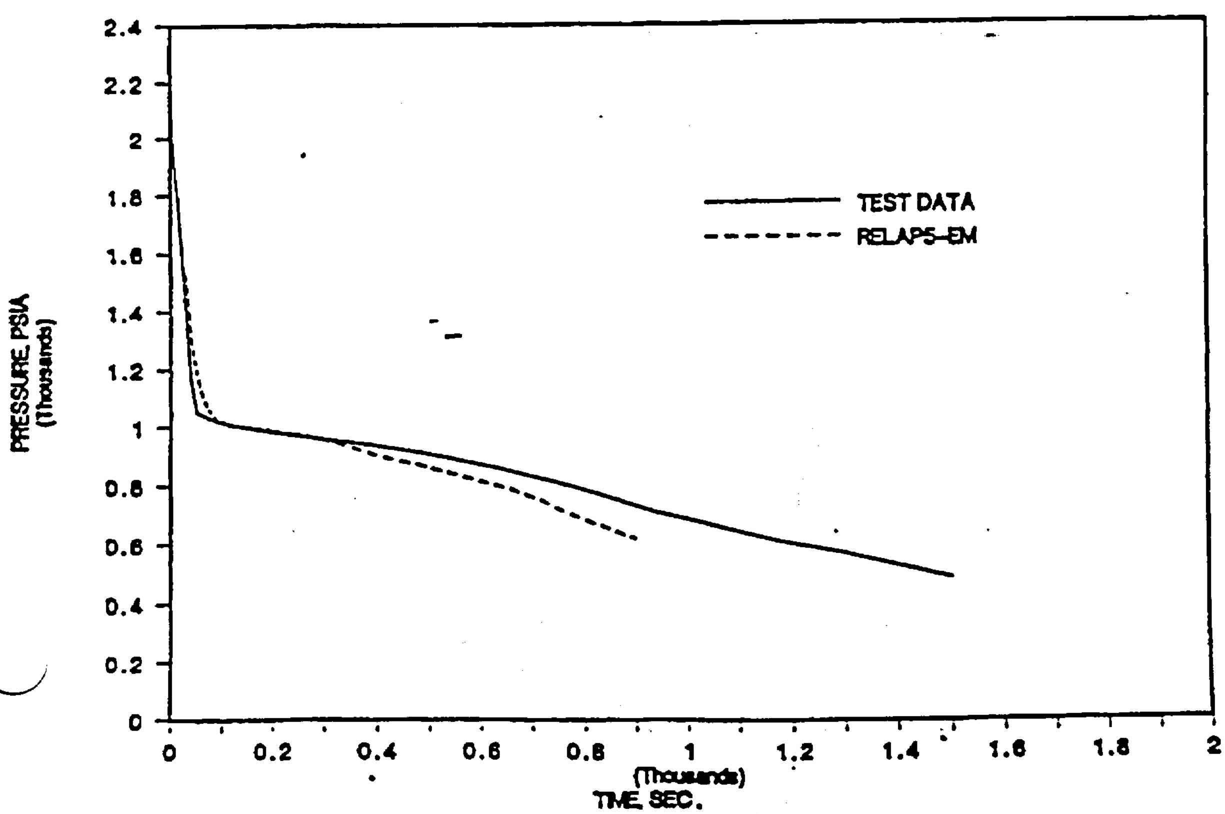

FIGURE 3-3. LOFT L-3-5, NORMALIZED RCS INVENTORY.

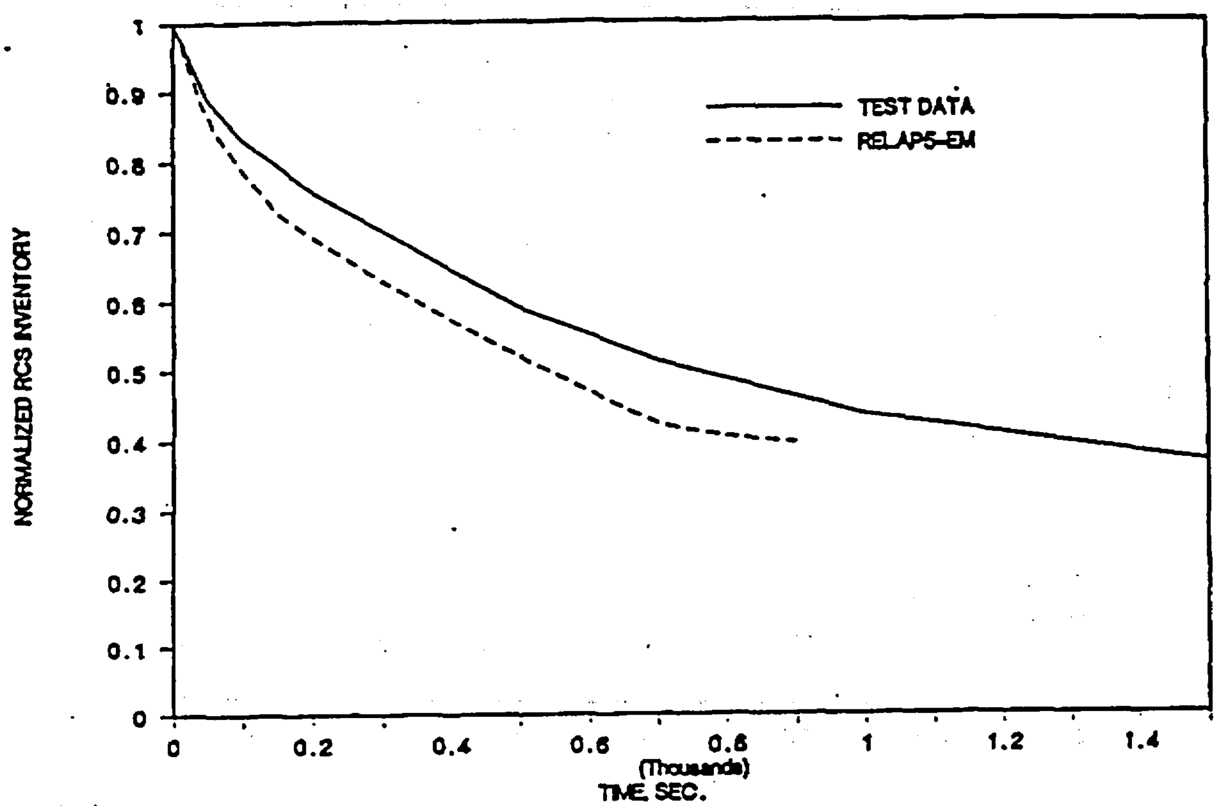

FIGURE 3-4. LOFT TEST L-3-5, HOT LEG DENSITY.

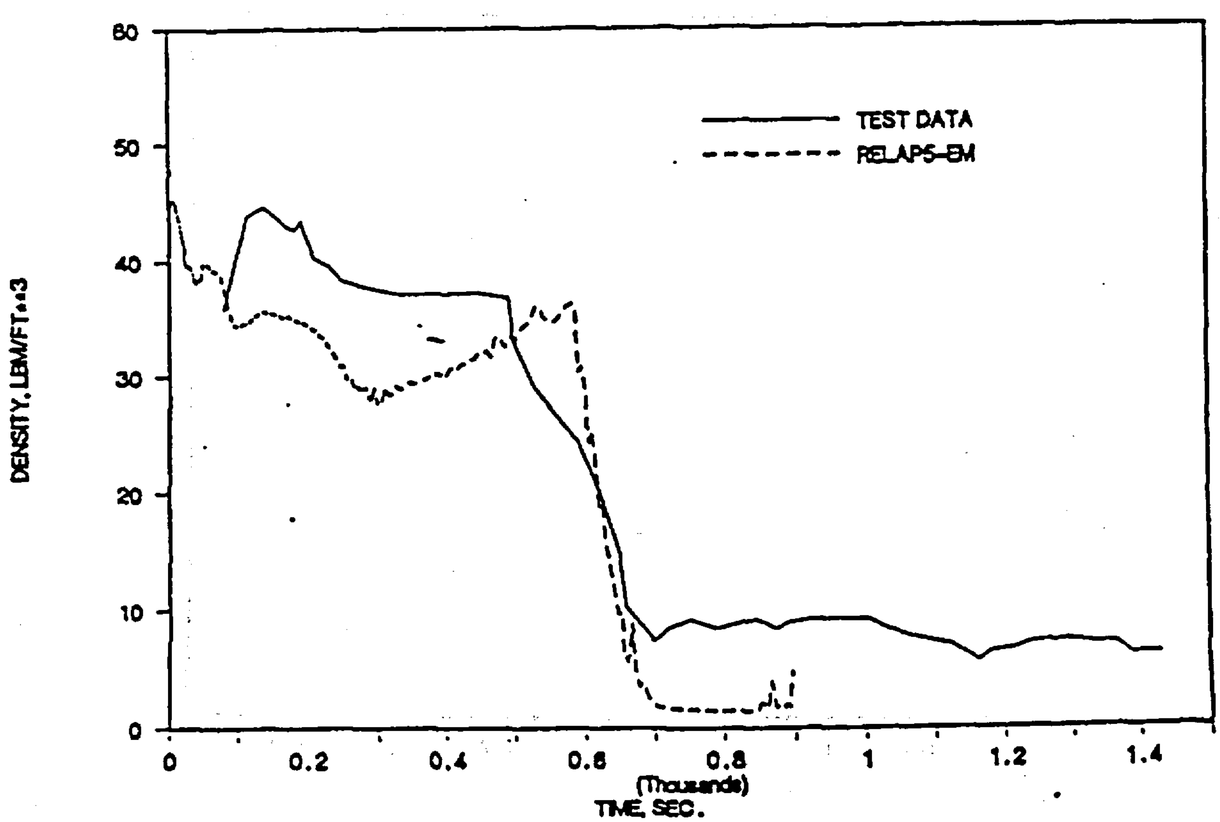

FIGURE 3-5. LOFT TEST L-3-5. COLD LEG DENSITY(PUMP DISCHARGE).

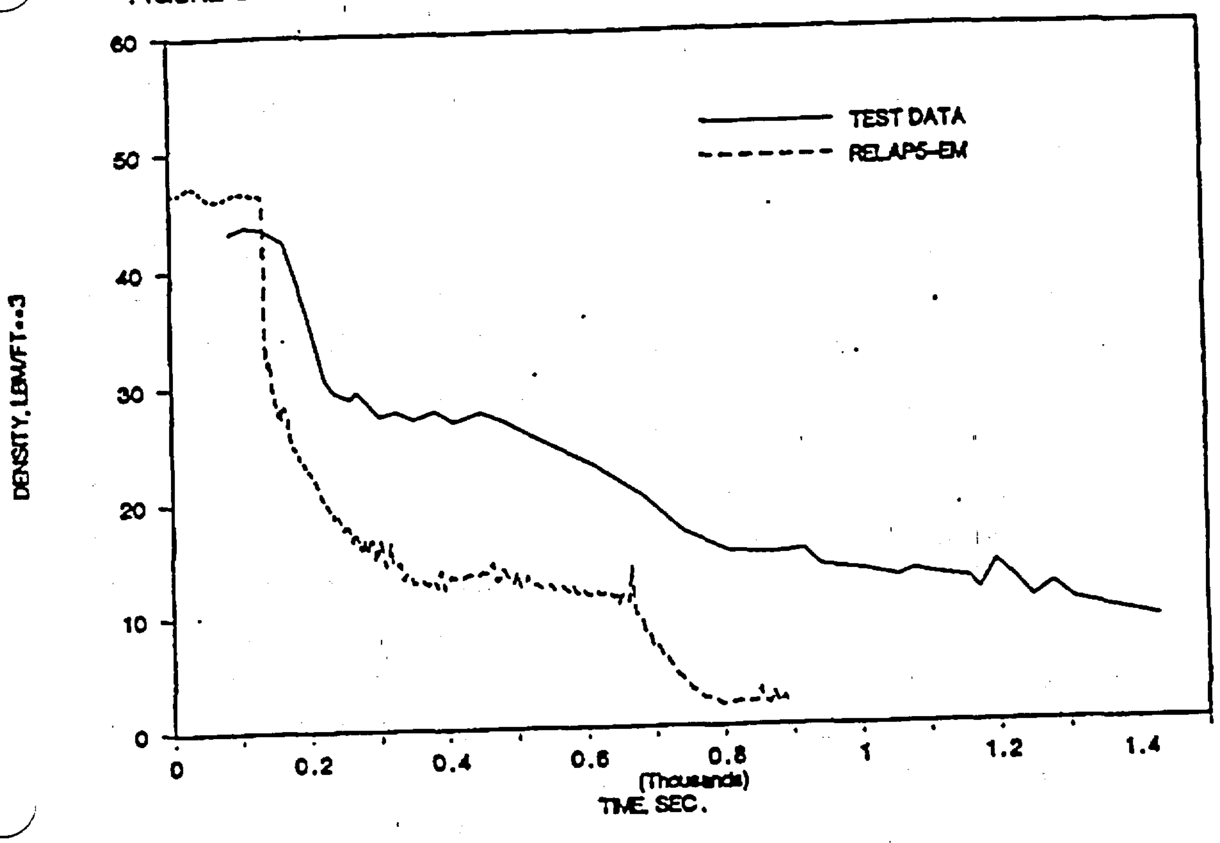

4. The following questions are related to the response to Question 16 regarding how RELAP5/MOD2-B&W meets the requirements of NUREG-0737, Item II.K.3.30.

a. The response stated that the RELAP5/MOD2 calculations of OTIS and MIST tests demonstrated the code was capable of properly predicting SBLOCA phenomena, and that the results showed the primary system pressure and mass inventory were well predicted. However, no comparisons were provided. Also, the OTIS and MIST tests were performed with the once through steam generator geometry of B&W plants whereas the RELAP5/MOD2-B&W is intended for use for plants with recirculating steam generators. Provide additional benchmark results for facilities with a RSG design to demonstrate the LOCA evaluation model and RELAP5/MOD2-B&W'S ability to calculate small break phenomena with RSG plants.

Response: A SBLOCA transient is characterized by a relatively slow depressurization of the RCS. It begins with subcooled blowdown to saturation pressure followed by saturated depressurization for an extended period of time. Following the RC pump trip, the primary system undergoes a transition from forced flow to natural circulation, and distinct liquid levels are developed in the reactor vessel and in portions of the primary loops. Manometric balances are developed in the primary system while the core decay heat is removed via the break, natural circulation, and reflux boiling. As the core liquid level continues to decrease, the hydrostatic balance causes clearing of the pump suction loop seals. The primary system liquid inventory continues to decrease until the ECCS overcomes the leak flow. The phenomena involved are generally common to both RSG and OTSG plant designs (excepting reflux boiling) and demonstration of code capabilities can be extended from one design to the other. The ability of RELAP5/MOD2-B&W to correctly predict these key phenomena and associated parameters is demonstrated by the results of benchmark analyses on three different facilities MIST (OTSG) test 320503, Semi-scale (RSG) S-LH-1 and LOFT (RSG) L-3-5.

Although the MIST facility represents a scaled B&W NSSS, and the performance of the OTSGs and its impact on natural circulation are not directly applicable to the RSG plant, the primary system inventory and depressurization rate are primarily controlled by the break size. The predictions of the primary system inventory and mass distribution within the primary system for the MIST test are applicable to any plant configuration. The benchmark of MIST test 320503 and the other benchmarks contained in reference 4.1 demonstrate RELAP5/MOD2s ability in fluid tracking, phase distribution, and heat removal through the natural circulation period and into the steam water separated boiling pot period.

The issue of the effects of the steam generator performance on natural circulation and reflux boiling is addressed by the benchmark of Semiscale test S-LH-1. As discussed in the response to question 17 of the round one questions on RELAP5/MOD2-B&W and question 5 of this question set, the results demonstrate the code's ability to correctly predict the SBLOCA transient. In addition, fluid velocities in the uphill side of the steam generators are provided, in response to question 5, to demonstrate that the code calculates natural circulation and reflux boiling during the period when the steam generators are effective. Figures 10-1 and 10-2 (round one questions on RELAP5/MOD2-B&W) show liquid and vapor velocities in the uphill side of the steam generator tubes. The negative liquid velocity (fall back) indicates the reflux mode cooling. No experimental data are available for comparison.

b. In discussing RELAP5/MOD2-B&W's ability to calculate the effects of non-condensible gases on the system response, the addition of a model to calculate surface condensation in the presence of a non-condensible was discussed. Benchmarking of this model against separate effects tests was also discussed by referencing a paper presented at the Eighth International Heat Transfer Conference in 1986 without providing the results. Provide appropriate results from this paper. Also, provide results which verify the code's ability to calculate the effects of non-condensibles on the overall system responses, including system pressure, heat transfer, natural circulation, and non-condensible transport, etc.

Response: The reference paper presented at the Eighth International Heat Transfer Conference is attached. The benchmark results of the separate effects tests demonstrate that RELAP5/MOD2-B&W is capable of handling the effect of noncondensible gas on surface condensation. However, the volume of noncondensible gas that can be trapped in the primary system during small break LOCA (SBLOCA) is too small to impact steam generator performance in the liquid natural circulation, two-phase natural circulation, or reflux boiling modes. Thus, the effects of noncondensible gas are not directly considered in the analysis. The remainder of this response deals comprehensively with the impact of noncondensibles on the results of SBLOCAs in five subsections: (1) the general effects of noncondensible gas on SBLOCA, (2) potential sources of gas, (3) effects on steam generator performance, (4) gas effects on larger SBLOCAs, and (5) conclusions.

Generalized Effects of Noncondensible Gas on SBLOCA

For the purpose of discussing the impact of noncondensible gas, SBLOCAs can be considered in two groups: (1) those that require the steam generator to remove energy for a substantial period of time and (2) those that do not. After reactor trip, pump coast down, and removal of the initial core stored energy, an SBLOCA depressurizes (or not) in accordance with a balance between the energy source of the core and the energy sinks of the break and the steam generators. If break flow is insufficient to cause a decrease in the system average specific energy then the system will depressurize to the just above the secondary pressure, and the energy removal necessary to keep the system from repressurizing will be accomplished by the steam generators. If break flow is sufficient to cause a decrease in system average specific energy then the system will depressurize until the break flow and the core decay heat are in balance. This balance point may vary with time, as different energy and fluid sources (the ECCS) and sinks (generally break quality) develop, but will generally act with the decay heat to produce a gradual system depressurization as decay heat is reduced. Similarly, the first group of SBLOCAs will become independent of the steam generators as the decay heat drops.

If sufficient noncondensible gas is present to interfere with the performance of the steam generators, the first group of small breaks either will not depressurize or will repressurize depending on the timing of the appearance of the gas. LOCAs of this class may depend strongly upon the ECCS injection capability for successful termination, such that, if the resultant pressure increase significantly decreases the injection capability of the ECCS, more severe core uncovery may be experienced. As will be shown below, however, the amount of gas releasable to the RCS is so small for these accidents that it does not substantially interfere with the performance of the steam generators.

The effect of noncondensibles on the second class of SBLOCAs is a result and consequence of the design of the ECCS. As the break size increases, depressurization becomes more rapid and the pressure at which the leak and decay heat balance becomes lower. At some break size, the balance point will coincide with the initiation of flow from the low pressure (RHR) injection system. If it is also true that the flow from the RHR system is required to assure core decay heat removal, it might be possible for the nitrogen cover gas from the accumulators to pressurize the system such that the flow from the low pressure system would be momentarily cutoff. As will be shown later, although it is possible that nitrogen is injected for these types of SBLOCA, the injection is insufficient to raise the RCS pressure up to the RHR system shutoff pressure or the gas enters at such a late time that the high pressure system can supply all of the required ECCS.

Sources of Noncondensible Gas

The sources of noncondensible gas that can affect steam generator performance during SBLOCA are the dissolved gas in the reactor coolant system (including the pressurizer liquid region, the charging system, and the refueling water storage tank); the gas in the steam space of the pressurizer; the gas generated by radiolytic decomposition of the coolant; the gas in the gap and plenum volumes of the fuel; and possibly gas resulting from cladding metal-water reaction. These can become free gas within the reactor coolant system (RCS) by boiling or flashing of liquid, by alteration of the solubility of the gas in water, or by direct generation. All three processes occur, to some extent, in LOCAs, resulting in a time varying concentration of free gas within the RCS. Accordingly, most arguments that the gas is inconsequential are based on the maximum releasable amounts of gas as opposed to the actual amount of gas expected. For typical small breaks this amounts to an overprediction of the gas volume by more than 500 percent.

Acounting for all sources of gas, except hydrogen from metal-water reaction, the total volume of gas available for release within the RCS of a 4-loop Westinghouse designed plant, including one hour of radiolytic decomposition, is about 117 cubic feet at the secondary control pressure of 1150 psia and 562 F. This amounts to 29 cubic feet per steam generator or about 5.7 percent of the tube volume (assuming 10% tube plugging). If the potential for metal-water reaction is included up to the limit allowed by 10CFR50.46 (1% of the core oxidizes), the total available gas would be about 231 cubic feet at 1150 psia and 561 F. This gives 58 cubic feet per generator or about 11 percent of the tube volume (again considering 10% tube plugging). Realistically, SBLOCAs are resolved in about half an hour or less with peak cladding temperatures below 1500 F. Under these conditions, only about 10% of the water storage tank is injected into the RCS, there is essentially no metal-water reaction, and only one half of the RCS is flashed or boiled. Thus the amount of released gas is only 36 cubic feet for the system or 9 cubic feet per generator, about 1.8% of the generator tube space. Notwithstanding this, the remainder of this answer considers the maximum releasable amounts of gas.

Effect of Noncondensibles on SBLOCAs Which Require Steam Generator Heat Removal

In sufficient quantity, noncondensible gas can impede the ability of the steam generator to transfer energy. For those SBLOCAs that rely on the steam generators to remove part or most of the decay heat, an alteration of steam generator performance might seriously change the course and consequences of the accident. The steam generators remove energy by liquid natural circulation, two-phase natural circulation, or reflux boiling. Typically, an SBLOCA will proceed through all three of these phases. The reflux mode is the most significant because it is during this mode that the core has a possibility of experiencing a cladding temperature excursion. During the other two modes, the core is covered with water or a two-phase mixture. The potential impact of noncondensible gas on each of these modes of cooling is discussed below.

Liquid natural circulation is characterized by the transfer of energy from the core to the steam generator by water in its liquid state. The process may occur with steam in the system but the steam must be trapped in regions away from the circulation path since the water in the circulation path is by definition subcooled (if saturated water is present then the plant is in two-phase natural circulation). Heat exchange within the steam generators is by a convection process and will not be interfered with by the presence of noncondensible gas. The only way that such gas could interfere would be to block the circulation flow. The total amount of noncondensible gas releasable, for a plant in this mode, is 29 cubic feet at the steam generator control pressure. If released, this gas would exist as small bubbles suspended within the RSC coolant and would be circulated around the coolant loop with the coolant. Separation may occur in regions of low velocity such as the steam generator plenums, the RC pump casings, the upper downcomer, or the reactor vessel upper head. Collection in any of these regions will not interfere with circulation because if collection threatens to interfere, the gas would be swept back into the circulating system to collect elsewhere.

A worst case assumption is that the gas all collects in the steam generator tube region. The maximum amount of the tube bundle length that could be occupied by the gas is less than three feet. Under this hypothesis, the gas would be pushed to the downside of the tubes and cause a 12 percent (51 feet is the length of the average steam generator tube) reduction in the cold side driving head for circulation. This, in turn, would slow the flow quickly causing an increase in heating of the coolant in the core, compensating for the loss of cold side head. The end result would be a slightly slower circulation rate operating at a slightly wider temperature differential, but transferring the same amount of energy. The effect would be barely noticeable.

As, or if, the primary coolant system continues to loose inventory, the capability to keep the hot leg temperature below saturation and still transfer the required heat will be lost. The core will start to generate steam that will flow to the steam generators and be condensed. The return coolant from the steam generator will remain subcooled and the process continue much like liquid natural circulation. This is the beginning of the two-phase natural circulation period. Noncondensibles, if present, will continue to flow throughout the system as in liquid natural circulation. Again, a worst case assumption could be made that the noncondensibles accumulate in the middle of the steam generator tubes. The existence of the plug of noncondensibles in the middle of the generator would be compensated for in the same way as occurs in liquid natural circulation. The circulation rate would slow slightly and the hot leg would develop a higher void fraction.

As two-phase circulation proceeds, the fluid loss is such that the downside of the steam generator tubes can no longer support a column of saturated water and steam to the height of the center of the tubes. At this time the plant makes a gradual transition into the reflux mode. The upper or highest of the steam generator tubes will make the transition first and the generator will perform in a mixed mode for a period of time. The noncondensible impact is also mixed. For those steam generator tubes in two-phase circulation the impact is as described above, very little. For those tubes in the reflux mode, the impact is a reduction in the tube surface area available for condensation. The noncondensibles collect in the steam generator tubes on the tube down side and act to reduce the heat transfer. As with the other modes, and as detailed below, the volume of the noncondensibles available is so small that little impact is possible.

Full refluxing in the presence of noncondensible gas has been studied experimentally. Single tube tests[4.2] and tests performed in the Semiscale Mod 2A facility[4.3] show that the addition of noncondensible gas to an RSG results in the division of the tube length into two zones. The upstream, active zone, experiences nearly no effect from the injection of noncondensibles, while the downstream passive zone experiences nearly total heat transfer blockage. The steam generators act as if their heat transfer areas have been reduced in proportion to the gas concentration. According to tests in the Semiscale facility[4.3], gas volumes up to about 5 percent of the tube volume have no detrimental impact on steam generator performance. Gas volumes above 5 percent require gradually increasing thermal potentials to maintain full heat transfer rates.

For SBLOCAs that do not involve cladding temperature excursions above 1500 F, an assumption that there is no significant core wide metal-water reaction is reasonable, and the maximum gas volume available for release is limited to 5.7 percent of the steam generator tubes. As this is essentially the upper limit for no effect demonstrated by Semiscale, there will be no detrimental effect on steam generator performance. Should the LOCA involve higher cladding temperatures, the inclusion of a 1 percent oxidation of the core zirconium would produce a maximum gas concentration of 11 percent of the steam generator tube volume. For this concentration the Semiscale tests show a 50 psia increase in system pressure to be required to compensate for the lowered steam generator heat transfer area. Such an increase, above the steam generator control pressure of 1150 psia, would not substantially reduce the injection capabilities for the centrifugal charging and safety injection systems. Therefore, for those SBLOCAs that rely on the steam generators for partial energy removal and pressure control, the evaluation need not directly consider the consequences of noncondensible gas in the RCS.

<u>Effect of Noncondensibles on SBLOCAs Which Do Not Require Steam Generator Heat Removal</u>

As discussed previously, the larger SBLOCAs will depressurize rapidly to pressures at which an equilibrium exists between the core decay heat and the break flow. During the depressurization, such gas as is present will expand, but, since the steam generators are now a heat source rather than a heat sink, the effect on steam generator performance is beneficial. A possible adverse effect of noncondensible gas occurs for SBLOCAs that reach approximate equilibrium at pressures just below the RHR injection system dead head pressure. If mitigation of these events requires RHR flow, and if the plant accumulators were to expel nitrogen at the critical time, the gas might repressurize the system above the dead head pressure and stop RHR injection. The system would shortly bleed down and reestablish RHR injection, but, if timing were crucial, the momentary lack of RHR injection could increase the severity of the event.

The effect of accumulator discharge of nitrogen has been studied for large break LOCA in the Semiscale facility[4.4]. Depending on the amount and rate of gas discharge into the RCS, the system responded with an abrupt pressure increase followed in a few seconds by a pressure decay to a stabilized value that was 20 to 30 psi above the pre-discharge pressure. The pressure increase continued far past the end of gas injection, indicating an interference with steam condensation. By the end of the reported data, the pressure seems to be falling gradually back to the pre-injection pressure. Aside from the pressure impact, the effect of the injection of gas was to push water from the downcomer into the core and momentarily increase the flooding rate. This, in turn, slightly reduced the cladding temperatures.

These experimental results are directly applicably only for large breaks. For SBLOCA, the slower system depressurization will alter the impact of nitrogen injection. System pressure will not be increased; rather the rate of depressurization will be slowed. The interference with steam condensation will not be as noticeable as in the Semiscale tests because condensation is not a strong effect in an SBLOCA at the time of nitrogen discharge. These trends are observable in the Semiscale results in Figure 31 of reference 4.4. Here the initial pressure spike is reduced as the rate of nitrogen injection is slowed. For the slowest injection rate there is no pressure surge but only a gradual pressure increase. SBLOCA injection rates will be considerably below the slowest of rates used in the Semiscale tests.

To address the potential for an adverse impact on SBLOCA because of accumulator gas injection, the break spectrum is divided into three more parts: (1) those breaks that will depressurize to inject nitrogen but will do so only after other ECCS systems (the two high pressure systems) can assure adequate core cooling without the RHR system, (2) those events that depressurize sooner than that but which do not fall to pressures well below the shutoff head of the RHR system, and (3) those events that depressurize to pressures well below the shutoff head of the RHR injection system. The demarkation of each category will be developed and finally the characteristics of the nitrogen effects identified to show that no adverse consequences occur.

For RCS pressures around 200 psia, both the centrifugal charging system (CC) and the safety injection system (SI) have reached a runout condition with a total injection flow of about 100 lbm/s. Such an injection flow is capable of removing all core decay heat for a 3500 Mwt plant at and after 300 seconds. Also, an expansion of the nitrogen in the accumulators at constant temperature shows that the accumulator gas will not expand beyond the tank at pressures above 200 psia. Therefore, any event that takes longer than 300 seconds to depressurize to 200 psia or lower does not require the RHR injection system to mitigate the accident and there are no adverse effects of nitrogen injection.

From the Semiscale results, the maximum impact on system pressure was about 30 psia. An examination of the system designs to be covered by this evaluation model shows that the lowest RHR injection system shutoff head is about 165 psia. As RHR injection builds fairly quickly with decreasing primary pressure, any accident that can be assured to hold pressure below 150 psia will receive abundant ECCS flow. Therefore, any accident that would depressurize to 120 psia (maximum impact is 30 psia) without nitrogen effects will not be adversely affected should gas injection occur.

The breaks between these two categories, those that depressurize to less than 200 psia prior to 300 seconds but stabilize at pressures greater than 120 psia, range from approximately 0.3 to 0.5 square feet in area. The break area is not actually significant but is useful as a tag for a normalized leak flow rate. An examination of the rate of system depressurization and the rate of accumulator depressurization for these accidents shows that accumulator injection takes place in two phases. The initial phase is predominately adiabatic and controlled by the initial energy of the pressurizing gas. This phase is responsible for the rapid injection of coolant and is active for 10 to 20 seconds longer than the system depressurization. The second phase is controlled by the heating of the gas within the tank by natural convection with the walls of the tank. This phase causes a very slow expansion of gas and/or water into the RCS.

An examination of a break that depressurizes to a stable pressure of 140 psia shows that the adiabatic expansion of the nitrogen does not cause gas expansion beyond the volume of the tank and that, with gas heating, the gas does not expand into the RCS until about 340 seconds. At this time the expansion of the gas into the RCS, allowing for heating to RCS temperatures, is about 2 cubic feet per second with excess leak flow (potential for steam leak flow above that required to relieve core decay heat) at 80 cubic feet per second.

For events that depressurize to 130 psia, the adiabatic expansion phase is essentially over at the same time that gas expansion into the RCS is predicted. Comparing the gas expansion rate for this event to the excess volumetric leak flow at 150 psia shows that the cumulative gas added to the RCS by 300 seconds could have been vented within 15 seconds if system pressure were to increase to 150 psia.

For an event that depressurizes to 120 psia, the adiabatic expansion is still effective as gas is being expanded into the RCS. A comparison of the nitrogen injection rate, with the gas heated to the RCS temperature after injection, to the excess volumetric leak flow at 150 psia shows that there is 30% more excess volumetric leak flow than is required to vent the accumulator gas being discharged. The rate of discharge continues to drop with time.

Taken together, these studies show that, for events that do not depressurize below 140 psia, accumulator gas discharge will not occur while the RHR injection system is required for core cooling, and that, for those events that do depressurize to below 140 psia, the effect of nitrogen injection would be to slow the depressurization of the system rather than cause a repressurization. This demonstrates that there are no adverse effects of nitrogen injection from the accumulators for SBLOCAs. To the contrary there are most likely beneficial effects. Semiscale observed that some water was pushed out of the downcomer and into the core. To a small degree that might occur during an SBLOCA. A larger benefit could accrue if the gas where flushed into the steam generators where it might interfere with the reverse heat transfer taking place.

Conclusions

An examination of the consequences of noncondensible gas on the results of SBLOCAs has shown that for smaller breaks which require the steam generators for energy removal, the amount of gas available for release to the RCS is small, the gas expected to be released is less than 20% of that releasable, and that the impact of a postulated nonmechanistic release of all available gas into the RCS is negligible. For larger breaks, it has been demonstrated that a potential adverse impact of nitrogen injection from the accumulators, as the accumulator water is depleted, does not occur and that there may in fact be a benefit from such an injection. Therefore, it is reasonable to neglect the effects of noncondensible gas within the small break LOCA evaluation model.

c. In discussing RELAP5/MOD2-B&W's ability to calculate natural circulation, two calculations of LOFT-OECD Test LP-SB-03 (by S. Guntay and P Hall, respectively) were referenced as demonstrating RELAP5/MOD2's ability to calculate natural circulation. You concluded that RELAP5/MOD2-B&W should perform as well as RELAP5/MOD2 because of the similarities between the two codes. However, no results were provided in the response to support this assertion. References to support the assertion that the code adequately calculates natural circulation were provided in response to Question 17. Because of the similarity of the references, it was concluded the reference for the work by Guntay was to a summary in an International Code Assessment Program report that did not discuss natural circulation. Also, the work by Ardron and Hass was shown as a private communication. This material does not acceptably demonstrate the code's ability to calculate natural circulation. Provide results of RELAP5/MOD2-B&W assessment calculations of a RSG geometry that verify the code's ability to calculate all three modes of natural circulation: single-phase, two-phase, and reflux.

Response: The calculation of natural circulation in a PWR is mainly dependent on the temperature difference between primary and secondary sides and the hydrodynamic models that affect flow regime and heat transfer. It is independent of steam generator design. For single-phase natural circulation, the benchmark results of MIST test 340213 are acceptable to demonstrate that RELAP5/MOD2-B&W is capable of calculating single-phase natural circulation when a positive temperature difference exists between the primary and secondary sides.

B&W's benchmark of the LOFT Experiment L-3-5 also demonstrates the ability of the code to calculate natural circulation. The code predicted single-phase natural circulation for the requisite period of time as shown in Figure G.2-8 of BAW-10164P and Figure 14.1. in the response to round one Question 14 on the RELAP5/MOD2-B&W topical report (BAW-10164P).

To demonstrates the code's ability to predict two-phase natural circulation and reflux cooling in the predicted and test benchmark of the S-LH-1 experiment, a comparison of flows, through the hot legs or steam generator tubes, was considered. However, test flow and density data are not readily usable to make a meaningful comparison. Therefore, a qualitative assessment is provided below.

The two-phase circulation and reflux mode cooling is believed to start after pump coastdown to zero speed, at about 90 seconds (Figure 24 in NUREG/CR-4438), and continues to approximately 250 seconds until the primary system pressure falls below the secondary side pressure. During this period, two-phase circulation and reflux cooling co-exist with two-phase natural circulation predominanting in the earlier period when the core, liquid level remains near the top of the core as shown in Figure 31 of NUREG/CR-4438, and with the reflux cooling mode dominant in the later period when the core is substantially uncovered. The primary system pressure and steam generator tube levels shown in Figures 5-4 through 5-8 (of Question 5 of this set of questions) indicate that the required conditions for two-phase circulation and reflux cooling exist during this period for both the test and prediction. An examination of the calculated steam generator tube phasic velocities in Figure 5-21 confirms that the RELAP5/MOD2-B&W code predicted two-phase circulation and reflux cooling.

To confirm that these modes of steam generator cooling existed in the experiment, the data from NUREG/CR-4438 (results of Semiscale MOD-2C Small break Loss-of-Coolant Accident Experiments S-LH-1 and S-LH-2) are used. The hot leg volumetric flow rates and densities shown in Figures 26 and 25, respectively, indicate that there is a two-phase natural circulation period to at least 140 seconds (end of data). The collapsed liquid level in the intact loop steam generator downflow leg, shown in Figure 23, actually increases at approximately 120 seconds. This is caused by two-phase mixture entering from the uphill side of the steam generator tubes, and further supports the existence of two-phase natural circulation in the test.

The characteristic signature of reflux cooling is to have a voided hot leg pipe and uphill side of the steam generator tubes in addition to a positive primary to secondary differential temperature. This is the case for both the intact and broken loops. An increase in hot leg volumetric flow (Figure 26) occurs at 105 seconds as steam travels to the intact loop tubes to replace fluid that is draining out. This is a good example of counter-current two-phase flow.

Additional evidence of reflux cooling can be seen in Figure 23 in NUREG/CR-4438. The collapsed liquid levels in the uphill sides of the steam generator tubes remain stable after 120 seconds while the downhill sides of the tubes continue to drain. This indicates a continuous supply of condensate to the uphill sides as a result of reflux cooling. Although no distinct period of transition from two-phase circulation to reflux cooling can be determined, the data indicate that, following the pump coastdown, steam generator cooling begins with predominantly two-phase natural circulation and changes to predominantly reflux of cooling at approximately 120 seconds as the primary system inventory continues to decrease.

Based on the above discussion, it is concluded that the RELAP5 code can adequately predict two-phase natural circulation and reflux cooling. In addition, good agreement in the leak flow rate (Figure 5-3) and the primary system pressure response (Figure 5-4) between the test and the calculation confirms that the quantitative performance of the code with respect to energy removal via two-phase natural circulation and reflux cooling is excellent.

In conclusion, the range of test comparisons provided is diverse to the extent that all phenomena involved in the prediction of single-phase and two-phase natural circulation, and reflux cooling in an RSG plant have been demonstrated. Therefore, B&W does not believe it is necessary to provide additional benchmarks.

d. The response did not discuss how the requirements of NUREG-0737, Item II.K.3.30, were met with respect to condensation/vaporization heat transfer in RELA5/MOD2-B&W. Clarify how there processes are modeled in the code and how well the models represent the condensation/vaporization processes important to accurately calculating the system response to a small break LOCA. At a minimum, how well the models represent the condensation of steam in the steam generator U-tubes, condensation due to the mixing of cold ECC water with steam in the primary system, and the vaporization of the core fluid and calculation of vapor superheat should be discussed.

Response: An assessment of the RELAP5/MOD2-B&W condensation-vaporization models is given below. From this assessment it is concluded that the RELAP5/MOD2-B&W condensation-vaporization models reasonably meet the NUREG-0737 requirements.

The RELAP5/MOD2 heat transfer package is used to calculate surface condensation in steam generator tubes. Nithianandan et al.[4.5] have evaluated these models using the B&W single tube test and MIT pressurizer test and found them to be satisfactory.

The vaporization of core fluid and the vapor superheat prediction depend on the surface heat transfer as well as the interphase heat transfer. All interphase heat transfer models in RELAP5/MOD2-B&W are the same as in RELAP5/MOD2. Dimenna et al.[4.6] at EG&G have made a detailed assessment of the interphase heat transfer models. They concluded that the models are reasonable approximations of the current understanding of the interphase heat transfer technology.

In the EM heat transfer package, the wall heat transfer during the subcooled and saturated nucleate boiling regimes is calculated using the Thom, Chen, and Schrock and Grossman correlations. These correlations have been widely used in the nuclear industry and are accepted by the heat transfer community. In the saturated nucleate boiling regime both vapor and liquid are near saturation condition and all the surface heat transfer is used to generate saturated steam. The voiding during the subcooled boiling heat transfer depends on the interphase heat transfer. Nithianandan et al.[4.7] has assessed the subcooled vapor generation models in RELAP5/MOD2 using two of Christensen's subcooled boiling tests and concluded that these models are satisfactory.

The wall heat transfer in the film boiling regime is calculated using the Condie-Bengston IV correlation. The McEligot correlation along with wall to vapor radiation are used to calculate the single-phase vapor heat transfer. In the response to Question 8 (round one on RELAP5/MOD2-B&W), the Condie-Bengston IV and McEligot correlations were assessed and concluded to be acceptable. The wall to vapor radiation is calculated using the Sun et al. correlation which is widely used in the industry.

The prediction of vapor superheat during film boiling depends on the interphase heat transfer. Lin et al.[4,8] assessed the RELAP5/MOD2 heat and mass transfer models using Chen's single tube tests conducted using the Lehigh test facility. The code was found to over-predict the vapor temperature for the high quality test and under-predict it for the low quality test. It is to be noted that it is difficult to measure the correct vapor temperature during two-phase flow conditions.

Even if RELAP5/MOD2-B&W does not calculate the vapor superheat correctly, it will have very little impact on the prediction of the peak cladding temperature. In the B&W SBLOCA methodology only the core collapsed liquid level is used from RELAP5/MOD2-B&W. The FOAM2 computer code uses this collapsed liquid level to calculate the mixture level and the steaming rate which are used in FRAP-T6-B&W. In FRAP-T6-B&W single-phase heat transfer is assumed above the mixture level irrespective of the vapor generation below the mixture level. This method conservatively eliminates pool entrainment of liquid. Therefore, the peak cladding temperature calculated by FRAP-T6-B&W will be conservative. In response to question 5 of this set, the methodology has been verified by simulating the Semiscale SBLOCA test S-LH-1 cladding heatup.

The condensation of steam in the cold legs by subcooled ECC water depends on the interphase heat transfer model. As mentioned earlier, from a detailed assessment of the interphase heat transfer models, Dimenna et al.[4.8], concluded that the models are reasonable. Development assessment at EG&G[4.9], using Bankoff's stratified flow condensation test and Aoki's steam water mixing tests provide indications of the applicability of these models.

Additional information regarding the acceptability of the interphase condensation models can be obtained from the B&W simulation of Semiscale LBLOCA test S-04-6, Semiscale SBLOCA test S-LH-1 and the LOFT SBLOCA test L-3-5. The S-04-6 results are given in response to question 12 (round one questions on RELAP5/MOD2-B&W). From the fluid temperature prediction near the injection location, shown in Figure 12.29, it can be concluded that the code calculated fluid temperature agrees reasonably well with the test data during the accumulator injection period. The mass flow rates near the injection location, shown in Figures 12.18 and 12.19, and the system pressure response, shown in Figures 12.4 through 12.19, do not show non-physical behavior during the accumulator injection period. Similar observations can be made from the pressure and temperature calculations near the injection location for tests S-LH-1 and L-3-5, Figures 4.1 through 4.4.

From this assessment of the RELAP5/MOD2-B&W condensation-vaporization models, it is concluded that these models reasonably meet the NUREG/0737 requirements.

References

4.1 J. A. Klingenfus, Mist Final Report Chapter 10: RELAP5/MOD2 Mist Analysis Comparisons, NRC-04-83-168, RP 2399-1, Preliminary copy NRC publication pending, February 1988.

4.2 D. Hein, R.Rippel, & P. Weiss, "The Distribution of Gas in a U-Tube Heat Exchanger and its Influence on the Condensation Process," International Heat Transfer Conference, Munich Germany, September 1982.

4.3 G. G. Loomis, Summary of the Semiscale Program (1965-1986), NUREG/CR-4945, EGG-2509, Idaho National Engineering Laboratory, July 1987, pages 197 - 199.

4.4 J. M. Cozzuol, Thermal-Hydraulic Analysis of Semiscale Mod-1 Integral Blowdown-Reflood Tests (Baseline ECC Series), TREE-NUREG-1077, Idaho National Engineering Laboratory, March 1977, pages 37 - 50.

4.5 Nithianandan, Morgan, Shah, & Miller, "RELAP5/MOD2 Models for Surface Condensation in the Presence of Non-condensible Gases," pp 1627-1633, Proceedings of the 8th Int. Heat Transfer Conference held in 1986 at San Francisco, USA, Published by Hemisphere Publishing Corporation.

4.6 R. A. Dimenna, et al., RELAP5/MOD2 Models and Correlations, NUREG/CR-5194, August 1988.

4.7 Nithianandan, Shah, Schomaker, & Turk, "RELAP5/MOD2 Assessment at Babcock & Wilcox," NUREG/CP-0072 Volume 5, pp 271-295, February 1986.

4.8 J. C. Lin, et al., "RELAP5/MOD2 Post-CHF Heat And Mass Transfer Models," Paper presented at the Int. Workshop on Fundamental Aspect of Post Dryout Heat Transfer, Salt Lake City, Utah, April 1-4, 1984.

4.9 V. H. Ransom, et al., RELAP5/MOD2 Code Manual Volume 3: Developmental Assessment Problems, EGG-SAAM-6377, April 1984.

FIGURE 4.1. S-LH-1 BROKEN LOOP ECC INJECTION NODE PRESSURE.

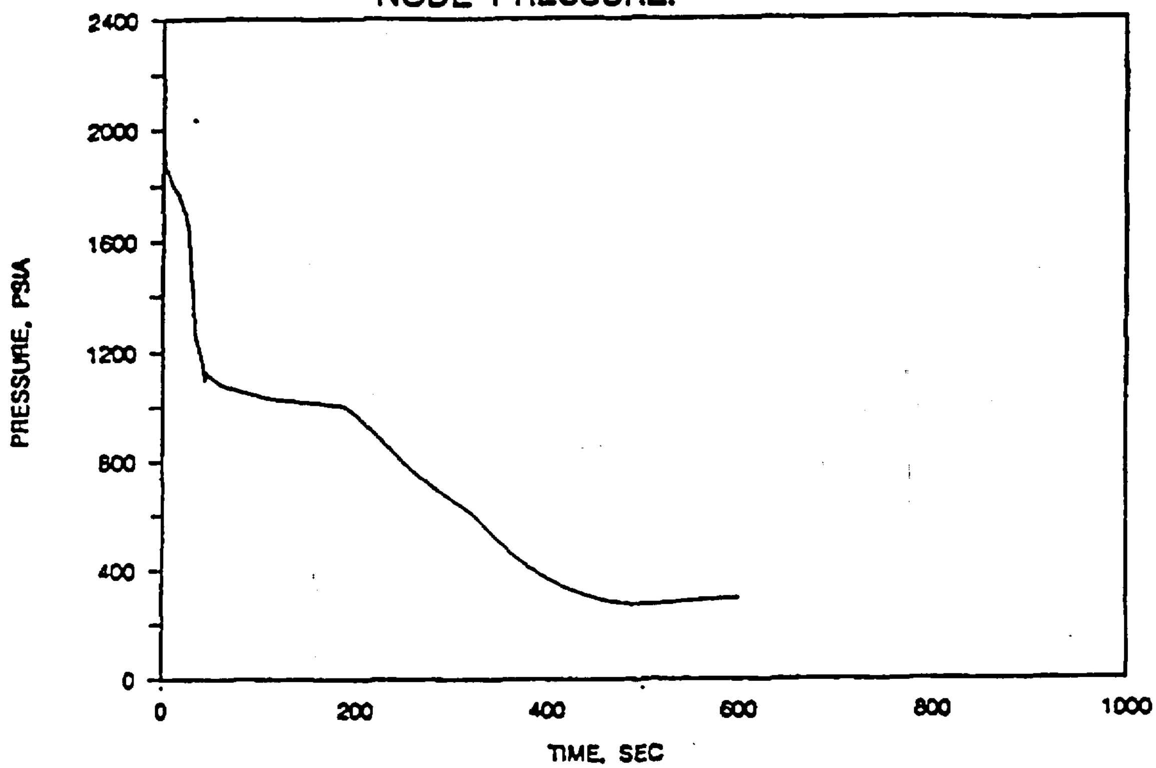

FIGURE 4.2. S-LH-1 BROKEN LOOP ECC INJECTION NODE TEMPERATURE.

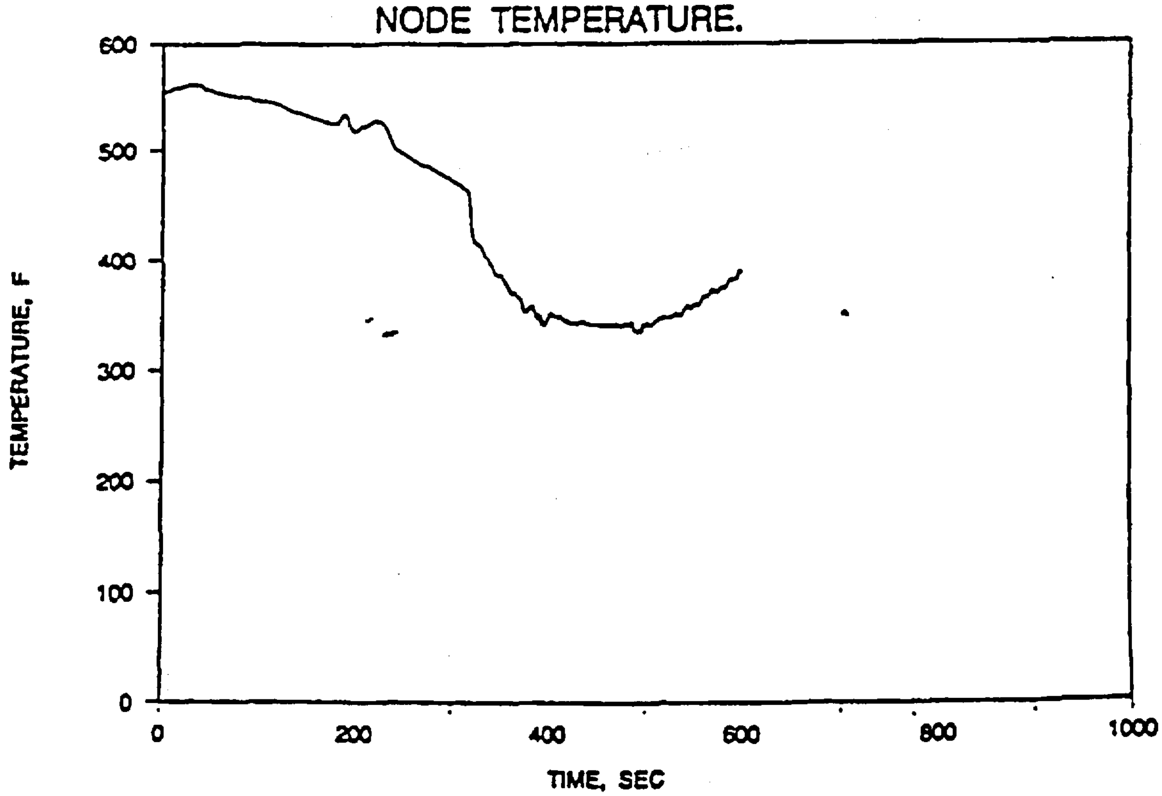

FIGURE 4.3. L-3-5 DOWNCOMER ECC INJECTION NODE PRESSURE.

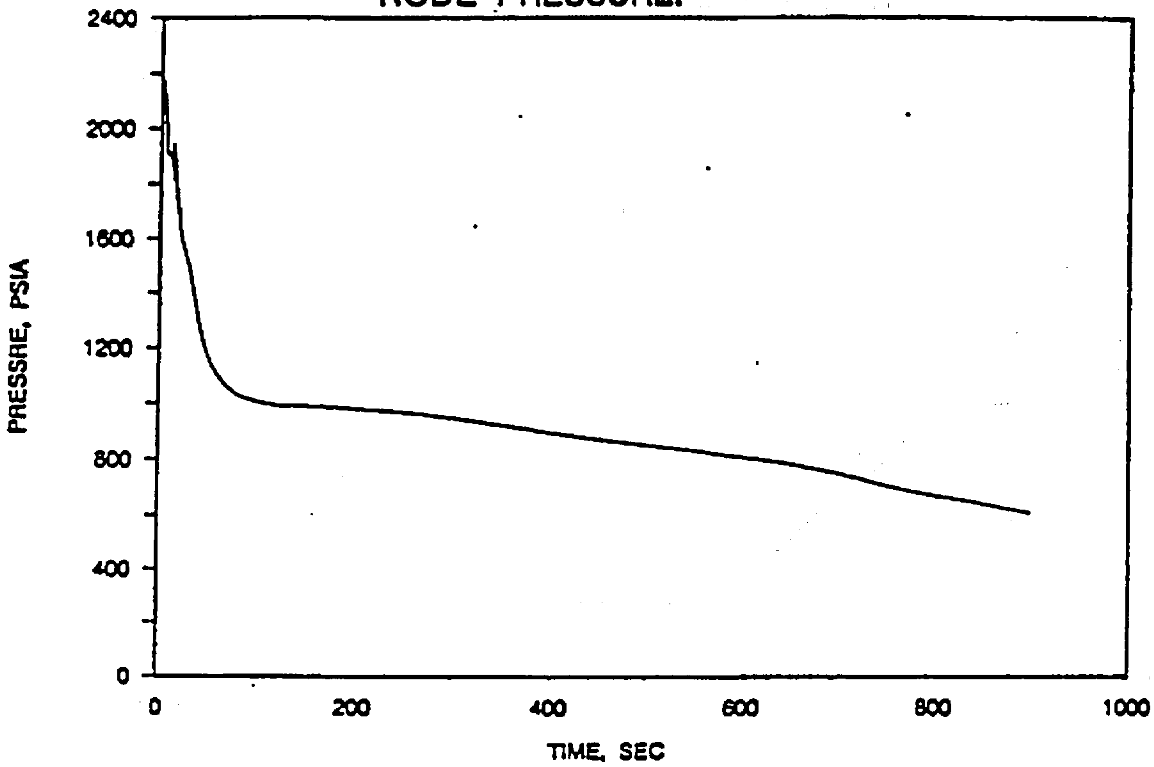

FIGURE 4.4. L-3-5 DOWNCOMER ECC INJECTION NODE TEMPERATURE.

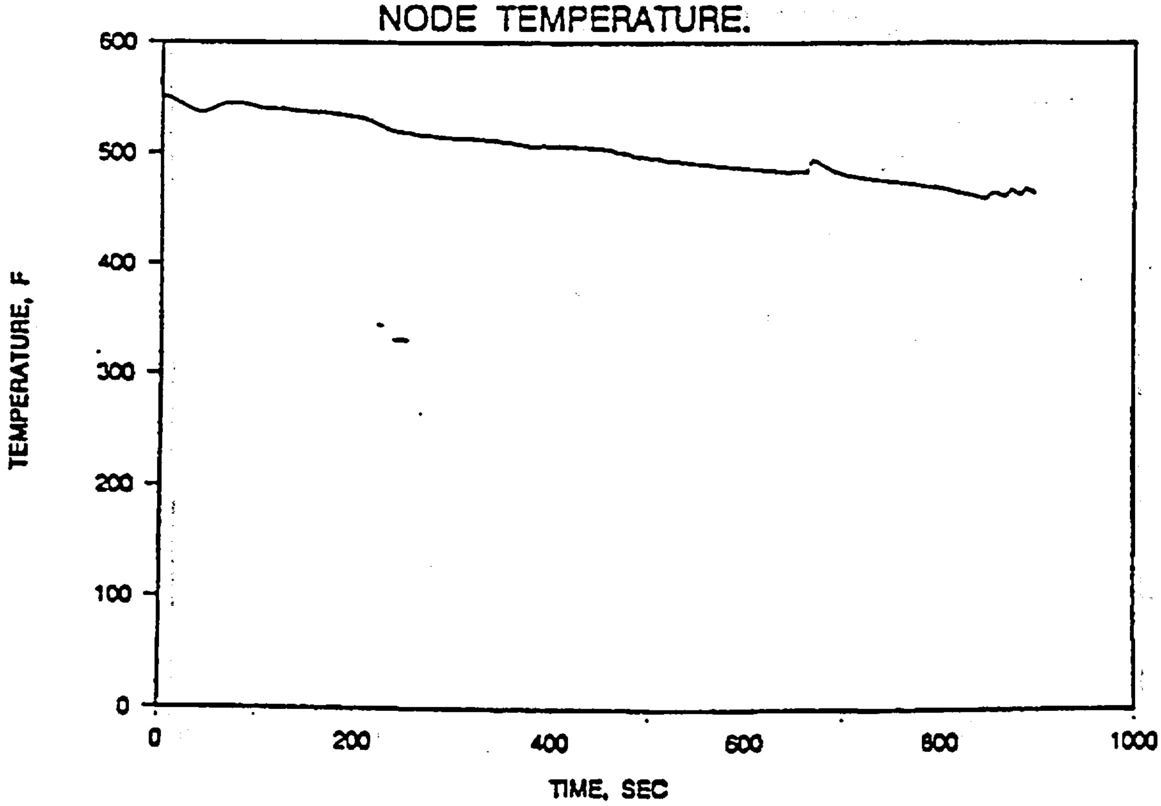

5. The following questions are related to the analysis of Semiscale Test S-LH-1 provided in response to Question 17.

a. Provide information to show how well the RELAP5/MOD2-B&W analysis calculated the rod temperatures in the Semiscale core, and discuss what effect the over-prediction of the core collapsed liquid level from 200 s to approximately 300 s had on the core thermal response.

b. The faster depressurization in the RELAP5/MOD2-B&W calculation after the loop seal cleared was stated to be due to steam venting. This response is not considered adequate. Because the loop seal cleared in both the test and the calculation, would not steam venting be occurring in both the test and calculation? Additional information is needed to clarify the reason or reasons for the difference between the calculated and measured depressurization rates.

c. The nodalization diagram for the Semiscale Test S-LH-1 analysis has more detailed nodalization than that recommended in BAW-10168P for SBLOCA EM model. For example, 16 volumes were used to model the U-tubes on the primary side of the steam generator versus eight in the EM model, and eight nodes in the downcomer versus three in the EM model. Because the peak cladding temperature calculation can be affected by the steam generator nodalization, clarify the effect of the analysis results of the more detailed nodalization used in the S-LH-1 analysis versus the nodalization recommended in BAW-10168P.

Response: B&W presented a benchmark of Semiscale test S-LH-1 as the response to Question 17 of the first round of questions on BAW-10164. As a result of further investigation into that benchmark and the test results, a revised benchmark has been run. The revision, which uses a tighter match to boundary conditions and recognition of some scale atypicalities, produces results that agree with the experiment far better than the original benchmark. The following response contains both the original and the revised benchmarks and supersedes the response to Question 17 of the first set. For convenience question 17 is quoted below.

17. " The experience with advanced thermal hydraulic computer programs has shown an important sensitivity to modeling of the steam generators when analyzing SBLOCAs. Specifically, the modeling of liquid entrainment, condensation, and hydraulic resistance (i.e., flow regime maps) could significantly depress the mixture level in the core. This phenomenon was observed in Semiscale Test S-UT-8 and later studied in Semiscale Tests S-LH-1 and S-LH-2. Recognizing Semiscale's atypicality, the staff nevertheless believes this phenomenon to be real and, therefore, possible in a full scale reactor. It is for this reason that we request validation of your computer program to predict this phenomenon, should it occur in a full scale reactor. Validation with Semiscale Tests S-LH-1 and S-LH-2 or demonstrating that the phenomenon observed in the Semiscale experiments is calculated to occur in a plant calculation would be acceptable. Use of other integral experiments for validation requires that these experiments simulate the hydraulic behavior observed in the Semiscale tests."

Semiscale S-LH-1 is a 5% break at the pump discharge pipe with a 0.9% core bypass flow from the downcomer to the upper head. The simulation of S-LH-1, using RELAP5/MOD2-B&W, demonstrates the capability of the code to predict SBLOCA phenomena, such as core uncovery/recovery, natural circulation including reflux boiling, loop seal clearing, and ECCS performance. The size of the break is such that decay heat removal via the steam generator is provided only briefly, and the steam generators do not play a significant role in mitigating the simulated accident. Numerous benchmarks of Semiscale test series S-NC, that demonstrate the adequacy of RELAP5/MOD2 to predict long-term core cooling by reflux boiling and natural circulation, have been performed by the industry.[5-1,5-2] The simulations of S-LH-1 presented herein confirm the industry results for RELAP5/MOD2-B&W with particular attention to the larger of the small breaks which form the most severe challenge to the ECCS.

Test Facility

The S-LH-1 test was conducted using the Semiscale MOD-2C facility shown in Figure 5-1. It consisted of a pressure vessel with simulated reactor internals and an external downcomer. The intact loop simulated three unaffected loops of a typical Westinghouse 4-loop PWR, while the broken loop simulated an affected loop in which the break is assumed to occur. The intact loop steam generator contained six inverted U-tubes, and the broken loop steam generator contained two inverted U-tubes. The reactor core simulator was a 5 x 5 bundle with electrically heated rods (23 rods were powered during the test). The upper head region contained a simulated control rod guide tube and two simulated support columns. The bypass line that extended from the external downcomer to the upper head was used to simulate the core bypass flow. A pressurizer was connected by a surge line to the intact loop hot leg. Both loops had primary coolant circulation pumps. Emergency core coolant from an accumulator and pumped injection system (LPI and HPI) were routed to the loop cold legs. An open loop secondary coolant system was used to control the secondary side pressure with feedwater and steam control valves.

Model Description

The Semiscale MOD-2C RELAP5 base model was originally developed by EG&G for the post-test analysis of experiments S-LH-1 and S-LH-2 (NUREG/CR-4438). The nodalization diagram is shown in Figure 5-2. The model consists of 181 hydrodynamic volumes, 172 junctions, and 256 heat structures. All volume and junction parameters are calculated with nonequilibrium and nonhomogeneous models. Steam generator secondaries, ECC injection, system environmental heat losses, and both vessel and piping external heaters are modelled in detail. The core axial power profile is modelled with twelve stacked heat structures over six two-foot long axial fluid volumes. The upper head region is nodalized to allow for junctions to be connected at the elevations of the top of the control rod guide tube, core bypass line and support columns, and at the elevation of the holes in the guide tube below the upper core support plate.

Changes were made to the original EG&G model to account for and distribute unrecoverable losses due to pipe bends, orifices at the pump discharge pipes, area changes at the steam generator inlet and outlet plenums, and flowmeters in the hot and cold leg pipes. A steady-state calculation was made with these changes to obtain the initial conditions presented in Table 5-1. The calculated initial conditions compared well with the test conditions except for the secondary side masses and pressures. These were adjusted to achieve the desired primary cold leg temperatures. The calculated pump speeds are slightly higher than the test measurements (8% and 3% for the intact and broken loops, respectively) as a result of higher pump discharge orifice resistances. The following changes that do not affect the steady-state initial conditions were made: the RELAP5/MOD2-B&W core surface heat transfer model was invoked, the leak discharge models were set to those for an evaluation model calculation, and thermal equilibrium was assumed in the core region.

As in the EG&G model, the external heaters were treated mechanistically in RELAP5, and the measured power to the heaters as a function of time was input as a boundary condition. The core decay power and pump coastdown speeds as a function of time were also input to the model. There was limited secondary side steam valve model information available from this experiment. Since the secondary system responses have an impact on the natural circulation and reflux boiling phases of the transient, the secondary side pressure responses from the experiment were used as boundary conditions in the calculation (see Table 5-2).

In order to improve the results several model changes were incorporated into the revised benchmark. The changes, detailed later in the section on <u>Revised Model Changes</u>, were:

1) Alteration of the discharge coefficient from 1.0 to 0.7 at a leak inlet void fraction of 70 percent.

2) Alteration of upper downcomer modelling to account for the bypass of the intact loop HPI.

3) A junction in the simulation of the guide tubes was made homogeneous and the connection of the core bypass to upper head adjusted.

4) Rearrangement of the vessel lower head flow paths.

5) Reduction of the loop exterior heat loses.

6) The secondary side pressure versus time curve was altered slightly.

Results of Base Analysis with a CD of 1.0

The sequence of major events is presented in Table 5-2 for the original and revised analyses. Figures 5-3 through 5-21 show the results of the benchmark calculations. The original results are indicated as dashed lines on all of the figures. The transient was initiated at zero seconds by opening the leak, and thereby causing a flow of subcooled primary fluid out the break, resulting in a rapid system depressurization. A leak discharge coefficient of 1.0 was applied to both the subcooled and saturated choke flow models. Figure 5-3 shows good agreement in the leak flow rate between the base RELAP5 calculation and the experimental data. The primary system pressure response is controlled by the leak flow, and Figure 5-4 shows that the calculated pressure is in good agreement with the experimental result up to 200 seconds. The calculated time to reach the safety injection system (SIS) setpoint, 1827.5 psia in the pressurizer is approximately 3 seconds later than the experiment, primarily due to a slower draining in the pressurizer. This is caused by a higher overall intact loop resistance. The calculated steady-state pump speed in the intact loop is approximately 8% higher than that of the experiment.

The draining of the steam generator tubes, shown in Figure 5-21, occurred after the pump speed coasted down to zero at 100 seconds. At this point, the primary system entered a reflux condensation cooling mode as evidenced by the counter-current flow shown in Figure 5-21. Figures 5-5 through 5-8 show U-tube liquid levels in both the intact and broken loops. It should be noted that the measured liquid levels using differential pressure cells can lead to considerable error during the pump coastdown period (0 - 100 seconds).[5-3] Both the prediction and the experimental data show that the upflow side of the U-tube consistently drained later than the downflow side due to de-entrainment and reflux condensation on the tube surface.

Following draining of the steam generator U-tubes, a liquid seal was formed in the pump suction of both loops. The seals caused a blockage of steam flow to the break. As a result, the primary system entered a period of manometric level depression in both the downflow side of the pump suction seals and in the core liquid level. To clear the pump suction loop seals, the liquid head imbalance between the downcomer and the core must accrue to the total of the loop seal level plus the liquid holdup, due to reflux condensation, in the upflow side of the U-tubes. As shown in Figures 5-5 and 5-7, the liquid level in the upflow side of the steam generator U-tubes is a significant contributor to the total ΔP that opposes loop seal clearing. The loop seals cleared at 175 seconds and 214 seconds for the intact loop and the broken loop, respectively.

Figures 5-9 through 5-12 show the liquid level in the pump suction pipes. The intact loop seal cleared first, followed by the broken loop, because the primary-to-secondary heat transfer was terminated earlier in the intact loop than in the broken loop. Clearing of the loop seals produces a continuous path to the break for steam generated in the core. The steam conditions at the leak result in lower leak mass flows, but higher volumetric flows. As a result, the primary system begins a rapid depressurization. The base model depressurization rate was faster than was observed in the experiment, in spite of good agreement in discharge mass flow rates between the calculation and the experiment. The effect would be consistent with a model that was discharging a higher quality at a larger volumetric rate than the corresponding experiment. This observation is part of the basis for the alterations made to the model for the second benchmark. It is unfortunate that there are no experimental results available by which the energy discharge rate or the heat loss to the ambient surroundings can be determined. With data of that sort the above hypothesis could be directly confirmed.

One of the important parameters used as an indicator for SBLOCA mitigation is core collapsed liquid level. This is shown in Figure 5-13. As a result of correctly predicting primary system mass inventory and reflux heat transfer, the agreement in the first core level depression between the calculation and the experiment is excellent. After clearing the loop seals, core decay heat continues to boil-off fluid in the core region and, since the HPIS flow alone is not sufficient to makeup for fluid lost out the break, the core liquid level continues to decrease until accumulator actuation is achieved.

Accumulator injection occurred much earlier in the base EM calculation than in the experiment due to the faster depressurization rate. However, the shortened core boil-off period was compensated for by increased flashing. Thus, the second core collapsed liquid level depression was calculated to be nearly the same as the measurement except for its timing. The experiment shows that a more significant and uniform core heat-up occurred during the second depression. The ability of RELAP5 to correctly predict the two distinct core liquid level depressions demonstrates that the code can accurately calculate important thermal-hydraulic system parameters.

Figure 5-14 shows the normalized primary system mass inventory. The mass inventory increased following accumulator injection. The HPIS injection flow rates for both the intact and broken loops are presented in Figure 5-15 and 5-16, respectively. The calculated flow rates are higher than those of the experiment due to the faster depressurization rate predicted by RELAP5 for this base EM model.

Following the completion of the base RELAP5 calculation, the collapsed liquid level was used with the power and pressure time histories to calculate core mixture levels with the FOAM2 code. The resultant mixture levels were input into FRAP-T6 with pressure, decay heat, core mass fluxes from FOAM2, and inlet enthalpy to compute a predicted cladding temperature excursion. The results of the FRAP-T6 calculations are shown in Figures 5-19 and 5-20 for the 8.2 and 10.2 foot core elevations. During both temperature excursions the calculated temperature peaks exceeded the experimental values for both elevations, demonstrating conservatism in the evaluation model steam cooling models.

Revised Model Changes

The first benchmark simulated the test using a leak discharge coefficient of 1.0 for the entire transient. After loop seal clearing, the calculated system depressurization, Figure 5-4, exceeded that of the test due to over-prediction by the Moody choked flow correlation. Based on experimental data, the Moody critical flow model is observed to over-predict two-phase leak flows for qualities greater than 10 percent while under-predicting the flow for lower qualities. To account for this the revised model used dual discharge coefficients, switching between the coefficients at a void fraction of 70 percent.

The RELAP5/MOD2-B&W EM choked flow model has an option to include four discharge coefficients as functions of the leak inlet conditions. Separate coefficients can be used for subcooled flow, during the transition to two-phase flow, during two-phase, and for steam (superheated) flow. In making adjustments to these coefficients it is equally important to maintain their relationships to each other as it is set individual coefficients correctly. Once relative values are determined specific values can be set by comparison to data or through a spectrum approach as is used in licensing. Although experimental data indicates that Moody under-predicts the discharge rates for low quality flow, the data also show that the same discharge coefficient should be applied to Henry-Fauske extended into the subcooled region and Moody at low qualities. Using 1.0 as the base discharge coefficient for extended Henry-Fauske suggests that 1.0 should also be used for the transition regime, a reduction to about 0.7 be used for the two-phase regime, and 1.0 be used under superheated conditions. The normalized values of discharge coefficients used in the revised model were 1.0, 1.0, 0.7, and 1.0.

The RELAP5/MOD2-B&W EM choked flow model also provides control over the conditions at which to apply the discharge coefficients. The lower bound for the transition regime is set to 1 percent void fraction and the upper bound at 70 percent void fraction. The subcooled coefficient applies whenever the leak inlet void fraction is less than 1 percent. The supperheat discharge coefficient is applied whenever the leak inlet enthalpy is greater than or equal to the leak node saturated steam enthalpy. The table that follows shows the coefficients and the switching in chart form.

Once the relative values of the discharge coefficients have been specified, the specific values to be used in a given evaluation can be determined. This can be done through an adjustment of the break area or through the multiplication of each of the discharge coefficients by a constant. In licensing calculations this is done by break area adjustment and is part of the spectrum approach to the identification of the worst case break. In experimental benchmarks this is usually done by adjusting one of the coefficients to match a measured flow and then adjusting the remaining coefficients to maintain their relationships with each other. Based upon the test data for S-LH-1 the subcooled and transition discharge coefficients were set to 1.13. Therefore, the two-phase value became 0.79 (= 0.7 * 1.13) and the superheated value 1.13.

Discharge Coefficients Relationships

Regime	Range of Application	Normalized Value	Value used in Revised Model
Subcooled	$\alpha_g <$ 1%	1.0	1.13
Transition	$\alpha_g \geq$ 1% & $\alpha_g \leq$ 70%	1.0	1.13
Two-phase	$\alpha_g >$ 70% & $H_{mix} < H_{g,sat}$	0.7	0.79
Superheat	$H_{mix} \geq H_{g,sat}$	1.0	1.13

System depressurization and inventory prediction of the original model were further complicated by a difference between the predicted and experimental break inlet conditions. Following loop seal clearing, the calculated break inlet flow was composed of steam from core boiling and system flashing and the broken loop ECCS liquid. The resultant break quality was between 85 and 90 percent. Evidence from the experiment -- measured break inlet quality, break flow rate, system mass balance, and the reactor vessel level decrease rates -- indicates that the break inlet quality should lie between 70 and 75 percent. Vessel and system mass balances calculated from the test data between 300 and 500 seconds cannot be matched using the intact loop HPI, decay heat, and flashing. The test break density indicated a quality of 70 to 80 percent. The break mass and energy discharges cannot be reasonably matched unless a quality of about 70 percent is used (break energy rate is inferred from the system energy balance and depresurization). On an individual basis the uncertainty of each measurement makes it difficult to be absolutely conclusive about the break inlet quality. However, taken in combination the evidence is compelling that the break quality averaged about 70 percent and that this was caused by bypassing of most of the intact loop HPI.

The intact loop HPI bypass was probably caused by a combination of the atypically short distance between inlet nozzles and high steam velocities in neighborhood of the broken leg nozzle. The intact cold leg mixture, which may not have been well mixed, transits the top of the downcomer so quickly that there is little time for a separation of steam and water prior to the high velocities at the broken loop nozzle. The result is essentially the entrainment of most of the HPI across the top of the downcomer. A change was made in the cold leg nozzle to downcomer connection for the revised model to essentially force bypass of the intact loop HPI. Noding changes included separation of volume 101 into two volumes (101 & 102) of equal height. The two cold leg nozzle junctions were modelled as one-half the original area and connected as upward oriented junctions to the top of control volume 101. A separate bypass junction (103) with one-half the cold leg nozzle area was connected as a downward oriented junction between the two cold legs. Associated changes were made to the junction connections from 101 to 102 to the rest of the downcomer. The arrangement is depicted in Figure 5-2a.

The reactor vessel upper head region drained too quickly in the original calculation. Phase separation in the guide tube allowed high upward steam flow which promoted draining. The junction between control volumes 183 and 184 was switched to a homogeneous condition. Justification of this switch is rooted in the atypical small size of this connection with the plugged drain holes. This type of model would not be used in plant applications. An associated change, which is currently used in the applications, was the modelling of the reactor vessel upper head connection of the bypass line. The junction was connected to the top of control volume 192 instead of the bottom of 193 to give a better bypass inlet phase condition.

The connection to the top of control volume 130 represented the Semiscale geometry; however, it allowed the bottom of the downcomer to trap steam during the last portion of the pump coast-down phase. At the end of the simulated pump coastdown the steam trapped in the downcomer was discharged out of the break and the system levels realigned. Moving the connection to the bottom of volume 140 allowed the core to serve as part of the steam discharge path. Plant application models use the revised model type of connection.

A change was made associated with the mechanistic loop heat loss modelling. Based on the mass and energy balance calculations on the core and downcomer during the core boil-off phase, the heat losses were considered to be too large. They were reduced by modelling the exterior heat loss as a heat transfer coefficient versus time. Initially a value of 1 Btu/hr-ft^2-s was chosen. This value was decreased by a factor of 100 to reduce the heat loss on the outside of the insulation during the transient.

The secondary side boundary conditions were also modified for the revised prediction. The original base calculation imposed the measured test secondary pressure as a boundary condition. A more appropriate boundary condition would be the primary-to-secondary temperature difference during the saturated phase of the transient. This boundary condition resulted in a slight reduction in the secondary pressure in the 100 to 300 second time frame. It maintained a similar potential for heat transfer in each loop, which is important because this heat transfer has a strong influence on individual loop seal level depressions. After 300 seconds a smooth linear ramp back to the test pressure was implemented. The imposed secondary pressure boundary conditions are shown in Table 5.2.

Revised Model Results.

The revised, best-estimate, model results are summarized in Table 5-2 and shown in Figures 5-3 through 5-21 as the dotted lines. The new set of discharge coefficients greatly improve the system pressure (Figure 5-4) and liquid mass inventoriey (Figure 5-14) predictions. The prediction of these parameters was improved primarily by matching the test leak fluid composition during the boil-off period while maintaining the appropriate total discharge. The downcomer bypass noding arrangement provided the mechanism to accurately simulate this behavior. Between 300 and 500 seconds the normalized mass prediction deviates somewhat from the test values. This deviation is partly due to the inventory in the broken loop pump suction piping, not clearing until 600 seconds.

Improvement in the prediction of the upper head level, shown in Figure 5-17, between 50 and 150 seconds helped to redistribute the system inventory such that it was more consistently with test observations. The lower downcomer model changed the steam storage in the lower downcomer; however, the forced bypass model in the nozzle belt region allowed more steam to be stored in the upper downcomer. The level behavior is shown in Figure 5-18. Upon intact loop seal clearing, the test, base, and revised model levels all resided at the cold leg nozzle elevation.

The timing of the intact loop seal clearing was the same as the base case and the test, although the duration and magnitude were slightly less than the previous values. The revised core collapsed level, shown in Figure 5-13, rose above the test data between 180 and 280 seconds. The over-prediction of the level was due to the rapid equalization of the downcomer and core levels. The difference appears to be due to a slight difference in the loop seal behavior. Once the downside of the intact pump suction clears, a steam venting path can be readily established. However, the facility seems to retain a small plug of liquid which acts as a resistance to the steam flow. The resistance remains partially in place until approximately 475 seconds. Its effect can be seen in the differential between the test downcomer and core collapsed levels.

The slight over-prediction of the core collapsed levels from the intact loop seal clearing until 450 seconds had minimal impact on the peak heater rod temperatures. The steam cooling above the mixture level in FRAP-T6 under-predicted the cooling; therefore, the temperature escalation was faster than that observed in the test.

At 500 seconds, the revised prediction was restarted and a path, that included one-tenth of the cold leg nozzle, was connected from the intact leg to the top of control volume 102. This path allowed a portion of the ECCS liquid to enter the downcomer and not be bypassed. The mass and energy balances on the test core region indicate that some of the intact loop ECCS fluid was still being bypassed after accumulator actuation. This path allowed approximately the same, but slightly less, liquid to enter the downcomer than occurred in the test. The system depressurization between 500 and 700 seconds, Figure 5-4, was more rapid than the test. The rapid depressurization was slowed at approximately 650 seconds due to boiling of small amounts of liquid that had swelled into the hot legs and inlet of the steam generator tubes. Since the depressurization was slowed, the rate of accumulator injection was lower and less steam condensation occurred. The revised calculation reached a pressure equilibrium at 850 seconds, thus halting the accumulator flow. The intact loop HPI was still insufficient to absorb all the core decay heat at this time and a second core boil-off began. The test appeared to be approaching this condition at 1000 seconds.

Conclusions

RELAP5/MOD2-B&W calculated the major events of the Semiscale S-LH-1 transient -- two-phase natural circulation, reflux boiling and liquid holdup, pump suction loop seal clearing, core liquid level depression, ECCS injection and core recovery -- in the proper sequence for both benchmarks provided in this response. Both benchmarks calculated the overall system responses in reasonable agreement with the experimental data. The assumptions and boundary conditions used for the base calculation resulted in a depressurization rate that effectively modeled a larger break. The SBLOCA code package, namely RELAP5/MOD2-B&W, FOAM2, and FRAP-T6, calculated a conservative heater rod surface temperature in both predictions, with the original and revised calculations producing similar peak temperatures. The revised RELAP5/MOD2-B&W calculation was able to closely match the test behavior for S-LH-1 including small scale facility effects.

Although the benchmarks were conducted to demonstrate basic code capabilities, most of the modeling used is representative of that for evaluation model calculations. The degree of nodalization employed in the benchmarks was higher than required. The detail used in the pressurizer, hot legs, UTSG secondary sides, UTSG primary sides, lower downcomer, and cold legs provides minimal benefit over lessor models. The noding near the bottom of the pump suction downside is required to preserve the proper timing for loop seal clearing. Steam generator noding should be sufficient to determine the total energy transport in or out of the primary system and to differentiate between upside or downside condensation for proper liquid tracking during reflux boiling. The emphasis in component noding should be to model the elevations of liquid traps correctly. Sufficient noding near the break should be provided to place the ECCS injection location properly for the event being studied.

Connections between and within components require careful consideration. Regions of particular importance are the hot and cold leg nozzles, upper head to upper plenum connections, and upper downcomer connections. Junctions will be connected to volumes, that may establish mixture levels, in an orientation that will tend to pass liquid or steam in accordance with the predicted levels. Double flow path modelling will be used for hot and cold leg nozzles. The S-LH-1 benchmark used crossflow junctions for the nozzle areas. Although the crossflow junctions perform similar to double flow paths, double flow path modelling has two advantages. It has the capacity to model liquid-liquid counter-current flows that may develop in the cold leg nozzles, and retains the full complement of momentum terms.

The noding proposed for the SBLOCA evaluations and described in BAW-10168 is sufficient to meet these computational needs. The benchmarking of Semiscale test S-LH-1, Loft test L-3-5, the Mist test series, and others demonstrate that RELAP5/MOD2-B&W can adequately predict system thermal-hydraulic responses during a SBLOCA with differing levels of detail used in the noding. Further the combination of noding and code packages selected for the small break evaluations produce conservative peak cladding temperature results for SBLOCAs that result in temperature excursions. Therefore, the RELAP5/MOD2-B&W, FRAP-T6-B&W, and FOAM2 computer codes are adequate for calculating SBLOCA fluid conditions and core cladding temperatures.

References

5-1. K. P. Ardron and P. C. Hall, "UK Experience with RELAP5/MOD2," Central Electricity Generating Board, Generation Development and Construction Division, Barnwood, Gloucester, UK (Private Communication).

5-2. P. Ting, R. Hanson, and R. Jenks, International Code Assessment and Applications Program, NUREG-1270, Vol. 1, March 1987.

5-3. G. G. Loomis and J. E. Streit, Results of Semiscale MOD-2C Small-Break (5%) Loss-of Coolant Accident Experiments S-LH-1 and S-LH-2, NUREG/CR-4438, November 1985.

Table 5-1. Comparison of Calculated and Measured Initial Conditions for Semiscale Test S-LH-1.

Parameter	RELAP5	Measured
Pressurizer Pressure, psia	2244.	2244.
Core Power, Kw	2015.	2015.
Pressurizer Liquid Level, inches	155.5	155.6
Cold Leg Fluid Temperature, F		
Intact Loop	552.1	552.2
Broken Loop	555.6	556.7
Primary System Flow Rate, lbm/s		
Intact Loop	15.7	15.6
Broken Loop	5.2	5.2
Core Bypass Flow (% of total core flow)	0.9	1.0
SG Secondary Pressure, psia		
Intact Loop	829.6	859.7
Broken Loop	881.8	857.2
Core ΔT, F	67.8	67.4
SG Secondary Side Mass, lbm		
Intact Loop	421.0	374.8
Broken Loop	94.8	78.0

Table 5-2. Comparison of Calculated and Measured Sequence of Events for Semiscale Test S-LH-1.

Event	Time, seconds		
		RELAP5 PREDICTIONS	
	Measured	BASE	REVISED
Break Opened	0.5	0.0	0.0
Pressurizer at 1827.5 psia (SIS)	14.67	17.65	17.35
Reactor Scram	19.57	22.60	22.30
Pump Coastdown Initiated			
Intact Loop	21.35	24.35	24.05
Broken Loop	20.76	23.75	23.45
Feedwater Off			
Intact Loop	19.67	22.70	22.40
Broken Loop	19.00	22.00	21.70
MSIV Closure			
Intact Loop	22.0	25.00	24.70
Broken Loop	22.0	25.00	24.70
HPIS Initiated			
Intact Loop	41.60	44.60	44.40
Broken Loop	40.98	44.60	44.40
Pressurizer Emptied	33.90	44.00	40.00
Intact Loop Seal Cleared	171.4	175.0	175.0
Broken Loop Seal Cleared	262.3	214.0	605.0

Table 5-2. Comparison of Calculated and Measured Sequence of Events for Semiscale Test S-LH-1 (continued).

Event	Time, seconds: Measured	RELAP5 PREDICTIONS: BASE	RELAP5 PREDICTIONS: REVISED
Accumulator Injection			
Intact Loop	503.8	324.0	490.0
Broken Loop	501.4	324.0	490.0

SG Secondary Side Pressure Used in the RELAP5 Predictions

BASE RELAP5 SECONDARY PRESSURE: Time sec	Intact Loop psia	Broken Loop psia	REVISED RELAP5 SECONDARY PRESSURE: Time sec	Intact Loop psia	Broken Loop psia
0	860	858	0	860	858
20	860	888	20	860	888
40	1016	1021	40	1016	1021
60	1000	1010	60	1000	1010
100	995	995	100	995	995
200	989	974	150	977	940
300	958	926	200	958	910
1000	863	700	250	929	890
			300	900	877
			1000	863	700

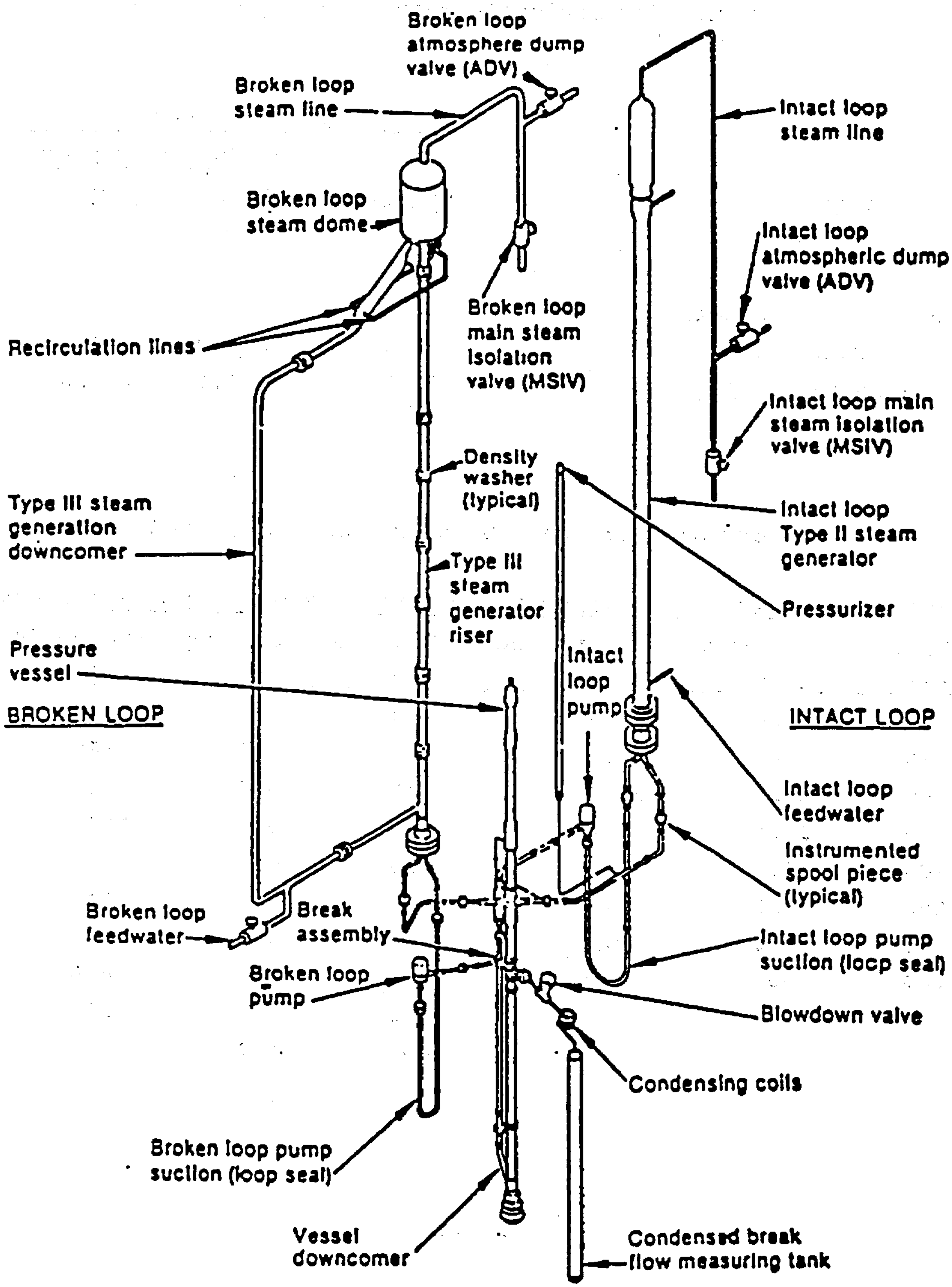

Figure 5-1. Semiscale MOD-2C System Configuration.

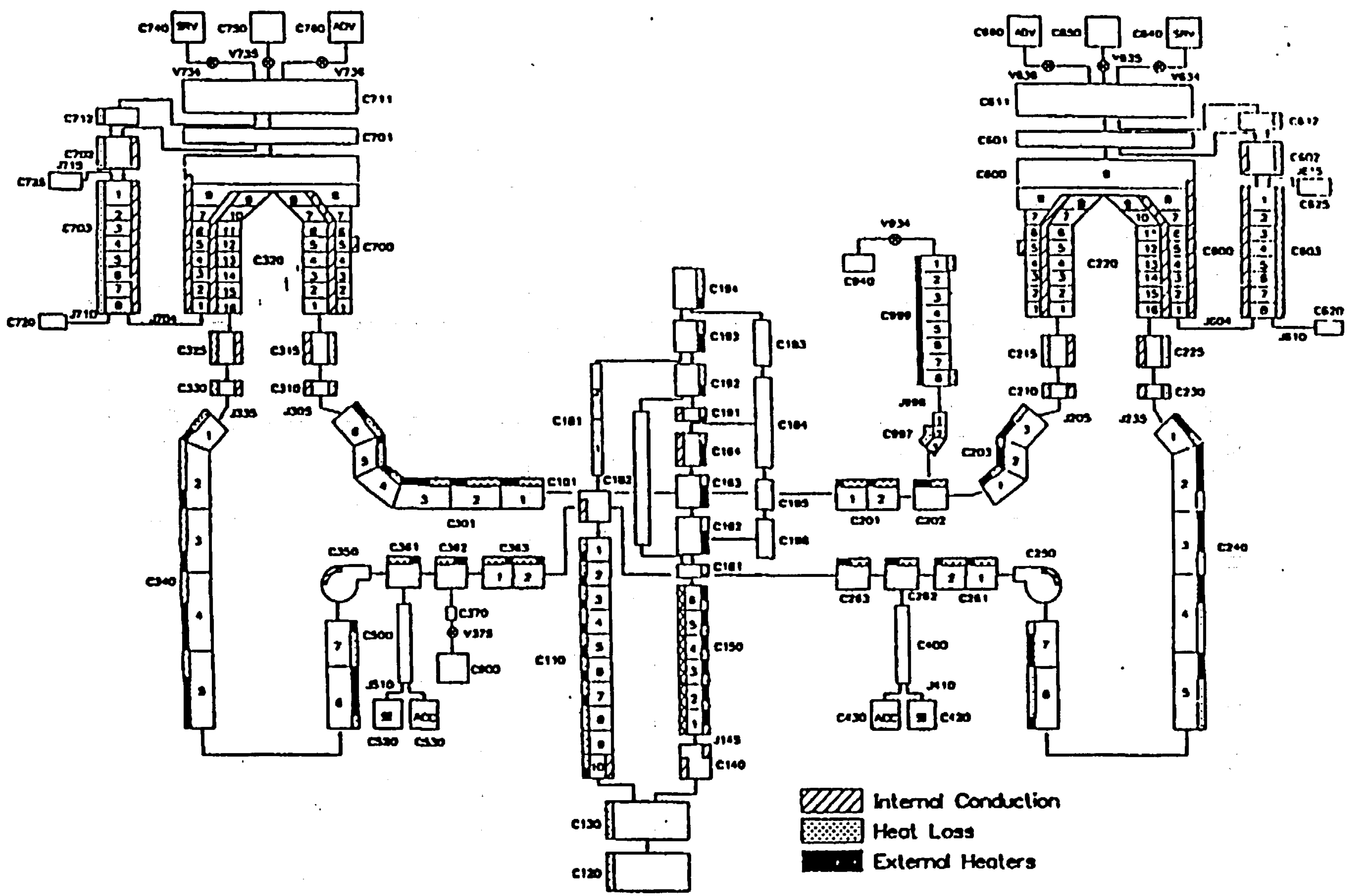

Figure 5-2. Semiscale Test S-LH-1 Base Model Noding Diagram

Figure 5-2a. Semiscale Test S-LH-1 Forced ECCS Bypass Downcomer Noding Diagram.

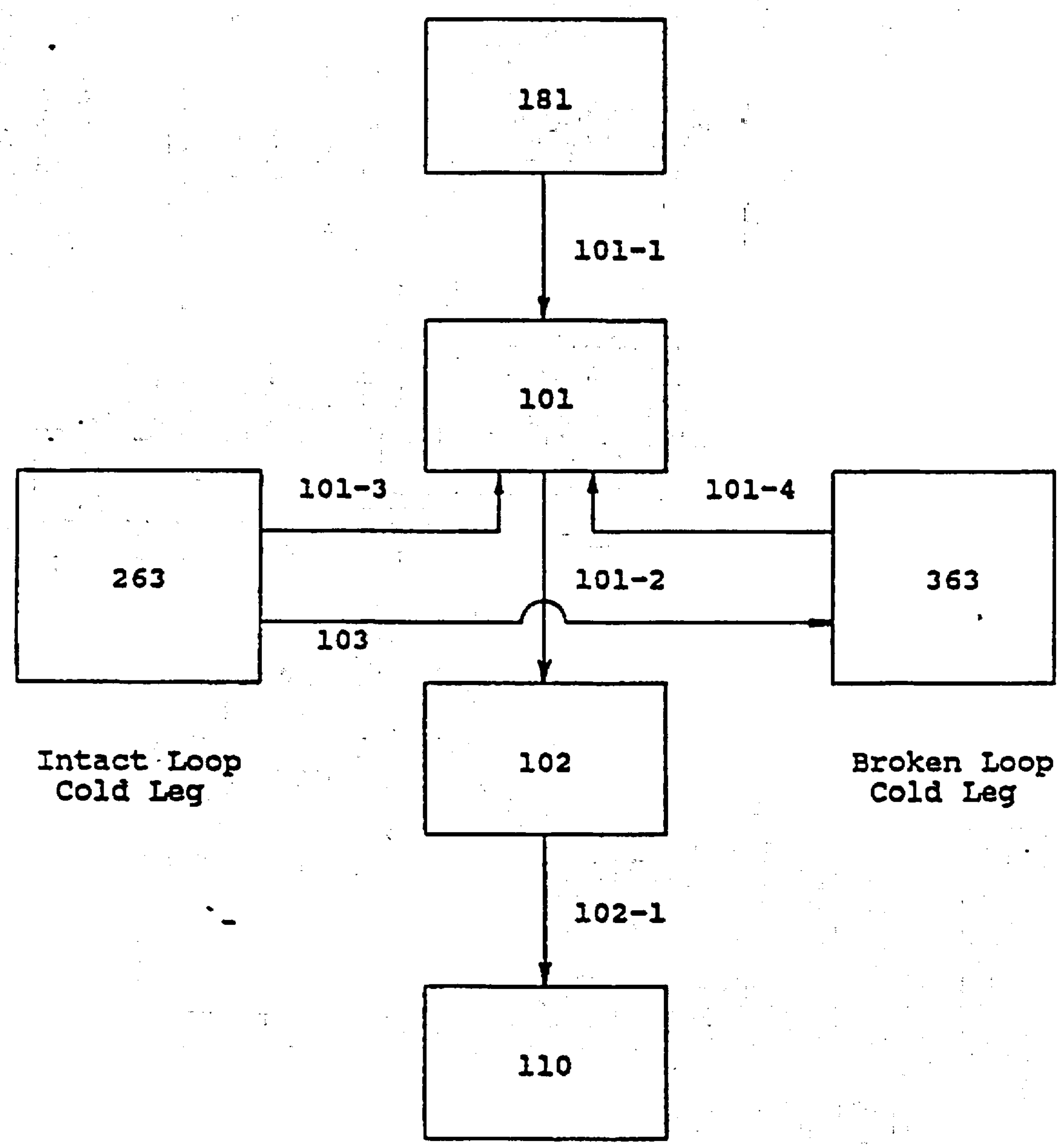

FIGURE 5-3. SEMISCALE TEST S-LH-1; LEAK FLOW RATE.

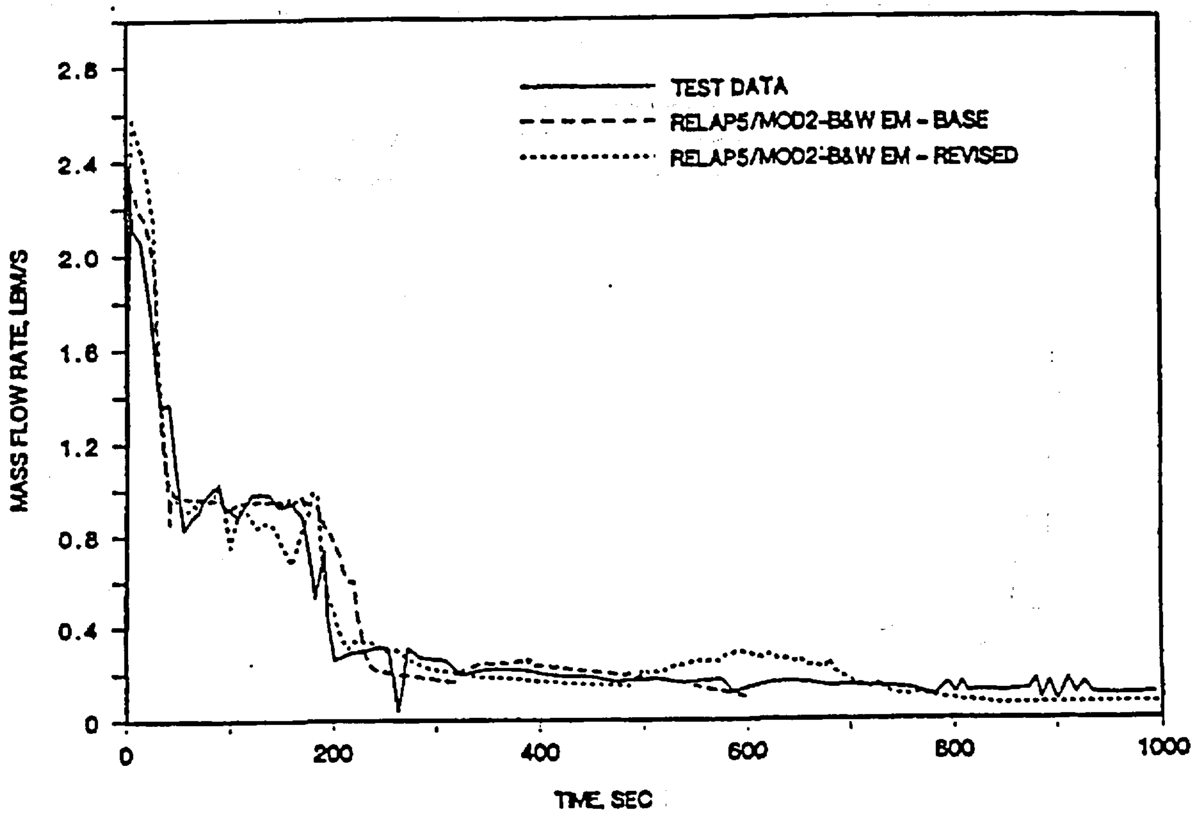

FIGURE 5-4. SEMISCALE TEST S-LH-1; PRIMARY SYSTEM PRESSURE.

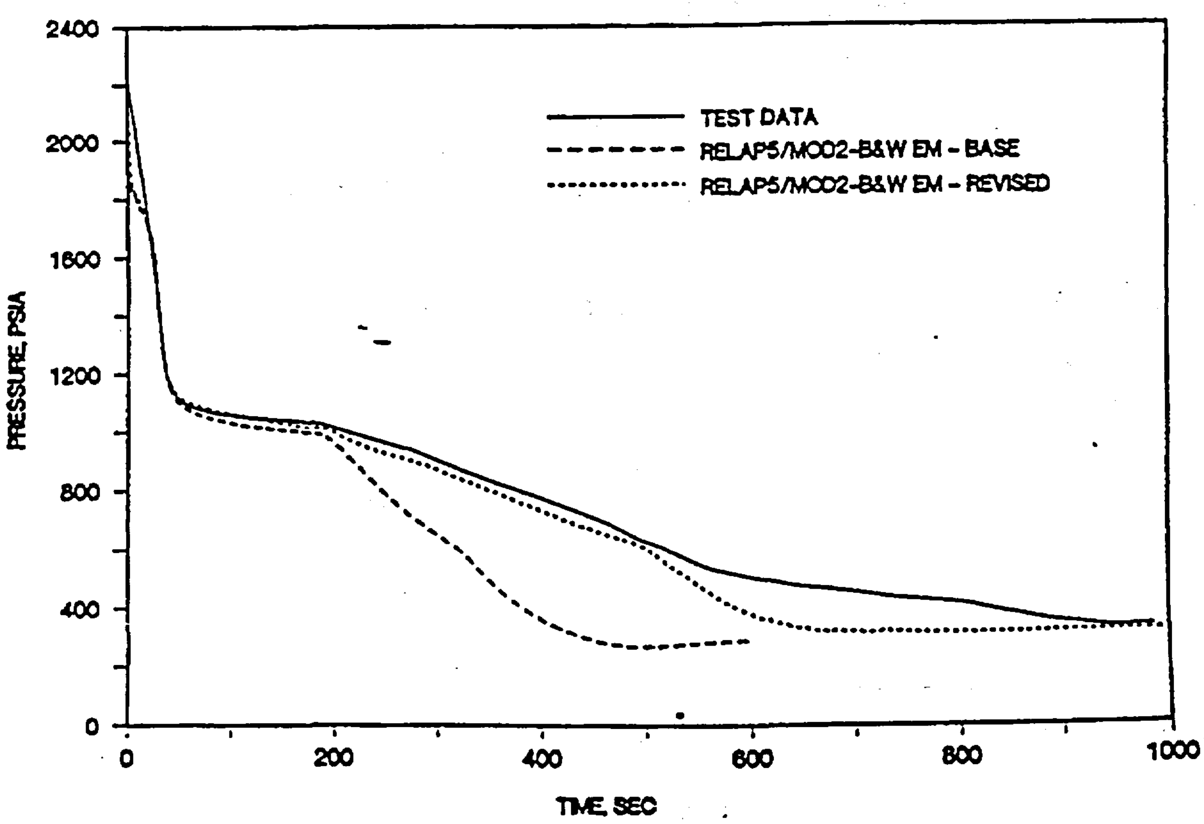

FIGURE 5-5. SEMISCALE TEST S-LH-1; INTACT LOOP STEAM GENERATOR TUBE LEVEL - UP SIDE.

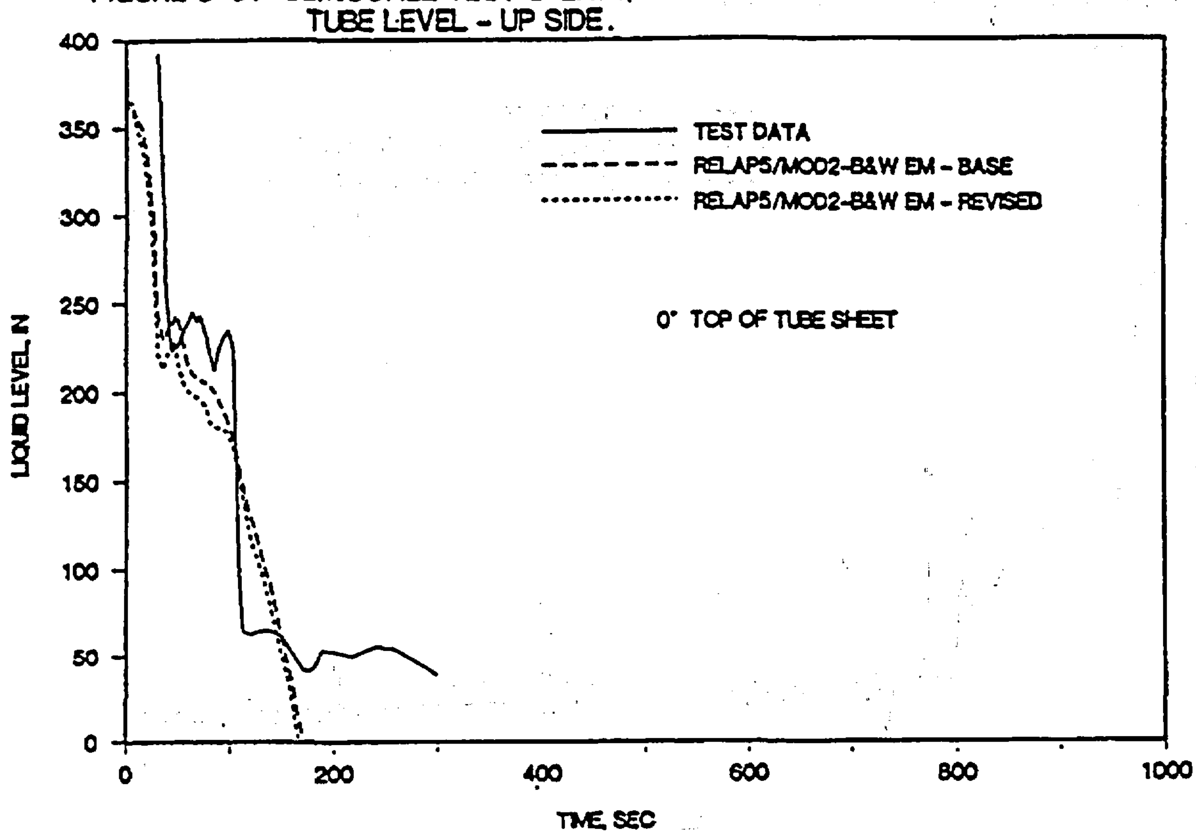

FIGURE 5-6. SEMISCALE TEST S-LH-1; INTACT LOOP STEAM GENERATOR TUBE LEVEL - DOWN SIDE.

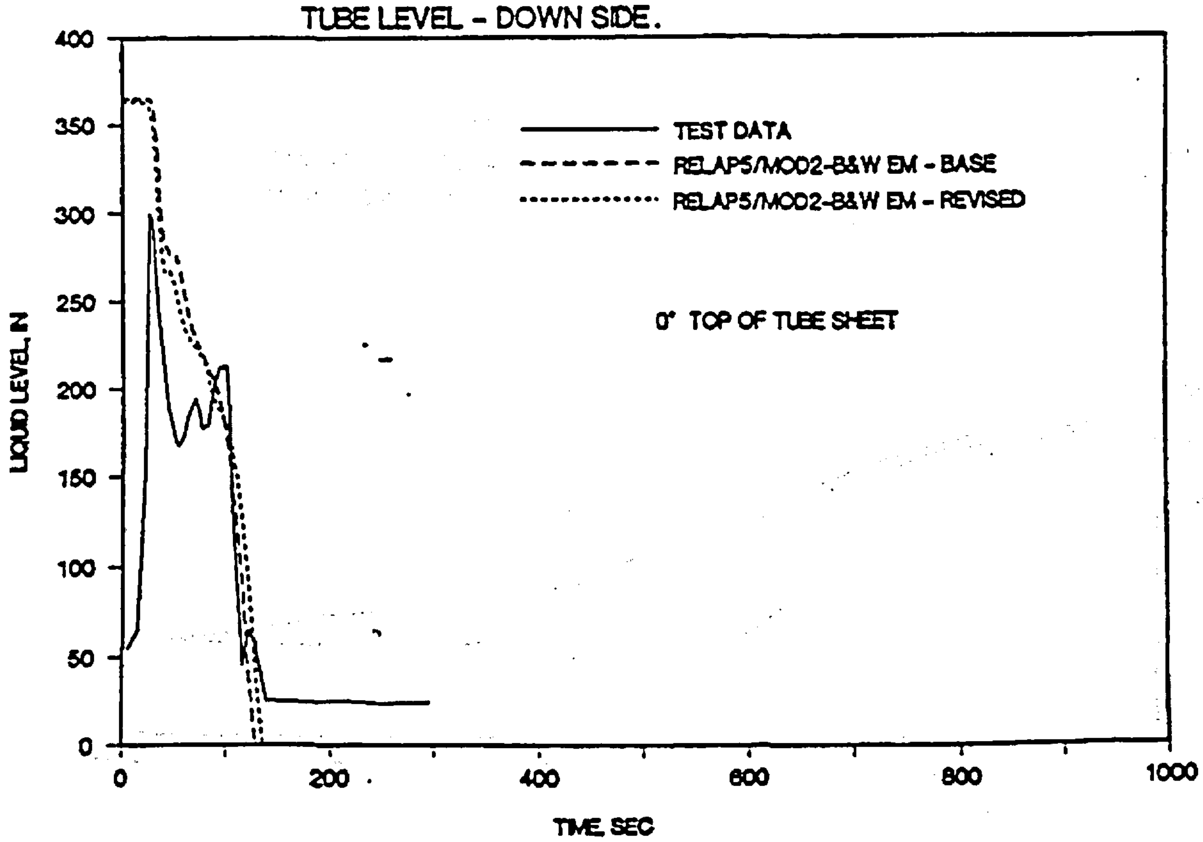

FIGURE 5-7. SEMISCALE TEST S-LH-1; BROKEN LOOP STEAM GENERATOR TUBE LEVEL - UP SIDE.

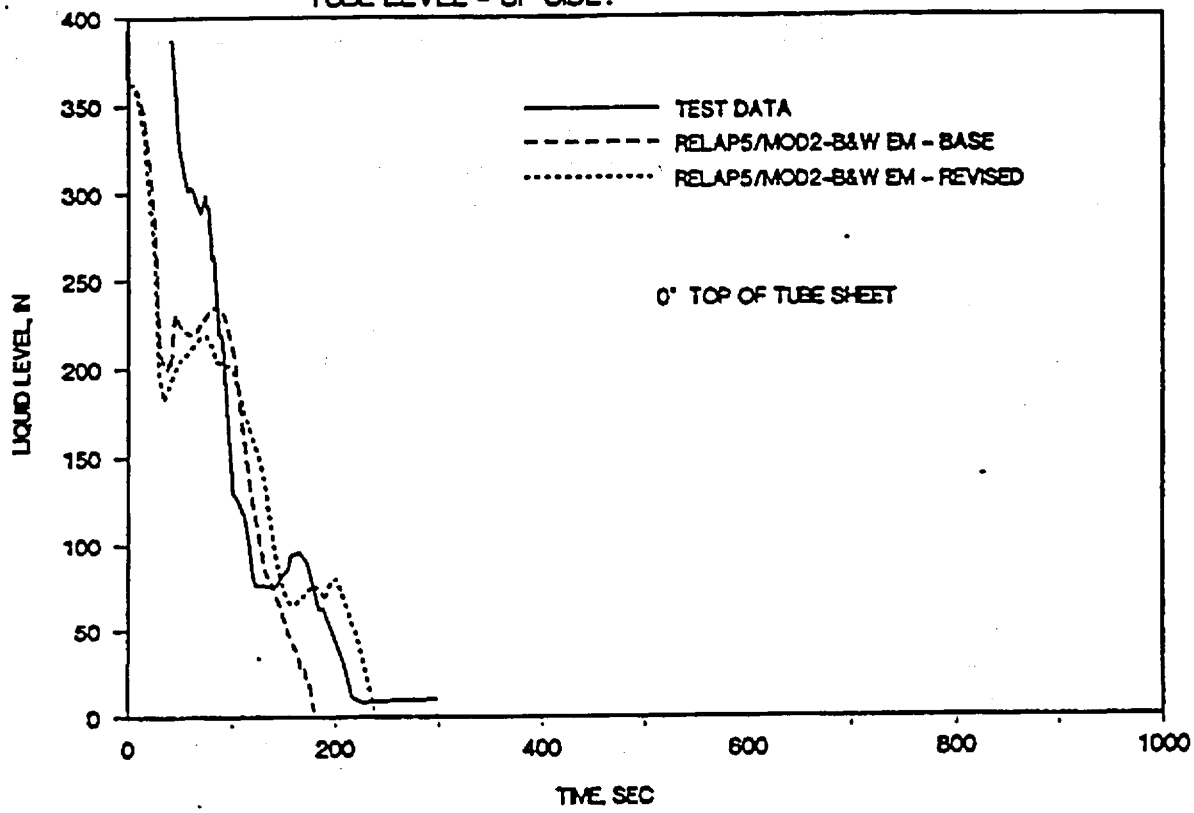

FIGURE 5-8. SEMISCALE TEST S-LH-1; BROKEN LOOP STEAM GENERATOR TUBE LEVEL - DOWN SIDE.

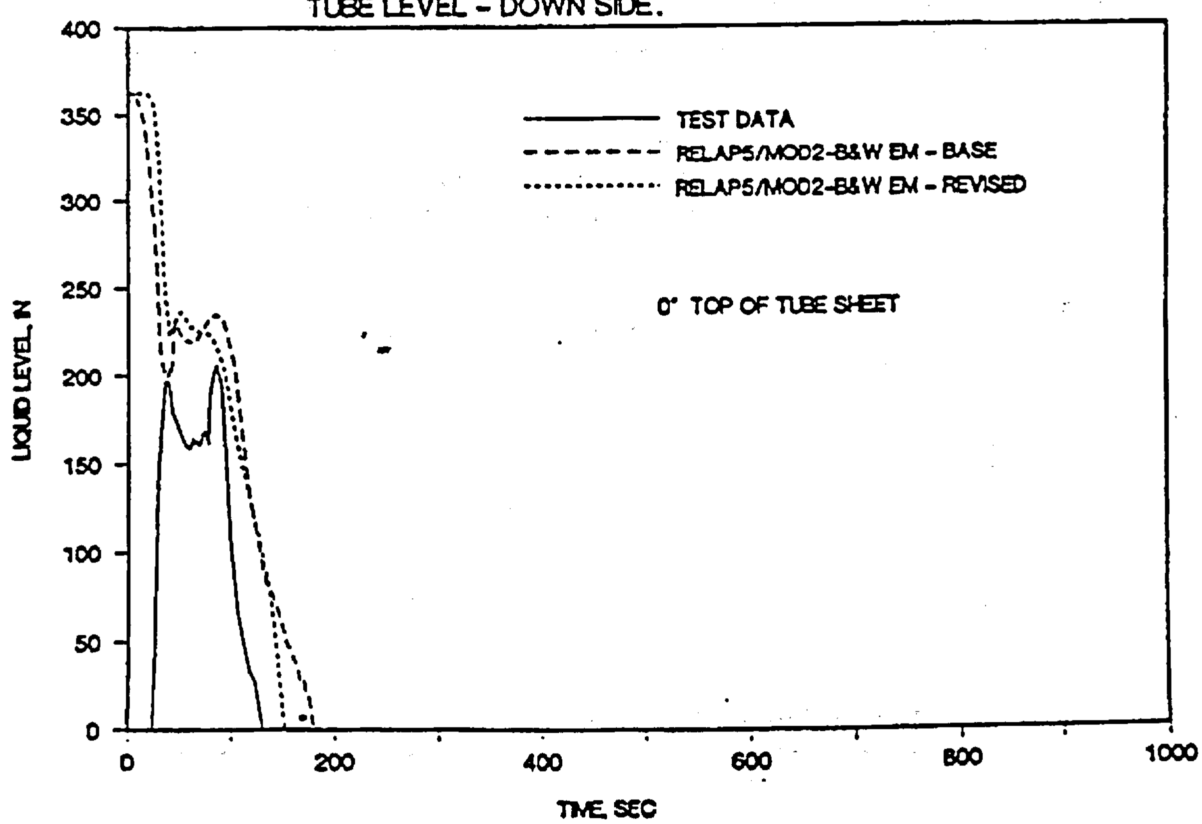

FIGURE 5-9. SEMISCALE TEST S-LH-1; INTACT LOOP PUMP SUCTION LEVEL - DOWN SIDE.

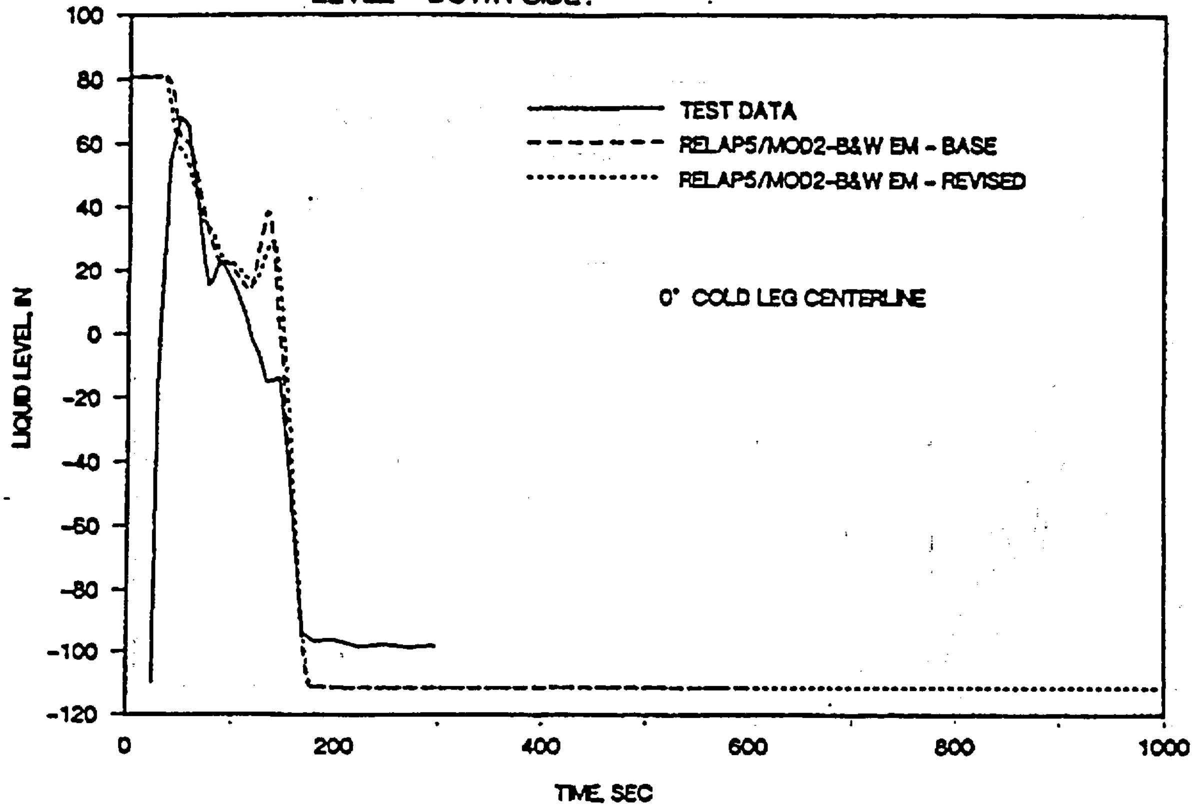

FIGURE 5-10. SEMISCALE TEST S-LH-1; INTACT LOOP PUMP SUCTION LEVEL - UP SIDE.

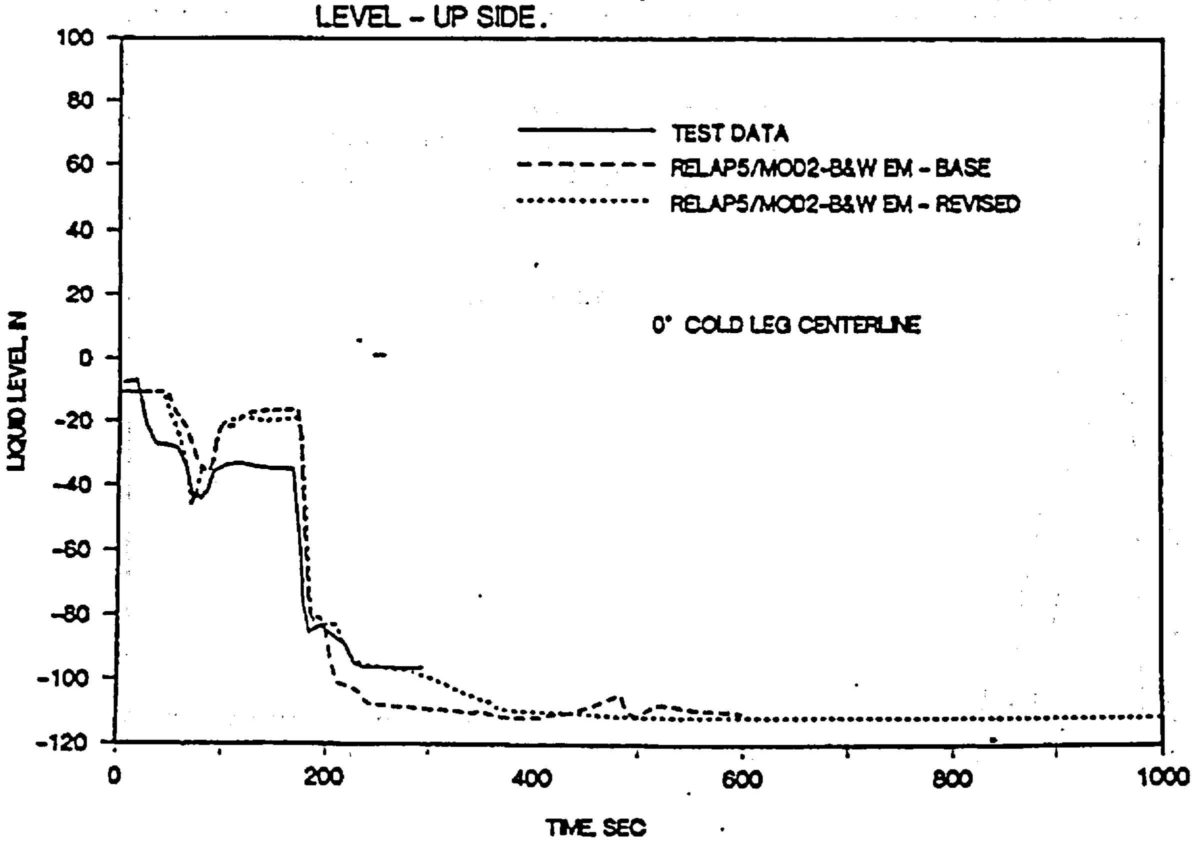

FIGURE 5-11. SEMISCALE TEST S-LH-1; BROKEN LOOP PUMP SUCTION LEVEL - DOWN SIDE.

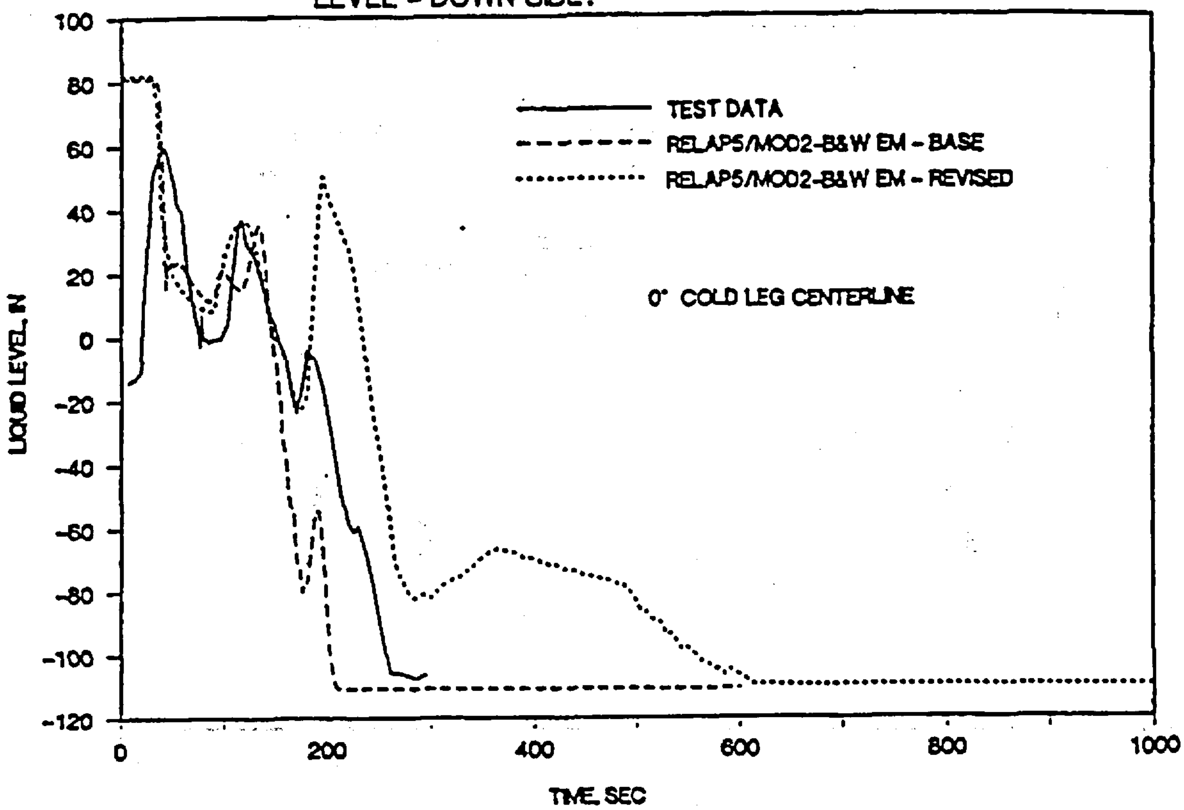

FIGURE 5-12. SEMISCALE TEST S-LH-1; BROKEN LOOP PUMP SUCTION LEVEL - UP SIDE.

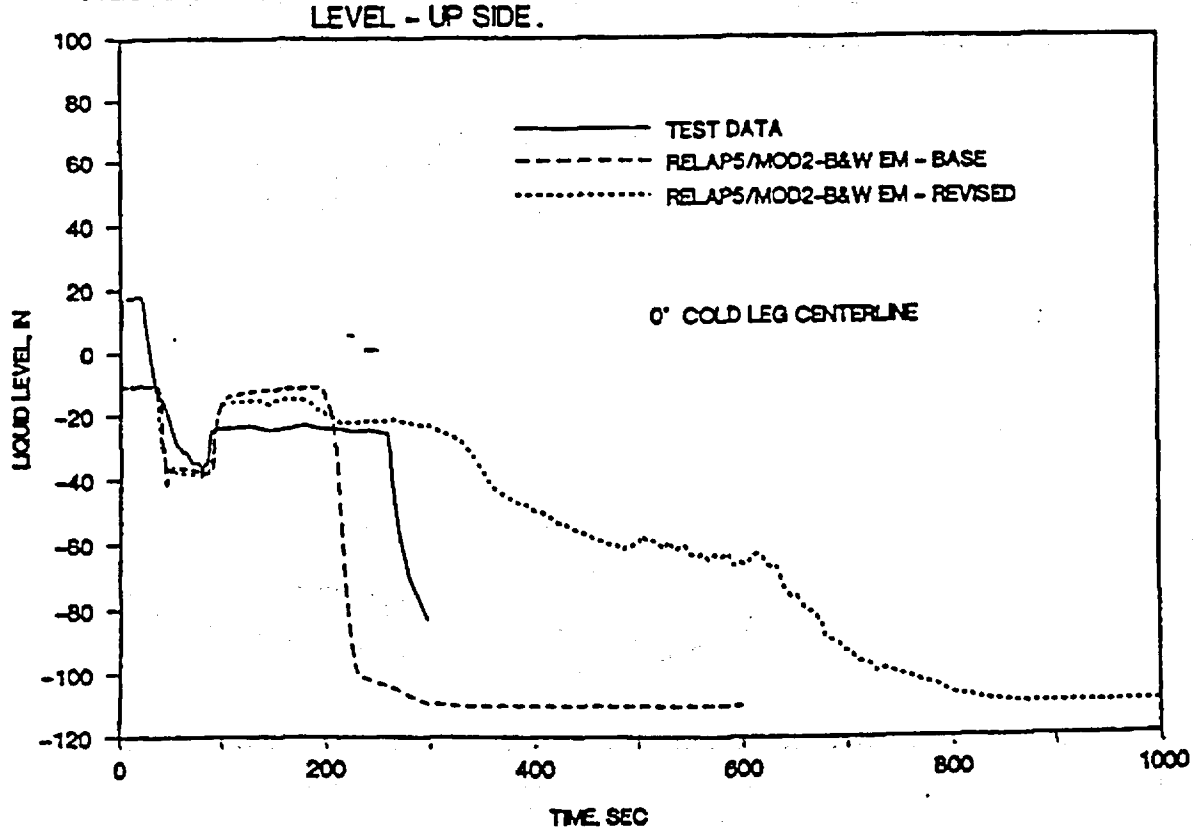

FIGURE 5-13. SEMISCALE TEST S-LH-1; VESSEL LIQUID LEVEL.

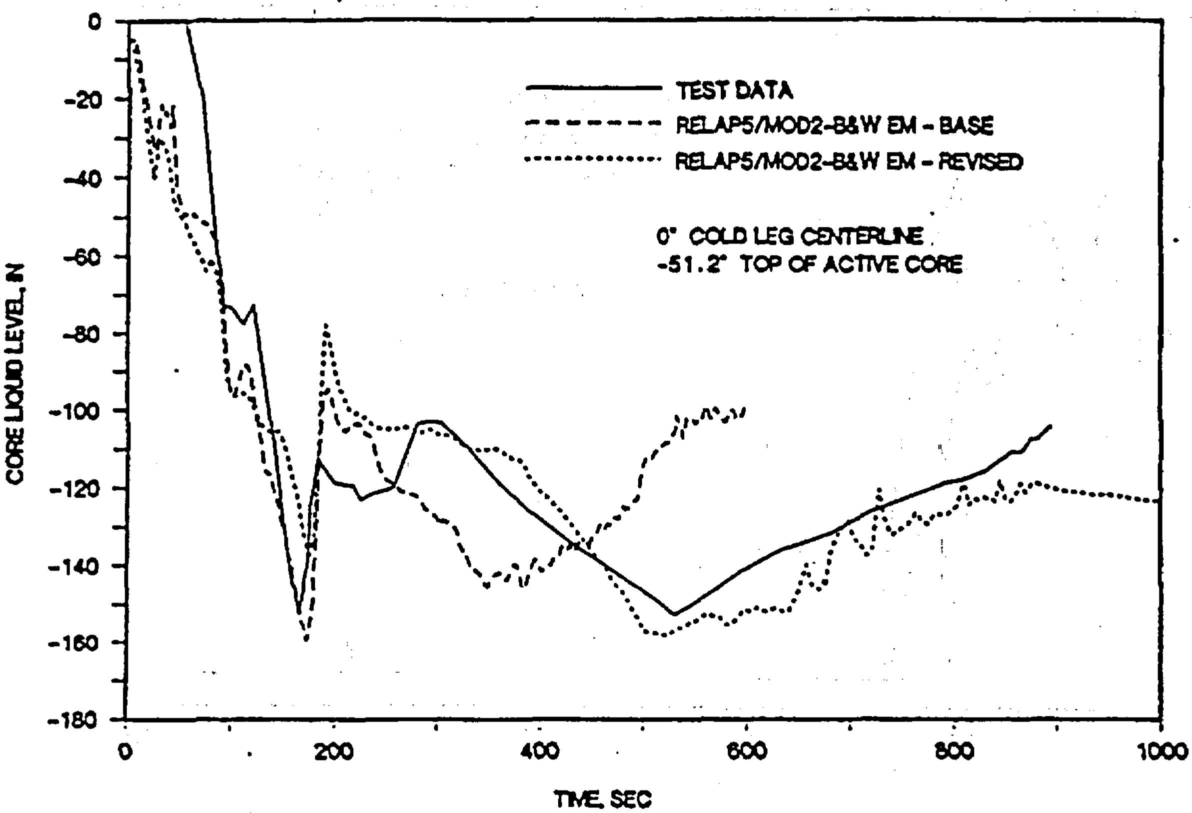

FIGURE 5-14. SEMISCALE TEST S-LH-1; PRIMARY SYSTEM NORMALIZED MASS.

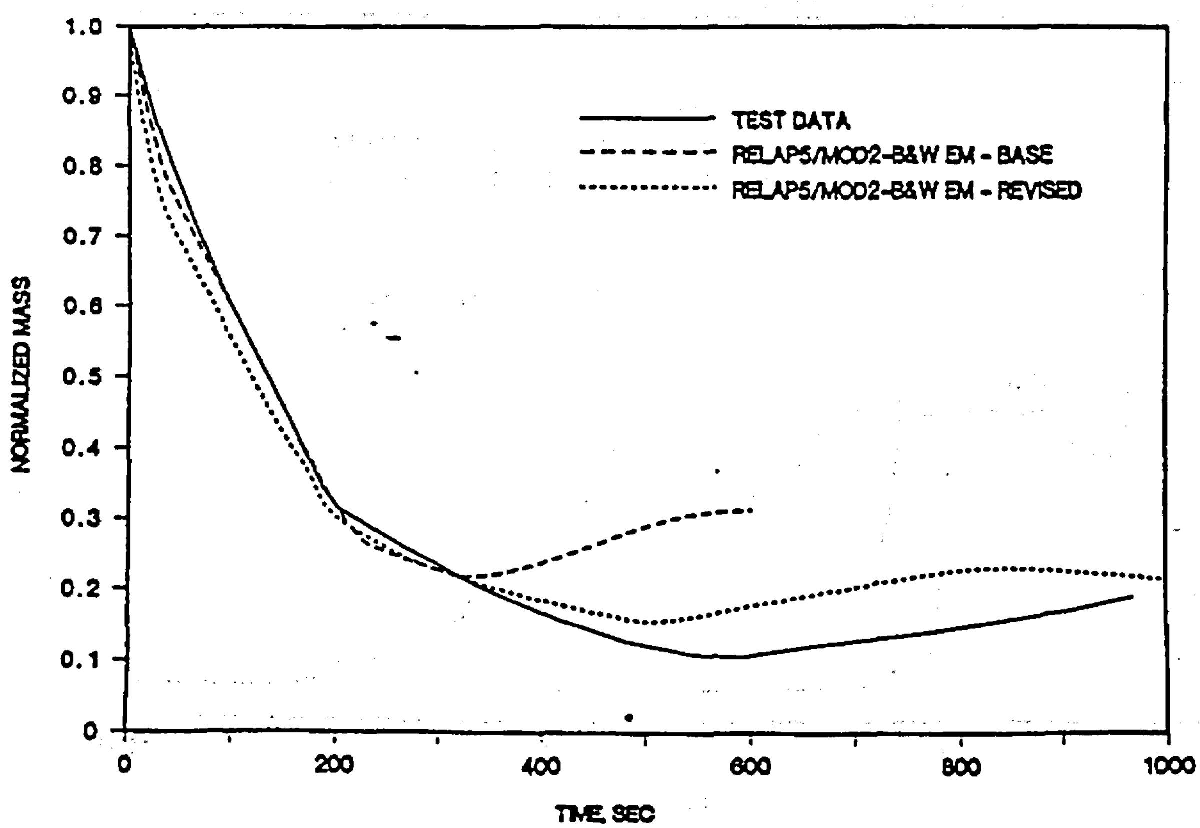

FIGURE 5-15. SEMISCALE TEST S-LH-1; INTACT LOOP ECC FLOW RATE.

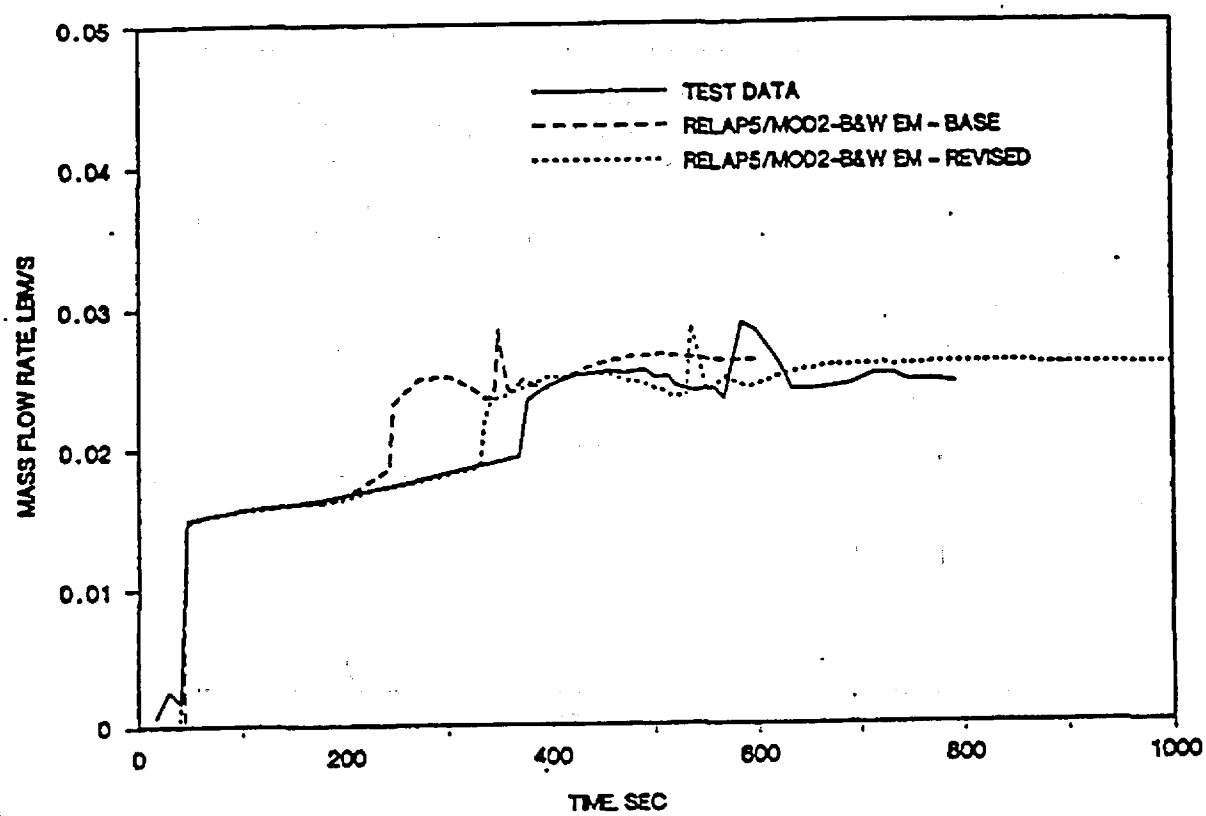

FIGURE 5-16. SEMISCALE TEST S-LH-1; BROKEN LOOP ECC FLOW RATE.

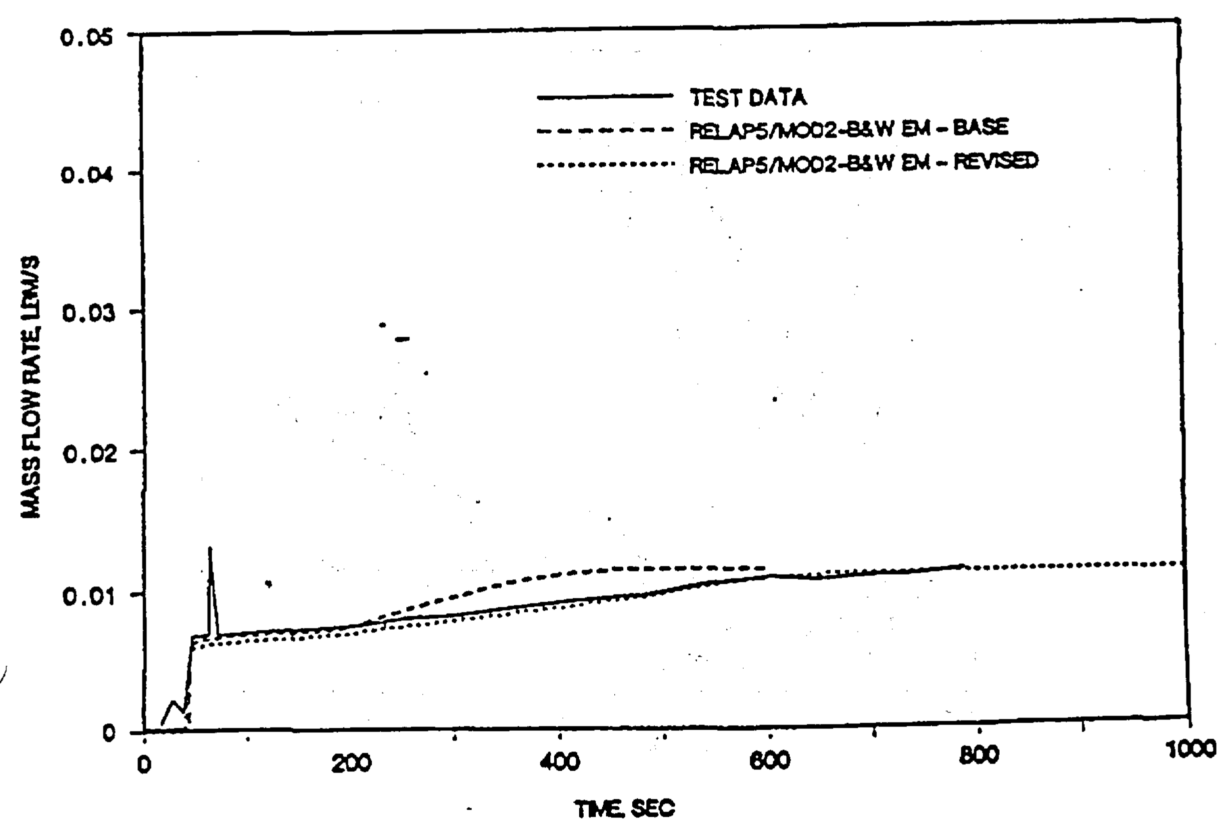

FIGURE 5-17. SEMISCALE TEST S-LH-1; VESSEL UPPER HEAD LIQUID LEVEL.

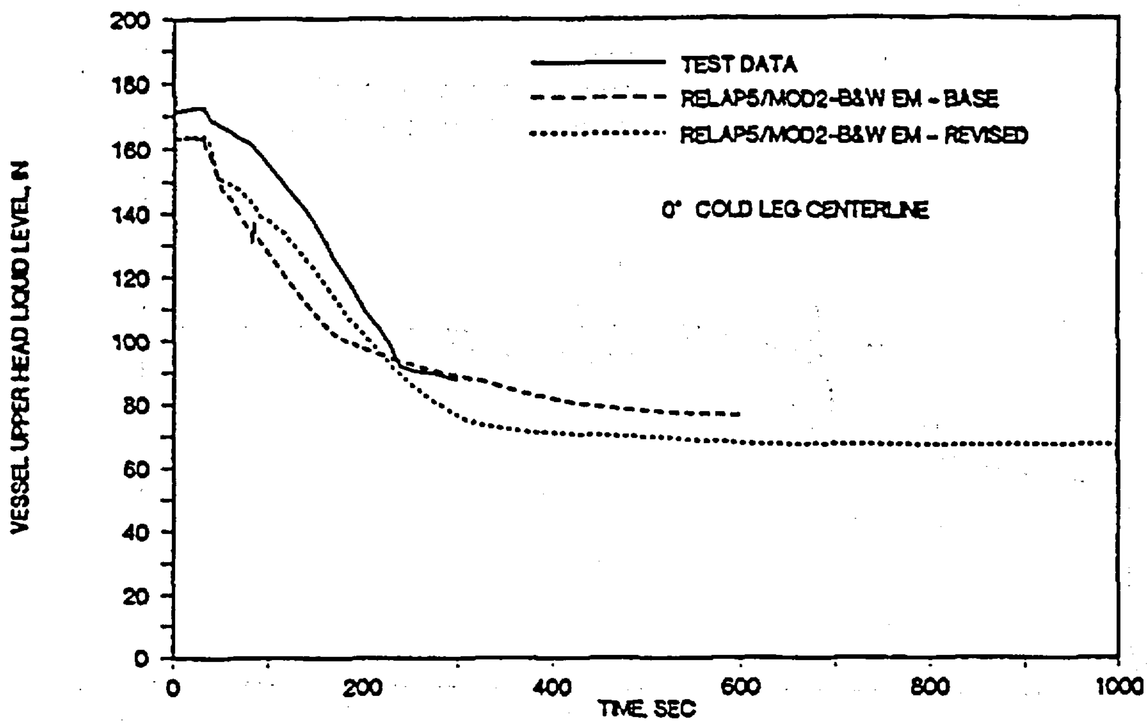

FIGURE 5-18. SEMISCALE TEST S-LH-1; DOWNCOMER LIQUID LEVEL.

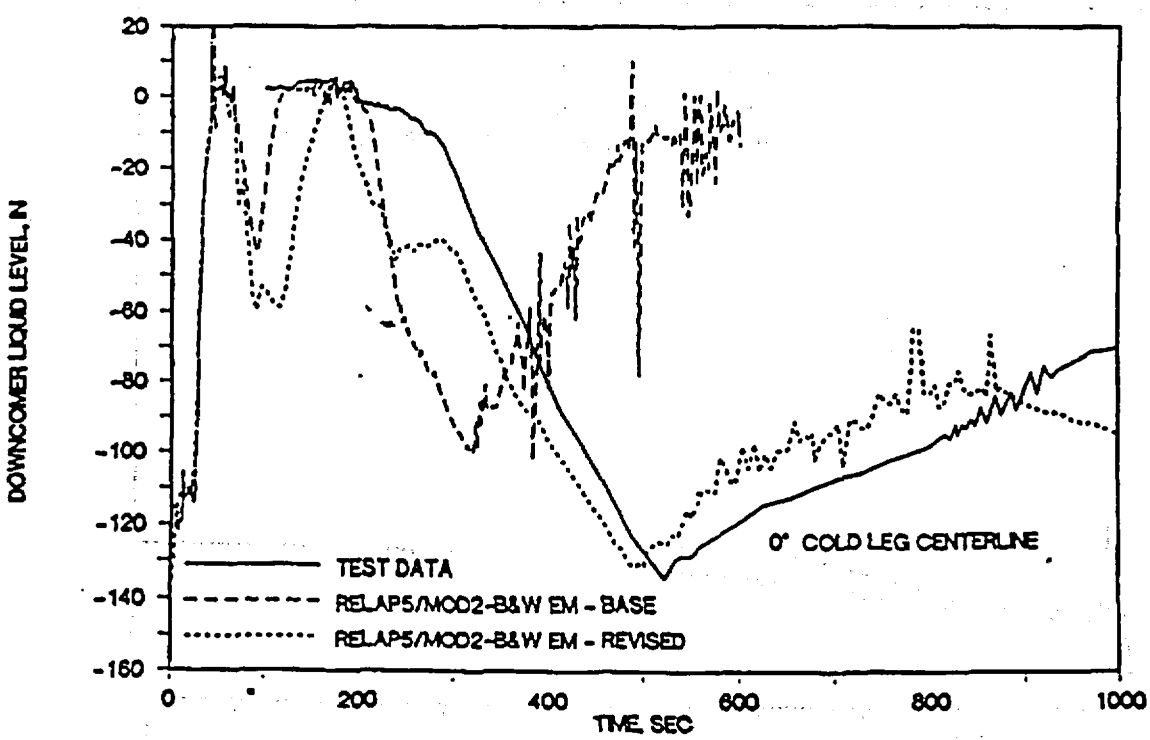

FIGURE 5-19. SEMISCALE TEST S-LH-1; 8 FOOT HEATER ROD SURFACE TEMPERATURE.

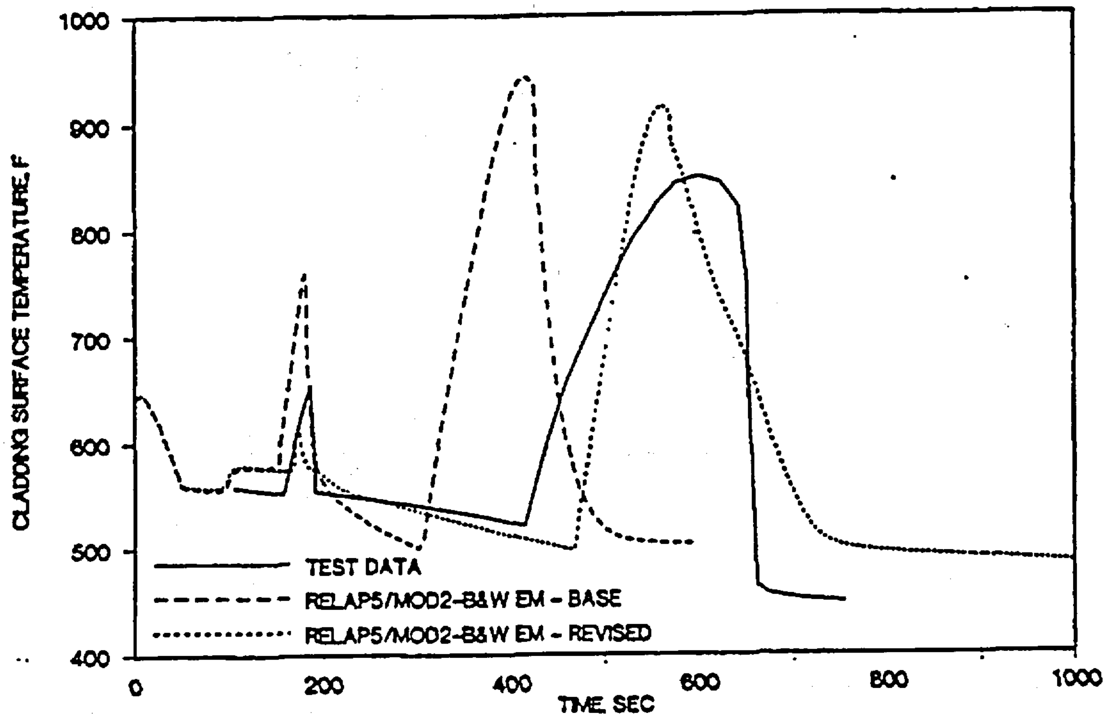

FIGURE 5-20. SEMISCALE TEST S-LH-1; 10 FOOT HEATER ROD SURFACE TEMPERATURE.

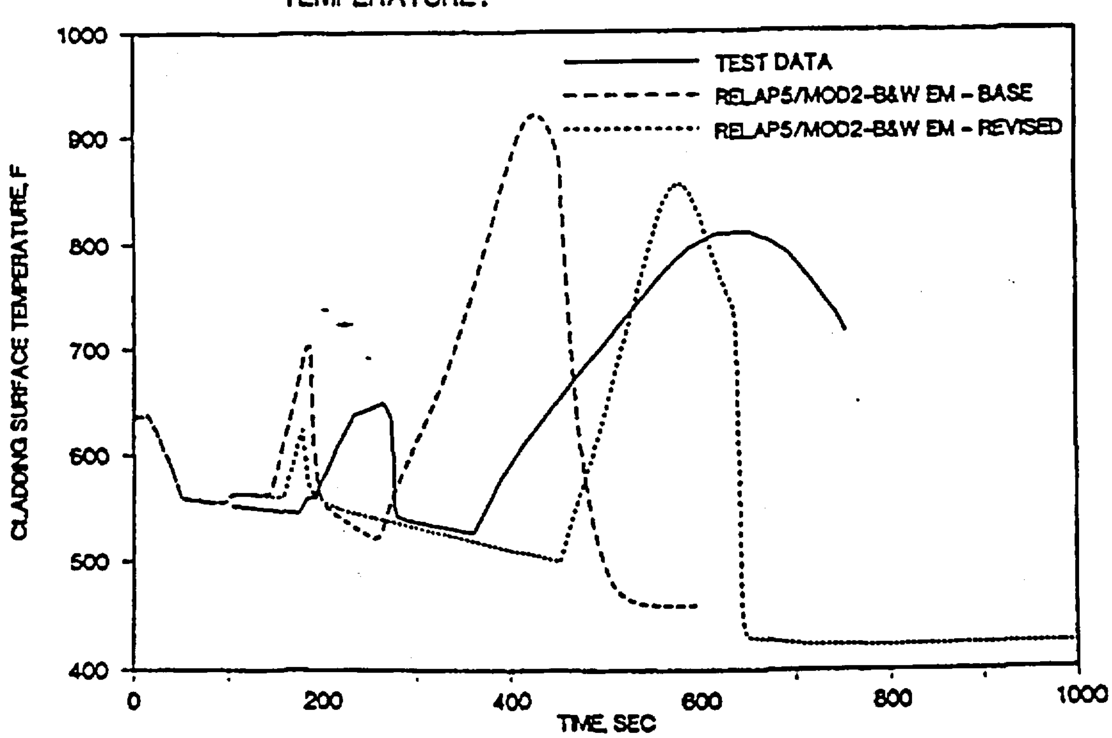

FIGURE 5-21. SEMISCALE TEST S-LH-1; RELAP5/MOD2 BASE CASE CALCULATED TUBE VELOCITIES.

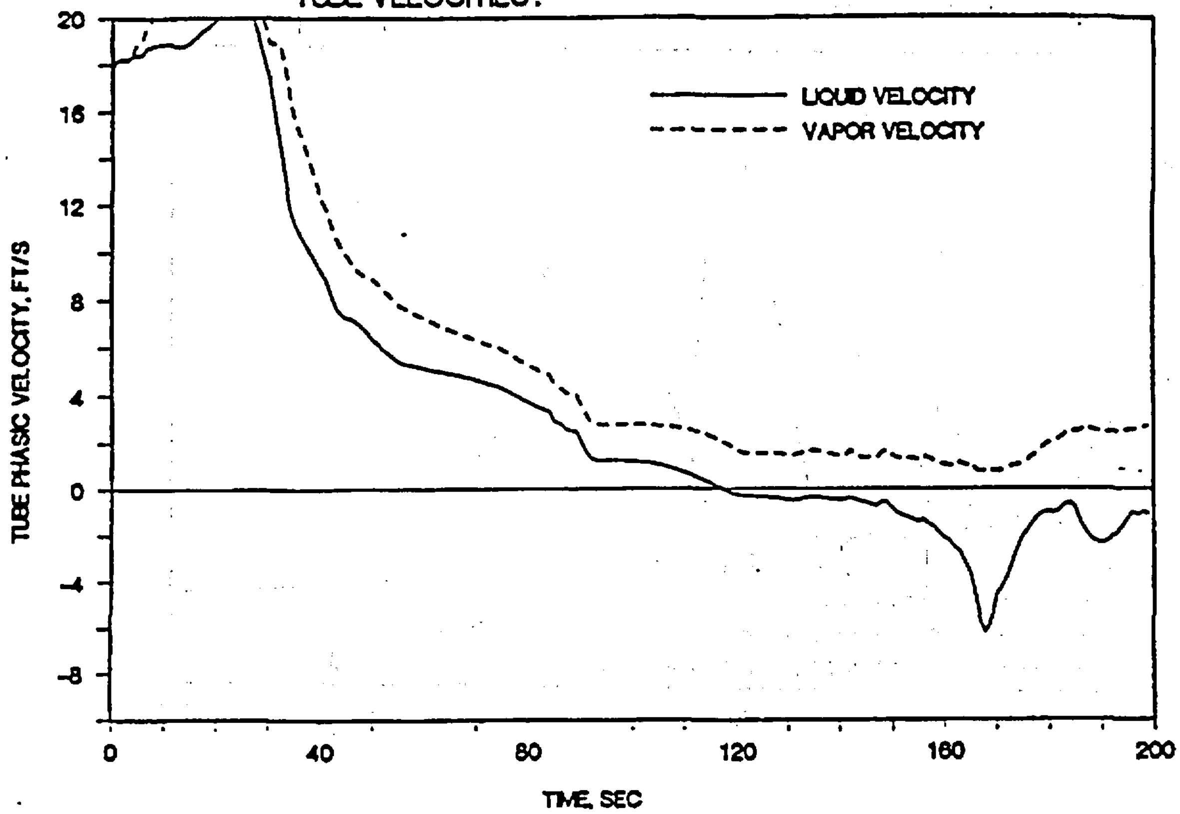

6. Your response to Question 18 stated that an assessment calculation for a 1.0 ft^2 break, which was selected as a transition point between the large- and small-break LOCA calculations, was not needed because this break size is not the limiting case for either large- or small-break LOCA. Confirm that your plant specific break spectrum analyses will include calculations, with both the large- and small-break LOCA EMs, of a 1.0 ft^2 break in order to demonstrate compliance with Section C.1.a of Appendix K to 10 CFR 50.

Response: The B&W recirculating steam generator LOCA evaluation model separates small breaks from large breaks at a break area of 1.0 ft^2. Should the evaluation of a break with that area become necessary as part of a spectrum or partial spectrum submittal for compliance with 10CFR50.46, the evaluation will be performed as both a large break and as a small break. Both results will be reported in the submittal and the deviations between the treatments evaluated and explained.

This page intentionally left blank.

5.3 Safety Evaluation Report of Revision 1

This section contains the safety evaluation report, dated April 18, 1990, issued as a result of NRC review of revision 1 of this topical report. The SER is based on the technical report produced by EG&G, Idaho National Laboratory, as part of the review process; this technical report is included in this section.

This page intentionally left blank.

UNITED STATES
NUCLEAR REGULATORY COMMISSION
WASHINGTON, D. C. 20555

April 18, 1990

Mr. J. H. Taylor, Manager
Licensing Services
B&W Nuclear Technologies
3315 Old Forest Road
P. O. Box 10935
Lynchburg, Virginia 24506-0935

Dear Mr. Taylor:

SUBJECT: ACCEPTANCE FOR REFERENCING OF LICENSING TOPICAL REPORT, BAW-10164P, REVISION 1, "RELAP5/MOD2-B&W, AN ADVANCED COMPUTER PROGRAM FOR LIGHT WATER REACTOR LOCA AND NON-LOCA TRANSIENT ANALYSIS"

We have completed our review of the subject topical report submitted by the Babcock & Wilcox Fuel Company (BWFC), a company of B&W Nuclear Technologies, by a letter of December 28, 1987, and revised by letters of November 2, 1988 and January 30, 1990. We find the report to be acceptable for referencing in license applications to the extent specified and under the limitations delineated in the report and the associated evaluation by the U. S. Nuclear Regulatory Commission (NRC), which is enclosed. The evaluation defines the basis for acceptance of the report.

We do not intend to repeat our review of the matters described in the report when the report appears as a reference in the license applications, except to ensure that the material presented is applicable to the specific plant involved. Our acceptance applies only to the matters described in the report.

In accordance with procedures established in NUREG-0390, NRC requests that BWFC publish accepted versions of this report, proprietary and non-proprietary, within three months of receipt of this letter. The accepted versions shall incorporate this letter and the enclosed evaluation between the title page and the abstract. The accepted versions shall include an "-A" (designating accepted) following the report identification symbol.

Should our criteria or regulations change such that our conclusions about the acceptability of the report are invalidated, we expect BWFC or the applicants referencing the topical report, or both, to revise and resubmit their respective documentation, or to submit justification for the continued effective applicability of the topical report without revision of their respective documentation.

Sincerely,

Ashok C. Thadani, Director
Division of Systems Technology
Office of Nuclear Reactor Regulation

Enclosures:
's stated

UNITED STATES
NUCLEAR REGULATORY COMMISSION
WASHINGTON, D. C. 20555

ENCLOSURE 1

SAFETY EVALUATION OF THE BABCOCK & WILCOX FUEL COMPANY TOPICAL REPORT BAW-10164P, REVISION 1, RELAP5/MOD2-B&W, AN ADVANCED COMPUTER PROGRAM FOR LIGHT WATER REACTOR LOCA AND NON-LOCA TRANSIENT ANALYSIS

1.0 INTRODUCTION

As part of safety analysis for fuel reloads of the pressurized water reactor (PWR) plants equipped with recirculating steam generators (RSGs), the Babcock & Wilcox Fuel Company (BWFC) developed reload safety analysis methodologies for loss-of-coolant accidents (LOCAs) and non-LOCA transients and accidents. The LOCA evaluation model is described in topical report BAW-10168P, "RSG LOCA" (Ref. 1). The approach for the safety analysis of non-LOCA transients is described in topical report BAW-10169P, "RSG Plant Safety Analysis" (Ref. 2). The system transient analysis code RELAP5/MOD2-B&W is used, complemented with other codes, to perform both LOCA and non-LOCA analyses. The RELAP5/MOD2-B&W code, which is the subject of this review, is described in the report BAW-10164P, Revision 1, submitted and amended by letters of December 28, 1987, November 2, 1988, and January 30, 1990 (Refs. 3, 4, 5).

For a large-break LOCA, the RELAP5/MOD2-B&W code is used to calculate reactor coolant system transients and core thermal hydraulic conditions during the blowdown phase. These calculations are followed by the use of the REFLOD3B and BEACH codes (Refs. 6 and 7) to calculate the refill and reflood responses. For a small-break LOCA (SBLOCA), the entire system response is analyzed with the RELAP5/MOD2-B&W code. If a core uncovery is predicted to occur, the FOAM2 code (Ref. 8) is used to calculate the mixture height inside the reactor core. The FRAP-T6-B&W code (Ref. 9) is then used in both large-break and small-break LOCAs to calculate the thermal response and peak cladding temperature (PCT) at the hot fuel rod.

The non-LOCA safety analysis methodology uses the RELAP5/MOD2-B&W code to model and calculate the system responses for each transient. Reactor core power during each transient is calculated using the point kinetics neutronic model in the RELAP5/MOD2-B&W code. The resulting thermal hydraulic conditions of the core calculated using the RELAP5/MOD2-B&W code are used as boundary conditions for another core thermal hydraulic code, such as LYNXT (Ref. 10), to determine the temperature and departure from nucleate boiling ratio (DNBR) of the hot rod.

This safety evaluation addresses only the acceptability of using the RELAP5/MOD2-B&W code with proper details of the reactor system noding for calculation of transient system response as part of the reload safety analysis of LOCA and non-LOCA transients and accidents. Implementation of the overall transient and accident analyses is addressed in the review of the LOCA evaluation model (EM) topical report BAW-10168P and the non-LOCA safety analysis method report BAW-10169P. Because the RELAP5/MOD2-B&W code is a part of the LOCA EM and the non-LOCA safety analysis, the restrictions imposed on RELAP5/MOD2-B&W will also affect these analyses, and vice versa.

2.0 DESCRIPTION OF RELAP5/MOD2-B&W

The RELAP5/MOD2-B&W code is a BWFC version of the advanced system analysis computer code RELAP5/MOD2. RELAP5/MOD2 was developed by the Idaho National Engineering Laboratory as a best-estimate code to simulate a wide variety of PWR system transients. The code, which is also organized into modules by components and functions, was designed to model the behavior of all major components in the reactor system during accidents ranging from large-break and small-break LOCAs to anticipated operational transients involving the plant control and protection systems. This code supports simulation of the primary system, secondary system, feedwater train, system controls, and core neutronics. Special component models include pumps, valves, heat structures, electric heaters, turbines, separators and accumulators.

The fundamental equations, constitutive models and correlations, and method of solution of RELAP5/MOD2 are described in NUREG/CR-4312 (Ref. 11). The recently published NUREG/CR-5194 (Ref. 12) contains a very detailed description of models and correlations used in the RELAP5/MOD2 code. RELAP5/MOD2-B&W preserves the original models of RELAP5/MOD2. However, new features and models have been added to ensure compliance with the requirements in Appendix K for LOCA ECCS evaluation model to permit licensing LOCA analysis. The more significant features added include:

(1) The Moody, extended Henry-Fauske, and Murdock-Bauman critical flow models.

(2) A core heat transfer model

(3) The return to nucleate boiling and transition boiling lockout logics

(4) New fuel rod behavior models to represent fuel rod fission gases, rod deformation, fuel-cladding swelling and rupture, gap conductance, and zircaloy-water reaction.

The RELAP5/MOD2-B&W hydrodynamic model is a one-dimensional (axial), transient, two-fluid model used to calculate the flow of a steam-water two-phase mixture. This two-fluid model uses six field equations: 2 phasic-continuity equations, 2 phasic-momentum equations and 2 phasic-energy equations. Therefore, RELAP5/MOD2-B&W is capable of calculating the characteristics of non-homogeneous, non-equilibrium flow. The hydrodynamics model also contains several options for invoking simpler hydrodynamics models, such as homogeneous flow, thermal equilibrium, and frictionless flow models, which can be used independently or in combination. The system model is solved numerically using a semi-implicit finite difference technique. The user can also select an option for solving the system model using a nearly-implicit finite difference technique that allows for violation of the material Courant limit, and is suitable for steady state calculations and for slowly-varying, quasi-steady transient calculations.

The RELAP5/MOD2-B&W code uses a point-kinetics model with six delayed neutron groups to calculate reactor power as a function of time. It contains provisions for fuel temperature, moderator temperature and density reactivity feedback. Other reactivity feedbacks such as those caused by boron concentration changes and tripped-rod reactivity are provided with input tables for generalized reactivity with respect to time.

The constitutive models in the RELAP5/MOD2-B&W code include models for defining flow regimes, and flow-regime-related models for calculating wall friction, interfacial mass transfer, heat transfer, and drag force. A core structure heat transfer model and a fuel pin heat conduction model with dynamic fuel cladding gap conductance model are included. The core heat transfer package can calculate heat transfer coefficients for various heat transfer regimes from single-phase convection, nucleate boiling, to post-critical heat flux (CHF) heat transfers.

Other special features of the RELAP5/MOD2-B&W that are very useful in the thermal-hydraulic analysis of PWRs include dynamic pressure loss models associated with abrupt area change for single-phase and two-phase flows, a centrifugal pump performance model with two-phase degradation effects, choked flow models with treatment for horizontal stratification, nonhomogeneous two-phase flow, counter-current flow models, crossflow junctions, decay heat models, a fine mesh renodalizing scheme for heat conduction, liquid entrainment, a motor valve model, a relief valve model, control system, and trip system.

3.0 STAFF EVALUATION

The staff performed the evaluation of the RELAP5/MOD2-B&W code with technical assistance from Idaho National Engineering Laboratory. A technical evaluation report (TER) regarding the acceptability of the RELAP5/MOD2-B&W code is attached as part of this evaluation. We have reviewed the TER and concurred with the conclusion.

Based on our review, we find that the RELAP5/MOD2-B&W code contains appropriate phenomenological models suitable for calculating both LOCA and non-LOCA transients. Also, the RELAP5/MOD2-B&W code contains nothing that is plant-specific in nature or that would preclude the application of the code to any of the recirculating steam generator plants. Therefore, the RELAP5/MOD2-B&W code can be applied to any of the proposed Westinghouse and Combustion Engineering plants.

BWFC has developed two plant-noding models with the RELAP5/MOD2-B&W code for the analysis of non-LOCA transients and accidents. One is a low-power model for analysis of steamline breaks at low power. The other is a full-power model for analysis of other transients such as a turbine trip, a locked reactor coolant pump rotor, and the uncontrolled withdrawal of a rod cluster control assembly bank, etc. The report BAW-10169P (Ref. 2) describes both models, and also presents the benchmark comparisons between the results of the RELAP5/MOD2-B&W calculations with these models and the results of selected final safety analysis reports (FSARs) of Westinghouse PWR-designed plants for the transients and accidents representing different transient categories to be analyzed in the safety analysis. The comparisons of several important parameters, such as neutron and thermal powers, pressurizer pressure and water level, core inlet and average temperatures, and flow rate, indicated a generally good agreement in the trends of these parameters. This agreement indicates the appropriateness of using the RELAP5/MOD2-B&W code with proper plant noding details to calculate the system responses to the transients. Therefore, it is acceptable to use the RELAP5/MOD2-B&W code for licensing calculations of transient reactor system responses. However, for a complete safety analysis, an approved core thermal hydraulic code and critical heat flux correlation should be used with the RELAP5/MOD2-B&W code. The noding details and inputs should be justified on a plant-specific basis. The choice of constitutive models including the empirical models and correlations should be justified to ensure that their use is within the ranges of applicability.

The RELAP5/MOD2-B&W code also contains the features and models necessary to satisfy the requirements of Appendix K to 10 CFR 50. Therefore, we find this code to be acceptable for use in integral system analyses for the large-break and small-break LOCAs, i.e. the calculation of the system blowdown response for large-break LOCAs and the calculation of the system hydraulic response for small-break LOCAs.

4.0 SUMMARY

The staff has reviewed Topical Report BAW-10164P, Revision 1. Except for the following conditions and restrictions, we find that the RELAP5/MOD2-B&W code is acceptable for calculating the reactor system responses in performing the safety analysis of transients and accidents, including large-break and small-break LOCAs.

(1) The Chen-Sundaram-Ozkaynak film-boiling correlation in the core heat transfer model and the B&W auxiliary feedwater model for once-through steam generators were not reviewed and, therefore, should not be used in licensing calculations without prior review and approval by the NRC.

(2) Prerupture cladding swell is not modeled because BWFC indicated that the swell is generally less than 20 percent with insignificant flow diversion effects. The acceptability of neglecting the effects of prerupture swelling is part of the LOCA EM review based on BWFC's analysis of the flow diversion effects. The SER on report BAW-10168P will address the resolution of this matter.

(3) The built-in kinetics data for decay heat calculations in the RELAP5/MOD2-B&W code are based on the 1973 and 1979 standards of the American Nuclear Society (ANS). Because Appendix K requires the use of a value that is 1.2 times the 1971 ANS standard for decay heat calculation, BWFC should ensure that the decay heat used in licensing LOCA analysis complies with Appendix K.

(4) The LOCA assessments of the Extended Henry-Fauske and Moody critical flow models were based on the use of the static properties as input to the critical flow tables. The LOCA licensing calculations should be performed accordingly.

(5) The interphase drag model of the RELAP5/MOD2-B&W code tends to overpredict interphase drag. This overprediction may cause nonconservative predictions of loop seal clearing phenomena in that liquid is cleared even when the steam flow is not sufficiently high to drag the liquid out of the loop seal. Therefore, this model may not accurately calculate the core uncovery and the peak cladding temperature (PCT). A resolution requiring a sensitivity study to choose a proper loop seal nodalization that results in the highest PCT calculation will be addressed in the LOCA EM review.

(6) Even though noncondensible gases are not modeled in the SBLOCA system analysis, BWFC demonstrated negligible effect that all sources of noncondensible gases will have on the overall response of the system for the range of SBLOCAs. However, BWFC noted that a 50 psi increase above the steam generator control pressure of 1150 psia could result from a worst case release of noncondensible gases. The staff believes that this pressure increase generally would not substantially reduce the injection capabilities of the charging and safety injection (SI) systems. However, because the performance characteristics of the SI pumps vary widely in the plants, verification should be made on a plant-specific basis to ensure that a 50 psi pressure increase will not greatly reduce SI flow such that the PCT would increase by more than 50°F. Otherwise, additional information should be provided to justify neglect of noncondensible gases, or the effect of the pressure increase caused by noncondensible gases should be included in the analysis.

(7) For a complete safety analysis, an approved core thermal hydraulic code and CHF correlation should be used with the RELAP5/MOD2-B&W code. The noding details and inputs should be justified on a plant-specific basis.

The choice of constitutive models including the empirical models and correlations should be justified to ensure their use is within the ranges of applicability.

REFERENCES

1. BAW-10168P, "RSG LOCA - B&W Loss-of-coolant Accident Evaluation Model for Recirculating Steam Generator Plants, Volume I - Large Break, Volume II - Small Break," July 1988.

2. BAW-10169P-A, "RSG Plant Safety Analysis - B&W Safety Analysis Methodology for Recirculating Steam Generator Plants," October 1989.

3. Letter from J. H. Taylor (BWFC) to J. A. Norberg (NRC), "ECCS Methodology for Licensing Catawba and McGuire Reloads," JHT/87-271, December 28, 1987.

4. Letter from J. H. Taylor (BWFC) to J. A. Norberg (NRC), "ECCS Methodology for Licensing Catawba and McGuire Reloads," JHT/88-203, November 2, 1988.

5. Letter from J. H. Taylor (BWFC) to Valeria Wilson (NRC), "RELAP5/MOD2 Topical Report, BAW-10168P (sic. BAW-10164P), JHT/90-8, January 30, 1990.

6. BAW-10171P, Revision 2, "REFLOD3B - Model for Multinode Core Reflood Analysis," February 1989.

7. BAW-10166P, Revision 1, "BEACH - Best Estimate Analysis Core Heat Transfer, A Computer Program For Reflood Heat Transfer During LOCA," December 1988.

8. BAW-10155-P, "FOAM2 - Computer Program to Calculate Core Swell Level and Mass Flow Rate During Small-Break LOCA," October 1987.

9. BAW-10165P, "FRAP-T6-B&W - A Computer Code for Transient Analysis of Light Water Reactor Fuel Rods," October 1987.

10. BAW-10156-A, "LYNXT - Core Transient Thermal-Hydraulic Program," February 1986.

11. NUREG/CR-4312, EGG-2396, "RELAP5/MOD2 Code Manual," Volumes 1 and 2, August 1985.

12. NUREG/CR-5194, EGG-2531, "RELAP5/MOD2 Models and Correlations," August 1988.

EGG-EAST-8695
February 1990

TECHNICAL EVALUATION REPORT

RELAP5/MOD2 - B&W, AN ADVANCED COMPUTER PROGRAM FOR LIGHT WATER REACTOR LOCA AND NON-LOCA TRANSIENT ANALYSES

C. P. Fineman

Prepared for the
U.S. NUCLEAR REGULATORY COMMISSION